



UNIVERSITAT
POLITÈCNICA
DE VALÈNCIA

**Nanocomposites of Multiphase Polymer Blend
Reinforced with Carbon Nanotubes:
Processing and Characterization**

by

Marcin Węgrzyn

Supervised by

Dr Enrique Giménez Torres

Dr Adolfo Benedito Borrás

INSTITUTO DE TECNOLOGÍA DE MATERIALES

Valencia – January 2014



UNIVERSITAT
POLITÈCNICA
DE VALÈNCIA

**Nanocompuestos de Mezcla de Polímeros Multifásicos
Reforzada con Nanotubos de Carbono:
Procesamiento y Caracterización**

Marcin Węgrzyn

Dirigida por

Dr Enrique Giménez Torres

Dr Adolfo Benedito Borrás

PROGRAMA DE DOCTORADO INGENIERÍA Y PRODUCCIÓN
INDUSTRIAL

TESIS DOCTORAL INTERNACIONAL

Valencia – Enero 2014

Work presented in this document has been done in
Institute for Plastic Research:

Instituto Tecnológico del Plástico AIMPLAS
Calle Gustave Eiffel 4
46980 Paterna, Spain



Results presented here are based on CONTACT project: *Marie Curie Initial Training Network for the tailored supply-chain development of CNT-filled composites with improved mechanical and electrical properties.*



Pracę tą dedykuję moim Najbliższym.

ACKNOWLEDGEMENTS

First and foremost I would like to express sincere thanks to my supervisor, Dr Enrique Giménez, whose motivation, understanding, and great deal of patience have made this research an interesting adventure. This project would have been incomplete without his immense knowledge and friendliness. Tremendous contribution occurred also on personal ground, by undefined amount of help he offered with bureaucracy at *Universitat Politècnica de València* and in *Aimplas*. Besides, I would like to thank my co-supervisor, Dr Adolfo Benedito from *Aimplas* for stimulating discussions and help in solving everyday issues.

Sincere thanks also to the staff of *Aimplas*. At first, sincere thanks to my coworkers from *Departamento de Materiales*, Pilar Martinez, Olivia Menes and Dr Amaya Ortega. Furthermore, thanks to all the colleagues from *Laboratorio Químico*, especially to César Gadea and Dr Belén Monje for the patient introductions to various characterization techniques. Kind and thankful bow to *Departamento de Compounding*, especially to Ignacio Buezas and Francisco Javier Royuela for their countless advices and for teaching me the twin-screw extrusion (thanks also to Patrick Weiss from *Fraunhofer ICT*), and to Begoña Galindo for stimulating discussions. Thanks to *Departamento de Extrusion* and *Departamento de Diseño y Inyección*. Sara Juan has to be mentioned for her undoubted help and endurance in injection molding of nanocomposites.

Very special thanks to Carolina Salinas for multiple offers of help. My stay in Spain would have been far more difficult without your unparalleled personality.

I would like to thank to Cristina Abad for frankness and for visualizing me the right things to do and to avoid. Sincere thanks also to Carlos Martinez for help with automotive issues and to all the people accidentally omitted in above text. Muchas gracias a Todos!

Special thanks go to the whole CONTACT project research team, especially to Jyri Tiusanen (*Promolding BV*) and to Shyam Sathyanarayana (*Fraunhofer ICT*) for the fruitful cooperation. Thanks to Dr Daniel Vlasveld and Dr Christof Hübner for supervision during my secondments.

Professionalism in the difficult task of coordination young researchers by Dr Hübner, Carolyn Fisher and Yvonne Hofmann has to be mentioned.

I would like to acknowledge also Javier Gomez (*University of Jaume I*) for help with electron microscopy, Oscar Sahuquillo (*Technical University of Valencia*) for nanoindentation measurements and *Institute for Polymer Materials Polymat* from San Sebastian for capillary rheometry. I also want to acknowledge Professor Tim Osswald's group from the *University of Wisconsin-Madison*: Dr Daniel Ramirez for performing theoretical calculations used in this work. Thank to Dr Robert Thatcher for help in correction of spelling mistakes.

Countless thanks to Min Ying Tsang for the constant support, undisturbed positive attitude and uncommon kindness.

I would also like to send sincere greetings to my parents for the support on every possible ground.

Finally, I have to mention that this research would not have been possible without the financial assistance of European Community's Seventh Framework Program.

*If the only tool you have is a hammer,
you tend to see every problem as a nail.*

Dr Abraham Maslow

ABSTRACT

This thesis presents the study of nanocomposites based on immiscible polymer blend of polycarbonate and acrylonitrile-butadiene-styrene (PC/ABS) filled with multi-walled carbon nanotubes (MWCNT). The aim is to achieve an improvement of mechanical properties and electrical conductivity of the nanocomposites.

In an initial stage, a twin-screw extruder was used to obtain nanocomposites by melt compounding. Three methods of carbon nanotubes addition were studied: direct addition, dilution from a masterbatch and feeding of MWCNT suspension in ethanol. For each method, the influence of nanofiller content and processing parameters on morphology and final properties of the nanocomposite was analyzed. Furthermore, the influence of two types of carbon nanotubes modifications was studied: covalent modification by surface-oxidation (MWCNT-COOH) and non-covalent modification by an addition of surfactant promoting the nanofiller-matrix interactions.

A good dispersion of the MWCNT was obtained for masterbatch dilution and suspension feeding. Both methods showed preferential localization of carbon nanotubes in polycarbonate phase (PC).

Samples processed by masterbatch dilution showed the 30 % increase of rigidity and a decrease of ductility of PC/ABS for 0.5 wt. % MWCNT. Electrical conductivity was influenced by processing temperature and carbon nanotubes type. The percolation threshold value was 2.0 wt. % for pristine MWCNT and 1.5 wt. % for modified MWCNT-COOH.

Better balance of mechanical properties and electrical conductivity was achieved in the samples obtained by the masterbatch route. These properties were studied in a subsequent phase, when the extruded nanocomposite was injection molded in order to obtain a defined geometry.

Injected samples showed higher homogeneity and thus, higher electrical conductivity when low injection speeds and intermediate melt temperatures were applied. This effect is related to the high orientation and concentration of carbon nanotubes, as well as to occurrence of a skin effect. However, the maximum electrical conductivity achieved after the injection process was reduced by orders of magnitude over the obtained in the compounding stage. Finally, a mathematical model of carbon nanotubes orientation in injection molded samples was calculated. The results showed a good agreement with the experimental values. A high orientation of carbon nanotubes, exceeding 75 %, in the direction of the flow at higher distances from the injection gate was observed. A loss of the orientation in the injection gate area due to flow disturbances was observed.

RESUMEN

En esta tesis se ha abordado el desarrollo de nanocompuestos basados en una mezcla inmiscible de policarbonato y acrilonitrilo-butadieno-estireno (PC/ABS) y la adición de nanotubos de carbono (MWCNT), con el objetivo de conseguir propiedades mecánicas y de conductividad eléctrica mejoradas.

En una primera fase, se empleó una extrusora de doble husillo para la obtención por mezclado en fundido de los nanocompuestos, y se estudiaron tres métodos de adición de los nanotubos de carbono: la adición directa, la dilución a partir de un masterbatch, y la incorporación de los MWCNT a partir de una suspensión en etanol. Para cada método, se analizó la influencia de del contenido de nanocarga y de los parámetros de procesado sobre la morfología y propiedades finales de los nanocompuestos. Asimismo, se estudió también la influencia de la adición de nanotubos de carbono con dos tipos de modificaciones superficiales. En particular, se adicionaron nanotubos de carbono modificados covalentemente mediante oxidación (MWCNT-COOH), así como la adición de un surfactante para favorecer las interacciones nanocarga-matriz.

Desde el punto de vista de la morfología, una buena dispersión de los MWCNT fue obtenida a partir de los métodos de dilución de un masterbatch y suspensión en etanol, mostrando en ambos casos una localización preferencial de los nanotubos de carbono en la fase policarbonato (PC).

En las muestras procesadas mediante masterbatch se observó que la rigidez aumentaba por encima del 30 %, a la vez que se reducía la ductilidad del PC/ABS, para adiciones de 0.5 % peso de MWCNT. Asimismo, se observó que los valores de conductividad eléctrica estaban influenciados por las temperaturas de procesado y la naturaleza de los nanotubos de

carbono, siendo el valor de percolación de 2.0 % peso para MWCNT puros y 1.5 % peso para MWCNT-COOH.

Atendiendo al mejor balance de propiedades mecánicas y de conductividad eléctrica logrado en las muestras obtenidas mediante la ruta de masterbatch, en una siguiente fase se estudió la variación producida en estas propiedades cuando el nanocompuesto extruido fue moldeado por inyección para obtener una geometría definida. Del estudio de los parámetros de inyección se observó que las muestras inyectadas presentaban una mayor homogeneidad, y por ende una mayor conductividad eléctrica, cuando se aplicaban bajas velocidades de inyección y temperaturas de fundido intermedias. Este efecto está relacionado con la mayor orientación de los nanotubos de carbono en las zonas internas con mayor concentración de MWCNT y a la existencia de un efecto piel. A pesar de ello, la conductividad eléctrica máxima alcanzada después del proceso de inyección se redujo varios órdenes de magnitud respecto al valor obtenido en la etapa previa de compounding.

Finalmente, se llevó a cabo un modelizado matemático de la orientación producida en los nanotubos de carbono durante el proceso de moldeo por inyección, y los resultados obtenidos mostraron un buen ajuste con los valores experimentales. Se observó una alta orientación de los nanotubos de carbono en la dirección del flujo a distancias alejadas del punto de inyección, con valores teóricos por encima del 75 %, así como una pérdida de la orientación en las proximidades del punto de inyección debido a perturbaciones en el flujo.

RESUM

En aquesta tesi s'ha abordat el desenvolupament de nanocompostos basats en una mescla immiscible de policarbonat i acrilonitril-butadié-estiré (PC/ABS) i l'addició de nanotubs de carboni (MWCNT), amb l'objectiu d'aconseguir propietats mecàniques i de conductivitat elèctrica millorades.

En una primera fase, es va utilitzar una extrusora de doble fuset per a l'obtenció per mesclat en estat fos dels nanocompostos i es van estudiar tres mètodes d'addició dels nanotubs de carboni: l'addició directa, la dilució a partir d'un masterbatch, i la incorporació dels MWCNT a partir d'una suspensió en etanol. Per a cada mètode, es va analitzar la influència del contingut de nanocàrrega i dels paràmetres de processament sobre la morfologia i propietats finals dels nanocompostos. Així mateix, es va estudiar també la influència de l'addició de nanotubs de carboni amb dos tipus de modificacions superficials. En particular, es van addicionar nanotubs de carboni modificats covalentment mitjançant oxidació (MWCNT-COOH), així com l'addició d'un surfactant per a afavorir les interaccions nanocàrrega-matriu.

Des del punt de vista de la morfologia es va obtenir una bona dispersió dels MWCNT a partir dels mètodes de dilució d'un masterbatch i suspensió en etanol, mostrant en tots dos casos una localització preferencial dels nanotubs de carboni en la fase policarbonat (PC).

En les mostres processades mitjançant masterbatch es va observar que la rigidesa augmentava per damunt del 30 %, alhora que es reduïa la ductilitat del PC/ABS. Per a addicions del 0.5 % en pes de MWCNT. Així mateix, es va observar que els valors de conductivitat elèctrica estaven influenciats per les temperatures de processament i la naturalesa dels nanotubs de carboni, sent el valor de percolació del 2.0 % en pes per als MWCNT purs i del 1.5 % en pes per als MWCNT-COOH.

Atenent al millor balanç de propietats mecàniques i de conductivitat elèctrica aconseguit en les mostres obtingudes mitjançant la ruta de masterbatch, en una següent fase es va estudiar la variació produïda en aquestes propietats quan el nanocompost extrudit va ser modelat per injecció per a obtenir una geometria definida. De l'estudi dels paràmetres d'injecció es va observar que les mostres injectades presentaven una major homogeneïtat, i per tant una major conductivitat elèctrica, quan s'aplicaven baixes velocitats d'injecció i temperatures intermèdies de fos. Aquest efecte està relacionat amb la major orientació dels nanotubs de carboni en les zones internes amb major concentració de MWCNT i a l'existència d'un efecte de pell. Malgrat açò, la conductivitat elèctrica màxima aconseguida després del procés d'injecció es va reduir diversos ordres de magnitud respecte al valor obtingut en l'etapa prèvia de compounding.

Finalment, es va dur a cap un modelitzat matemàtic de l'orientació produïda en els nanotubs de carboni durant el procés de moldeig per injecció, i els resultats obtinguts van mostrar un bon ajust amb els valors experimentals. Es va observar una alta orientació dels nanotubs de carboni en la direcció del flux a distàncies allunyades del punt d'injecció, amb valors teòrics per damunt del 75 %, així com una pèrdua de l'orientació en les proximitats del punt d'injecció degut a pertorbacions en el flux.

INDEX

CHAPTER 1

1. Introduction	15
1.1. Overview of the thesis	16
1.1.1. Motivation	16
1.1.2. Challenges	17
1.2. Objectives	18
1.3. Structure of the thesis	19

CHAPTER 2

2. Literature review	22
2.1. Engineering plastics	22
2.1.1. PC/ABS Polymer blends	23
2.1.2. Carbon nanotubes	25
<i>2.1.2.1. Synthesis overview</i>	25
<i>2.1.2.2. Properties overview</i>	28
2.2. Polymer-carbon nanotube nanocomposites	30
2.2.1. Preparation and processing of MWCNT nanocomposites	32
<i>2.2.1.1. Compounding of nanocomposites</i>	33
<i>2.2.1.2. Injection molding of nanocomposites</i>	34
2.2.2. Properties of MWCNT nanocomposites	39

2.2.2.1. <i>Morphology of MWCNT nanocomposites and nanofiller functionalization</i>	39
2.2.2.2. <i>Mechanical properties of MWCNT nanocomposites</i>	44
2.2.2.3. <i>Electrical properties of MWCNT nanocomposites</i>	45
2.2.3. Prediction of properties of MWCNT nanocomposites	50
2.2.4. MWCNT nanocomposites of multiphase blends	53

CHAPTER 3

3. Materials and experimental method	57
3.1. Materials	57
3.1.1. PC/ABS blend	57
3.1.2. Multi-walled carbon nanotubes (MWCNT)	57
3.1.3. Surfactants	58
3.2. Melt processing conditions	59
3.2.1. Instruments	59
3.2.2. Nanocomposites processing routes	62
3.2.2.1. <i>Common nanofiller feeding method</i>	62
3.2.2.2. <i>Masterbatch dilution method</i>	63
3.2.2.3. <i>Suspension method</i>	65
3.3. Sample preparation	66
3.3.1. Compression molding	67
3.4. Samples Characterization	68

3.4.1. Analyses of morphology	68
3.4.1.1. <i>Light Transmission Microscopy (OM)</i>	68
3.4.1.2. <i>Scanning Electron Microscopy (SEM)</i>	70
3.4.1.3. <i>Transmission Electron Microscopy (TEM)</i>	73
3.4.1.4. <i>Raman spectroscopy</i>	74
3.4.2. Thermal properties	75
3.4.2.1. <i>Differential Scanning Calorimetry (DSC)</i>	76
3.4.2.2. <i>Thermo-Gravimetric Analysis (TGA)</i>	78
3.4.2.3. <i>Dynamic Mechanical Analysis (DMA)</i>	79
3.4.3. Mechanical properties	81
3.4.3.1. <i>Tensile testing</i>	81
3.4.3.2. <i>Nanoindentation</i>	84
3.4.4. Rheology	85
3.4.5. Electrical properties	89
3.4.6. Flammability	91

CHAPTER 4

4. Conventional melt mixing	96
4.1. Study of PC/ABS-MWCNT nanocomposites morphology	96
4.1.1. Characterization of PC/ABS and MWCNT	96
4.1.2. Influence of processing method on morphology of PC/ABS-MWCNT nanocomposites	99

4.1.3.	Influence of MWCNT modification on morphology of PC/ABS-MWCNT nanocomposites	107
4.2.	Study of thermal properties of nanocomposites	112
4.2.1.	Thermal characterization of PC/ABS	112
4.2.2.	Study of thermal behavior of PC/ABS-MWCNT nanocomposites	114
4.3.	Mechanical properties of PC/ABS-MWCNT nanocomposites	122
4.3.1.	Influence of MWCNT modification on mechanical properties of PC/ABS-MWCNT nanocomposites	125
4.3.2.	Comparison between experimental data and theoretical predictions of the nanocomposite tensile modulus	128
4.4.	Rheological properties of nanocomposites	133
4.5.	Influence of carbon nanotube content on electrical properties of PC/ABS-MWCNT nanocomposites	139
4.6.	Preliminary conclusion	143
4.7.	Selection of samples with the best balance of properties	145

CHAPTER 5

5.	Modification of conventional extrusion	147
5.1.	Study of PC/ABS-MWCNT nanocomposites morphology	147
5.1.1.	Influence of nanocomposite processing on the morphology of PC/ABS-MWCNT nanocomposites	147

5.1.2.	Influence of MWNCT modification on morphology of PC/ABS nanocomposites	155
5.2.	Study of thermal properties of nanocomposites processed by suspension method	160
5.2.1.	Thermal stability of nanocomposites	160
5.3.	Study of mechanical properties in nanocomposites processed by suspension method	168
5.4.	Comparison of electrical properties of nanocomposites	171
5.5.	Preliminary conclusions	174

CHAPTER 6

6.	Injection molding	177
6.1.	Processing conditions	177
6.1.1.	Common injection molding process	179
6.1.2.	Masterbatch dilution in injection molding	180
6.2.	Study of MWCNT dispersion	180
6.2.1.	Morphology of injection samples	181
6.2.2.	Carbon nanotubes location in the sample	189
6.2.3.	Orientation of carbon nanotubes	196
6.3.	Flammability of injection molded nanocomposites	200
6.4.	Mechanical reinforcement in injection molded nanocomposites	204
6.5.	Electrical properties of injection molded nanocomposites	214

6.5.1. Recovery of conductive network 219

6.6. Preliminary conclusions 222

CHAPTER 7

7. Modelling of injection molded nanocomposites 225

7.1. Methodology and basic assumptions 225

7.1.1. A short description of numerical models 225

7.1.2. Assumptions used for the calculation 227

7.2. Calculation results 229

7.2.1. Comparison between theoretical and experimental data 235

7.3. Preliminary conclusion 236

CHAPTER 8

8. Conclusions and future research 239

8.1. Conclusions 239

8.2. Suggestions for future research 241

9. Literature 244

1. Introduction

Nanotechnology has recently gained attention of scientific environment due to the solutions offered in main areas of the human activity. Ceramic-, metal- and inorganic-based nanomaterials have found applications in areas from medicine to construction sector. Carbon-based structures have unique position among the researched and applied nanomaterials. Single- and multi-walled carbon nanotubes representing 1D structures share this attention with the graphene sheet (2D) and the more complex systems, *e.g.* fullerenes. Nevertheless, carbon nanotubes with their excellent properties, well established production process (*e.g.* variations of carbon vapor deposition – CVD) and characterization methods have become an important material in nowadays technology. The homogeneity of commercial batches and the precise control of the structures allow application of these nanomaterials in technologies requiring designed parameters, *e.g.* aspect ratio, purity (including the residual catalyst content), length distribution or alignment in the substrate.

Global market of engineering plastics production, according to various sources, has exceeded 19.6 million metric tons in 2013 and is expected to increase reaching 29.1 million metric tons by 2020. Multiple solutions offered by polymer materials are becoming bases of the new applications involving engineering plastics. Polymer blends participating in these numbers, seem to attain attention again in the last years. Besides the unfilled multi-facial materials with controlled size of the dispersed phase, the nanocomposites based on such matrices are being researched intensively.

Excellent properties of carbon nanotubes boost electrical conductivity of polymer materials and improve mechanical properties the orders of magnitude higher than the common fillers at similar concentrations. Furthermore, the phenomenon of nanofiller migration between the phases of

the immiscible polymer blend occurs with the co-continuity of the filler creating the percolated network with high selectivity regarding localization. The issues related to the dispersion of carbon nanotubes in polymer matrices are reported to be solved by a covalent- and non-covalent modification of the filler or by a proper adjustment of machine parameters. Nevertheless, homogeneous morphology is rarely obtained during the processing. Polymer melt and carbon nanotubes have various flow abilities, what causes challenges *e.g.* in injection molding. The difference of nanofiller concentration in several areas of the injected sample as a consequence of the shear-induced flow is a drawback in this technology. Finding the solutions for disadvantages in carbon nanotube-based nanocomposites formation and processing would bring a great number of new, interesting applications.

1.1. Overview of the thesis

1.1.1. Motivation

Research on nanocomposites based on multiphase polymer blend filled with multi-walled carbon nanotubes was done with the aim of matrix properties improvement. The challenge and interest in this research are focused on understanding the behavior of carbon nanotubes in immiscible blend. Formation and processing of nanocomposites with the common methods from commercially available materials was carried out in order to provide conditions applicable for industry. The work was done within the CONTACT project funded from the European Community's Seventh Framework Program (FP7/2007-2013) under grant agreement no. 238363. Initial Training Network (ITN) was oriented on various fields related to carbon

nanotubes: synthesis and characterization of nanomaterials, formation processing of nanocomposites and application of designed technology.

Recent studies offer great number of information about carbon nanoparticle-filled polymers. Nevertheless, only minor part of these reports are related to the multiphase matrix-based nanocomposites. Multi-walled carbon nanotubes with a unique structure of rolled graphene sheet providing uncommon properties of this material allows achievement of elevated values of electrical properties. Besides, an increase of other properties has been achieved in polymer nanocomposites. Performance achieved after the formation of polymer blend and after the introduction of nanofiller giving various properties increase is defined as the main aim of this research.

1.1.2. Challenges

The common issues related to carbon nanotubes-filled polymer-based nanocomposites can be divided into sections and summarized as:

- Agglomeration of nanofiller during nanocomposite formation
- Importance of wetting properties between matrix and filler (possibly tuned by functionalization)
- Importance of applied shear value necessary to break primary- and secondary agglomerates with keeping high-aspect ratio of carbon nanotubes
- Difficulty of maintaining the good morphology of the nanocomposite along the whole specimen after processing by injection molding
- Importance of controlling the orientation of carbon nanotubes inside the mold during injection molding

1.2. Objectives

The aim of this thesis is to produce nanocomposites of multiphase polymer matrix filled with multi-walled carbon nanotubes. The goals include study of properties evolution during the path from nanocomposite formation to processing. Commercially available materials and scalable methods are used. Therefore the specific objectives are:

- Formation of nanocomposites based on PC/ABS multiphase polymer blend filled with carbon nanotubes:
 - Study of the influence of processing parameters (screw speed, barrel temperature)
 - Study of the influence of carbon nanotube feeding method
 - Study of the influence of carbon nanotubes modification
- Extended characterization of nanocomposites including morphology and the other main properties
- Processing of the selected nanocomposites by injection molding:
 - Study of the influence of processing parameters (injection velocity, melt temperature)
 - Study of the influence of the number of processing steps
- Characterization of the specimens including morphology with carbon nanotubes orientation, mechanical- and electrical properties
- Theoretical calculations of carbon nanotubes orientation after injection molding and comparison of the results with experimental data

1.3. Structure of the thesis

This thesis is organized into eight chapters in order to clearly lay out the research developed on formation and processing of nanocomposites with multiphase polymer blend filled with multi-walled carbon nanotubes.

Chapter 2 presents the state of the art on related polymer-based nanocomposites filled with carbon nanotubes.

Methods used during formation and characterization of PC/ABS-MWCNT nanocomposites are described in *Chapter 3*. Principles of twin-screw extrusion and various analytical techniques used in this work are described. Methods of nanofiller introduction and conditions applied during nanocomposite formation are shown along with the conditions of each performed test.

Information in *Chapter 4* contains presentation and discussion of the results obtained in the nanocomposites formation step. Twin-screw extrusion was carried out with the commonly applied nanofiller introduction: dry powder feeding and masterbatch dilution. Morphology, thermal-, mechanical- and electrical properties are described. Preliminary conclusions about the performance achieved after the introduction of carbon nanotubes to PC/ABS are located at the end of this chapter.

Chapter 5 gives information about the modification of the nanofiller feeding method during twin-screw extrusion. Formation of PC/ABS-MWCNT was carried out with the introduction of carbon nanotubes in the form of suspension in ethyl alcohol. Crucial areas are studied: morphology, thermal-, mechanical- and electrical properties. Besides, non-covalent modification of carbon nanotubes with surfactants is studied.

Chapter 6 is constructed of presentation and discussion of the results obtained in injection molding. Furthermore, processing parameters are given and applied methods are described. Morphology including carbon nanotubes orientation and localization, thermal-, mechanical- and electrical properties are described. Preliminary conclusions about the performance achieved after nanocomposite processing are located at the end of this chapter.

Theoretical calculations of carbon nanotubes behavior in polymer melt during injection molding are presented in *Chapter 7*. Expected location of nanofiller and orientation is corroborated with the experimental results.

In *Chapter 8* general conclusions and suggestion for continuation of this research are presented.

2. Literature review

2.1. Plastic Materials

Following the analysts of Plastics Europe, in 2012 the entire polymer industry in European Union had a combined turnover of above 300 billion euro. This is a minor part of the world market, which is shown in Figure 2.1.1. Therefore, great expectations of actual and future research carried out in this field are related to the most universally-used materials in the global economy. Plastics became an important part of modern technology, providing the state-of-the-art solutions to the automotive, aerospace or electronic industries.

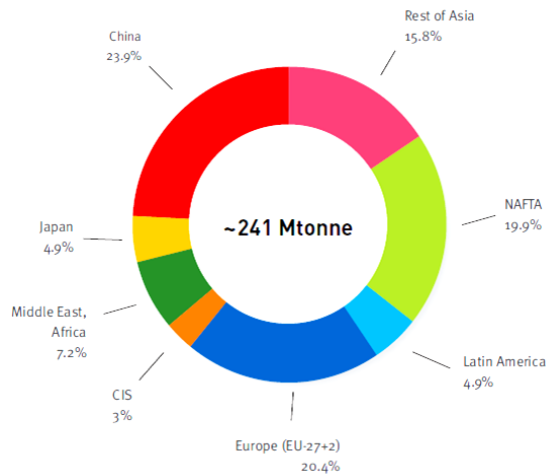


Figure 2.1.1: World plastic production in 2012 [Plastics Europe].

Regarding the further advance in plastic materials, the combination of mutually beneficial polymers was introduced into the market in the form of blends. Miscible and multiphase polymer blends create over 36 % of the polymer production industry,^[1] which is a considerable area. Besides,

nanocomposites are another method of plastics improvement on the path of advanced materials development. Nanocomposites getting the recent attention of both research and industry are estimated to be consumed annually in the amount of over 330 metric tons in 2016 according to BCC research. Such an amount should be regarded as significant, especially that these materials are novel and new solutions are rarely directly applied in rather conservative industry.

2.1.1. PC/ABS Polymer blends

Polycarbonate, produced annually in billion tons,^[2] is one of the most common engineering thermoplastic polymer with good transparency and properties similar to poly(methyl methacrylate) (PMMA). Polycondensation of bisphenol A and phosgene results with polycarbonate but detailed production process involves the intermediate step of the bisphenol A sodium salt formation, further conversed into the final material. Bisphenol A can be exchanged by the similar structure monomers to improve particular properties (*e.g.* introduction of halogen atoms increases flame retardancy). High impact-resistance of polycarbonate is confronted with the low scratch resistance. Nevertheless, good mechanical properties (Table 2.1.1) make a wide range of applications possible, despite the required high temperatures of processing tools. Except the common automotive and electronic applications there is significant area of special destination materials, like optical lenses, riot shields or medical materials.

Table 2.1.1: Comparison of Bisphenol A polycarbonate (PC) and ABS.^[3]

Properties	PC	ABS
Glass Transition Temperature [°C]	145	105
Melting Temperature [°C]	225	-
Density [gcm ⁻³]	1.20	1.05
MFI [g 10min ⁻¹]	8.3	13.2
Hardness Rockwell R	118	108
Tensile Strength [MPa]	63.1	43.4
Elongation at break [%]	50.4	25.6
Izod impact strength [Jm ⁻¹]	640-850	340
Elastic Modulus [MPa]	2360	2350
Electrical Resistivity [Ω cm ⁻¹]	1.4 e14	1.3 e16
Surface Resistance [Ω]	1.2 e15	3.2 e15
Thermal Conductivity [W m ⁻¹ K]	0.17	0.19
Vicat Softening point [°C]	147	101
Flammability, UM94	V-2	HB-5VA
Refractive Index	1.59	-
Processing Window [°C]	280-300	200-250
Drying Temperature [°C]	120	75-90

Polycarbonate blended with acrylonitrile-butadiene-styrene terpolymer (ABS) forms immiscible,^[4] largest selling commercial polymer blend in the world. The multiphase PC/ABS exhibits unique properties due to the combination of polymers with various characteristics.^[5] Besides, morphology of the PC/ABS blend depends on many factors, but the blend type components, their share and shear rates during the processing are most important.^[4] Interfacial interactions can be based also on the differential shrinkage between polymers, which is minimized by co-polymerization reducing the inter-laminar gaps. Reasonably small injection molding shrinkage (near 0.3 % for reinforced material) promotes such a processing method with a standard

melt temperature ranging between 240 °C and 280 °C, and mold temperatures below 100 °C. According to ISO 294, the injection velocity is 240 mms⁻¹, although after mixing with solid particles (*e.g.* carbon nanotubes) this value could be rapidly reduced due to the increase of melt viscosity.

2.1.2. Carbon nanotubes

Various types of carbon nanomaterials, one-dimensional carbon nanotubes or two-dimensional nanographene platelets, earned a stable position in the area of additives for industrial plastics. Well-studied multi-walled carbon nanotubes (MWCNT) with a unique structure and properties became an important group due to the offered improvement of properties. MWCNT in nanocomposites can boost electrical and thermal conductivity^[6-8] by orders of magnitude over the performance achievable with traditional carbon fillers in similar weight percentages.^[9] Two main types of carbon nanostructures with different origin and properties are present in nowadays technology. Single-walled carbon nanotubes (SWCNT) are constructed of a rolled monolayer graphene sheet while the aforementioned multi-walled carbon nanotubes (MWCNT) are a structure build of many concentric SWCNT. The most commonly applied synthesis methods need to be discussed in order to understand the behavior of this nanomaterial.

2.1.2.1. Synthesis overview

Production process of carbon nanotubes has evolved since the discovery in 1990's. The issued related to single-walled carbon nanotubes production are in majority an academic interest, while MWCNT are already introduced in the industry. Both types are principally prepared in arc-discharge process or by laser-ablation in an inert gas atmosphere with a use of metal catalyst.^[10-11] Nevertheless, Catalytic Chemical Vapor Deposition (CCVD)

(Figure 2.1.2) is the commonly applied method providing repeatability required in industry.^[12-13] The product formation depends strongly on the metal catalyst center, inert gas and electric currents. The plasma control variation of the CCVD method has been studied as an alternative method.^[14] With this method the microscopic and macroscopic parameters of the product are precisely controlled. Furthermore, further development of new technologies of carbon nanotubes production is reported, *e.g.* the fluidized bed reactors are studied and the technology is being adapted for the industrial use.^[15-16]

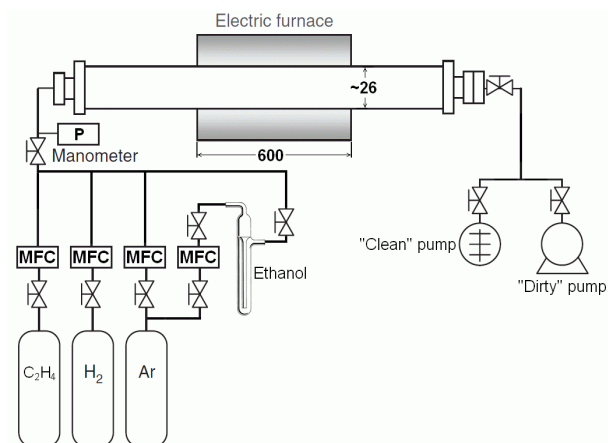


Figure 2.1.2: Scheme of low pressure CCVD installation.^[17]

Highly controlled pyrolysis of a hydrocarbon-organometallic solution like ferrocene-benzene, thiophene or methane can yield in carbon nanotubes when correct conditions are applied. The decomposition of a simple hydrocarbon or hydrocarbon mixtures over metal substrates usually gives satisfactory results, too. Besides, simply alcohols as starting materials to obtain mono-layered graphene tubes with sufficient purity and efficiency were studied.^[18] Selection of an appropriate metal catalyst is crucial in the nanotube growth process. This is usually correlated with the formation

method, *e.g.* two-step plasma-enhanced CVD shows a Ni as the most suitable catalyst to obtain MWCNT.^[19] Water enhanced catalysts introduced to CVD method by Iijima *et al.*^[13] can induce the growth of a dense and vertically aligned nanotube forest but the satisfactory control of this process has not been achieved yet. Industrial approach drives the research in the catalyst area. CoMoCat commercialized by South-West Nanotechnologies Inc. is an interesting example due to the scalability and possibility to change of the process from periodic to continuous.^[19]

There are various recognized mechanisms of carbon nanotubes formation with a slight predominance of a few. The mechanism clarifying hydrocarbon pyrolysis proposed in 1978 by Baker and Harris^[20] slightly modified by Oberlin^[21] involves the C-H bond breaking with hydrogen release followed by the diffusion of carbon through the metal substrate. Further deactivation of the catalyst and over-coating causes termination of a nanotube growth. The size of metal catalyst determines the product and MWCNT are preferably grown on medium-sized particles.

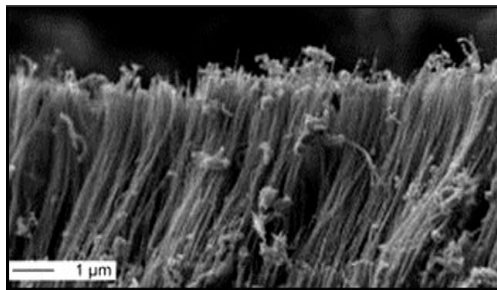


Figure 2.1.3: Aligned carbon nanotubes forest grown by CVD method.^[22]

Besides, a formation mechanism including the hemispherical structures giving the beginning of nanotube growth is one of the considered theories^[23] This is often correlated with the growth model regarding the individual nanotube being formed on one metal particle. Some computational models

supported by the laboratory tests showed the formation of CNT directly by closing a large one-layer graphite sheet.^[24] This is reported as a more energetically favorable mechanism than growing individual nanotube by the addition of carbon atoms to the structure.

Intensive research on carbon nanotubes production methods resulted in a bowl-like cathodes or an open-air synthesis giving higher yields, purity and improved oxidation resistance.^[13] Laser vaporization was developed by Smalley *et al.*^[12] where a beam is directed into graphite at the high pressure of an inert gas. Nevertheless, Chemical Carbon Vapor Deposition (Figure 2.1.2) with the advantage of scalability is preferred due to facilitated industrial application of this method. Resulting material in the form of aligned carbon nanotube *forest* (Figure 2.1.3) contains the primary agglomerates that need to be destroyed in the nanocomposite formation process. Combination of these methods, a laser-assisted CVD can selectively produce MWCNT or SWCNT. Besides an aerogel-supported CVD with control provided by the change of a fed gas or a surface area is an alternative.

2.1.2.2. Properties overview

Novel and uncommon properties of carbon nanotubes make this material an important field in recent research. With the comparison to carbon fibers, carbon nanotubes Young modulus and strength are improved by over 30 %, showing 1800 GPa and 40 GPa, respectively (Table 2.1.2). Multi walled carbon nanotubes are structured of up to 30 concentric layers of graphene with a diameter in a range of 10-50 nm,^[25] abnormally high length-to-diameter ratio (L/D)^[26] and standard length in a range of 500-1000 nm, dependable on synthesis method.^[25] Besides, the outer layer of an individual carbon nanotube exists in three main structural versions: zigzag, armchair and chiral.^[27]

Purification and characterization methods play a key role in the nanomaterials production process. The greatest share of impurities comes as an amorphous carbon and graphite nanoparticles, but this is the least problematic one. The residual metal catalyst gives more difficulties, *e.g.* influences the low-temperature oxidation process of polycarbonate causing drawbacks during the nanocomposite formation. The most common procedures in MWCNT refining process are mechanical centrifugation and filtration or oxidation: gas-phase or vapor-phase oxidation and wet chemical oxidation.^[11] Acid treatment combined with the high-temperature gives the requested level of product purity.^[24] The other methods are still being investigated.^[28-29] Nevertheless, the most promising path to obtain pure material is to improve the synthetic way rather than purification methods.

Table 2.1.2: Properties comparison between SWCNT, MWCNT and the other commonly known materials: steel and Kevlar®.

Properties	SWCNT	MWCNT	HS Steel	Kevlar
Diameter [nm]	1.0-1.5 ^[30]	10-100 ^[30]	-	-
Length [μm]	0.5-4.0 [17]		-	-
Young 's modulus [GPa]	1300 ^[31]	1800 ^[32]	200 ^[33]	130 ^[33]
Tensile strength [GPa]	10-60 ^[33]		4.1 ^[33]	3.9 ^[33]
Elongation failure [%]	20-30 ^[34]		<10 ^[33]	2.8 ^[33]

Regarding the application area of carbon nanotubes, electronic and electrical industry seems to be the key area. The material already holds an important place in engineering.^[4,35] Electrical characteristics of carbon nanotubes match with the requirements of energetic industry. The potential application gives solutions in the market of batteries, solar cells, hydrogen storage, display devices and loudspeakers. The other applications take advantage

from electromagnetic properties of the carbon nanotubes: artificial muscles, electric motor brushes and magnets or superconductors.^[4] Optoelectronic industry can benefit from the phonon transport possibilities in MWCNT while the mechanical properties can be exploited in the surface and membrane industry or in radiation chemistry-related branches.^[6,36] Despite the mentioned applications, the great majority of solutions are based on polymer-matrix nanocomposites filled with MWCNT.

2.2. Polymer-carbon nanotube nanocomposites

Without any doubts plastics and their composites poses already strong and constantly growing domination in everyday life. Advanced materials have reached the high importance in modern world. This brings the necessity of the application-oriented research.

The development of advanced materials is usually driven by the idea of future use. Electronic sector including the application of plastics and polymer-based-composites is a dynamically changing branch of technology with long history dated back to 1950's.^[37] Even though the conductive polymers are present in science and technology, engineering plastics tend to show poor electrical properties not sufficient for the application in this sector. This drawback is commonly solved by the formation of composite with electrically conductive filler.^[38] Nevertheless, such a material often shows the decrease of mechanical properties coming from the low homogeneity.^[39] Besides, the other parameters, like thermal properties with the degradation behavior or the procesability (often correlated with the visco-elastic properties) need to be controlled. The recent, well-settled study of conductive plastics^[7,40] shows the possibilities of material control and variations of research areas that need to be covered in order to provide the data necessary for the application. Polymer-based electronics with only trace amounts of silicon or copper are concurrent to metals and semiconductors.

The new elements are flexible, light and cost-efficient. Besides, plastics are expected to create an alternative for indium tin oxide (ITO) widely used in optoelectronic technology.^[41]



Figure 2.1.4: Example applications of polymer-based MWCNT-filled nanocomposites.

Considering carbon nanotubes as reinforcement in engineering plastics, a group of specific applications needs to be mentioned. First of all, EMI (electromagnetic interaction) shielding of material reinforced with carbon nanotubes gets more attention, despite relatively high complexity of this technology.^[42] The great-scale electrochemical metallization of industrial elements (*e.g.* car elements or house-hold equipment elements) demand electrically conductive elements (Figure 2.1.4). Furthermore, according to the information provided by the Nanocyl during CNPComp 2013, automotive uses MWCNT replacing carbon black in the fuel systems (pumps, tanks, connectors), due to the required electrostatic properties. Carbon nanotubes-filled nanocomposites are present in simply applications like polyurethans for

wheels or elastomers for tubings, as well as in more sophisticated ones: ATM machines, sport goods or sensors.

Despite the thermoplastic materials, the thermosetting resins have an important place in carbon nanotube composites technology. Considerable improvement in the dispersion of carbon nanotubes in epoxy resins is obtained, with the respect to the decreased viscosity in some cases (comparing with an average thermoplastic polymer melt at processing temperature).^[43-45] This creates the greater possibility of the use of surfactant as a physical modification of the nanofiller, which finally leads to the better dispersion.^[46-47] However, additional issues that need to be discussed are outside of the area of interest of this project.

2.2.1. Preparation and processing of MWCNT nanocomposites

Formation of carbon nanotube-based nanocomposites with the ability to control the properties is within the main goals of researchers nowadays. Melt mixing is the commonly applied preparation method preferred by industry, though. Various material improvement is being reported for this method.^[48] However, the problem of carbon nanotubes dispersion disappears when the other processing methods are used (*e.g.* solution processing and in-situ polymerization).^[35,43,49-51] Morphology of carbon nanotube-based nanocomposites influences the main features of the final material. The actual state of knowledge shows that the dispersion of carbon nanotubes in the polymer matrix needs to be improved before such composites will enter the market with the ability to replace the common engineering plastics. Alignment of the nanofiller play less important role in determining material behavior, although the properties as electrical conductivity or isotropy of mechanical reinforcement are sensitive to this factor.^[52]

Processing of the nanocomposites regarding shaping of the previously formed material can be non-invasive for the nanofiller dispersion state, *e.g.* compression molding. Usually no significant change to the morphology of pellets is observed, while in the injection molded specimens a level of dependence on processing parameters is clearly higher.^[53] MWCNT dispersion varies a lot with the change of position inside the specimen regarding the distance of mold walls.^[53-54] Due to different flow abilities of polymers and nanotubes related to the spatial behavior, there is a significant change in the filler concentration also with the respect to the gate.^[25] Well dispersed nanofiller in samples processed at small injection velocity exist,^[25,53] which can be understood as positive signal for the further research in this field. Nevertheless, processing methods of nanocomposites at actual state are still at the embryonic level.

2.2.1.1. Compounding of nanocomposites

High aspect ratio of carbon nanotubes causes the boost of electrical- and thermal conductivity in isolating polymers at relatively low loads.^[55-56] Likewise, shape and properties of MWCNT allow improving mechanical properties of polymer matrix when homogeneous dispersion is achieved. This is related to the mechanical percolation based on interactions between carbon nanotubes and polymer chains.^[57] Nevertheless, achieving of good dispersion of carbon nanotubes in polymers by melt-mixing is one of the key challenges. Agglomeration level based on attractive Van der Waals forces between individual nanotubes appears to be tunable when twin-screw extrusion is applied.^[58-59] Tailoring the key processing parameters during nanocomposite preparation and further processing^[60] allows significant decrease of agglomeration and control of alignment in the final part.^[61] Specific mechanical energy (SME) is recognized parameter describing energy applied to the material during melt mixing.^[62] Proper control of the

compounding process and selection of correct processing parameters, in particular with the design of screw profile, is a significant factor in the quality of the final nanocomposite.^[58]

Twin screw extrusion has disadvantages, that could affect the incorporated nanofillers (*e.g.* MWCNT breakage at high-shear conditions). Great number of twin-screw extrusion of major engineering polymer-based nanocomposites exists. High impact polystyrene (HIPS),^[63] polypropylene (PP),^[64-71] acrylonitrile-butadiene-styrene terpolymer (ABS),^[8,71-74] polyamide 6 (PA6)^[75-82] or polycarbonates (PC)^[5,56,83-86] and polyurethanes (PUR)^[87-89] are already widely investigated.

Machine selection is an important part of the process of material preparation. The co-rotating twin-screw extruder is often employed in the initial part of this process and the presence of such technology in polymer processing industries gives various advantages. The factors controlling entire extrusion process include the machine integral parts (screw geometry, die geometry) and setting parameters (barrel temperatures, throughput, screw speed) related also with the material parameters.^[90] The complex mutual dependences between these parameters seems to be commonly shown as a set included in the Specific Mechanical Energy (SME) which shows the final influence of the processing on the nanocomposite.^[91-92] Material conduction and dissipative melting mechanisms are used in twin-screw extruders during the processing.^[93] Besides, an effective mixing of nanofiller and polymer matrix occurs when the kneading elements (Figure 2.1.5) are used in screw profile. Sufficient mixing forces are not provided when the regular (transporting) screw elements are used. Nevertheless, character of the screw should be balanced between mild and aggressive, taking into account matrix properties and effects influencing quality of the final material (*e.g.* carbon nanotubes shortening).^[94] Final screw profile depends on the thermal, rheological and morphological characteristics of polymer, combined with

heat and shear sensitivity of this material. Mathematical calculation supporting the issue of screw profile selection usually gives positive results. Nevertheless, highlighting the critical points in the system for nanocomposites processing is still being developed.

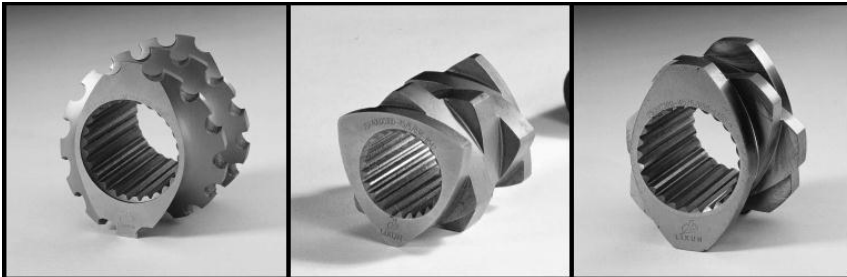


Figure 2.1.5: Elements increasing shear in twin-screw extruder.^[90]

Alig *et al.*^[95] reported strong dependence between electrical conductivity, MWCNT content and processing parameters for nanocomposites based on polycarbonate. The destruction of nanofiller network and, thus a decrease of electrical conductivity was reported when a high screw speed was used. *Primary-* and *secondary agglomeration* theory explains nanofiller bundling what is related to electrical conductivity reinforcement in plastics.^[56] Presence of tightly packed agglomerates in the nanofiller before extrusion makes de-agglomeration more difficult and, thus decreases the homogeneity of MWCNT dispersion. However, it is claimed that the size on carbon macrostructures can be modified with changed shear conditions, *e.g.* with ball mill treatment of nanotubes before further processing.^[96] Proper parameters (high screw speed, low barrel temperature) guarantee better dispersion, so increased contact between the individual nanotubes and matrix.

2.2.1.2. Injection molding of nanocomposites

Injection molding is one of the most widely used plastics processing method for the mass production of complex geometry parts. The well-established

technology offers complete solutions often accepted by the industry. The introduction of forming technology is focused on the key issues ignoring the principals of the process. Multiple effects were observed after the injection molding of the nanocomposites of polymer matrix filled with carbon nanotubes (*e.g.* nanotubes breakage or alignment).^[97] The studies on macrofillers processing, sometimes extrapolated to nanofillers, revealed the significant damage of particles in the transition section of the screw.^[98] Moreover, the presence of much shorter glass fibers in the skin region of the final specimen is compared with the central part of the sample.^[99] These results can give frames for the results expected on nanocomposites. Furthermore, it is reported that the distribution of fiber-like filler in the whole specimen depends on the filler length. Considering double processing of carbon nanotubes (compounding followed by injection molding), it is rather difficult to maintain the initial nanofiller length.

Important role of processing parameters in injection molding were studied on various nanofiller-based systems.^[52,60] Kim *et al.* reported the influence of the holding and injection pressures, mold temperature, and injection speed on the morphology of the final specimen of PA6 filled with MWCNT.^[52] Observations show that the latter two parameters have the greater influence on electrical conductivity of the final part. Gate position in the mold was also investigated, although the results seem to be not clear. Pötschke *et al.* reported behavior of PC/MWCNT with 2 wt. % and 5 wt. % nanofiller loads.^[60] Increase of injection speed and decrease of melt temperature is responsible for high orientation of the nanofiller. Formation of the nanotubes network leads to the increase of electrical conductivity of up to six orders of magnitude when the opposite trend of aforementioned parameters is used.

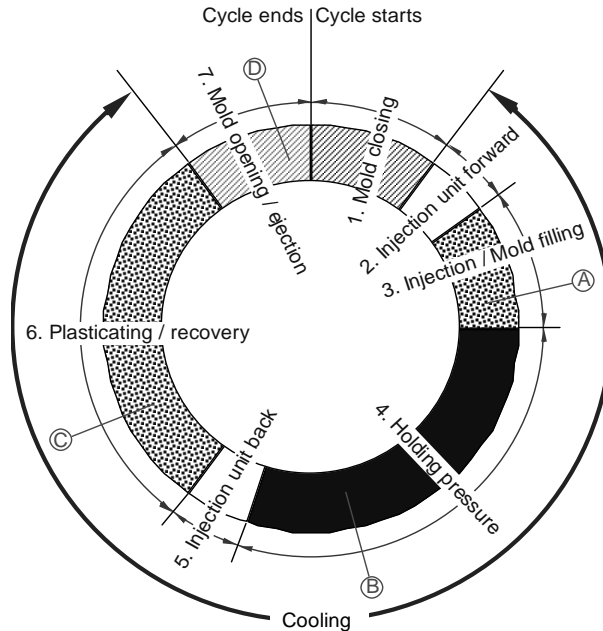


Figure 2.3.6: Time layout of injection molding cycle.^[100]

Besides, precise characterization of the injection molding process requires an introduction of the injection cycle – the basic process repeated during the production (Figure 2.3.6). Melt injection into the mold cavity is followed by the application of holding pressure compensating the shrinkage of the material. Moreover, during the latter process the pressure applied to the material possibly affects the final morphology of the nanocomposite. Therefore, the optimization of conditions by proper selection of pressures and temperatures reduces thermal degradation and the common defects, *e.g.* short shot or flashing.

Regarding the high quality of specimens, many factors need to be optimized and monitored with the respect to the melt fluidity, processing temperatures, and overall melt process ability. Keeping the responding parameters on the constant level throughout the production is a key issue as well. Injection molding is based on the heat exchange between the machine and the

material, so the thermal balance during the processing is determining the quality of the final element. In a case of mass production, the importance of injected parts reproducibility and the precision of dimensions decreases for economic reasons, favoring shorter cycle.^[80]

Polymer-carbon nanotubes nanocomposites processing by injection molding gets more attention in the literature during the last years. Additionally, various modifications of the common aforementioned method were introduced in order to improve the final morphology and properties of the nanocomposite. Shang *et al.* showed the injection molding of PP/MWCNT nanocomposites involving study of the influence of vibration field on the final morphology and electrical properties of the specimen.^[55] Unexpected results showed values relatively similar to the compression molding, which usually only slightly affects morphology. Steady electrical conductivity is achieved most probably due to contacts between oriented carbon nanotube bundles. Furthermore, the quality of injection molded specimen can be improved with the change of the gate position and controlling the melt flow management in the mold.^[52] Other issue, related almost exclusively to electrical conductivity, is the time after which the carbon nanotube network recovers in polymer melt during the short injection molding cycle. This time is relatively long and sometimes is interpreted as a proof for difficulty of the full network recreation.^[97] Besides, with the change of mold temperature the differences in MWCNT and polymer flow were reduced causing significant increase of morphology along the whole specimen.^[52]

Injection molding of polymer blends filled with MWCNT, is not a subject of intensive studies. Similarly to twin-screw extrusion, additional issues of phases compatibility occur. Li *et al.*^[101] shown the formation of PC microfibrils reinforced by MWCNT in PP matrix. After the injection molding the carbon nanotubes remains almost exclusively in PC, which is in

agreement with the aforementioned results.^[5] These results contradict with the other published statement^[102] about the MWCNT presence in both phases of PC/polyolefin nanocomposite. Nevertheless, various nanocomposites formation methods and different characteristics of both nanocomposites could have influenced migration of the nanofiller.

It has been reported that injection molding gives less homogeneous dispersion of the carbon nanotubes and greater dependence of the final material on processing parameters than compounding.^[59-60,103] The difference of nanofiller concentration in several areas of the injected sample as a consequence of the shear-induced flow is also a drawback in this technology. Studies carried out on injected samples of polycarbonate by Park *et al.* show the differences in nanofiller concentration between different parts of the specimen.^[52] Though injection molding is a complex process controlled with many parameters, usually the melt temperature^[104] and injection speed^[60] are chosen as main factors influencing electrical conductivity in injection molded carbon nanotubes-filled nanocomposites.

2.2.2. Properties of MWCNT nanocomposites

2.2.2.1. Morphology of MWCNT nanocomposites and MWCNT functionalization

Improvement of Young modulus and tensile strength with just unitary addition of carbon nanotubes is an average range of 30 % of the initial value, which makes MWCNT one of the best known materials to be mixed with commercial plastics. The requirements for mechanical reinforcement can be summarized with the respect to the filler as: high aspect ratio, best possible dispersion and alignment, centers of interfacial stress transfer distributed in the whole specimen volume.^[51,105-107] Material with some degree of nanofiller alignment is expected in fibers but not in constructing

material.^[27] Incorporating carbon nanotubes into the polymer matrix can be done with the previous formation of chemical bonds between the rolled graphene surface and macromolecules. The destructive method is favorable only in some cases.

Pötschke *et al.* reported the study of the type of carbon nanotubes on the PC-based nanocomposite.^[59] Various commercially available nanotubes are mixed with the same plastic giving different results. The dependence of nanofiller sedimentation was checked with the respect to conductive network formation and compared to the nanocomposites production by masterbatch dilution. Results recorded for various processing parameters show the individual carbon nanotubes for low processing temperatures and short pressing time. High temperatures promoted secondary agglomeration, though. The primary- and secondary agglomeration relates to the recreation of network after the nanocomposite processing. Primary agglomerates present in raw nanofiller material are destroyed during the nanocomposite formation. Further processing result with the formation of secondary agglomerates. Additionally, the appearance of similar particles is compared with the other thermoplastic materials and with epoxy resins.

Agglomeration was also investigated by Pötschke *et al.*^[108] in 1.0 wt. % MWCNT nanocomposites. Mainly particle formation mechanisms were studied including the rupture and erosion. The stress applied to the nanomaterial differs dependently on the compound. The observation shows both mechanisms responsible for agglomerates formation when low screw speeds are applied, while rupture dominated at higher speeds. PC/MWCNT material was studied in order to determine the viscoelastic behavior dependence on the nanocomposite formation.^[102] The results collected on compression molded specimens clearly show the relation between the viscosity and the storage modulus. Besides, loss modulus shows similar behavior at lower strengths. Carbon nanotubes tend to cause the increase of

viscosity. Above 2.0 wt. % a large decrease of viscosity with frequency appears showing non-Newtonian behavior at low frequencies. Such rheological threshold is slightly higher than the electrical percolation threshold (between 1.0 wt. % and 2.0 wt. %). Besides, the higher viscosity values than in material based on nanofibers or on carbon black can be explained as a dependence on the high aspect ratio of carbon nanotubes. An interesting comprehensive research results are published by Youn *et al.*^[50] showing the influence of filler geometry on the selected properties of PC nanocomposites. Composites are formed by melt mixing with various fillers: carbon black, graphite nanofibers and carbon nanotubes. Percolation threshold is observed in the latter case between 1.0 wt. % and 3.0 wt. %. The final conductivity is reported as 10^{-3} Sm^{-1} . Carbon black/polycarbonate and graphite nanofibers/polycarbonate showed Newtonian behavior, just like the pure PC matrix. This is similar to the nanocomposite reported by Pötschke *et al.*^[83] with MWCNT load below 2.0 wt. %.

Better carbon nanotubes dispersion is achieved in compression molding than in injection molding.^[53] TEM micrographs of the layers cut with the different distance from the specimen edges provide the image of skin effect in injected samples. Samples with rather high resistivity show the best nanotubes alignment. Spatial statistics are estimated for PC/MWCNT nanocomposite and the parameters are ordered with the following order of importance: MWCNT content (first order parameter), dispersion together with the distribution and alignment (second order parameter). The incorporation of additional elements into the structure results with more variables. More materials are investigated, including: polystyrene/MWCNT,^[63] poly(styrene-co-acrylonitrile)/MWCNT (SAN/MWCNT)^[109] and finally to terpolymer-based nanocomposite poly(styrene-co-acrylonitrile-co-butadiene)/MWCNT (ABS/MWCNT).^[8,72-73,75] This brings the investigation to

the desired point: PC/ABS-MWCNT nanocomposite^[4,5] and PC/ABS as a final material.^[74,150]

Orientation of nanotubes in skin layer was found in samples processed with high injection speeds and reduced temperature, while the opposite sequence of parameters gave no alignment.^[60] Holding pressure and mold temperature seems to have little influence on the final properties while melt temperature is an important factor. Carbon nanotubes orientation in the final nanocomposite and agglomeration effect appearing during injection molding has been investigated with rheology tests showing the indication of nanofiller alignment sensitivity to the high shear conditions.^[103] Visco-elastic properties of matrix in presence of nanofiller network is strongly related to CNT re-agglomeration process. Further process modifications reported by Li *et al.* showed the polypropylene-MWCNT reinforced with polycarbonate micro-fibrils and the relation between dynamic sample production.^[101] Shear controlled orientation injection molding has been compared with the conventional process. The dynamic samples show clear improvement over the conventional ones, indicating also carbon nanotubes located in the micro-fibrils and aligned along their long axes.

- *MWCNT functionalization for polymer nanocomposites*

Grafting polymer chains to the nanostructures makes the whole system miscible in proper matrixes and improves the viscoelastic behavior as well as mechanical properties. Although there are significant benefits from such a treatment, the decrease of electrical properties occurs in covalent modifications due to the fact of interrupting in π -networks on the single nanotubes.^[106] Macromolecules have great spatial hindrance and reduced chemical reactivity – both facts are the disadvantage in *grafting-to* method based on formation of only small number of covalent bonds in the process. Pre-synthesized oligomers or polymers terminated with the functional group

are connected to the oxidized carbon nanotube by carboxylic groups. Diffusion of the consecutive macromolecules after first part of the functionalization process is hampered by the already attached chains which causes rather low grafting density in this method. Other limitation is a necessity of terminating polymers with an appropriate functional group ready to react with an active center on MWCNT surface. The last argument is difficult to avoid because of the chemistry of carbon nanotubes and conditions of the functionalization process often carried out with condensation mechanism. Radical mechanism, nucleophilic coupling and nucleophilic addition mechanisms are also investigated, but the efficiency in the former one is highest. The possibility of using commercial macromolecules with well-known weight distribution is beneficial for the industry. Examples of amine-terminated polymers are present in the literature already.^[106] Improvement of *grafting-to* method was made to increase reactivity of side groups. *Grafting-from* is the result of this work with an advantage of controllable and designable process. Method is based on growing polymer chains from the active centers on carbon nanotubes surface by surface-initiated polymerization, which is a one-pot reaction with surface-oxidized MWCNT as a starting material. Obtaining great molecular weights (MW) of carbon nanotube side chains is not limited by the diffusion problems as the molecules in motion are no longer macromolecules. High density grafting is reachable much easier because the equal growth of terminal nanotube substituent and equal level of accessibility to the active centers (for monomers) in every moment of the process are provided. Various methods are used to carry out such functionalization, with the use of main types polymerizations including ionic,^[110-112] redox^[113] and metallocene catalysis^[114-115] as well as electrochemical grafting^[116] used widely *e.g.* in liquid crystalline polymers engineering. Other, more sophisticated methods of grafting polymers on MWCNT are being

investigated: atom transfer radical polymerization (ATRP),^[117-118] reversible addition-fragmentation transfer (RAFT),^[119-120] ring opening polymerization (ROP).^[121-122] The solution of some synthetic problems may be application of mixed mechanism. The reactivity of carbon nanotubes is sensitive to the curvature and surface defects density.^[123] Application of wet chemical oxidants,

e.g. acids and mixtures or peroxides and ozone gives conclusion of the sensitivity of product creation on the type of oxidant over the reaction conditions. Less aggressive chemicals (H_2O_2 , $(\text{NH}_4)_2\text{S}_2\text{O}_8$) gave greater number of hydroxyl and carbonyl groups, while the aggressive oxidants (*e.g.* HNO_3 , KMnO_4) result with the high fractional concentrations of carboxyl groups. Kim *et al.* report the amidation, esterification, thiolation and silanization as the most common ways of carbon nanotube surface modification.^[124]

The other possibility of functionalization is the physical absorption of π -conjugated polymers or polymer chains with heteroatoms in the structure on MWCNT surface. Clearly weaker interactions can be obtained with wrapping chains around the nanotube. Besides, the influence on mechanical properties of pure nanostructure is remarkably lower with an advantage of almost unchanged π -network. This is related to the charge mobility retained on high level.^[106] Such an option is often utilized when MWCNT are modified with the surfactants and no chemical bonding occurs.

2.2.2.2. Mechanical properties of MWCNT nanocomposites

Multi walled carbon nanotubes, due to their size comparable with the size of polymer chains and related interactions provide improvement of mechanical properties. An example increase of Young modulus is observed for PA6/ABS blend and for Nylon 6 with 7.5 wt. % and 2.0 wt. % MWCNT, respectively. The final result is 1.24 MPa for PA6 and very similar improvement observed

for the blend. This is 153 % of the pristine matrix and cannot be compared with any other filler.^[27] Poor dispersion of carbon nanotubes in polymer matrix is usually directly influencing the main mechanical properties. The decrease of mechanical stability is caused by the formation of agglomerates.^[51,106,125] Due to this, stress is distributed in nanocomposite not in a regular manner. The usual distribution through the individually dispersed carbon nanotubes is changed to the partial distribution through the agglomerates acting as macrofillers. Furthermore, the higher the distance between individual nanotubes the more stress is transferred to the matrix. This can be checked with a relatively high accuracy by Raman spectroscopy. Band near 1550-1600 cm^{-1} varies if the nanotubes are under tension.^[126] Mechanism responsible for mechanical reinforcement is limited after reaching the maximum strength value for the nanocomposite with the debonding of the matrix-filler surface. The value of interfacial stress share (IFSS) responsible for this effect is reported below 100 MPa for common commercial polymers. This value is improved after the incorporation of MWCNT.^[77,127]

Fortunately, from the economical point of view, MWCNT are giving the highest improvement of mechanical properties, although the stress strength exhibits lower values than it is expected from computational studies.^[35,61,71]

2.2.2.3. Electrical properties of MWCNT nanocomposites

Great majority of many outstanding carbon nanotube properties, able to carry the immense current 100 MA/cm^2 , is related in some way to electronic properties. Electrical conductivity of one-dimensional structures like carbon nanotubes occur over the tube lengths enabling them to carry high voltages without any significant energy wastes, *e.g.* in the form of heat emission. The change from the semi conductive to metallic character of carbon nanotubes depends on chirality of the hexagon cylinders.^[52] Electrons, as

well as phonons, can be easily transported through the single nanotube^[12] which explains potential application in optoelectronic technology. Electrical conductivity, next to mechanical properties is one of the most significant characteristic of polymer-carbon nanotubes nanocomposites. Early report of the charge mobility improvement in such materials was investigated on the substituted polyvinylene (PmPV). The lowest measured conductivity was reported to be 10^4 Sm^{-1} in PMMA with SWCNT treated with SOCl_2 .^[128] Such huge matrix electrical conductivity improvement of hundreds orders of magnitude shows an enormous importance of these nanocomposites in industry. Possible applications like optoelectronic memory devices with charge storages in nanotube composite transducers^[22] can be significant in the future. Network formation from the not entangled carbon nanotubes provides good charge-path system dispersed in the matrix.

Percolation threshold (Figure 2.1.7) tends to be the most often mentioned property in the related literature.^[8,45,50,56,77,83,93,129] This parameter is a mathematical term describing the randomly formed network and probability of interconnection between particles. Lattices of filler in matrix are theoretically forming ordered or random pattern described mathematically. Fillers of various shapes are defined in systems, *e.g.* discs oriented in the three-dimensional space making a fine model for graphene dispersions.^[130] The value of percolation threshold changes with many factors. Carbon nanotubes percolation is sensitive to the wall-multiplicity and the purity. Besides, eventual functionalization or further processing methods show some influence. The most efficient mass load of carbon nanotubes in the composite given by Bauhofer *et al.* on the electrical behavior of MWCNT-filled nanocomposites is 0.2 wt. % for nearly every MWCNT system in the single-phase matrix.^[128] This value is based on an average load described in a large number of related articles. Nevertheless, there is a deviation from this value for epoxy composites, due to the different matrix character and

the higher possibility of self-creating network exhibiting kinetic percolation.^[43,131-133] However, kinetic percolation is mainly investigated in the polymerization systems with the respect to monomer concentration and is rather absent in industrial approaches.^[131]

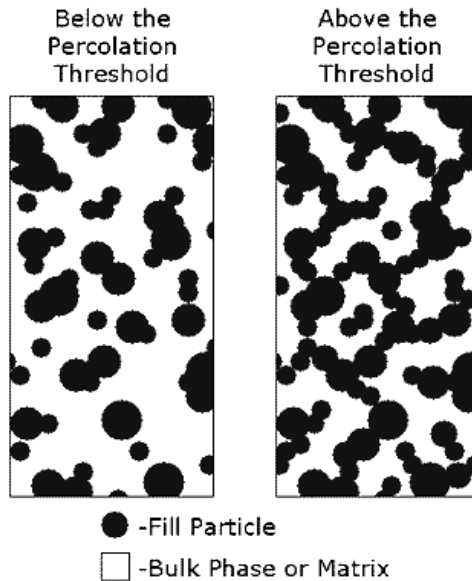


Figure 2.3.7: percolation threshold scheme – material filled with particles differing in size.^[134]

In general, thermosets differ in properties from thermoplastic composites, also in relation between the filler concentration and its alignment, melt rheology and the conductivity of the final specimen. Percolation threshold in the former materials is situated above the rheological threshold, which is opposite to the thermoplastic nanocomposites.

Two main often measured parameters of electrical properties in carbon nanotube-filled nanocomposites are surface and volumetric conductivities. The former one is more dependent on the filler load showing the decrease

of increasing MWCNT load for compression molded specimens, just until reaching the point of the network formation.^[74] However, after the percolation threshold the decrease of the influence on surface conductivity appears. For more complex system of injection molded samples, this parameter is greater in the same nanotubes load. Conductivity measured in-line in injection molding machine on PC matrix with MWCNT, showed the greater dependence on throughput and temperature than on the other parameters. Up to 7 orders of magnitude differences were observed with just a slight variation of these factors.^[74] Shear or elongation stress can also break the alignment of nanofiller network resulting in the conductivity drop. Furthermore, electrical conductivity recovery was observed during the rheology testing. After the shear forces were stopped, carbon nanotubes network is rebuilt. Alig *et al.*^[74] reported a bunch of inline and offline experiments with conductivity measurements carried out directly in the melt near the screws or outside the machine, respectively. These experiments on the injection molding machine or extruder gave the image of how the conductivity of polymer-MWCNT nanocomposite is influenced by shear. Few factors were reported to have higher significance. Vitrification for amorphous polymers or crystallization for semi-crystalline ones and the reorganization of MWCNT network are mentioned. Besides, mold and melt temperatures influence the conductivity of the specimen as well. However, the former parameter is clearly more significant^[60] The best conductivity values are obtained at rather high melt temperature but low injection velocity. The temperature decrease in the mold during the lateral steps of the injection cycle seems to play an important role, too.^[52] Uneven cooling causes the differences in conductivity between two opposite specimen edges. Mold wall that has higher temperature promotes particle migration and reorganization due to decreased viscosity. Furthermore, some semi-crystalline materials after the temperature treatment above the T_g show the affection

of crystallization behavior.^[135] In that case also toughness characteristics are changed due to the heat exchange modifications. Opposite theory says that slow cooling would promote crystallization and further change of the filler alignment.

PC is a plastic with a possibility of great prospective electronic application. This is due to the relatively good control of the nanofiller dispersion. An example of such study is a formation of MWCNT conductive layers in polycarbonate substrate, which can be used in antistatic application.^[136] In-line measurements show the possibility of conductive network re-creation in PC melt with 0.5 wt. %, 0.875 wt. % and 2.0 wt. % of MWCNT.^[95] Experiment set up was based on a slit dye in the outlet of a twin-screw extruder equipped with pressure, temperature and electric sensors. After stopping the extrusion and keeping the parameters constant the conductivity of the material increased. Such recovery of electrical conductivity is similar to the results of the experiment carried out on PA6. This can be understood as a minor dependence of the sample crystallinity on the studied effect. Conductivity of polycarbonate measured in shaped samples was done by Alig *et al.*^[56] on material with the nanofiller concentration between 0.5 wt. % and 5.0 wt. % prepared by melt mixing with 15 wt. % masterbatch dilution method. Percolation threshold occurs between 1.0 wt. % and 1.5 wt. %. The experiment was done in internal mixer with 5 minutes of resident time in extruder. The standard industrial machines with higher screw speed provide the resident time not longer than 90 seconds. This publication is based on dielectric spectroscopy used for nanocomposites morphology evaluation.

Further processing after nanocomposite creation is based on injection molding, as it is stated above. Villmow *et al.* shows the dependence of polycarbonate filled with 2.0 wt. % and 5.0 wt. % MWCNT on processing parameters during injection molding.^[60] Holding pressure, injection speed

and temperatures of melt and mold were studied as factors determining surface and volume electrical conductivity of the final material. These parameters should be chosen respecting the nanotubes content in the material. Besides, obvious presence of skin effect mentioned elsewhere as a principal of this processing method is also reported.

Chandra *et al.* reported varying electrical resistivity across the length and the width of injected PC specimen independently of process parameters^[137] Electrical conductivity was higher in regions farthest from the injection gate and in the central part of the sample. The crystallization behavior of the matrix has been proved to be influenced by CNT presence in polypropylene.^[65]

2.2.3. Prediction of properties of MWCNT nanocomposites

Experimental investigation of carbon nanotubes-based nanocomposites can be supported by the computational methods of mathematical modelling. There are suitable mathematical theories showing MWCNT behavior at various conditions as well as describing carbon nanotube-polymer composites.^[138] However, due to the relatively new topic, nanocomposites are still not very well defined regarding the interactions between polymer chains and *e.g.* nanotubes. Two examples of mathematical models were compared Coleman *et al.*: *Halpin-Tsai* and *Rule of Mixtures*.^[27] Both methods give values of the calculation results precise enough to estimate the influence of nanofiller load in the final material. The purpose of this estimation is an evaluation of the mechanical properties increase. However, there are some negative aspects in these methodologies. *Halpin-Tsai* method^[139] has a disadvantage of underestimating the stiffness in high volume fractions, avoided in the second model. The *Rule of Mixtures* describes the composite with fillers as an elastic, isotropic matrix of well aligned, elastic fibers spanning on all the length of the specimen. Such an

inaccuracy of an idealized model contradicts with the actual situation, where the nanotubes are individually separated and fully covered by the polymer. Improvements of this method allowed introducing the *Cox factor* indicating the stress-transfer between carbon nanotubes and polymer matrix. Due to the huge difference between the specimen length and individual filler particles dimensions. Finally, the stress is controlled by matrix and nanostructures, not always as well dispersed and aligned as it was mentioned in the former model.^[27] Besides, the estimated properties in the *Rule of Mixtures* are a volume-weighted average of matrix and filler. Commonly estimated shear and elastic modulus are supplemented by density, tensile values and Poisson's ratio. *Halpin-Tsai* equations based on elastic calculations tend to be more exact, although good agreement with experimental data is reached mainly for semi-crystalline plastics. The geometry of filler plays an important role, as well as the entire packing geometry, defined as a sphere, a fiber or an intermediate.^[139] Numerical tools are often used together with experimental methods in order to evaluate the actual state of material.^[140] However, mathematical tools can play an important role in the final material design on many stages of this process, including experiment design and understanding of the results. Furthermore, mathematical model is developed at the initial stage of nanocomposite formation in order to provide good control over all parameters. It causes difficulties with the randomly selected parameters, though. Apart from the mentioned basic factors, more mutually related parameters exist. The structure parameters are usually being calculated along with the dispersion control correlated with the morphology and the phase size distribution in the final material. This part follows the selection of process (throughput, temperatures and screw speed) and extruder parameters (L/D, screw profile). The final step of calculations after the verification of structure parameters is based on selection of target

parameters. This is done on the base of designed product properties with an appropriate mechanical and morphological characteristic of the final composite.

The Tucker-Folgar mathematical model^[141] is a common method used to predict the behavior of macro-scale fibers in injection molded materials.^[142] Folgar and Tucker reported the asymmetrical behavior of the orientation curves of filler under a simple shear flow.^[141] This method is a derivative of the Fokker-Planck method^[143] modified by decreasing the number of numerical solutions. The necessity of such extended calculations the disable application of Fokker-Planck model to solve large scale industrial problems. Characteristics of such flow allow building the relatively precise mathematical model of the fiber-like filler alignment and orientation. Jeffery orbits effect^[144] is one of the key behaviors defined in this case. Fibers aligned in an oriented flow slow down its rotation, while when the orientation of the particle is perpendicular to the flow, rotation increases again. Following Londono, the decrease of the fiber ratio increases the time it spends aligned with the flow and decreases the time it spends in rotation.^[146] Anisotropic rotary diffusion was added to Jeffery-type model in order to improve definition of the fiber behavior.^[146] This caused better fitting between the experimental data and the calculations, comparing to the isotropic Folgar-Tucker model. Another issue is related to the definition of the fiber itself. Commonly it is solved by regarding the individual fiber as made up of lined up spheres.^[147-148] Each element of such system can independently bend or stretch showing high flexibility. Yamamoto and Matsuoka report also dependence on the fibers rigidity on the melt viscosity.^[149] This is because of the change from the orientation in the flow direction to the planar orientation of rigid fibers. Nevertheless, the majority of mathematical calculations are related to the macro-scale systems with

fillers defined as similar to *e.g.* glass fibers. Such models cannot be adapted for nanocomposites freely because the interactions between individual nanofiller particles and polymer chains are significantly higher than in the aforementioned systems.

2.2.4. MWCNT nanocomposites of multiphase blends

Polymer blends provide technological solutions due to the combination of parameters of the components. Usually, the formation of multi-phase blends are a compromise that need to made in order to develop the material. Miscible blends are a desired solution, but with moderate compatibility of components, like in polycarbonate/acrylonitrile-butadiene-styrene (PC/ABS) material, homogeneous morphology cannot be obtained.

Formation of high impact polystyrene (HIPS) nanocomposite with multi-walled carbon nanotubes is investigated by McNally *et al.* with the special influence of screw speed on electrical properties.^[63] The desired parameter is improved 12 orders of magnitude regarding the pure matrix (resistivity varies between $10 \cdot e^4$ and $10 \cdot e^{16}$). Besides, the best dispersion is achieved with an intermediate screw speed rather than with the high value of this parameter. The authors claim that short resident time (caused by elevated screw speeds) promotes the formation of agglomerates. The G-band in Raman spectra characterizing MWCNT is shifted *c.a.* 24 cm^{-1} , which is explained by the authors as a strong interaction between the two materials. For more complex matrices, *e.g.* blends, double percolation has to be considered as a parameter influencing final properties. Related research is done on polyamide 6 (PA6) with MWCNT melt-mixed with ABS.^[8,75] Friedrich *et al.* observed that the nanofiller, at first located in PA6 matrix, after extrusion still shows the preference to stay in this material rather than in ABS.^[75] Low filler loads (2.0 to 3.0 wt. %) give electrical conductivity onset due to the confinement of the conductive filler which is related to double

percolation. Comparing these results to the previous reported in this paper, PA6 showed better electrical conductivity improvement when is researched as mono-phase material than in co-continuous blend. However, it is also reported that the incorporation of carbon nanotubes into polymer matrices generally gives an improvement of electrical conductivity and in the same time slightly reduce the mechanical properties. Nevertheless, this reduction is smaller than in case of carbon black or other similar fillers often compared to MWCNT. ABS with various carbon nanotubes content tends to host nanofiller in SAN rather than in polybutadiene, which is confirmed by broadened T_g peak of SAN measured by mechanical spectroscopy.^[73] Mechanical properties and sound insulating properties as a function of CB content is reported as well.^[72]

The number of publications regarding an industrial blend PC/ABS-MWCNT nanocomposite rapidly decreases to only few from the significant number of over 650 published in 2013. Despite the research groups working on this matrix,^[150] the importance of this work is still minor at the moment. Older research on this material and on the derivative: maleic anhydride grafted to ABS and further composed to PC/MABS, is based on rheology.^[4] The deviation from the rule of mixtures between the composition containing between 25 and 65 wt. % of polycarbonate gives an idea of material behavior also respecting greater deviation for neat ABS over the modified ABS. In general, after blending the processability of PC is improved with the reduction of melt viscosity. More recent publication finally shows the incorporation of MWCNT into PC/ABS.^[5] PC usually hosts the nanotubes, but this can be slightly controlled with the change of rubber content in ABS. This effect is explained by the kinetic and thermodynamic relations. The influence of MWCNT localization on electrical conductivity is shown as well. Conductivity increase is surprisingly reported in the material with MWCNT located in ABS that is dispersed in PC. Besides, the wetting test of carbon

nanotubes gives important information. PC/PB-MWCNT nanocomposite shows most of the nanofiller in polybutadiene phase while for PC/SAN-MWCNT the majority of nanotubes is in polycarbonate.

Pötschke *et al.*^[102] investigated PC-MWCNT and PC/PP-MWCNT nanocomposites aiming to decrease the filler content and study the double percolation threshold phenomenon. The experiment of combining two immiscible plastics gives the co-continuous blend with PC/CNT load of 30 wt. % to 80 wt. %. Carbon nanotubes content of 0.4 wt. % improved electrical conductivity. Volume resistivity of the samples ranges between $10^{15} \Omega\text{cm}^{-1}$ before blending and 10^6 to $10^7 \Omega\text{cm}^{-1}$ after the processing. Nanotubes are present in both matrices after extrusion which is confirmed by the selective PC extraction and following by the SEM investigation.

Miscible- and multiphase polymer blends create over 36% of polymer production industry.^[1] Development of nanocomposites based on such matrix filled with multi-walled carbon nanotubes (MWCNT) offer novel possibilities to produce materials with tailored properties. Both: miscible^[151] and immiscible^[5,152] blends exhibit desired performance characteristics after incorporation of MWCNT. PC/ABS blends filled with carbon nanotubes were studied by Xiong *et al.*^[152] and Sun *et al.*^[5] In both cases blends were prepared by researchers from the neat components and migration or controlled location of MWCNT was reported. Besides, affinity of carbon nanotubes to polycarbonate component at defined PC-to-ABS ratio was explained showing the challenge of achieving a uniform distribution of MWCNT in both components when commercial PC/ABS blends are used.

3. Materials and experimental methods

3.1. Materials

3.1.1. PC/ABS blend

Matrix used in this study was an amorphous thermoplastic, commercially available polymer blend of polycarbonate (PC) with acrylonitrile-butadiene-styrene copolymer (ABS) supplied by Bayer MaterialScience AG (Germany) as Bayblend® T85. Selected data of the material is showed in Table 3.1.1.

Table 3.1.1: Selected properties of PC/ABS blend.

Property ⁽¹⁾	Unit	Bayblend® T85
PC content	wt. %	85
ABS content	wt. %	15
Density	kg/m ³	1150
Melt volume-flow rate	cm ³ /10 min	12
Melt viscosity (260 °C)	Pa·s	290
Tensile modulus	MPa	2300
Izod impact strength	kJ/m ²	50
Vicat softening temperature (50N, 50	°C	129/131
Flammability (UL 94)	Class	HB
Volume electrical resistivity	Ohm·m	1E14
Surface electrical resistivity	Ohm	1E16
Water absorption (at 23 °C)	%	0.7

⁽¹⁾Data supplied by producer

3.1.2. Multi-walled carbon nanotubes (MWCNT)

Two types of carbon nanotubes were used in this study. Commercially available multi-wall carbon nanotubes (MWCNT) supplied as NC7000 by Nanocyl (Belgium) of 90% purity were used as non-modified nanofiller. Surface-oxidized multi-wall carbon nanotubes (MWCNT-COOH) supplied by CheapTubes Inc. (USA) with 95% purity were used as modified nanofiller. Both materials were produced by catalytic carbon vapor deposition (CCVD) method. Parameters of the materials are presented in Table 3.1.2.

Table 3.1.2: Comparison of MWCNT and MWCNT-COOH properties.

Property	Unit	MWCNT (Nanocyl)	MWCNT- COOH
Purity	%	90 ⁽¹⁾	95 ⁽¹⁾
Average length	µm	1.5 ⁽¹⁾	[0.7 ± 0.1] ⁽²⁾
Average diameter	nm	9.5 ⁽¹⁾	[10.4 ± 0.3] ⁽²⁾
Average aspect ratio		160	[70 ± 10] ⁽²⁾
Surface area (BET)	m ² /g	250-300 ⁽¹⁾	[15 ± 4] ⁽²⁾
Density	g/cm ³		[1.85 ± 0.02] ⁽²⁾
Bulk density	g/cm ³		2.1 ⁽¹⁾
			0.15 ⁽¹⁾

⁽¹⁾ Data supplied by producers; ⁽²⁾ Data from literature^[54]

3.1.3. Surfactant

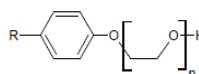
A non-ionic surfactant, *Triton® X-100* (octylphenol ethoxylate) was selected after comparison with other commercial surfactants (e.g. *Tergitol®*, polyglycol ether) from Sigma Aldrich. The surface tension of Triton X-100 is higher than ethyl alcohol (below 24 dynes cm⁻¹). The foaming index of Triton X-100, related to the effectiveness of surfactant, is higher than in the other surfactants considered for this study. The values of Triton X-100 are

shown in Table 3.1.3. Surfactant was used without additional treatment or purification.

Table 3.1.3: Properties of Triton ® X-100.

Property ⁽¹⁾	Triton X-100
Surfactant character	non-ionic
Reaction ⁽²⁾ [pH]	6.0
Density ⁽³⁾ [g mL ⁻¹]	1.061
Viscosity ⁽³⁾ [Pas]	0.240
Surface tension ⁽³⁾ [dynes cm ⁻¹]	33
Foam height: 0min/5min ⁽⁴⁾ [mm]	128/107

Molecular structure



⁽¹⁾ Data supplied by manufacturer; ⁽²⁾ 5% aq. solution; ⁽³⁾ At 25 °C; ⁽⁴⁾ According to Ross-Miles foaming test, 0.1 wt.%

3.2. Melt processing conditions

3.2.1. Instruments

Nanocomposites were prepared by melt compounding on a Prism Eurolab 16 (Thermo Fisher Scientific) twin-screw co-rotating laboratory extruder with barrel diameter 16 mm and barrel length L/D 25. Throughput during all experiments was set to 1 kgh⁻¹. Screw speed was adjusted between 100 and 600 rpm, dependently on the design of the experiment. Barrels temperature was maintained between 220 °C and 280 °C, following the recommended conditions of matrix supplier. No temperature profile was applied.

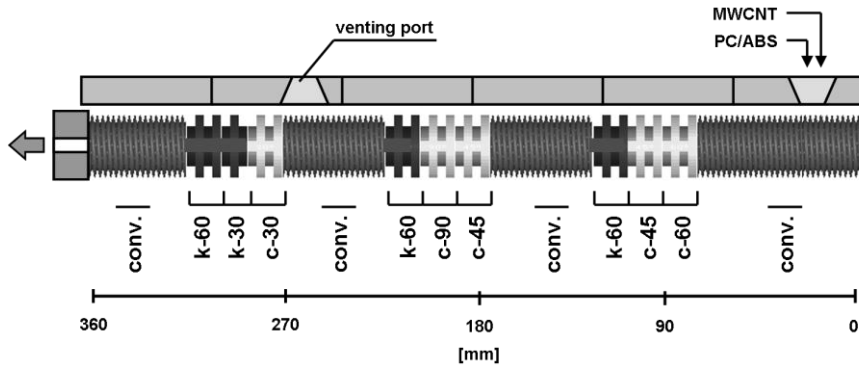


Figure 3.1.1: Screw design for PC/ABS-MWCNT melt compounding; conv. – conveying transport zones c-30, -45, -60, -90 – kneading conveying zones with elements twisted 30°, 45°, 60° or 90°; k-60 – kneading reverse zone with elements twisted 60°.

PC/ABS was kept in a Conair dehumidifying hopper drier for 4 hours at 100 °C before the experiments to avoid degradation (hydrolysis) during processing.

All experiments were conducted using the screw profile showed in Figure 3.1.1, which was designed using Ludovic software package (Sciences Computers Consultants). Temperature and energy distribution along the screw was calculated using parameters from the AIMPLAS experimental database. Most significant energy applied to the material (based on calculation for masterbatch formation) during melt mixing was the dissipated energy coming from the screw (41 %) and the combined conduction energy coming from the screw and nozzle (47 %). The mean residence time for the material in the machine was 52.6 seconds ranging from 42 seconds to 56 seconds.

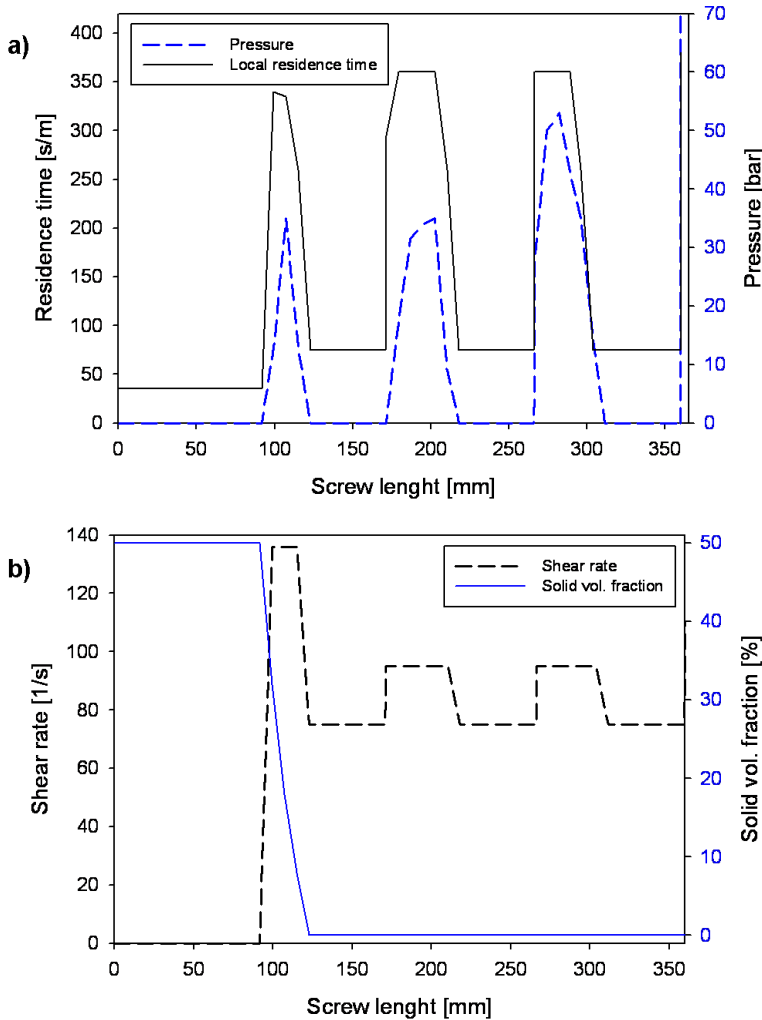


Figure 3.1.2: Selected parameters calculated for melt compounding of PC/ABS-MWCNT nanocomposites: a) residence time and pressure during processing versus screw length, b) shear rate and solid volume fraction versus screw length.

Figure 3.1.2 shows selected parameters depending on the position of the screw and kneading zones. According to Figure 3.2a the time in which the material passes the screw zones is significantly higher for kneading areas.

Moreover, pressure increases in these zones and an increased number of reverse kneading elements is present for both effects. Sudden increase of the shear rate presented in Figure 3.1.2b is related to the solid volume fraction. The remaining half of the total amount of polymeric matrix is melted when the material reaches first kneading zone. The presence of not melted polymer causes an increase in shear rate at around 100 mm distance from the feeding gate. The other two high-shear zones are related to the kneading elements.

3.2.2. Nanocomposite processing routes

Three main nanocomposite formation methods have been demonstrated in this work resulting in varied carbon nanotubes dispersion qualities in the PC/ABS matrix. Multi-walled carbon nanotubes, modified or non-modified, were used to form nanocomposites with concentrations between 0.5 wt. % and 5.0 wt. %. Nanofiller was fed to the machine in the form of powder, as a masterbatch or as a suspension in ethyl alcohol.

3.2.2.1. Common nanofiller feeding method

Nanocomposites were obtained by addition of MWCNT in the form of powder together with the matrix pellets through the principal feeding gate of the extruder (Figure 3.2.1). Multi-walled carbon nanotubes were fed to the extruder with a pneumatic feeder Brabender Flex Wall. Materials with the final nanofiller concentration were obtained in this way at various temperatures and with various screw speeds (Table 3.2.1).

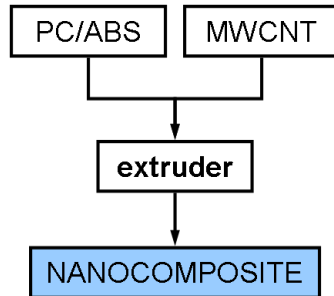


Figure 3.2.1: Scheme of Powder method.

Table 3.2.1: Samples obtained with Powder method.

Sample code	MWCNT	Screw speed	Barrels temperature
	concentration		
	[wt.%]	[rpm]	[°C]
P	1.0	200	280
	2.0	200 / 400	280
	3.0	100 / 200 / 400	280
	5.0	100 / 200 / 400 ⁽³⁾	280

⁽¹⁾ Masterbatch

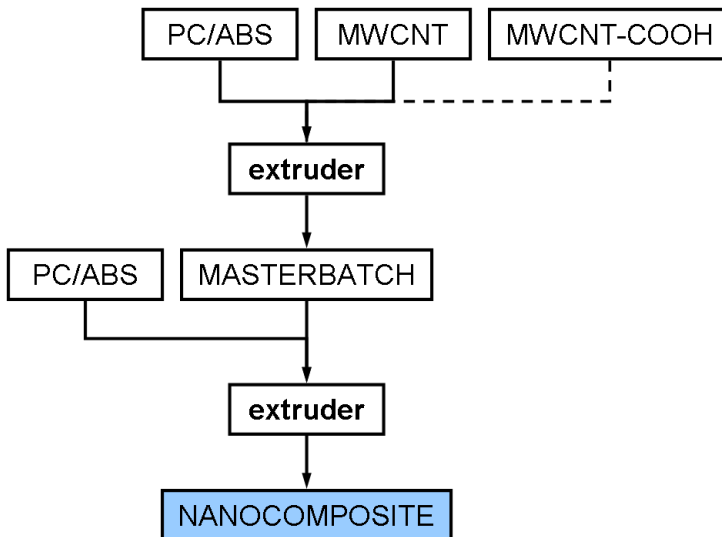
3.2.2.2. Masterbatch dilution method

Masterbatch with 5.0 wt. % MWCNT or MWCNT-COOH loading were prepared by the Powder method with screw speed of 400 rpm in both cases. Masterbatches were then diluted to the desired concentrations with various processing parameters (Table 3.2.2). Masterbatch pellets were fed together with the matrix pellets to the first feeding gate of the extruder. Figure 3.2.2 shows that the pre-dispersed masterbatch requires one more processing step comparing to the powder method.

Table 3.2.2: Samples obtained with Masterbatch method.

Sample code	MWCNT	Screw speed	Barrels
	concentration [wt.%]	[rpm]	temperature [°C]
MB ⁽¹⁾	0.5	400 / 600	260 / 280
	1.0	400 / 600	260 / 280
	1.5	400 / 600	260 / 280
	2.0	400 / 600	260 / 280
	2.5	400 / 600	260 / 280
	3.0	400 / 600	260 / 280
MB-COOH ⁽²⁾	0.5	400 / 600	260 / 280
	1.0	400 / 600	260 / 280
	1.5	400 / 600	260 / 280
	2.0	400 / 600	260 / 280
	3.0	400 / 600	260 / 280

⁽¹⁾ Nanocomposite with MWCNT; ⁽²⁾ Nanocomposite with MWCNT-COOH

**Figure 3.2.2:** Scheme of Masterbatch method.

3.2.2.3. Suspension method

A scheme of the suspension method is presented in Figure 3.2.3. A suspension of multi-walled carbon nanotubes in absolute ethyl alcohol (4 g/100 ml) was prepared by sonicating a stirring mixture with a Bandelin UV 2200 ultrasound probe for 5 minutes (20 W power). The suspension was fed by a Masterflex peristaltic pump, together with the pellets of PC/ABS blend, into the first feeding gate of the extruder. A vacuum was applied to the final extruder barrel to remove any residual alcohol from the final material, although, theoretically the solvent should evaporate immediately in the feeding region (ethanol boiling point: 78.5 °C). Nanocomposites of various concentrations were prepared (Table 3.2.3).

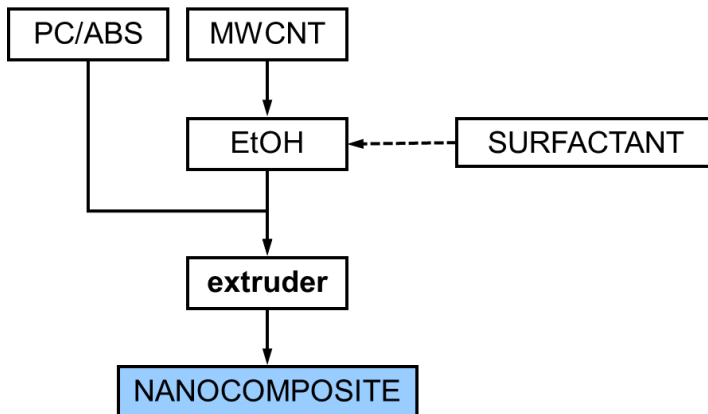


Figure 3.2.3: Scheme of suspension method.

Additionally non-covalent modification of carbon nanotubes with surfactant was carried out within using this feeding method. Triton® X-100 was added to the suspension of MWCNT in ethyl alcohol before being fed into the reactor using slightly modified processing parameters.

Table 3.2.3: *Samples obtained with Suspension method.*

Sample code	Additive	MWCNT	Screw	Barrels
		concentration [wt.%]	speed [rpm]	temperature [°C]
S ⁽¹⁾	-	1.0	400/600	220/240/260/280
	-	1.5	400/600	220/240/260/280
	-	2.0	400/600	220/240/260/280
	-	3.0	400/600	220/240/260/280
S-Triton ⁽²⁾	S1	0.5	400/600	240/260
	S1	1.0	400/600	240/260
	S1	1.5	400/600	240/260
	S1	2.0	400/600	240/260
	S1	3.0	400/600	240/260



⁽¹⁾ Nanocomposite with no additives; ⁽²⁾ Nanocomposite with Triton X-100;

3.3. Sample preparation

Rectangular and dog-bone shaped specimens prepared according to EN ISO 527-3 were characterized (Table 3.3.1). Rectangular specimens tested for morphology, thermal-, mechanical-, electrical properties and flammability. Dog-bone specimens were tested for morphology and mechanical properties only.

All nanocomposites were dried under vacuum at 110 °C for 4 hours before processing.

Table 3.3.1: Dimensions of PC/ABS-MWCNT samples.

Property	Rectangular	Dog-bone specimen
Shape		
Overall length	60.0 ± 0.2	115.0 ± 0.5
Gauge length	-	35.0 ± 0.1
Overall width	10.0 ± 0.2	19.0 ± 0.1
Gauge width [mm]	-	6.0 ± 0.1
Thickness [mm]	2.0 ± 0.1	4.0 ± 0.1

3.3.1. Compression molding

Compression molding was carried out at 260 °C for the lower and upper plates on a Collin 6300 press. The five-step, 30 minutes-long program includes an increasing pressure gradient between the steps 1 and 4 finished with the mold cooling to 80 °C. Program details are showed in Table 3.3.2.

Table 3.3.2: Compression molding program details.

Step	Time [sec.]	Pressure [bar]
1 st	240	2
2 nd	180	60
3 rd	180	120
4 th	300	210
5 th	900	70

Additionally, discs with 30 μm thickness were compressed from pellets in order to investigate morphology of nanocomposites by light transmission microscopy. The compression was carried out using a Specac hydraulic press

at 260 °C with aluminum discs separating press surface and the nanocomposite.

3.4. Samples characterization

All samples obtained by melt mixing were extensively characterized in the form of pellets or compressed bars with the most attended: morphology and electrical properties which are in the main interest of this work. These results were complimented with thermal, mechanical and rheological properties determination, and flammability testing. The effect of varying the processing parameters of the sample preparation on the final properties of the product could be determined using the further methods.

3.4.1. Analyses of morphology

3.4.1.1. Light Transmission Microscopy (OM)

Theoretical background

Optical microscopy is a useful characterization method that, depending on the experimental set-up, can provide various information of material characterization. The changes include, *e.g.* technique of illumination (light transmission or -reflecting microscopy), contrast mode (conventional bright field- or polarized light microscopy) or lens configuration (single lens- or compound microscopy). A typical microscope contains a light source, condenser lens, objective lens and projection (ocular) lens.

Light-transmission microscopy bases on the interaction between light and sample, and refraction of this light by the set of lenses. Figure 3.4.1a shows the scheme of light path between the source and the image plane. Poor contrast occurs when there is insufficient light in the projection plane. This can be reduced by application of Köhler illumination which involved the defocusing of the light source Following the research needs, multiple-lens microscopes are currently used, where double magnification occurs: by

objective lens and by ocular. This system allows separating light transmitted through (or reflected by) the sample between the objective and digital camera. In this case image is collected with improved numerical aperture NA and reduced chromatic aberration improving resolution d .

$$(3.1) \quad NA = n \sin \alpha$$

$$(3.2) \quad d = \frac{\lambda}{NA_{obj.} + NA_{condenser}}$$

Maximum obtainable magnification of 1500x relates to image resolution, limited by the wavelength of light (370-740 nm) and is a sum of objective and lens magnification. The concept of numerical aperture based on light-collecting ability (α – light reflection angle for medium) of the lenses introduces oil replacing air as medium surrounding optics (Equation 3.1). More favorable refractive index n of oil improves the final resolution (Equation 3.2). Another issue of transmission light microscopy is optical aberration, which relates to the complexity of white light. Wavelengths of light beam passing through the peripheral part of lens are not brought into the same point with the beam passing through its center, which causes chromatic or spherical aberrations. Most common solution for this problem is replacing one lens with the set of lenses with different curvature and made of various materials.

Methodology

The dispersion quality of the nanocomposites was studied on Leica DMRX light transmission microscope using the Leica Application Suite. Carbon nanotubes agglomeration was analyzed using the Leica Materials Workstation software. Samples were cut on a microtome to slices of 30-45 μm . The total possible area of at least three discs or slices of each

material was investigated and representative images in two magnifications were collected. Particle distribution, carried out for selected nanocomposites after melt mixing, was determined based on ten images taken in different discs of the same material. The limit of agglomerate detection for this test was $5\ \mu\text{m}$ due to ISO 18553 and to avoid errors of imperfections on the disc surface.

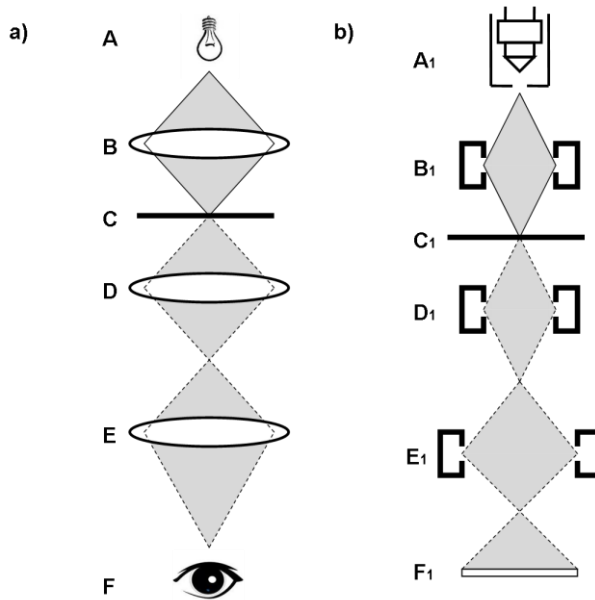


Figure 3.4.1: Scheme of a) light transmission microscope and b) transmission electron microscope; A – light source, A₁ – electron gun, B, B₁ – condenser lens, C, C₁ – specimen, D, D₁ – objective lens, E, E₁ – Projection lens, F, F₁ – image plane.

3.4.1.2 Scanning Electron Microscopy (SEM)

Theoretical background

The magnification limit of light-transmission microscopy allows observation objects with $1\ \mu\text{m}$ scale. Further magnification to nanometric scale requires employment of electron microscope (EM). In order to carry out EM, the

sample must be conductive which can be achieved by coating with conductive medium before measurement. Common materials to increase EM sample conductivity included gold, platinum or carbon which is by physical vapor deposition or sputtering.

Figure 3.4.2 shows a scheme of a scanning electron microscope and the source. An electron beam thermionically emitted from electron gun goes through the set of condenser lens and hits the sample under vacuum conditions. The Lorenz force controls the diameter of the beam and the strike point on the sample surface by electromagnetic lenses. Electrons after interaction with the specimen are collected giving information about near-surface region. In a whole range of reactions, *e.g.* back-scattered electrons or X-rays radiation, secondary electrons play the crucial role as a main mean of the final image.

$$(3.3) \quad \rho = \frac{0.6\lambda}{n \sin \alpha}$$

The resolution of the SEM experiment (Equation 3.3) depends on radiation wavelength, λ , and numerical aperture (Equation 3.1). The angle of reflection, α , is *c.a.* 70° in optical microscopy and below 1° for SEM which, together with the change other parameters, gives the difference in theoretical maximum resolution between $0.21 \mu\text{m}$ and *c.a.* 4 \AA , for optical and scanning electron microscopy respectively. Magnification in scanning electron microscope is controlled by reduction of area swept by electrons, changing the current in scanning coils.

A significant problem in electron based microscopy is the charging the sample by the electron beam. This causes distortions in the image and unwanted contrast increase. Preventing this phenomenon is usually done by

proper selection (reduction) of observation parameters: vacuum quality and accelerating voltage.

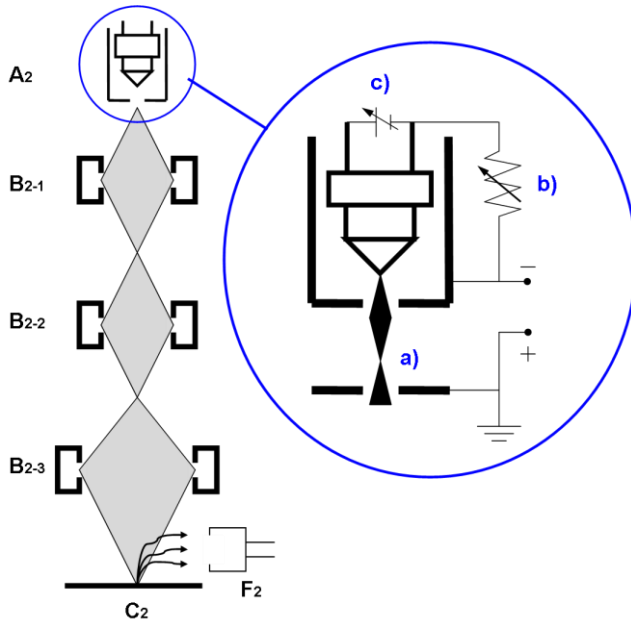


Figure 3.4.2: Scheme of scanning electron microscope and electron gun; A_2 – electron gun, B_{2-1} , B_{2-2} , B_{2-3} – condenser lens, C_2 – specimen, F_2 – signal detector, a) – cross-over, b) – bias resistor, c) – filament current supply.

Methodology

Nanocomposite samples were studied on JEOL 7001F scanning electron microscope with electron gun ranging between 0.1 kV and 30 kV. Samples were previously platinum-coated using sputtering device Baltec SCMCS010 and evaporator Fisons Polaron SC7650. Software used for images acquisition was INCA Wave 200. Images were collected with electron gun voltage 5.0 kV with magnification between 10^3 and 10^5 times.

3.4.1.3. Transmission Electron Microscopy (TEM)

Theoretical background

Transmission electron microscopy (Figure 3.4.1b), a derivative of the scanning electron microscopy, allows penetration and observation of internal structure of the sample. Instrument components include electron gun as a source and electromagnetic lenses used for controlling beam parameters, similarly to SEM. The sample is located between objective lens and condenser lens, on electron beam path so electrons pass through the sample returning an image on fluorescent screen.

The specimen for this test is a 1 μ m-thick slice cut from bigger piece with keeping the characteristics of the material. Thickness of the slice has to be controlled to avoid beam spreading inside the sample. Such piece is placed on copper grid which provides conductive contact.

TEM methods are susceptible to image distortions and artifacts. Conventional TEM (CTEM) is sensitive to aberration of objective lenses while scanning TEM (STEM) is sensitive to beam diameter.

Corrections of spherical and chromatic aberrations are present in both instrument types as well. Moreover, resolution limits related to this can be significantly changed, allowing determination of atom positions.

Methodology

Transmission electron microscopy images of nanocomposites were collected on JEOL JEM-1010 with electron gun at 100kV and a MegaView III digital camera. Samples were prepared on a copper grid (300 mesh) and coated with carbon film.

3.4.1.4. Raman spectroscopy

Theoretical background

Raman spectroscopy is a vibrational spectroscopic technique which provides information on specific functional groups and overall symmetry of the material. A basic Raman spectrometer contains an excitation source, *e.g.* laser, light collection optics, wavelength selector and detector.

The method observes the inelastic scattering of light after interaction with a sample. The resulting spectrum depends on the change of molecular polarizability. Absorbed light excites the molecule from the ground state to a higher-energy virtual state (Figure 3.4.3) which then undergoes relaxation and reemission of the photons at a different frequency. This shift contains information about low frequency transitions in the material (*e.g.* vibrational or rotational deformations)

There are three main possible outcomes of interactions between the sample and photon during Raman spectroscopy (Figure 3.4.3). The overwhelming majority is classified as elastic Rayleigh scattering, where the excited molecule returns to the same vibrational state and emits a photon with the same frequency as the incoming radiation. Elastic scattering does not give a signal in Raman spectroscopy. Stokes- and anti-Stokes frequencies occur when the incoming photon either gains or loses energy, respectively. The difference between these two incidents is related to the change of frequency between absorbed and emitted photons. For Stokes scattering no full relaxation is observed giving lower frequency of emitted photon (Figure 3.4.3). The anti-Stokes frequency is higher than the Rayleigh frequency due to the excitation of molecule being already on the other than the ground vibrational state. Relaxation occurs to the ground state causing higher emitted than absorbed energy.

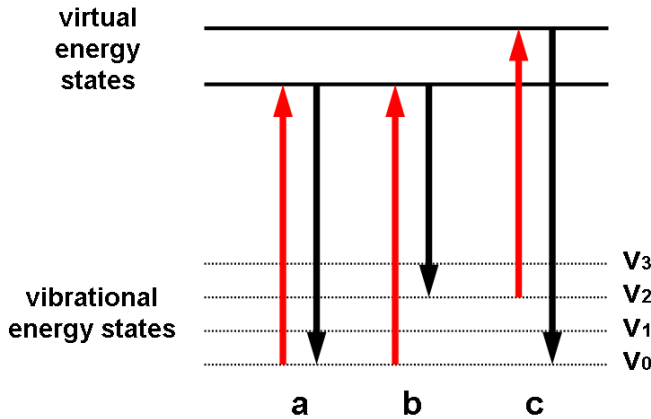


Figure 3.4.3: Diagram of energy states involved in Raman signal and scattering types: Rayleigh (a), Stokes (b) and anti-Stokes (c).

Methodology

Raman spectroscopy was carried out on a Horiba XploRA instrument with a Olympus BX41 light reflection microscope, LCS-S-11 laser source and an air-cooled CCD detector. Two wavelengths were used during measurements: 532 nm or 785 nm with radiation filters 300 μm (hole) and 50 μm (slit). Slices from the cross-section of rectangular sample were investigated. The experiment was divided in to two parts with principal spotted the region on the surface of the sample with microscope. Then the spectrum was collected with the laser beam hitting the selected point.

3.4.2. Thermal properties

In the study of thermoplastic polymers, temperature is an important consideration for processing and application. An increase in processing temperature can change the polymer viscosity, it's response to shear rate, ability to disperse fillers, increases degradation or influence final visual properties. In terms of material application, processing temperature is also

an important factor influencing polymer state at T_g which results with changes of mechanical properties of the final part.

3.4.2.1. Differential Scanning Calorimetry (DSC)

Theoretical background

The state of matter changes with temperature giving indication of material properties. Heat effects associated with phase transitions are recorded as a function of time and temperature during differential scanning calorimetry (DSC) measurements. Characterization of polymers results usually with glass transition temperature (T_g) or melting point (T_m) for amorphous or semi-crystalline materials, respectively. Additionally specific heat and purity of the sample can be determined.

$$(3.4) \quad \left(\frac{dq}{dt} \right)_p = \frac{dH}{dt}$$

$$(3.5) \quad \Delta \frac{dH}{dt} = \left(\frac{dH}{dt} \right)_{sample} - \left(\frac{dH}{dt} \right)_{reference}$$

A typical DSC instrument is pictured schematically in Figure 3.4.4 and contains an aluminum pan with the test sample and an empty pan used as a reference. Both are located in the chamber purged with an inert gas. Both pans are heated with the defined rate and the heat exchange differences between the sample and the reference is continually corrected. Typically an experiment includes heating and cooling cycles that usually follow heating performed in order to erase the thermal history of the material. The resulting heat exchange differences recorded at the constant pressure (equal to enthalpy change dH) as a function of temperature (Equation 3.4) can be explained as a heat flow change (Equation 3.5). Dependently on the

endo- or exothermic character of the process, heat is absorbed or emitted, respectively. These effects are shown in Figure 3.4.4 as a response on the heat flow curve.

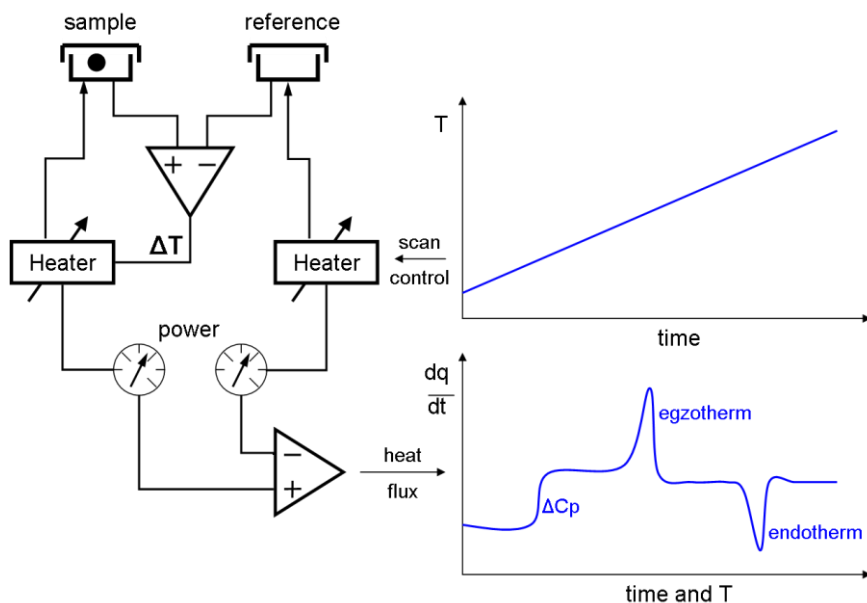


Figure 3.4.4: Scheme of DSC instrument with resulting curve.

Semi-crystalline polymers undergo glass transition, which is simply change between brittle and rubber-like state, not being a phase transition of any kind. Relaxation of polymeric chains interactions related to free Gibbs energy appear above characteristic temperature, so immiscible polymeric blends show individual T_g for each phase. Parameter more representative for material and not dependent on heat exchange rate commonly measured by DSC is heat capacity, C_p (amount of heat required to rise the temperature of 1 g of material of temperature 1°). During the experiment, this is measured as an absolute value of the heat flow dH/dt divided by the heating rate, which is shown in Equation 3.6.

$$(3.6) \quad \Delta C_p = \Delta \left(\frac{dH}{dT} \right) = \Delta \frac{dH}{dt} \frac{dt}{dT}$$

Methodology

Differential scanning calorimetry measurements were carried out on Perkin-Elmer Diamond DSC. Approximately 10 mg of the samples in the form of pellets were placed in aluminium pan closed with lid. The lid was pierced in order to release eventual gases. Samples were initially heated in temperature range between 20 °C and 200 °C with a heating rate of 20 °Cmin⁻¹. This run was performed to erase the thermal history on the nanocomposite. Then sample was cooled from 200 °C to 20 °C with the same heat exchange rate and the first heating was repeated with unchanged parameters. Transition temperatures were collected from the second heating cycle.

3.4.2.2. Thermo-Gravimetric Analysis (TGA)

Theoretical background

Thermal stability of materials determined basing on weight loss is measured by thermo-gravimetric analysis. Heating of the sample with constant rate is done simultaneously with weight monitoring, resulting with mass loss plotted versus temperature. A typical instrument setup is shown schematically in Figure 3.4.5. Inert gas is introduced into the furnace to avoid rapid oxidation that can not be controlled by heating rate. Position of point in degradation curve can be changed of up to 50 °C with varying atmosphere or heating rate.

TGA is useful in polymers characterization providing information about moisture absorbed, inorganic content and copolymer mass contribution for complex materials.

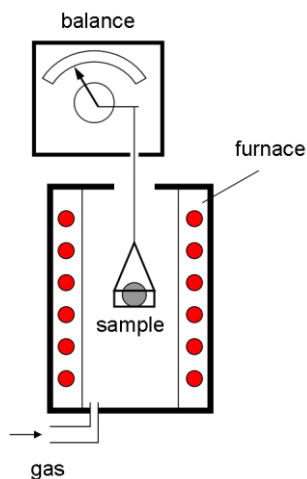


Figure 3.4.5: Scheme of thermo-gravimetric analysis.

Methodology

Thermal degradation of nanocomposites was investigated by thermo-gravimetric analysis on a TA Instruments TGA Q5000 instrument. The resulting curve of mass change versus temperature provides information of thermal stability for nanocomposites. 10-20 mg of sample was heated under nitrogen atmosphere from 50 °C to 600 °C with heating rate of 10 °Cmin⁻¹ and in air flow from 600 °C to 800 °C with the same heat exchange rate. Prior to each testing equilibration of the instrument was carried out at 50 °C. The final step above 600 °C was carried out without an inert gas in order to confirm the nanofiller content. Each material was tested at least two times.

3.4.2.3. Dynamic Mechanical Analysis (DMA)

Theoretical background

Wide applicability of polymers can be explained, among the other issues, by the viscoelastic properties of the material. Dynamic mechanical analysis (DMA) is the method most commonly used to determine these properties by

application of sinusoidal stress in a cyclic manner at various temperatures. Actually, stiffness and dumping (energy dissipation) are measured and reported as the storage modulus (E') and $\tan \delta$. The latter parameter is a measure of energy loss in oscillation mode in a dissipative system. This oscillatory test is different from other methods such as thermo-mechanical analysis, where a static force is applied and dimensional changes are recorded as a response.

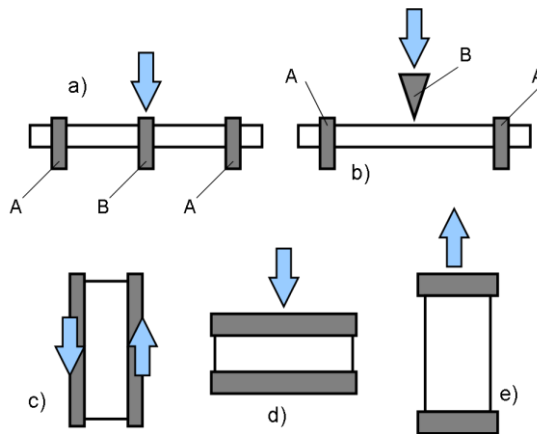


Figure 3.4.6: Common clamp geometries in DMA: a) dual cantilever, b) three-point bending, c) shear, d) compression, e) tensile; A – fixed clamps, B – movable clamp.

Oscillatory stress is applied to the material clamped in one of the geometries through the part of clamp. Geometry is related to the type of experiment and to the expected results, *e.g.* compression or tensile geometry (Figure 3.4.6) for storage modulus in a range 30-60 MPa and 30-120 MPa, respectively. Flexure geometries, three-point bending, cantilever and dual cantilever, are also employed below expected storage modulus values. Selection of proper clamp is additionally based on sample dimensions and character, *e.g.* thermoplastic-, thermosetting material will demand different geometries.

The storage modulus is usually measured as a function of temperature, which allows observation of the structural changes in material, including T_g . The glass temperature observed in DMA usually differs from the one recorded by DSC measurement, which is related to the applied frequency, which is absent in the latter experiment. The region between glassy plateau (before T_g) and rubbery plateau allows us to see the influence of various factors on polymeric material. In addition to an obvious alpha transition (T_g), DMA allows beta transitions to be observed as well as secondary dispersions and Hookean behavior.

Methodology

The dependence of mechanical properties on temperature for PC/ABS-MWCNT nanocomposites was investigated by dynamic mechanical analysis on TA Instruments DMA-2980 instrument. Dynamic temperature spectra of the samples were obtained in a dual cantilever clamp at vibration frequency 1 Hz. Temperatures were ranging from 35 °C to 200 °C and the scan rate was 3 °Cmin⁻¹. Each specimen was mounted in the clamp with the use of torque wrench to apply reproducible force. A dual cantilever clamp was selected due to the universal character of the test. The dependence of $\tan \delta$ (delta) and storage modulus (E') on temperature was recorded.

3.4.3. Mechanical properties

3.4.3.1. Tensile testing

Theoretical background

The elastic and plastic characteristics of a material represented by its mechanical behavior determine the eventual applicability. Testing a sample by subjecting it to a uniaxial tension until failure is a recognized characterization method for various materials. The tensile test for thermoplastic polymeric materials was carried out on shaped dog-bone

specimens being rectangular bars with wider grip sections on both ends. After placing the sample in clamps, the material was stretched vertically by electromechanical or hydraulic system. The measurements of deformations in the sample were done by load cell. Such transducer converting a force into an electrical signal is usually selected according to the expected ultimate stress.

The interaction between the elasticity and viscosity of material is modelled by common laws. Hooke's law, being one of the principals of mechanics, says that stress is directly proportional to strain. It is showing relation between forces applied to the spring and its elasticity (Equation 3.7) including k and x , spring constant defining stiffness of the object, and spring displacement, respectively. However, only linear elasticity responds well to Hooke's law. Viscous behavior is defined by Equation 3.8.

$$(3.7) \quad F = -kx$$

A plot of resulting stress versus strain curve, pictured in Figure 3.4.7, can provide various data, including Young's modulus, tensile strength or elongation at break for the material. Elastic behavior shows lower stress values for ductile than for stiff materials at the same strain (Figure 3.4.7a, b, c). The failure point also varied depending on the character of material, appearing before yield point for brittle materials (Figure 3.4.7b). This characteristic point on curve separates elastic area where material acts (theoretically) following Hooke law, from plastic area. Cold drawing, composing the latter part, represents irreversible deformation followed by necking – the last stage before failure. Young's modulus can be calculated basing on the Hookean behavior: the ratio of uniaxial stress over the uniaxial strain.

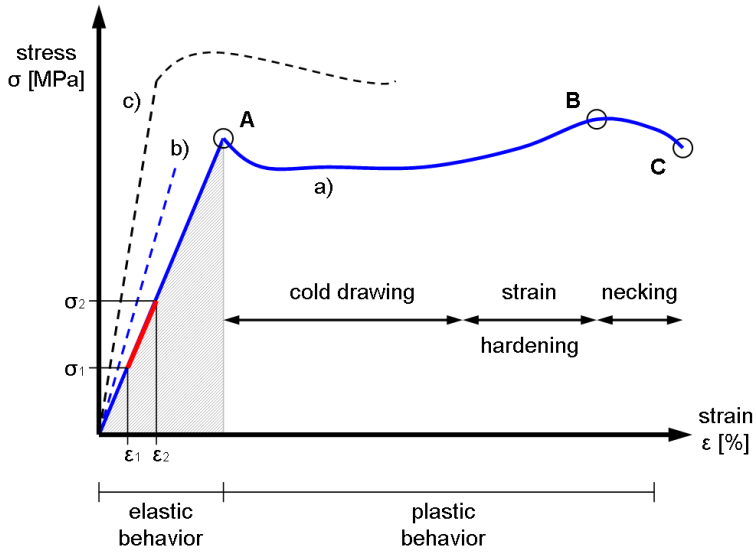


Figure 3.4.7: Stress-strain curves for various materials: a) ductile, b) brittle, c) strong and stiff; Characteristic points on curve a): A – yield point, B – ultimate stress, C – failure; elastic region is dimmed.

Methodology

Tensile measurements were performed on Instron Universal 3343 Machine following the ASTM D-638 standard. Samples with dog-bone geometry were clamped between grips and stretched at the velocity 5 mmmin^{-1} . A 1 kN load cell was used for this test. Experiments were carried out at constant conditions: $50 \pm 5 \text{ \% HR}$ and $24 \pm 2 \text{ }^\circ\text{C}$. The curves of stress dependence on strain were recorded and parameters characterizing nanocomposites were determined basing on this relation: tensile strength σ , Young's modulus E , elongation at break ϵ_b and at yield point ϵ_y . Toughness K of the material was calculated from the curves for selected nanocomposites.

3.4.3.2. Nanoindentation

Theoretical background

Nanoindentation is a method of mechanical testing at the submicron scale. Usually hardness is measured, however the elastic modulus, hardening exponents or creep parameters can be determined as well. The technique is widely used in material sciences and is often utilized in conjunction with other common characterization methods.

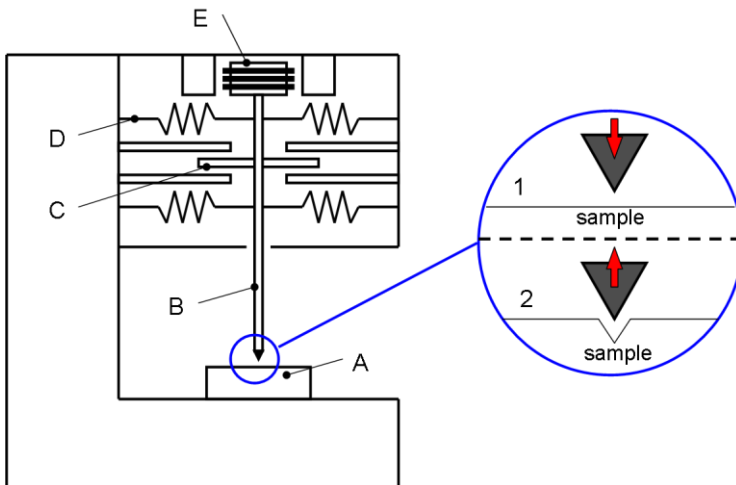


Figure 3.4.8: Scheme of nanoindenter: A – sample; B – indenter column; C – capacitive displacement gauge; D – support springs; E – load application cell; 1, 2 – stages of the process with sample surface indication.

Nanoindentation is based on pressing defined geometry to the material (Figure 3.4.8) and recording the response. Force and displacement are recorded during both steps. The crucial elements of the equipment are sensors and actuators providing correct reading of material response. The indenter tip, conventionally made of diamond, is tetrahedral which helps simplify analysis. Moreover, efforts have been made to create the proper method for nanoindenter tip characterization.

Interesting phenomena take place during the nanoindentation measurements due to the small quantity of material used for the test. Usually discontinuities on the load-displacement curves are related to the dislocation or shear activities in the material, or to the phase transformation. However, the latter situation exists mainly for metal or alloys.

Methodology

Nanoindentation tests were carried out using a G-200 nanoindenter from Agilent Technologies with a Berkovich diamond tip, previously calibrated on standard silica. The tip was pushed into the material until a 250 nm depth was reached, the force was maintained for 5 seconds and released. Measurements were carried out at nine different points for each sample separated by 120 μm . Stiffness used for evaluating mechanical properties was calculated by a Continuous Stiffness Measurement mode (CSM) set at 45 Hz oscillation frequency and 2 nm harmonic oscillation amplitude at a strain rate of $5 \times 10^{-2} \text{s}^{-1}$. The plasticity index Ψ was calculated from the ratio between areas under the loading and unloading curves.

3.4.4. Rheology

The viscoelastic behavior of polymer nanocomposites is fundamental for the processing of compounded material. This behavior includes relation between shear rate, angular frequency and temperature with material quality, *e.g.* nanofiller dispersion state. Interactions between polymeric chains and individual carbon nanotubes or agglomerates influence rheology of molten polymer even at low concentrations due to the high aspect ratio of nanofiller. An increase of viscoelasticity occurs above the mechanical percolation^[153].

Theoretical background

Viscosity, being one of the key parameters of visco-elastic materials depends strongly on sample homogeneity, including filler dispersion, molecular chain length or blend composition. Fluids are usually divided according to the dynamics into two main material types: Newtonian and non-Newtonian (Figure 3.4.9b) with the former one satisfying Equation 3.8. Shear stress τ depends on viscosity μ and strain rate explained as gradient of velocity which can create a situation of direct proportion between stress and strain. In a non-Newtonian fluid, like most of the polymer melts, the relation between shear stress and shear rate is not linear and can not be characterized by constant viscosity coefficient.

$$(3.8) \quad \tau = \mu \frac{dv}{dx}$$

$$(3.9) \quad De = \frac{t_c}{t_p}$$

Viscosity in polymer melts decrease with increased shear rate which is important for processing issues and is commonly investigated with oscillatory shear in a range of frequencies *e.g.* on rotational rheometer. Low and high shear rates representing different material behavior which is related to polymer chains relaxation time. Deborah number De (Equation 3.9) as a ratio between stress relaxation time t_c and processes time t_p is an important processing parameter increasing between Newtonian and non-Newtonian fluids.

Importance of material morphology is literally related to filler influence on melt viscosity at lower share rate. Dependently on shape, size or load of filler various viscosity increase is usually observed. This is extinguished at higher shear, where matrix contribution dominates. Blend composition also

changes viscosity dependently on the compatibility of components. The Deborah number varies significantly with formation of the blend, which is related to much longer t_c time for dispersed phase.

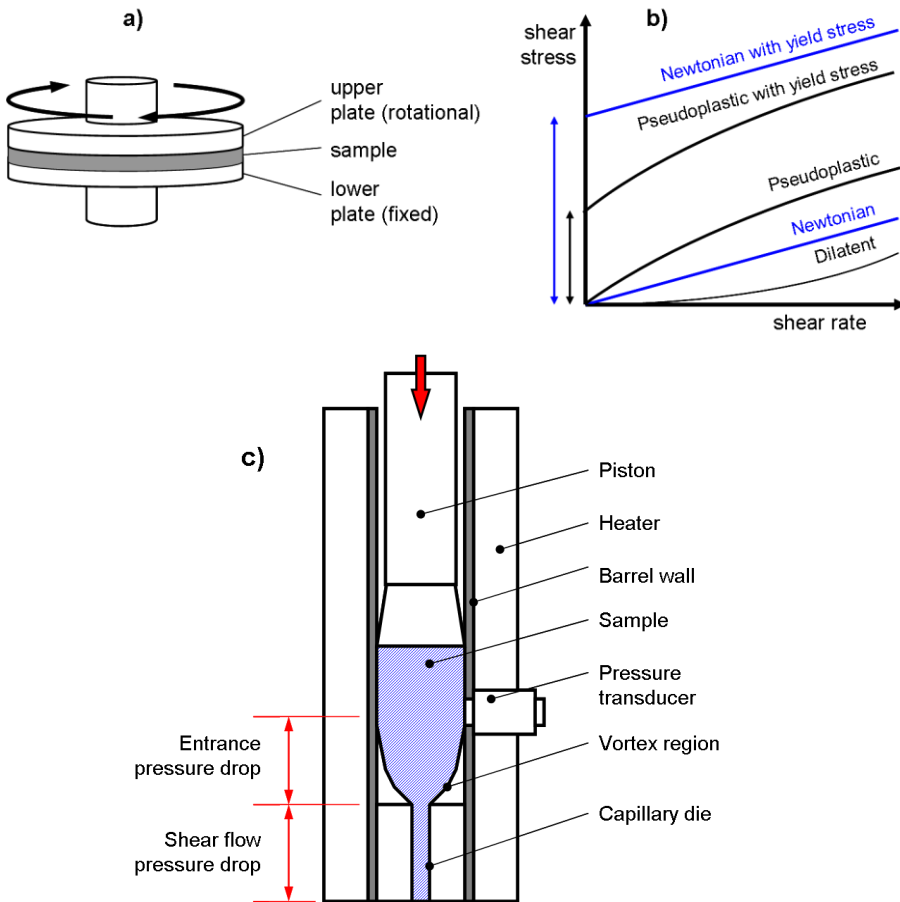


Figure 3.4.9: Scheme of parallel plate geometry in rotational rheometer (a), characteristic flow diagrams of various materials (b) and scheme of capillary rheometer (c).

The instrument for rheology determination is usually equipped with rods of various geometries providing different testing conditions. For a rotational

rheometer, besides the parallel plate geometry pictured in Figure 3.4.9a, the common one is a concentric cylinder with increased instrument-sample surface contact. For capillary rheometer (Figure 3.4.9c), providing shear high enough to simulate injection molding, melted polymer is pushed through die of defined diameter.

Data collected from the instrument allows plotting the storage modulus G' (strain energy reversibly stored in the substance) and complex viscosity η^* .

Methodology

Viscoelastic properties of nanocomposites were investigated at low shear rates (from 10^0 s^{-1} to 10^3 s^{-1}) on TA Instruments AR G2 rotational rheometer with parallel plate geometry. Plate diameter was 25 mm and the software used for data processing was AR instrument Control RS232. Testing at higher shear (from 10^1 s^{-1} to 10^4 s^{-1}) was carried out on a Göttfert Rheo Tester 1000 capillary rheometer with nozzle diameter 9.5mm and capillary L/D ratio 30. Weissenberg-Rabinowitsch correction was applied to the readings from the machine in the later case. The test materials were in the form of pellets and were dried under vacuum at 100 °C for 4h before testing. The measurements were carried out at 280 °C. The gap between the plates in the rotational rheometer was set at 1mm before each run. During the test, pellets were placed on the lower plate and melted. Samples were equilibrated in the rheometer in nitrogen atmosphere for 3 minutes. According to the results, strain was set to 1 % and the elastic modulus (G'), loss modulus (G'') and complex viscosity (η^*) were recorded.

3.4.5. Electrical properties

Improvement of electrical conductivity in PC/ABS melt mixed with carbon nanotubes is one of the main aims of this work. Nanofiller with high aspect ratio in define concentrations creates a conductive network inside insulating polymer, which is known as percolation threshold. This value obtained with MWCNT differs significantly from the other materials, making electrical conductivity of carbon nanotubes-filled polymers a determining parameter. The structure of the network is one of the most important parameters for both industry and science, due to the recognized influence also on rheological and mechanical properties.

Theoretical background

Determination of electrical conductivity by electrical resistance measurement in normalized samples is commonly carried out following the Van der Pauw method. Volumetric and surface conductivity can be investigated with application of four- or two-point measurements (Figure 3.4.10). Filled polymeric materials exhibit electrical conductivity due to the formation of a filler conductive path inside the material, allowing charge carrier movement between the network ends. These interactions between different materials: filler (carbon nanotubes in this example) in the form of well dispersed particles or agglomerates and matrix (polymeric blend) require a normalized experimental protocol to allow reasonable comparison.

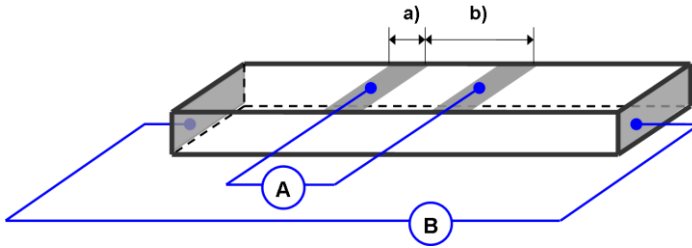


Figure 3.4.10: Scheme of electrical resistance measurement: A – surface resistance, A+B – volumetric resistance; a) 5 mm, b) 20 mm.

The Van der Pauw method is carried out on a sample with at least one dimension greater than the others. The specimen is clamped between electrodes, taking care to ensure contact is only through parallel edges of the sample. The current is applied as DC, providing a unidirectional flow of electrons and passive resistance. A current is passed through each parallel couple of edges and mean value is given as a result. The method can be modified in order to measure electrical resistivity of reinforcement polymers and required full contact between the sample and the electrode in the cross-section and contact between two reference electrodes on the surface to assure four-point reading. Volumetric conductivity is calculated from resistance value as a current is passed through electrodes B (Figure 3.4.10) and read by electrodes A. Surface conductivity is obtained analogous to volumetric conductivity but with two point measurement by Electrodes A reading the voltage drop on the sample. In Equation 3.10 and Equation 3.11 used for volumetric and surface conductivity determination, resistance is related with sample cross-section ab (or sample width a) and electrodes distance l .

$$(3.10) \quad \rho_v = R \frac{ab}{l}$$

$$(3.11) \quad \rho_s = R \frac{a}{l}$$

Methodology

The electrical properties of PC/ABS-MWCNT nanocomposites were investigated on rectangular specimens. Sample preparation included painting the silver electrodes on both sides and the surface of each specimen using Electrodag 1415 silver paint supplied by Agar Scientific (Figure 3.4.10). In the case of injection molded samples approximately 0.1 mm of material was removed from the surface before painting the electrodes on. Measurements were carried out following a modified Van der Pauw method and from ISO 3915. Electrical resistance was recorded with two- (surface resistance) and four-point (volumetric resistance) contact configuration. A Keithley 2000 Multimeter was used as source and reader.

3.4.6. Flammability

Determining material flammability is crucial for the characterization of new material due to safety issues. Fire retardant properties represented mainly by ignitability and flammability are measured as smoke opacity, heat release, dripping and flame spread. These criteria vary between applications, with the strictest being for the aerospace industry. Nanocomposites with carbon nanotubes have increased fire retardancy which is explained by barrier formation between burned and unburned parts. Such a protective layer depends strongly on nanofiller dispersion quality.

Theoretical background

The flame propagation characteristic of a polymeric material is a crucial parameter independent on the final application. Horizontal- and vertical burning are common methods of flammability verification accepted by

industry. Errors due to subjective testing can be minimized by following defined sample preparation and testing procedures (UL49) as burning characteristics are significantly dependent on homogeneity of the specimen. Parameters expected after flammability test include ease of ignition, intensity of burning and fuel contribution, usually presented with burning rate and flame spread.

Table 3.4.1: Material classification for 20mm vertical burning test.

Criteria conditions	V-0	V-1	V-2
	[sec]		
Afterflame time (t_1 or t_2)	10	30	30
Total afterflame time (t_1 and t_2)	50	250	250
Afterflame and afterglow time (t_2 and t_3)	30	60	60
Afterflame and afterglow reached to the clamp	No	No	No
Cotton indicator ignited by flaming drops	No	No	Yes

The dimensions of the specimen for this test are defined: length of 125.0 ± 5.0 mm, width of 13.0 ± 0.5 mm and thickness of $3.0 (-0.0 +2.0)$ mm. For each material, eight samples were tested: three for horizontal- and five for vertical burning. Materials were conditioned before the test for 48 h at 23 ± 2 °C and 50 ± 5 % relative humidity (RH). For the horizontal burning test the specimen was mounted on the stand (Figure 3.4.11) and two lines perpendicular to the long axis were marked 25 mm and 100 mm from the free end. The sample was ignited with a normalized burner, which impinges the sample for 30 seconds. After that time the ignition flame is removed and burning process is observed until afterflame forehead reaches the first mark. In that stage materials with the best flammability parameters are self-extinguished or afterglow appears after removal of the ignition

source. If the specimen continues to burn, the time of flame-travel between the two marks is recorded. The linear burning rate V is calculated as a ratio between length of burned part of the specimen and the recorded time.

For the vertical burning test, a similar to previous specimen is mounted on the stand with the long axis perpendicular to the ground and cotton is located underneath the specimen (Figure 3.4.11). A normalized flame is applied to the bottom of the specimen for 10 seconds. After that time the flame is removed and the time of afterflame is recorded as t_1 . When after-flaming is ceased, the ignition procedure is repeated and another afterflame or afterglow time is recorded as t_2 and t_3 , respectively. The classification of the material flammability is gauged based on the data in Table 3.4.1.

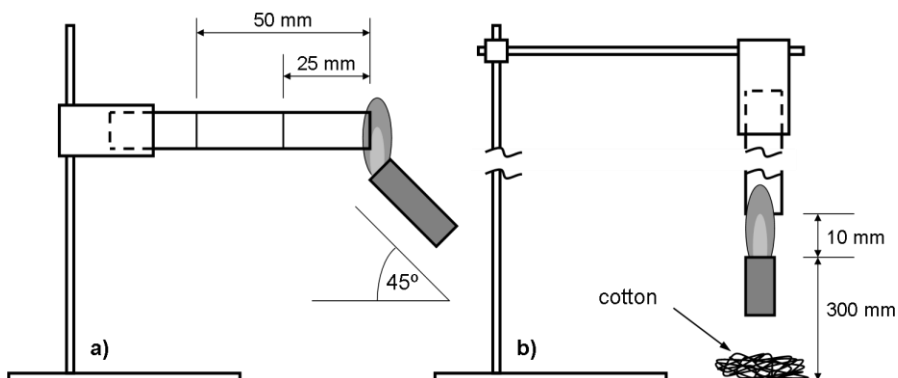


Figure 3.4.11: Experimental setup for nanocomposites flammability determination adapted from UL94; a) horizontal burning, b) vertical burning.

Methodology

The fire retardant properties of PC/ABS nanocomposites were done on selected compression and injection molded samples conditioned before the test at 50 ± 5 % HR and 24 ± 2 °C. Tests were performed following horizontal burning for HB classification and vertical burning guidelines from norm UL 94, modified for this project: size of the specimens suggested in

this document was reduced to the size of samples obtained in this work. This resulted with change of the position of second mark to 50 mm. Such prepared specimens were tested, classified and the linear burning rate was calculated. Materials were tested three times by each method.

4. Conventional melt mixing

Formation of nanocomposites by twin screw extrusion is a common, industrially recognized process. Specific mechanical energy (SME) is an important parameter characterizing that process and shows the effectiveness of the selected processing conditions. Equation 4.1, presenting the calculation method, can be understood as a relation between various mutually correlated values. Therefore SME is directly proportional to the torque (influenced by the melt viscosity) and the screw speed, but indirectly proportional to the throughput. Nevertheless, these parameters need to be correlated in order to reach the optimum conditions. Significant changes of SME at various combinations of processing parameters are described below. The parameter εP is the real power of the motor (including the efficiency of 0.97) in kW, T is torque while v_{proc} and v_{max} are screw speeds during processing and maximum, respectively. Throughput Q was maintained at 1 kg h^{-1} for all experiments, although research regarding changes of that parameter exists in the literature.^[62]

$$(4.1) \quad SME \left[\frac{\text{kW}}{\text{kg/h}} \right] = \frac{\varepsilon P \cdot T \cdot \frac{v_{proc}}{v_{max}}}{Q}$$

4.1. Study of PC/ABS-MWCNT nanocomposites morphology

4.1.1. Characterization of PC/ABS and MWCNT

An immiscible amorphous blend of the polycarbonate (PC) and the terpolymer acrylonitrile-butadiene-styrene (ABS) can contain more than two phases. The latter phase, is formed from poly(styrene-*co*-acrylonitrile) copolymerized in the presence of butadiene, which gives polymer chains

including three types of mers. The immiscibility of PC and ABS is not visible in light-transmission microscopy but can be observed by electron microscopy (*e.g.* SEM) as the presence of smooth polycarbonate and rough ABS^[74] (Figure 4.1.1). Besides, the major part of polybutadiene spheres is present in the latter phase. Some amount of polybutadiene is transferred to PC during blending process.

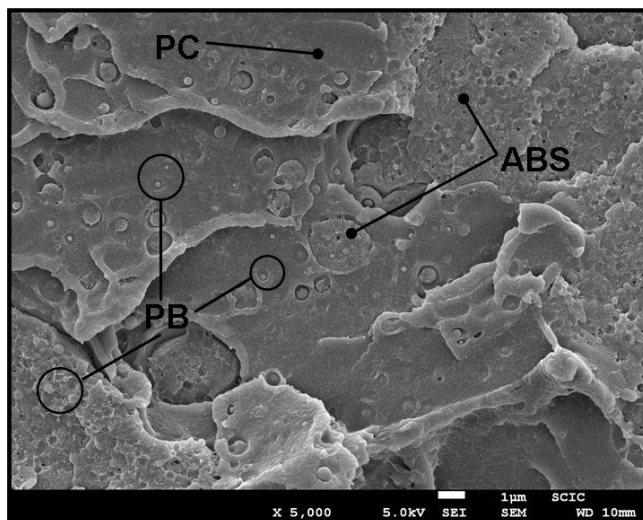


Figure 4.1.1: SEM micrograph of PC/ABS blend with indication of the main phases.

Spectroscopic characterization of the matrix by Raman spectroscopy is shown in Figure 4.1.2. The vibrational spectrum of PC/ABS shows characteristic bands between 600 cm^{-1} and 2000 cm^{-1} . The signals at 1880 cm^{-1} , 1112 cm^{-1} and 885 cm^{-1} are assigned to C-H in-plane and out-of-plane wagging modes. The broad band between 1200 cm^{-1} and 600 cm^{-1} arise due to C-O stretching and C-H deformations respectively.^[154]

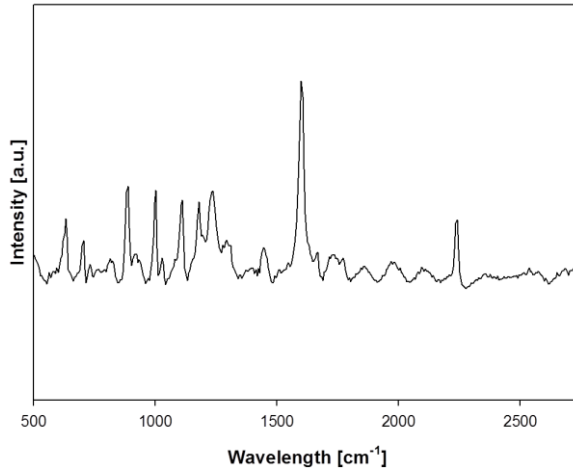


Figure 4.1.2: Raman spectra of PC/ABS.

The calculation of surface energies and wetting coefficient (ω) between the matrix and carbon nanotubes allows prediction of the nanofiller localization in the blend and eventual tuning of the material.^[152] Values of selected materials investigated^[152,155-156] are shown in Table 4.1.1. The interfacial tension (Y_{int}) obtained from partial surface tensions between the defined phases of the blend show higher value for ABS/MWCNT than for PC/MWCNT. Moreover, the same results are obtained with each of the applied calculation methods. The MWCNT wetting coefficients calculated with Equation 4.2 is -2.3^[155] or -1.5,^[156] which is constant with higher carbon nanotubes affinity for polycarbonate than to ABS in both cases.^[157] This is a main drawback in even division of the nanofiller between both components of PC/ABS blend. Besides, significantly lower content of ABS in the blend decreases the driving force to locate nanofiller in this phase.

Table 4.1.1: Surface tension (γ) and interfacial tension (γ_{int}) of MWCNT, PC and ABS at 250 °C.

Material	γ [mNm ⁻¹]	γ_{int} [mNm ⁻¹]
MWCNT ⁽¹⁾	45.3	-
PC ⁽²⁾	29.1	-
ABS ⁽²⁾	28.6	-
ABS/PC ⁽¹⁾	-	7.1
ABS/MWCNT ⁽¹⁾	-	28.1
PC/MWCNT ⁽¹⁾	-	11.7

(1) [155], (2) [152]

$$(4.2) \quad \omega = \frac{\gamma_{PC/MWCNT} - \gamma_{ABS/MWCNT}}{\gamma_{ABS/PC}}$$

4.1.2. Influence of the processing method on morphology of PC/ABS-MWCNT nanocomposites

Processing method during nanocomposite formation is a crucial factor showing significant influence on the final properties. Twin screw extrusion shows some advantages of tunable screw design and the shear control with temperature and screw speed.^[58,158-159] Various methods of MWCNT addition to the polymeric matrix can be understood as another factor in the modification of the material properties.

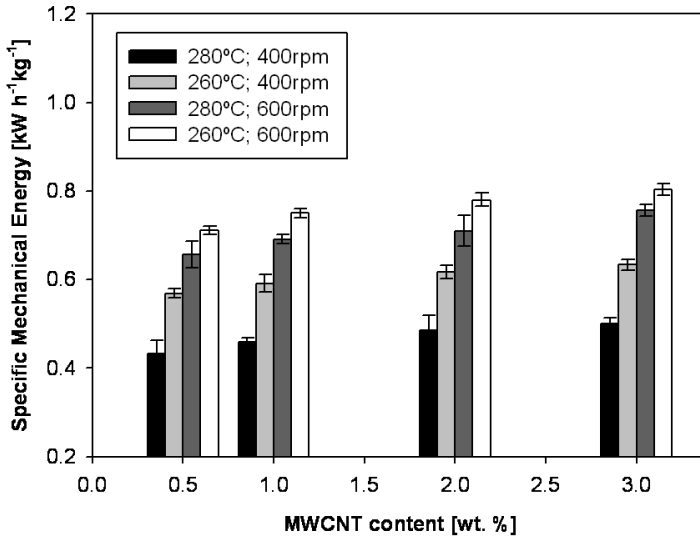


Figure 4.1.3: Specific Mechanical Energy dependence on MWCNT concentration and the processing parameters for masterbatch dilution (*MB*).

The increase of MWCNT load did not result with significantly stronger agglomeration. However, the morphology changes significantly with the change of other processing conditions, namely barrels temperature and the screw speed. Regarding the earlier reports about the relation between SME and the morphology of polymer nanocomposites,^[62] this phenomenon can be explained with the data present in Figure 4.1.3. Morphology quality clearly increases with SME. Both processing parameters involved in this study, melt temperature and screw speed, give a clear change in specific mechanical energy. The highest SME observed for the material processed at 260 °C and 600 rpm is a response of the energy provided to the material by the high screw speed at higher viscosity. The increase of melt temperature leads to a decrease in viscosity, which in turn has negative influence on SME. Further, the decrease of screw speed to 400 rpm results in the same nanocomposite behavior within the investigated range of temperatures. Figure 4.1.3 shows the necessity of correlating processing parameters during

nanocomposite compounding. Melt temperature, to a large extent, is responsible for resulting viscosity in this process, along with the screw speed determining shear forces needs to be seen as a correlated set of parameters rather than as two separate, mutually independent factors.

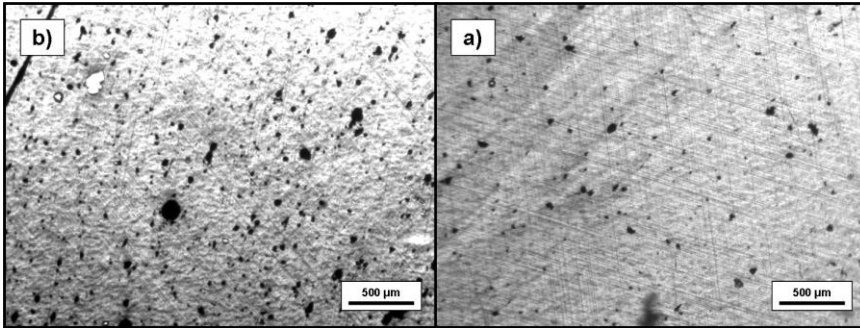


Figure 4.1.4: Light-transmission microscopy image of nanocomposite (3.0 wt. %) processed by powder addition (**P**) at 280 °C with: a) 100 rpm, b) 400 rpm.

Attempts to directly feed nanofiller to the extruder in the form of powder give poor morphologies. This is possibly due to the low SME applied to the material at single processing and relatively short material resident time in the machine (reduced approximately 50 % when compared to **MB**). The influence of screw speed is studied in **P** nanocomposites due to the high sensitivity to this parameter related with reduced processing. Screw speed influences the morphology mainly at low values, basically between 100 and 400 rpm. Figure 4.1.4 shows **P** materials processed with high temperatures but with various screw speeds ranging from low to middle values. The breakage of primary agglomerates carried out by the not completely melted polymer pellets appears in **P** method similarly as in the first step (pre-dispersion) of **MB** method. A significant reduction of both the size dispersion and the number of agglomerates can be seen when screw speed is increased from 100 rpm (Figure 4.1.4a) to 400 rpm (Figure 4.1.4b). This is

true for all methods applied in this study, leading to better morphologies for high screw speed values. There is no significant improvement observed with further increase screw speed to 600 rpm.

The control experiment carried out done during the nanocomposite formation with **P** method where MWCNT was added to the melted polymer in the middle of the screw. Particle resident time in the machine was reduced and the regions MWCNT were included showed significantly worse morphology at identical to **P** conditions. Therefore, resident time, morphology and the energy applied to the material during extrusion process are co-related.

Table 4.1.2: Agglomerates size distribution in nanocomposites (2.0 wt. %) formed with powder addition method (**P**); difference indicates the decrease of the value between screw speeds.

	Nanocomposite		
	100 rpm	200 rpm	400 rpm
Av. agglomerate area [μm^2]	159.08 (± 2.06)	99.78 (± 1.13)	34.38 (± 0.92)
Av. agglomerate length [μm]	16.41 (± 0.85)	11.26 (± 0.31)	6.57 (± 0.09)
Av. agglomerate aspect ratio [μm]	1.63 (± 0.05)	1.65 (± 0.08)	1.65 (± 0.07)
Agglomeration density [%]	11.15 (± 0.09)	9.13 (± 0.06)	1.21 (± 0.03)

The influence of screw speed was also investigated by the study of particle distribution in **P 2.0 wt. %**. Agglomeration parameters listed in Table 4.1.2 show significant improvement of morphology at higher screw speed rates. Average agglomerate area and length (both based on Feret axes) decrease

over 40-60 % between 200 rpm and 400 rpm with constant agglomerate aspect ratio. This suggests a reduction in of individual agglomerates, but not a change in shape. Agglomeration density, the factor describing the quality of nanocomposite morphology, is significantly reduced. Agglomeration density is defined as the ratio between the total area of agglomerates and the particle-free area in the image. Such behavior confirms the necessity of high shear presence in order to obtain well-dispersed carbon nanotubes in polymeric matrix. Correct selection of screw speed seems to be an important factor in this approach.

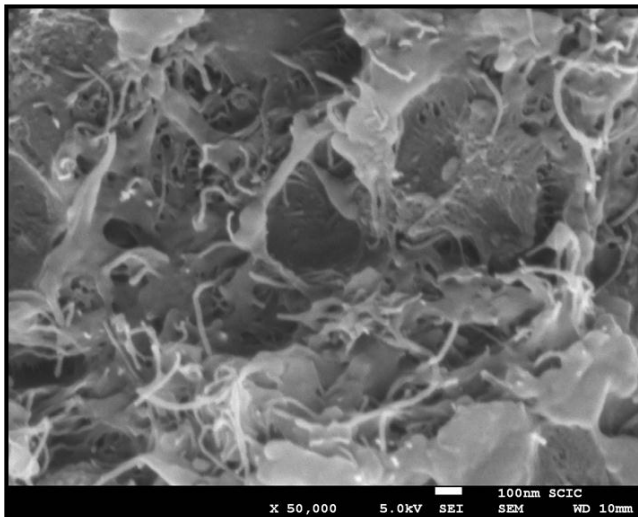


Figure 4.1.5: SEM micrograph of nanocomposite (**P 2.0 wt. %**) processed at 280 °C and 200 rpm.

Dry powder method **P** gives strong agglomeration of MWCNT as shown in SEM micrographs (Figure 4.1.5). This agglomeration is minimized with the application of further processing such as masterbatch dilution or addition of additives. The agglomeration of individual carbon nanotubes is not tight and the bundled nanotubes are likely to be separated following the processing

step. Again this emphasizes the influence of a second extrusion (*e.g.* masterbatch dilution).

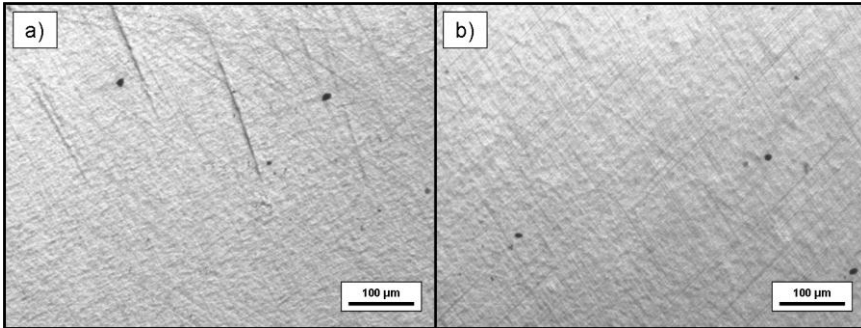


Figure 4.1.6: Light-transmission microscopy image of nanocomposites processed by masterbatch dilution (**MB**) at 260 °C with 400 rpm: a) 0.5 wt. %, b) 1.0 wt. %.

Masterbatch dilution method **MB**, further developed of the powder addition method, provides significant improvement of the final nanocomposite morphology. Longer resident time in the machine and the related higher total shear applied to the material gives more homogeneous materials studied on OM images (Figure 4.1.6). The morphology of **MB** nanocomposites is also relatively independent on MWCNT load, which was studied above 400 rpm. No significant change on carbon nanotube dispersion is observed between 0.5 wt. % and 1.0 wt. % MWCNT. The influence of processing temperature during the masterbatch dilution on morphology is similar to the effect of this parameter on SME (Figure 4.1.3). the relation between viscosity (controlled by the mentioned MWCNT load, barrels temperatures and screw speed) and final morphology is difficult to observe in OM images at relatively low carbon nanotubes concentrations applied in this study. Good dispersions are mainly a result of double processing in **MB** method.

No homogeneous distribution of the nanofiller between the blend components is observed in PC/ABS-based nanocomposites, as can be seen in the representative Figure 4.1.7. This situation is present for all studied compositions. Besides, MWCNT localization in polycarbonate and in the interface region proves the statements present in Table 4.1.1 related to the calculated affinity between the phases.

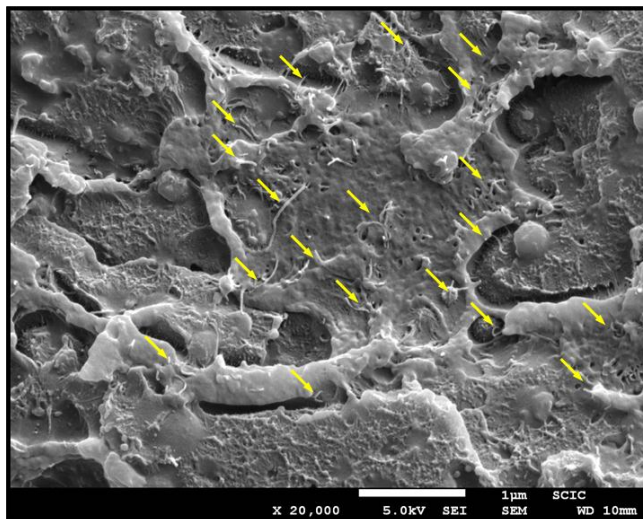


Figure 4.1.7: SEM micrograph of nanocomposite **MB 1.5 wt. %** processed at 260 °C with 600 rpm.

Raman spectroscopy of various nanocomposites demonstrates the dependence of characteristic band position and intensities on the nature of the processing methods. Characteristic bands for pristine multi-walled carbon nanotubes appear at 1340 cm^{-1} and 1475 cm^{-1} for D-band and G-band, respectively. The D-band arises from disordered graphite structures while the G-band is assigned to C-C bond stretching.^[160] For the studied nanocomposites, the bands are shifted towards the higher wave-number (blue shift) showing the positions at *c.a.* 1350 cm^{-1} (10 cm^{-1} shift) and

c.a. 1600 cm⁻¹ (25 cm⁻¹ shift) for D-band and G-band, respectively (Table 4.1.3).

Table 4.1.3: Raman spectroscopy shifts of characteristic MWCNT bands in pristine nanofiller and in nanocomposites.

Material		Band shift [cm ⁻¹]	
		D band	G band
MWCNT		1339	1575
P	(2.0 wt.%, 400 rpm)	1349	1592
MB	(2.0 wt.%, 400 rpm)	1347	1599

The difference in D- and G-band shifts between the nanofiller and the nanocomposite is greater than between the various nanocomposites. This is related to the local strains between MWCNT and the polymer,^[161-162] represented mainly by the mechanical compression transferred from the matrix to MWCNT.^[163] The G-band shift towards the higher values is explained as disentanglement of primary agglomerates and subsequent dispersion.^[160] However, measurement of the G-band in the nanocomposites has some uncertainty due to overlying with the peak at 1600 cm⁻¹ from aromatic groups of polymer (Figure 4.1.2). Moreover, the vibrations perpendicular to the long nanotube axis are affected by aromatic structures from polymer interacting with MWCNT.^[165-166] Nevertheless, the G-band shift of the nanocomposites presented in Table 4.1.3 can be understood as the indicator of MWCNT dispersion quality (*e.g.* for powder processing **P**).

PC/ABS-MWCNT nanocomposites formed by melt mixing with one- (powder addition **P**) or two-step (masterbatch dilution **MB**) processing method give moderate morphologies. Significant improvement of carbon nanotubes

dispersion is observed for the masterbatch method for all studied processing conditions. Nevertheless, regarding both methods, rather high shear should be applied to the material in order to improve the morphology. Therefore, moderate or higher screw speed is required, as no significant change occurs above 400 rpm. Also moderate processing temperatures are observed to give the best results due to providence of the proper melt viscosity of the blend.

4.1.3. Influence of MWCNT modification on morphology of PC/ABS-MWCNT nanocomposites

The main modifications of multi-walled carbon nanotubes applied in industry approach are shown in Figure 4.1.8. Direct covalent modification allows the formation of functional groups chemically bonded to the outer layer of MWCNT, while non-covalent modification with selected surfactants bases on the physical bonding of the additives to carbon nanotubes. Both types of modification result with the change of MWCNT location in the blend components and the change in defined nanocomposite properties. Figure 4.1.8a pictures the surface-oxidized MWCNT with the commonly higher concentration of COOH groups on the end caps. Pentagonal structures generally suffer more strain, which leads to higher reactivity with respect to defects on the outer shell.^[166]

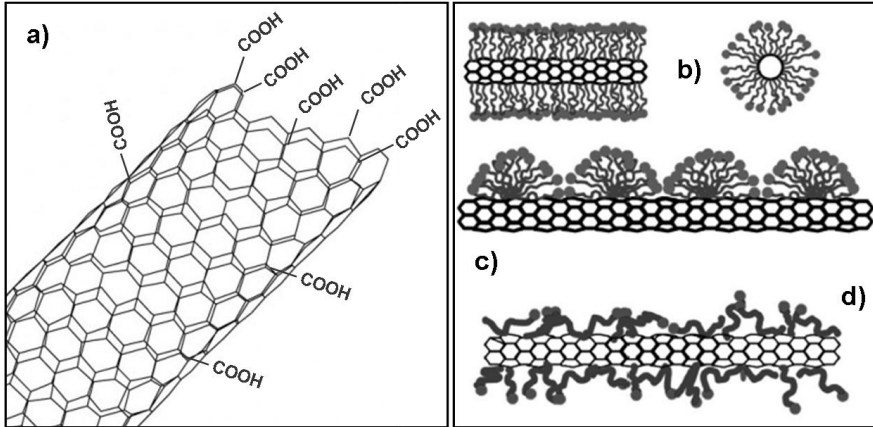


Figure 4.1.8: Schematic presentation of a) covalent- and b)-d)^[166] non-covalent MWCNT modification.

Covalent modification of multi walled carbon nanotubes resulted in significant improvement of nanocomposite morphology. Similar behavior after the nanofiller modification was reported by other authors.^[167-169] Homogeneous morphology is shown in Figure 4.1.9 on an example of nanocomposite with 1.0 wt. % and 5.0 wt. % MWCNT. Such improvement of MWCNT dispersion was absent in other modifications or other processing methods applied in this study. The strong increase of nanofiller load does not influence interactions between the individual nanofiller. Combining rather effective MWCNT dispersion method, masterbatch dilution, with the covalent modification of carbon nanotubes gave excellent homogeneity. Comparing the quality of the nanofiller dispersion of nanocomposite obtained with MWCNT-COOH (Figure 4.1.9a) with the material with non-modified carbon nanotubes (Figure 4.1.6b), the improvement after the modification of the nanofiller is clear.

The change of surface energies was achieved giving different MWCNT affinities to blend phases. Besides that, bulkiness of the groups terminating individual nanotubes most probably play an important role in the formation

of not so tightly bundled agglomerates. Good dispersion of individual carbon nanotubes with surface modification of MWCNT can be observed in SEM micrographs of the material (Figure 4.1.10).

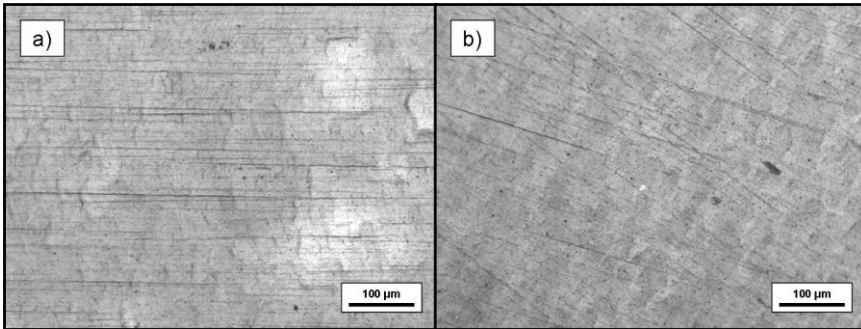


Figure 4.1.9: Light-transmission microscopy image of nanocomposites processed by masterbatch dilution with surface-modified carbon nanotubes (**MB-COOH**) at 260 °C with 400 rpm: a) 1.0 wt. %, b) 5.0 wt. %.

Very few bundles or agglomerates are observed, with the majority of the nanofiller dispersed homogeneously. As the carboxylic acid groups are present mainly near the tip of the nanotube (Figure 4.1.8) changing the affinity between the materials, some of the carbon nanotubes are dipped with both ends in the material. Such situation does not exist when the non-modified carbon nanotubes are used. Nevertheless, no significant change of the nanofiller location is observed and the polycarbonate phase is hosting the majority of MWCNT.

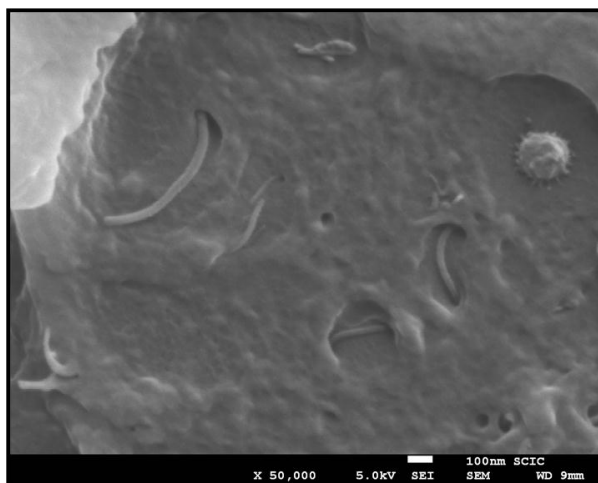


Figure 4.1.10: SEM micrograph of polycarbonate phase of nanocomposite **MB-COOH 1.0 wt. %** processed at 260 °C with 400 rpm.

Figure 4.1.11 shows the Raman D/G peak intensities ratios for various nanocomposites. This parameter is related to the quality of dispersion and to the tension between carbon nanotubes and polymer matrix. The **MB-COOH** ratio is value clearly lower than for the common **MB** method consistent with a decrease of agglomeration in the nanocomposite, according to the aforementioned explanations. This is in agreement with the SEM micrographs and OM images data indicating improvement of the morphology of the nanocomposites when MWCNT-COOH are used. D/G peak intensities parameter for powder addition method **P**, showing worse morphology than the other studied nanocomposites, is greater than **MB** and **MB-COOH**.

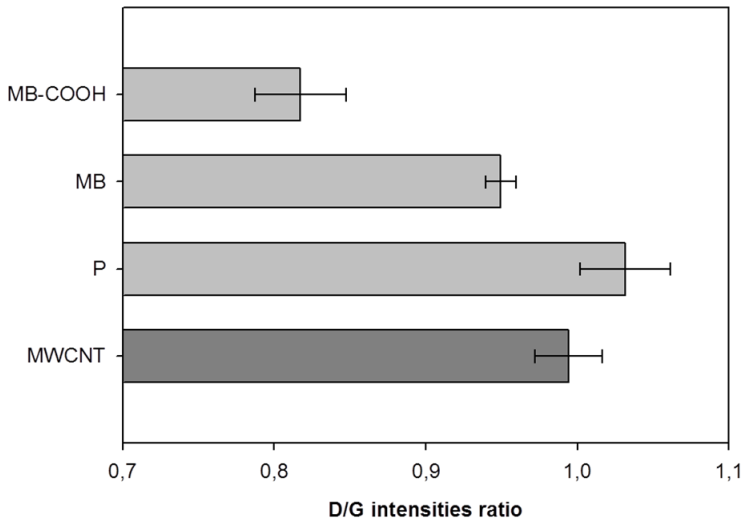


Figure 4.1.11: *D/G peaks intensity ratio for different nanocomposites (2.0 wt. %, 400 rpm) compared with pristine MWCNT.*

Transmission electron microscopy shows interesting results in agreement with the previous findings. Agglomerates present TEM micrographs of **MB-COOH 1.0 wt. %** (Figure 4.1.12) show the difficulty in totally overcoming the Van der Waals attractive forces between the nanotubes. Nevertheless, the remaining agglomerate size is significantly reduced with the surface-oxidation of the nanofiller. However, remaining tight bundles are difficult to destroy along the common processing path. The size of agglomerates below 400 nm proves the dispersion improvement (also when compared to the powder addition method, Table 4.1.2).

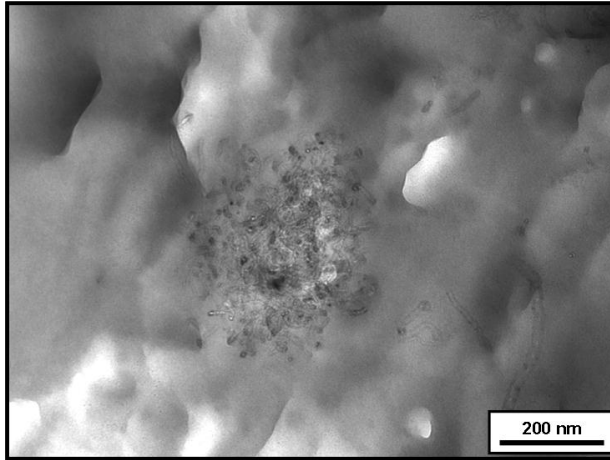


Figure 4.1.12: TEM micrograph of nanocomposite **MB-COOH 1.0 wt. %** processed at 260 °C with 600 rpm.

4.2. Study of thermal properties of nanocomposites

4.2.1. Thermal characterization of PC/ABS

The thermal properties of polymer-MWCNT nanocomposites determine material processing and the future applications by affecting various properties, *e.g.* the upper limit use temperature and the dimensional stability.^[170] The thermal decomposition behavior of polymeric matrix is a crucial factor in understanding the mechanism of nanocomposite degradation. High-resolution thermo-gravimetric analyses of neat PC/ABS carried out in dry nitrogen revealed multi-step decomposition, absent in the common test. The conditions of the test including isothermal steps activated with the increased weight loss influence the degradation of polybutadiene. This material is reported to decompose at 50 °C lower when the isothermal conditions are applied.^[171-172] Thermal decomposition of PC/ABS blend present in Figure 4.2.1 agrees with the earlier findings.^[173-174] The major phase of the blend is known for high thermal stability.^[175] The decomposition of neat polycarbonate under the nitrogen atmosphere occurs

between 400 °C and 500 °C, showing two broad peaks on the weight derivative curve.^[176] Two-step process includes oxidation and further depolymerization caused by the by-products cleavage. However, the first step based on radical mechanism can be retarded by the application of nitrogen atmosphere and eliminating water from the sample.^[177] The other known mechanism includes hydrolysis and condensation with the scission of polymer chains obeying the first order kinetics.^[178-180]

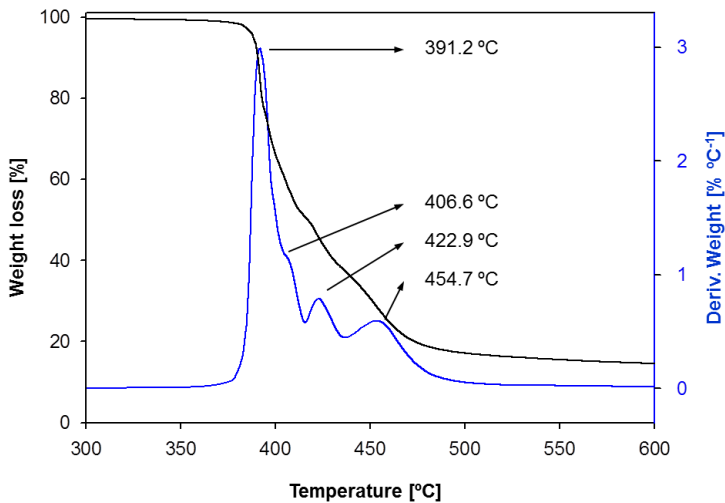


Figure 4.2.1: Hi-resolution TGA of PC/ABS blend.

An intensive peak at 391.2 °C present in Figure 4.2.1 is related to the first stage of PC degradation. Due to the separation of the decomposition of blend components, degradation of ABS phase is observed between the two steps of PC decomposition. Peaks at 406.6 °C and 422.9 °C are related to poly(styrene-*co*-acrylonitrile) (SAN) and polybutadiene, respectively.^[172] Detailed analyses of ABS material have been reported, revealing the multiple degradation stability dependences between the components and the terpolymer.^[181] The pure poly(styrene-*co*-acrylonitrile) degrades at

significantly lower temperature than the components and after the formation of SAN-*g*-polybutadiene, the decomposition temperature of SAN decreases. Such destabilization of the components appears also after blending to form PC/ABS.

4.2.2. Study of thermal behavior of PC/ABS-MWCNT nanocomposites

Reports on thermal behavior of PC-based nanocomposites show the general increase of thermal stability,^[176] while the ABS-based nanocomposites are reported to decrease the thermal stability of the matrix.^[174,182] When the flake-like nanofiller (*e.g.* nanoclay) is mixed with PC/ABS the thermal stability increases due to the strong barrier effects.^[183,184] For all nanocomposites studied in this work (Figure 4.2.2 and Figure 4.2.3) carbon nanotubes show decrease of thermal stability of polycarbonate and increase of this parameter for ABS phase. This observation can be related to the presence of MWCNT impurities affecting rather polycarbonate than the ABS. Carbon nanotubes used for this project are industrial grade material, which means they contain the impurities of amorphous carbon and the residual metal catalysts. It has been reported that the latter impurities or the defects such as carboxylic acid functional groups in MWCNT lead to the decrease of thermal stability of the nanocomposites by the reduction of the scavenging capabilities of free radicals.^[185] The investigation of PC/ABS-MWCNT nanocomposites thermal stability follows different methodology than the experiment presented in Figure 4.2.1. Non-isothermal experiments are carried out in order to study thermal degradation behavior. Curves shift towards the higher temperatures shows sensitivity reported earlier.^[171]

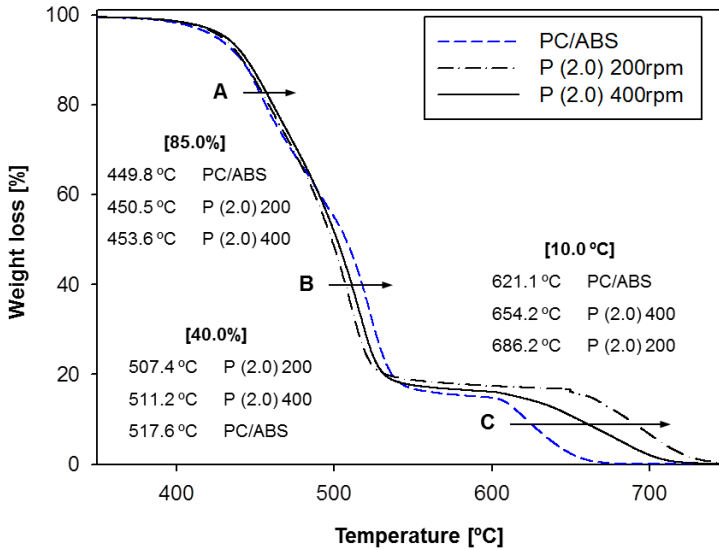


Figure 4.2.2: Thermal decomposition of PC/ABS-MWCNT processed by powder addition method **P**.

The influence of nanocomposite formation method on thermal properties of the final nanocomposite material is mainly related to the additives and the number of processing steps. Degradation curves of **P** material in Figure 4.2.2 show different behaviors of both blend phases. Furthermore, this behavior is amplified at higher MWCNT loads. Besides, the influence of screw speed during the **P** nanocomposite formation is shown in Figure 4.2.2. Three characteristic points are marked on the curves indicating the points of 85 wt. %, 40 wt. % and 10 wt. % of the initial mass. ABS phase stability does not change significantly (A) for both values. The behavior of polycarbonate (B) observed at the higher temperature range is opposite to ABS. Moreover, higher thermal stability for nanocomposites processed at 400 rpm indicates the influence of shear, which is related to more homogeneous morphology obtained at higher screw speeds (Figure 4.1.5).

Decomposition of the char (C) created in the principal stages of the degradation shows strong influence of processing parameters over the shown carbon nanotubes content. An increase of the final decomposition temperature is probably related to slightly higher agglomeration degree in the samples processed at 200 rpm. A MWCNT network is desired to include the individual nanotubes improving barrier properties. This approach should be changed, when the final oxidation step begins. A char formed during the first step, consisting the semi-degraded polymer and MWCNT, shows higher thermal stability for nanocomposites with worse morphology. The char consist of the agglomerated carbon nanotubes forming the better barrier and increasing the final degradation temperatures.

The nanocomposites **MB** in Figure 4.2.3a show the behavior similar to the **P** material. Thermal stability for this material is studied on weight derivative graphs in order to provide clearance of results. Slight decrease of the weight derivative maximum is observed for PC phase with the increase of MWCNT load. On the contrary, an increase of the temperature for ABS phase was observed. No significant change regarding the neat matrix was present. The reduction of a peak between the two maximums characteristic for both phases appears after the nanocomposite formation for both concentrations. This can be explained as a slight reduction of system sensitivity related to the presence of thermally conductive filler.

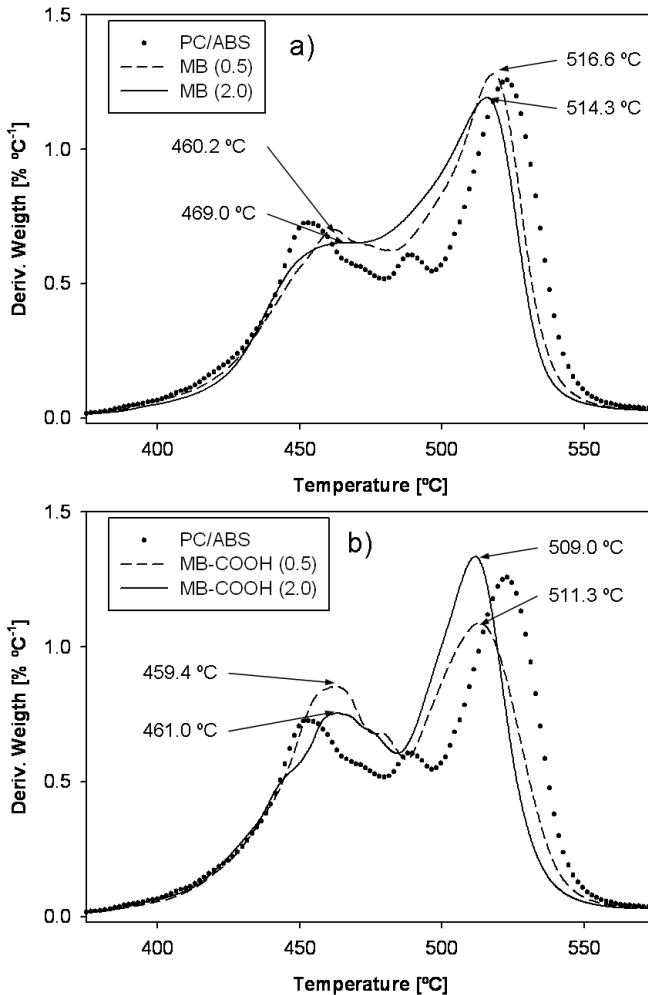


Figure 4.2.3: Weight derivative for nanocomposites formed with masterbatch dilution method (400 rpm, 260 °C): a) **MB**, b) **MB-COOH**.

The behavior of degradation temperatures in **MB** nanocomposites is improved when the carbon nanotubes are surface-oxidized (Figure 4.2.3b). Despite this fact, the degradation temperature of polycarbonate decreases with MWCNT-COOH load but ABS shows decrease in such a case. Comparison of **MB** material with the nanocomposite **MB-COOH** shows

further decrease of the degradation temperature for PC with no significant change for ABS phase, for the latter material. This is related to the possible relocation of nanofiller to the interphase region.

Table 4.2.1: Glass temperature (T_g) and change of heat capacity (ΔC_p) at glass temperature for **P** nanocomposites processed at 280°C and 200 rpm.

Material	MWCNT [wt. %]	T_g [°C]		ΔC_p [J g ⁻¹ deg ⁻¹]	
		PC	ABS	PC	ABS
PC/ABS	0.0	151.06	119.19	1.939	0.669
PC/ABS (proc.)	0.0	145.49	112.06	0.203	0.082
P	1.0	144.00	112.62	-	-
P	2.0	142.50	112.00	-	-
P	3.0	141.54	111.03	-	-

The results of differential scanning calorimetry, revealing the glass temperatures (T_g) of **P** nanocomposites and the change of heat capacity for this transition (ΔC_p), are shown in Table 4.2.1. Clear gradual decrease of these parameters for both blend components after the incorporation of MWCNT in one step processing is observed. Additionally, the processing affects the matrix itself what can be observed in a difference of ΔC_p values between PC/ABS and PC/ABS (proc.). It seems that the greatest variation is caused by shear applied during the nanocomposite formation process. The glass temperature change recorded along the increase of MWCNT load differs much less than between the processed and as-received matrix.

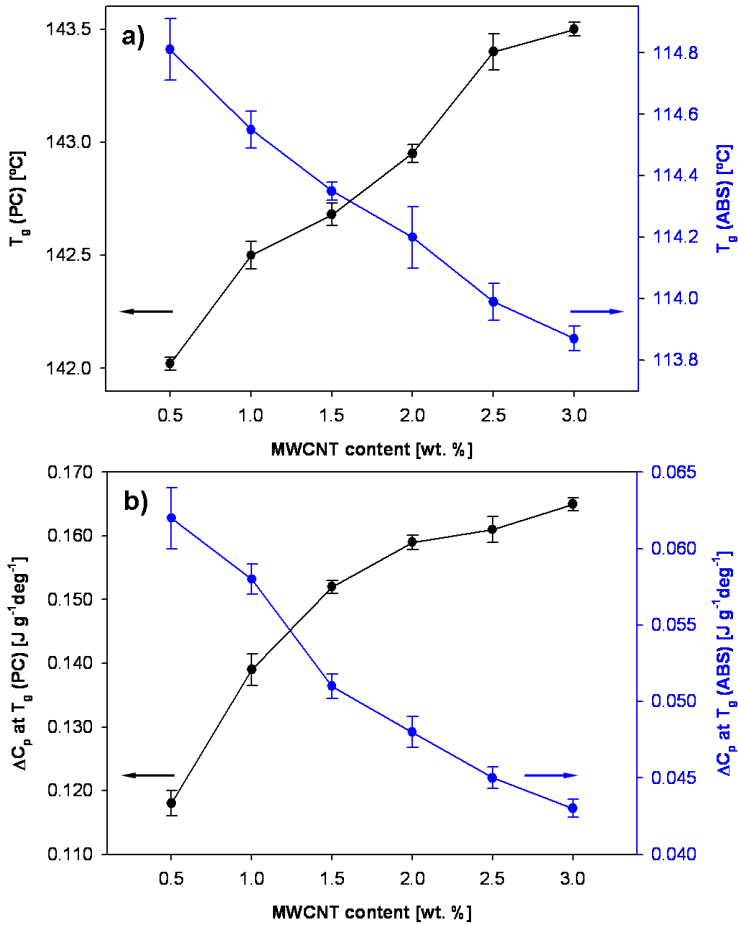


Figure 4.2.4: DSC summary of **MB** nanocomposites (400 rpm, 260 °C): a) T_g , b) ΔC_p .

The results of differential scanning calorimetry, revealing the glass temperatures (T_g) of **MB** nanocomposites and the change of heat capacity for this transition (ΔC_p), are shown in Figure 4.2.4. Collected data shows the decrease of both reported T_g values, similarly to nanocomposites **P** (Table 4.2.1). This is based on much stronger agglomeration in the latter material **P**. Chain mobility is greater for nanocomposites with agglomerated filler due to the reduced interactions between the matrix chains and individual

MWCNT. The decrease of PC and ABS glass temperatures agrees then with the previous findings.

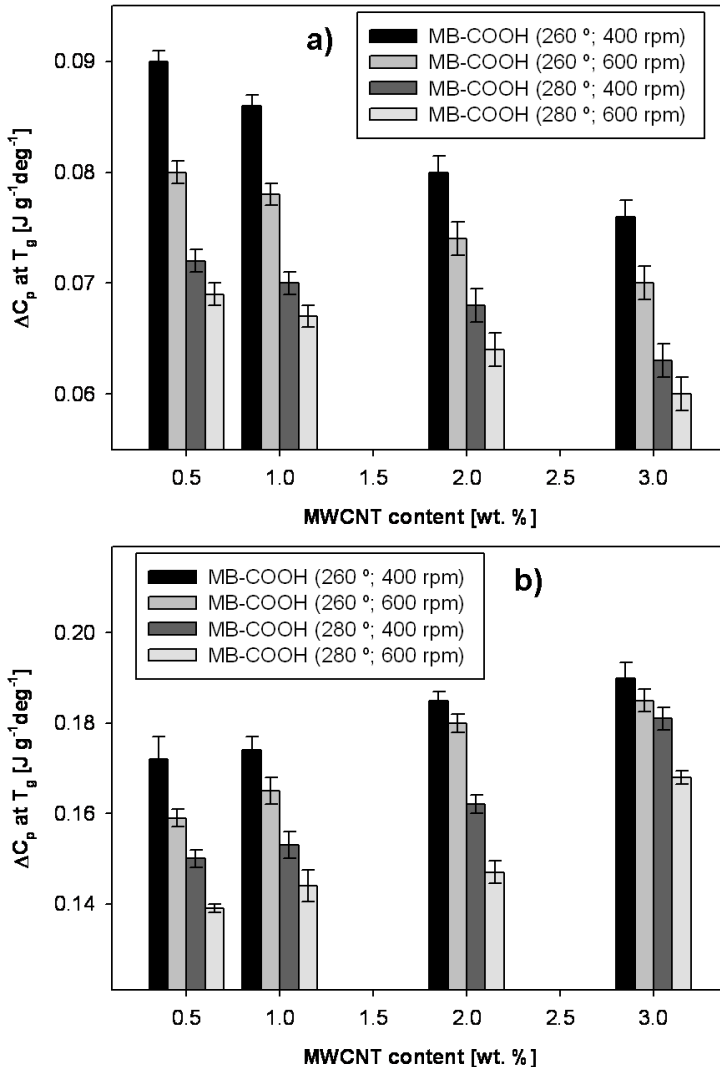


Figure 4.2.5: Change of heat capacity (ΔC_p) at glass temperature (T_g) for MB-COOH nanocomposites for: a) ABS, b) PC.

There is no significant difference in T_g before and after MWCNT-filled nanocomposite formation. A ΔC_p should rather be used as a reliable parameter.^[170] Figure 4.2.4a shows the opposite trends for both blend components, which can be understood as a confirmation for MWCNT separation between PC and ABS. Polymer chains mobility is affected by carbon nanotubes forming network and a good dispersion obtained in case of presented nanocomposites (**MB**) with the reported opposite trend for both blend components allows to assume the relocation of MWCNT at higher loads. This is concluded due to the increase of ΔC_p of the main nanofiller hosting phase. At the same time the MWCNT-free ABS phase shows the decrease of ΔC_p . Therefore, above a certain MWCNT load in an immiscible blend some amount of nanofiller is likely to fill the phase that is not thermodynamically favored.

The surface oxidation of nanofiller causes higher MWCNT loads in the interphase region of PC/ABS. Figure 4.2.5 with ΔC_p values for both blend components formed at various conditions shows similar trends observed in Figure 4.2.4b. Significant decrease of the specific heat capacity for ABS phase with the increase of MWCNT load confirms the change of polymer chains dynamics. This effect means that the increase of the nanofiller in ABS is identical with the effect shown in Figure 4.2.4.

The influence of processing parameters on ΔC_p of PC/ABS-MWCNT nanocomposites decreases with the nanofiller load for both components. Low value of both applied parameters, barrels temperature and screw speed, allows reaching the higher heat capacity. The correlated increase of screw speed and barrels temperature causes the decrease of heat capacity. This can be related to the higher degree of carbon nanotubes dispersion obtained at high shear conditions. As the ΔC_p can be understood as a polymer chain mobility, it should be reduced for better MWCNT dispersion in the nanocomposite with the same load. This is due to the fact that the

agglomerate usually shows lower interactions with the matrix than with individual nanotubes creating a network. Such a theory agrees with the findings present in Figure 4.2.5.

4.3. Mechanical properties of PC/ABS-MWCNT nanocomposites

The mechanical properties of polymer-based nanocomposites are strictly related to the morphology. Besides, blends show some advantages of the combined properties of components. Table 4.3.1 shows Young's modulus of the pristine matrix value 2200 MPa. The direct MWNCT feeding in powder form **P** results with the gradual increase of Young's modulus with the nanofiller content (Table 4.3.1).

Table 4.3.1: Tensile test results of nanocomposites formed with powder addition method.

Method	Nanocomposite		Mechanical properties		
	MWCNT [wt. %]	Proc.	$E^{(1)}$ [MPa]	$\sigma\text{-}y^{(2)}$ [MPa]	$\epsilon\text{-}b^{(3)}$ [%]
PC/ABS	0.0	-	2200 (± 15.0)	45.0 (± 1.0)	10.0 (± 0.1)
P	1.0	200 rpm; 280 °C	2888 (± 16.2)	53.6 (± 2.0)	4.9 (± 0.1)
P	2.0	200 rpm; 280 °C	3078 (± 11.0)	55.2 (± 1.2)	4.2 (± 0.2)
P	3.0	200 rpm; 280 °C	3248 (± 13.8)	53.9 (± 0.9)	3.3 (± 0.2)

⁽¹⁾ Young's modulus; ⁽²⁾ Stress at yield point; ⁽³⁾ Elongation at break.

Relatively high E values are present for **P** nanocomposites probably due to the poor final morphology and low matrix degradation during the processing thanks to the low value of overall shear (200 rpm and single processing). Micro-scale reinforcement of agglomerates rather than nano-scale reinforcement should be reported for this material. Besides, the stress at a yield point seems to be relatively constant with MWNT load, while elongation at break decreases at higher carbon nanotube concentrations. This is typical behavior for filled polymers with disturbed polymer-polymer interactions.

Table 4.3.2: Tensile test results of nanocomposites formed with masterbatch dilution method.

Method	Nanocomposite		Mechanical properties		
	MWCNT [wt. %]	Proc.	E ⁽¹⁾ [MPa]	σ -y ⁽²⁾ [MPa]	ϵ -b ⁽³⁾ [%]
MB	1.0	400 rpm;	2929	56.1	3.9
		260 °C	(±28.5)	(±1.5)	(±0.2)
MB	2.0	400 rpm;	2942	56.6	5.6
		260 °C	(±56.0)	(±2.1)	(±0.2)
MB	3.0	400 rpm;	3037	57.1	5.7
		260 °C	(±43.1)	(±1.2)	(±0.2)

⁽¹⁾ Young's modulus; ⁽²⁾ Stress at yield point; ⁽³⁾ Elongation at break.

Tensile test results of masterbatch dilution method **MB** present in Table 4.3.2 show behavior similar to the one-step processing **P** method. Gradual increase of Young's modulus with an increase of MWCNT load confirms the reinforcement of PC/ABS. Furthermore, stress at yield point shows higher values at elevated carbon nanotubes concentrations. Such a behavior of higher stress observed for stiffer nanocomposites is interpreted as better

reinforcement. Higher stress necessary for material to reach plastic deformation region can be related to better dispersion of the nanofiller. Insignificant increase of elongation at break is within the error and should be understood as a constant.

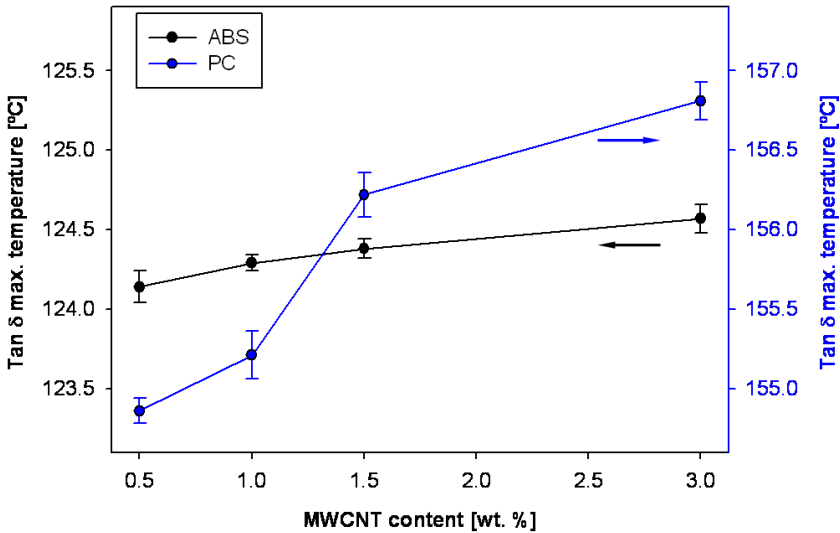


Figure 4.3.1: The dependence of $\tan \delta$ peak maximum on MWCNT load in **MB** nanocomposites (400 rpm, 260 °C).

Dispersion degree, orientation and the shape of the nanofiller along with the dispersion of the continuous phase play an important role in the final improvement of the researched material. $\tan \delta$ is read as a midpoint between the glassy and rubbery state of polymeric material. The common masterbatch dilution method **MB** of nanocomposite formation gives an expected increase in $\tan \delta$ peak maximum with an increase of MWCNT load for both blend components (Figure 4.3.1). This can be explained as relatively equal MWCNT division between both blend components at various nanofiller loads. It is understood, that the change observed for ABS will be minor when compared to PC, probably due to the lower content of the

former phase in the blend. Both vertical scales in Figure 4.3.1 have the same tick interval in order to emphasize the difference. Nevertheless, the impact on both blends appears to be similar when the phase share is taken into consideration.

Both applied processing methods show an increase of mechanical properties of PC/ABS matrix. Differences between the methods should be observed with respecting different processing conditions of **P** and **MB** nanocomposites studied here. Generally higher values of Young's modulus for the former material can be related with the slightly different mechanism of reinforcement. Majority of carbon nanotubes in **MB** are in dispersed state causing nano-scale reinforcement, while micro-scale agglomerates in **P** interact with polymer matrix differently. Besides, lower degradation of polymer chains during **P** processing is a major issue. Elongation at break relatively constant for **MB** nanocomposite is related with the better dispersion of nanofiller than observed in the other material.

4.3.1. Influence of MWCNT modification on mechanical properties of PC/ABS-MWCNT nanocomposites

The covalent modification of carbon nanotubes result with a slight increase of mechanical properties when compared to the non-modified nanocomposites (Figure 4.3.2). Characteristic behavior of **MB-COOH** and **MB** show a clearly higher performance for the former material with surface-oxidized carbon nanotubes. Young's modulus of **MB**, similarly to the stress at yield point, is lower along the whole studied MWCNT concentration range. This observation is explained as improved interactions between PC/ABS and **MB-COOH**. Besides, minor difference between **MB-COOH 1.0 wt. %** and **MB-COOH 2.0 wt. %** confirms weak influence of MWCNT loads at higher concentrations.

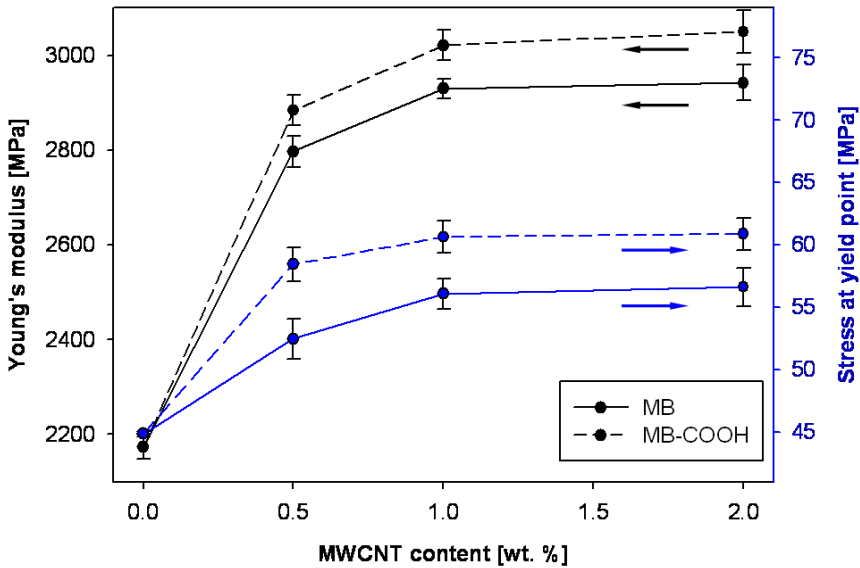


Figure 4.3.2: Mechanical properties of nanocomposites processed by masterbatch dilution with MWCNT (**MB**) and MWCNT-COOH (**MB-COOH**) (400 rpm, 260 °C).

The influence of processing parameters on mechanical properties of nanocomposites filled with covalently-modified carbon nanotubes in Figure 4.3.3 shows the aforementioned necessity of screw speed correlation with the melt temperature during processing. In these materials, higher Young's modulus is obtained for low screw speed at higher barrels temperature. Therefore, low melt viscosity with rather moderate shear is needed for good dispersion and for improvement of mechanical properties of the final material. This trend is present along the investigated MWCNT concentrations.

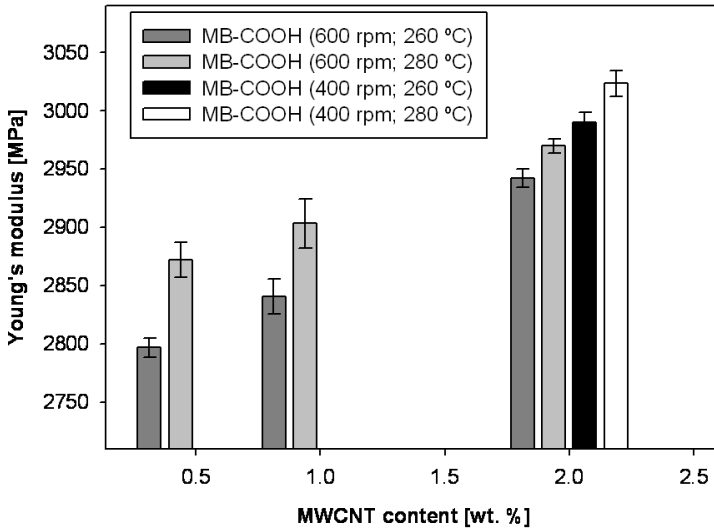


Figure 4.3.3: Young's modulus of **MB-COOH** nanocomposites processed at various conditions.

Further performance achieved for the surface oxidation of carbon nanotubes processed by masterbatch dilution method is present in Figure 4.3.4. Young's modulus and stress at a yield point for both presented parameters shows an increased mechanical performance. Moreover, slightly higher values of both parameters for **MB-COOH** material are observed, which can be related to the better morphology achieved when modified nanotubes are used (Figure 4.1.11).

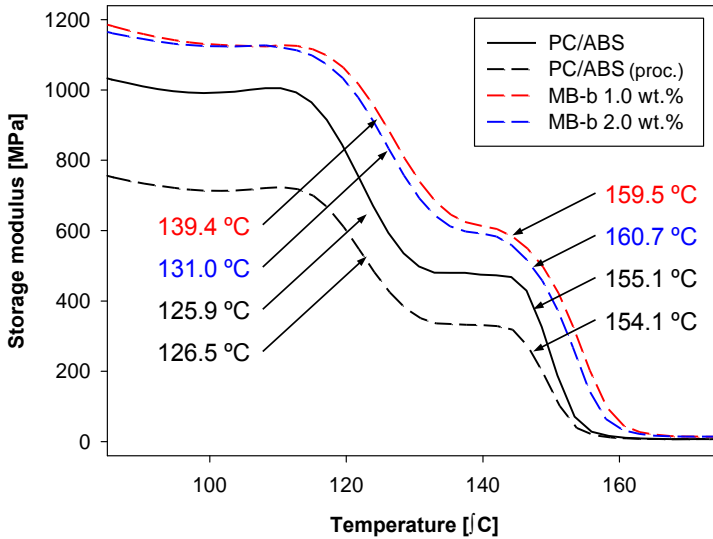


Figure 4.3.4: Storage modulus of PC/ABS and **MB-COOH** (400 rpm, 260 °C).

4.3.2. Comparison between experimental and theoretical data of the nanocomposite tensile modulus

Young modulus of polymer-based composites can be predicted with the use of Halpin-Tsai equations.^[139] Nevertheless, this method is designed to describe interactions between micro-scale fillers and matrix. Protocol regarding the significant scale difference between such fillers (*e.g.* glass fibers) and polymer chains disables direct application of Halpin-Tsai model for nanocomposite calculations. Modification of this method carried out to improve accuracy of the calculations for nanocomposites are reported in the literature.^[186-188] The most accurate fitting of the experimental data of PC/ABS-MWCNT are obtained by method A represented by Equation 4.3 and method B represented by Equation 4.4. These attempts result from the modified methods reported in literature.^[186,188]

$$(4.3) \quad E_m = k_A \frac{1 + \zeta \eta V_{CNT}}{1 - \eta V_{CNT}} E_m$$

$$(4.4) \quad E_c = F(V_f) \left[\frac{3}{8} \left(\frac{1 + \zeta \eta_L V_f}{1 - \eta_L V_f} \right) + \frac{5}{8} \left(\frac{1 + 2\zeta \eta_T V_f}{1 - \eta_T V_f} \right) \right] E_m$$

In a method A, Young's modulus is calculated with the experimental factor k_A (1.18) related to the accuracy between the experimental data and predictions. Method B is applied with the two variations of different functions $F(V_f)$ representing the accuracy coefficient.

Young's modulus of carbon nanotubes (E_f) and of PC/ABS (E_m) is 980 GPa^[188] and 2200 MPa (Table 4.3.1), respectively. Factor ξ calculated with Equation 4.4 is related to the geometry and the boundary conditions of the reinforcement and includes the aspect ratio of the individual nanotube. The volume fraction of MWCNT V_f respects densities of the nanofiller and the matrix.

$$(4.5) \quad \zeta = \frac{2l}{d}$$

$$(4.5) \quad \eta_L = \frac{\alpha \frac{E_{CNT}}{E_m} - 1}{\alpha \frac{E_{CNT}}{E_m} + \zeta}$$

$$(4.6) \quad \eta_T = \frac{\alpha \frac{E_{CNT}}{E_m} - 1}{\alpha \frac{E_{CNT}}{E_m} + 2}$$

$$(4.7) \quad \eta = \frac{K_{\omega} \left(\alpha \frac{E_f}{E_m} \right) - 1}{K_{\omega} \left(\alpha \frac{E_f}{E_m} \right) - \zeta}$$

Besides, factors η_L (Equation 4.5) and η_T (Equation 4.6) in the method B signify the efficiency of the nanofiller in the direction parallel and perpendicular to the tensile direction, respectively. In the method A this element is simplified to one factor η (Equation 4.7). Waviness coefficient K_{ω} used in the method A ranges between 0 and 1 and represents the share of force transferred by MWCNT along the central axis. Moreover, the orientation factor α related to the position of individual filler in the specimen is used during all calculations. According to the literature,^[186] α value 0.17 represents randomly oriented MWCNT, so the situation observed in the compression molded specimens.

$$(4.8) \quad F_1(V_f) = 1 - \gamma V_f$$

$$(4.9) \quad F_2(V_f) = \beta - \beta \ln(V_f)^n$$

The low accuracy of Halpin-Tsai prediction method at high MWCNT loads was reported^[106] and independently observed in PC/ABS-MWCNT. Nanofiller-matrix interactions occurring above 0.5 wt. % MWCNT need to be defined with higher precision in order to improve the accuracy of predictions. Besides, a significant increase of the agglomeration with the increase of nanofiller content is not taken into account during the calculation. Hence, the efficiency factor $F(V_f)$ (Equation 4.8 and Equation 4.9) was used to provide better fitting between the predictions and the experimental data. Factors γ , β and n are found to be 5.3, 0.1 and 2.1, respectively.

Both calculation methods described by Equation 4.3 and Equation 4.4 exhibit acceptable level of predicted data fitting with the experimental values only at low MWCNT loads. Above 0.5 wt. % MWCNT the results from method A and B are rather poor. Figure 4.3.5 shows results from modified and non-modified method A. Despite the presence of orientation factor and different values of waviness coefficient K_{ω} , the results vary from the experimental data. Relatively low value of the waviness coefficient suggests minimal orientation or straightness of carbon nanotubes. This can be related to low shear conditions during the preparation of the specimens by compression molding and therefore no orientation of individual nanotubes. Finally, the introduction of k_A factor and reduction of waviness coefficient gave satisfactory results.

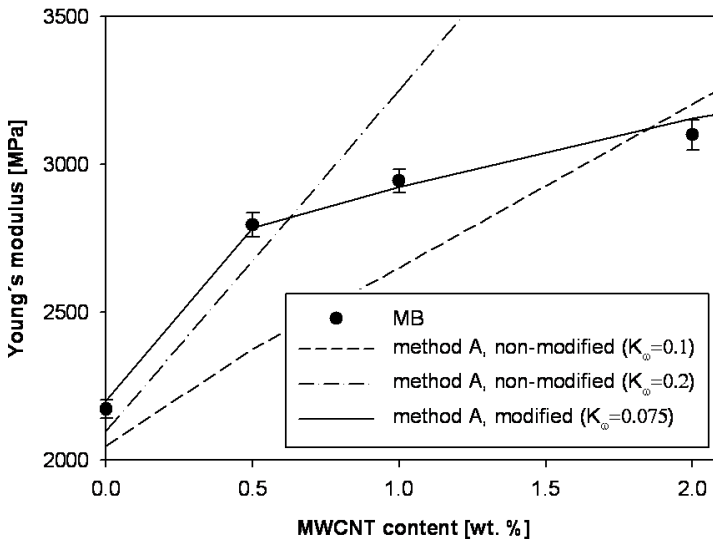


Figure 4.3.5: Prediction of Young's modulus for nanocomposites with modified and non-modified method A ($\alpha=0.17$) compared with experimental data for **MB** (400 rpm, 260 °C).

Non-modified method B pictured in Figure 4.3.6 gives equally imprecise results as method A. Nevertheless, after the incorporation of factors described with Equation 4.8 and Equation 4.9, the fitting the experimental data is improved. Coefficient $F_1(V_f)$ seems to provide results agreeing with the measured ones along the investigated nanofiller concentrations. The disagreement between the predictions and the experimental data increases with the increase of carbon nanotubes content for all applied methods. This is most probably related to the higher agglomeration. Due to this fact the load is transferred through the macrostructures rather than through the individual nanotubes reducing the importance of factors, *e.g.* related to the aspect ratio.

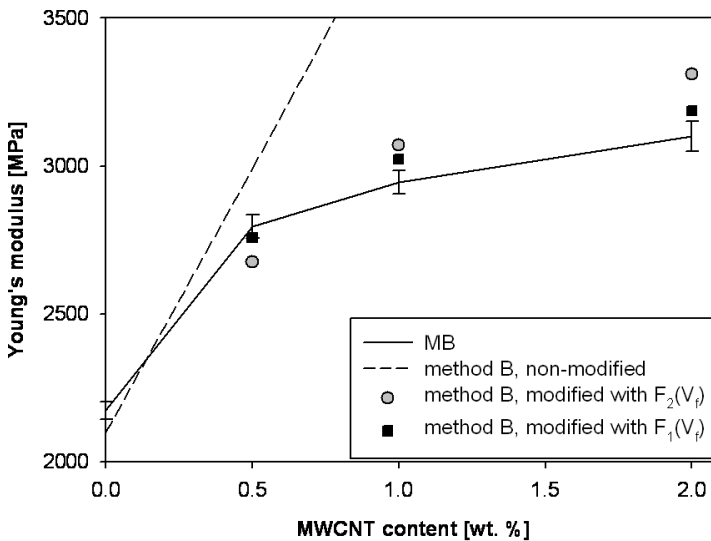


Figure 4.3.6: Prediction of Young's modulus for nanocomposites with modified and non-modified method B ($\alpha=0.17$) compared with experimental data for **MB** (400 rpm, 260 °C).

The above results show possibility of mechanical properties prediction for PC/ABS-MWCNT nanocomposites. Good agreement between experimental

data and mathematical model is achieved for modified Halpin-Tsai method. Nevertheless, further modification and standardization of this method should be carried out in order to improve the experimental data fitting.

4.4. Rheological properties of nanocomposites

Visco-elastic properties of polymeric materials are influenced by the introduction of nanofiller.^[83,106] Factors controlling this effect depend mainly on molecular weight of the macromolecules and on thermal history of the material. During the nanocomposite formation, viscosity can be controlled by the processing temperature or shear applied to the material.

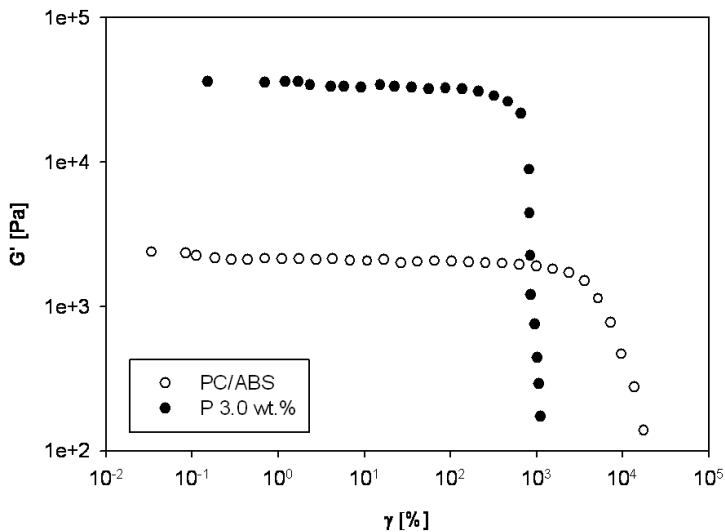


Figure 4.4.1: Strain sweep done on pure material and on nanocomposite **P 3.0 wt. %** processed at 280 °C, 200 rpm.

Pristine matrix investigated at the strain sweep mode shows constant behavior in a wide range. Besides, Figure 4.4.2 gives an indication of PC/ABS degradation during processing. Clearly decreased storage modulus

of the processed matrix is related to the shortening of polymeric chains due to the degradation.

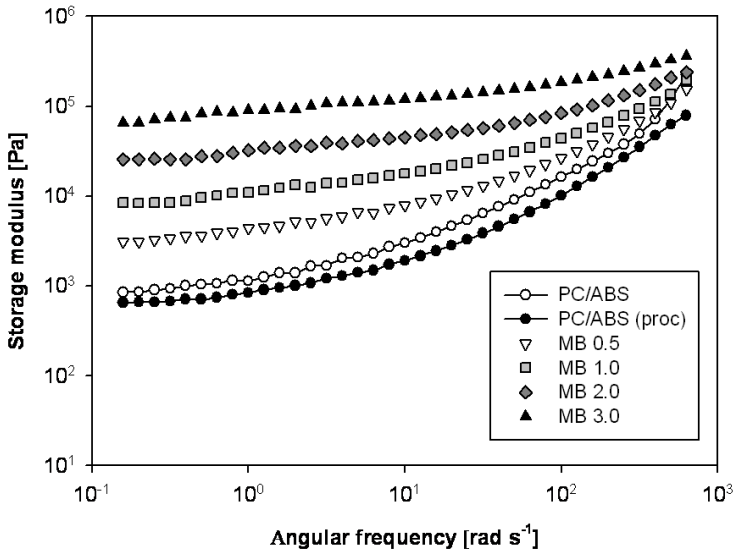


Figure 4.4.2: Storage modulus (G') as a function of angular frequency (ω) for nanocomposites processed with masterbatch dilution.

Investigation on the rheological properties of PC/ABS-MWCNT nanocomposites starts from securing the strain region with constant elastic modulus in order to provide the stable conditions during the measurements. Figure 4.4.1 shows curves for the neat matrix and the selected nanocomposite recorded at 280 °C at frequency 1 Hz. Material **P 3.0 wt. %** was selected for this test due to the high MWCNT load and to rather low shear applied during the previous processing (Figure 4.1.7). The curves are sensitive to the presence of carbon nanotubes. The effect of narrowing the *plateau* for **P 3.0 wt. %** with an order of magnitude increase of the G' values are observed. Therefore, the following tests are performed at a strain of 1.0 %, which is a compromise between the necessary low strain value and the linear viscoelastic properties of both materials.

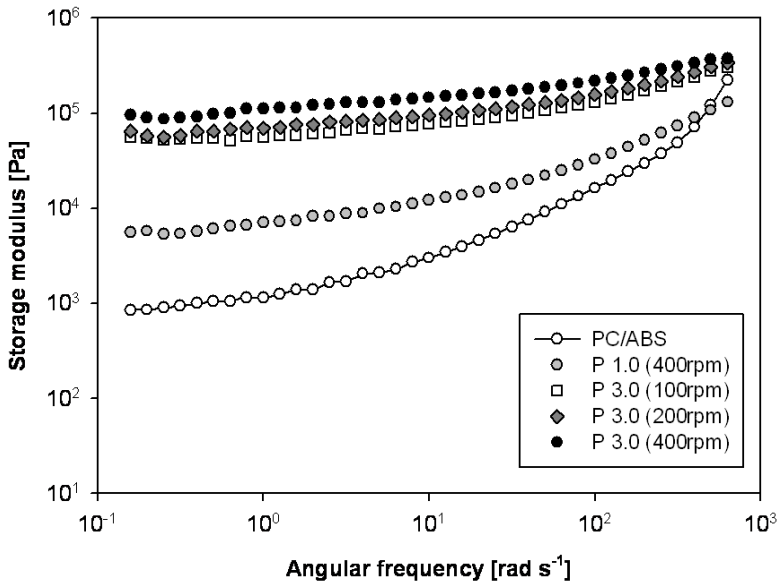


Figure 4.4.3: Storage modulus (G') as a function of angular frequency (ω) for nanocomposites processed with powder feeding.

Storage modulus of the processed PC/ABS matrix is lower than the one recorded for an as-received blend, as it is shown in Figure 4.4.2. This is caused by the reduction of molecular weight during two processing steps (the masterbatch creation and further dilution) resulting with the increased movability of macromolecules in the melt. The thermal degradation of both components of the blend occurs with the reduction of molecular weight rather than with the cross-linking.^[83,179] Even though the cross-linking appears at the initial stage of polybutadiene degradation, the content of this material in the blend is far too little to influence the rheology.^[189] The gradual increase of carbon nanotubes load causes an increase of storage modulus, giving the Bingham plastic behavior at loads 3.0 wt. % MWCNT. This can be explained by the presence of percolated carbon nanotubes network.^[153] The effect of storage modulus similarity at high frequencies

comes from the confinement of polymer chains within the carbon nanotubes network.

Carbon nanotube content and dispersion show significantly higher influence on the rheology than the processing parameters. Curves showed in Figure 4.4.3 represents the material processed by powder addition **P** at various screw speeds. The difference between processing methods can be observed between these curves and the results shown in Figure 4.4.2. The increase of storage modulus is measured at 1 rads^{-1} for **P** and **MB** with carbon nanotubes loads 1.0 wt. % and 3.0 wt. %. With an increase of MWCNT content the values changes between $10\text{e}^3 \text{ Pa}$ to $90\text{e}^3 \text{ Pa}$ and $7 \text{ e}^3 \text{ Pa}$ to $110 \text{ e}^3 \text{ Pa}$ for **P** (processed at 400 rpm) and **MB**, respectively. The tendency $G'_P < G'_{MB}$ at low frequencies and $G'_P > G'_{MB}$ at high frequencies states different nanocomposites behaviors. Good nanofiller dispersion in **MB** nanocomposite increases the relaxation time at low frequencies. This is because the carbon nanotube network does not allow free movements of polymer chains. Besides, interactions between agglomerates and macromolecules are significantly weaker than between the individual nanotubes and polymeric chains. Therefore, the **P** nanocomposite shows lower values at low rotational frequency. At higher frequencies, when the solid-like behavior is inherited, the storage modulus is higher for **P** material. This can be related to the lower degree of matrix degradation due to less processing steps. Besides, agglomerates are present along the whole test in **P** nanocomposite while in **MB** material the network of carbon nanotubes is broken.

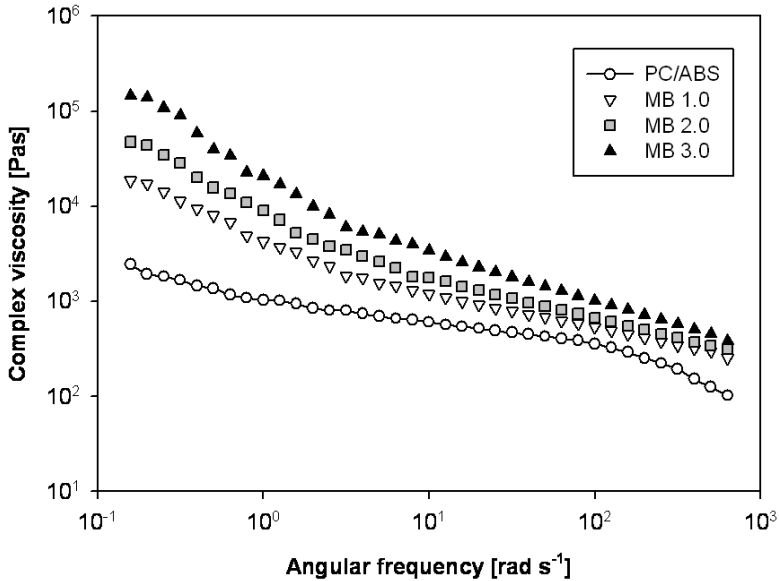


Figure 4.4.4: Complex viscosity (η^*) of nanocomposites processed with masterbatch dilution.

Additionally, changes related to the dispersion quality are observed when **P 3.0 wt.%** is processed at the various screw speeds. Even though the low shear during nanocomposite formation results with the stronger agglomeration (Table 4.1.3), storage modulus reported in Figure 4.4.3 gradually increases with the screw speed. This minor increase is in contrary with the previous findings. However, assuming the absence of well-defined carbon nanotubes network in **P** nanocomposite and clearly worse morphology than in **MB** material, this effect can be related to the degradation of PC/ABS during the processing reported in Figure 4.4.2.

$$(4.10) \quad \eta^* = \frac{G^*}{i\omega}$$

The selective filling of one component of an immiscible blend should result with the improved continuity of the components. Nevertheless, such an effect has not been reported clearly.^[1] The complex viscosity presented in Figure 4.4.4 increases with the MWCNT content. Cox-Merz rule explained in Formula 4.10 shows the origin of the complex viscosity (η^*)^[190] for the unfilled polymers. It is proved that the steady-state shear viscosity plotted against the shear rate corresponds to the complex viscosity plotted against the angular frequency (ω). This rule applies to a broad range of polymer melts.^[191] However, for the multiphase systems where the microstructure is affected by the flow, the rheological responses in dynamic and steady-shear are independent. It has been reported, that Cox-Merz rule holds for the relatively low MWCNT concentrations but becomes inaccurate above 3.0 wt. % of carbon nanotubes.^[192] Due to the characteristics of the nanocomposites based on fillers with high aspect ratio and the possible tight network formed when good morphology is obtained, the dependence of melt viscosity and MWCNT content increases at low frequencies. This is attributed to percolation of the nanofiller network inside PC and percolation of PC-MWCNT phase within the co-continuous blend.^[1] Complex viscosities in Figure 4.4.5 show stronger influence of screw speed than the effect of carbon nanotube load. This is in agreement with the observations from Figure 4.4.3. Light transmission images of **P** nanocomposites (Figure 4.1.7) showing the dependence of screw speed on the dispersion of nanofiller can be correlated with Figure 4.4.5. Despite clear improvement of the morphology with the screw speed, the impact on complex viscosity is rather minor. Moreover, the powder feeding similarly to masterbatch dilution gives the decrease of complex viscosity with an increase of rotational frequency.

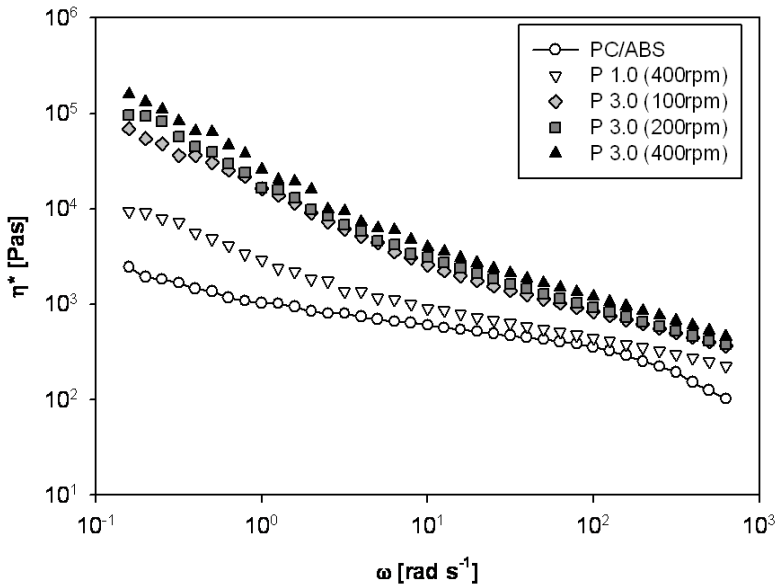


Figure 4.4.5: Complex viscosity (η^*) of nanocomposites processed with powder method.

Relationship between the dispersion of carbon nanotubes and the SME can be explained on **MB** material. Even though no significant change of the dispersion quality with an increase of MWCNT load is shown in Figure 4.1.5, the frequency sweep curve in Figure 4.4.4 shows significant change of this parameter.

4.5. Influence of carbon nanotube content on electrical properties of PC/ABS-MWCNT nanocomposites

Carbon nanotubes boost electrical conductivity of polymers many orders of magnitude changing the insulator into conductor.^[152] This can be additionally controlled with the additives and processing parameters. Electrical conductivity of PC/ABS blend (Table 4.5.1) disables any application of this material related to the electrical properties. Nevertheless, the

incorporation of MWCNT allows the aforementioned increase of electrical conductivity.^[152] Modification of nanofiller-polymer interactions gives additional benefits, *e.g.* the reduction of percolation threshold.^[193] Electrical conductivity of the pristine matrix is improved over 12 orders of magnitude with the introduction of 1.0 wt. % of MWCNT. Besides, percolation threshold^[194] is observed in PC/ABS blends. In fact double percolation threshold needs to occur, as this is the condition that must be fulfilled to reach conductivity in multi-phase blends. This phenomenon has been reported in polymers and is related to the formation of conductive network of the nanofiller in the hosting phase and to the continuous character of this phase in the blend^[195-196] (in PC/ABS case polycarbonate is considered as the main phase).

Table 4.5.1: Surface and volumetric electrical conductivities of PC/ABS and selected nanocomposites.

Material	[wt. %]	Processing		Electrical conductivity	
		[rpm]	[°C]	$\rho_s^{(1)}$ [S]	$\rho_v^{(2)}$ [S cm ⁻¹]
PC/ABS	-	-	-	5.7e-15 (± 1.2e-13)	6.3e-13 (± 1.6e-12)
P	2.0	100	280	9.6e-3 (± 0.5e-4)	4.1e-2 (± 0.2e-3)
P	2.0	200	280	2.8e-2 (± 1.1e-4)	6.0e-2 (± 2.3e-4)
P	3.0	200	280	3.1e-1 (± 3.1e-3)	3.9e-1 (± 1.8e-3)

⁽¹⁾ surface electrical conductivity; ⁽²⁾ volumetric electrical conductivity

Powder feeding-based processing method **P** gives rather poor morphology (Figure 4.1.7). Up to three orders of magnitude lower values of electrical

conductivity are the result of agglomeration of the nanofiller over the formation of the conductive network. Nevertheless, the processing methods influence can be observed in these materials. The increase of electrical conductivity between **P 2.0 wt. %** processed at 100 rpm and 200 rpm can be also explained with the morphology improvement at higher shear. At higher screw speeds better dispersion of carbon nanotubes is achieved and the quality of conductive network is improved.

Figure 4.5.1 shows the electrical percolation above 2.0 wt. % carbon nanotubes for the material formed in masterbatch dilution method **MB**. This observation can be understood as a confirmation of the presence of MWCNT in ABS phase. Regarding the amount of ABS phase in the blend and the fact of MWCNT presence in PC, the percolation should appear at lower nanofiller loads if all carbon nanotubes are located in the main blend component. Besides, Figure 4.5.1 shows slightly better electrical properties when the nanocomposite is obtained at lower processing temperatures. Such an effect is explained by the aforementioned relation between the dispersion quality and the melt viscosity. Possibly, co-continuous structure of the polycarbonate affected by the processing parameters should be studied. The latter parameter needs to be selected to maintain the balance between the ability of agglomerates melt penetration and the ability to break the agglomerates by shear transfer.

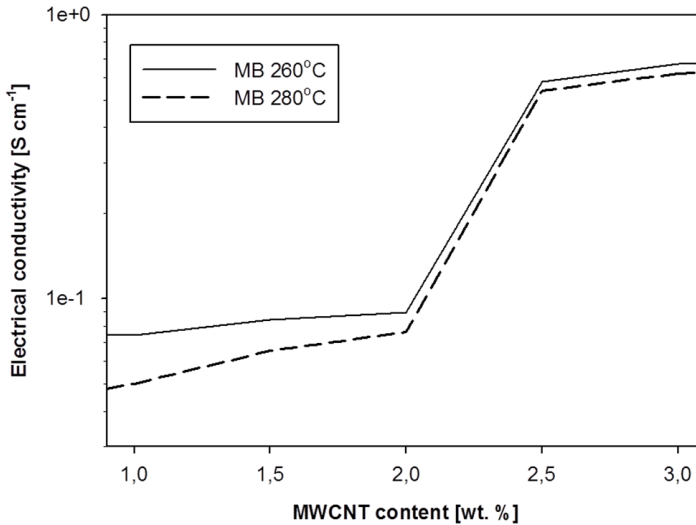


Figure 4.5.1: Volumetric electrical conductivity of selected nanocomposites processed at 400 rpm.

On the other hand, the incorporation of carbon nanotubes after their covalent modification results with the decrease of electrical conductivity when compared to pristine MWCNT (Figure 4.5.2). Carboxylic groups present on the surface of individual carbon nanotubes destroy the charge carrier paths. These electron paths are located mainly on the outer shell of the individual MWCNT. Moreover, the surface oxidation forming functional groups mainly on the ends of the individual nanotube (Figure 4.1.9a) creates the hindrance for the possible connections and formation of the network. The recognized carbon nanotube connections tip-tip, wall-tip and the most probable wall-wall are disturbed. This elevates the energetic barrier for the charge transfer between two individual, interconnected nanotubes. Such an effect is observed as the low electrical conductivity of the nanocomposite. Simple surface-oxidation of carbon nanotubes as nanofiller cannot be applied in the formation of highly-conductive nanocomposites.

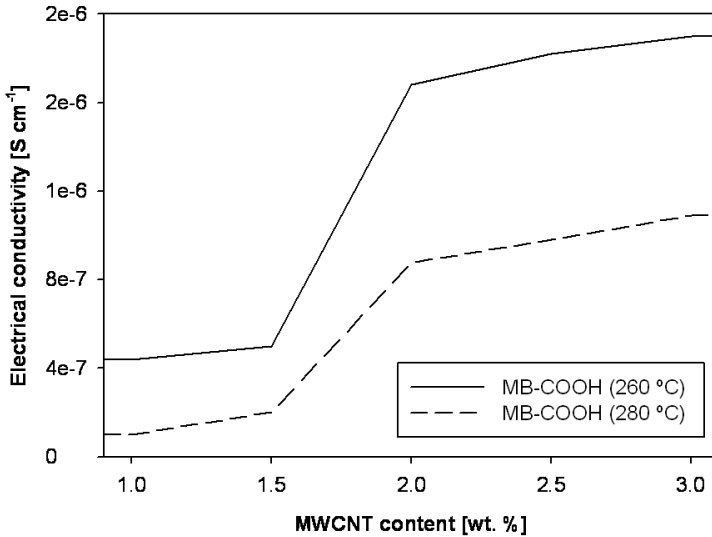


Figure 4.5.2: Volumetric electrical conductivity of nanocomposites filled with MWCNT-COOH.

Nevertheless, the percolation threshold for MWCNT-COOH is observed at lower nanofiller concentrations than for the analogous **MB** material, what can be related to the better dispersion. The change of MWCNT location in the blend due to the change of nanofiller-polymer interactions with surface oxidation of MWCNT plays a key role in this phenomenon, too. Besides, the influence of processing temperature is investigated for this nanocomposite revealing the lower electrical conductivity for material formed at higher temperature. Such dependence of the morphology on the processing temperature is explained by the effect of efficient energy for agglomerates breakage. At higher barrels temperature the required SME cannot be reached and the nanotubes network is fully formed.

4.6. Preliminary conclusions

Preliminary conclusions after twin screw extrusion gives insight into the performance obtained with various processing method at various conditions.

Table 4.6.1: Summary of PC/ABS-MWCNT nanocomposites (processed with powder addition method) performance; behavior relates to the increase of parameters defining columns.

Property	MWCNT load	Melt temp.	Screw speed ⁽¹⁾
<u>Powder Addition (P)</u>			
Dispersion quality	▼▼	NA	▲▲
Thermal stability	▲	NA	▲
Mechanical	▲	NA	▲
Melt viscosity	▲▲	NA	▲
Electrical	▲▲	NA	▲▲
<u>Masterbatch dilution (MB) / (MB-COOH)</u>			
Dispersion quality	▼ / ▼	▲ / ▼	▲▲ / ▲
Thermal stability	▼ / ●	▼ / ▼	● / ▼
Mechanical	▲▲ / ▲	▲ / ▲▲	▲ / ▼▼
Melt viscosity	▲▲ / ▲▲	▼ / ▼	▲ / ▲
Electrical	▲▲ / ▲▲	▼ / ▼	▲ / ▲

⁽¹⁾ performance relates mainly to higher values of the parameter; ▲▲/▼▼ – significant increase/decrease of value, ▲/▲ – moderate increase/decrease of value, ● – no significant or not defined change.

Conclusions summary is present in Table 4.6.1. Melt mixing of immiscible PC/ABS blend with commercial multi walled carbon nanotubes results with the similar material behavior. Nevertheless, the dispersion quality decreases more with MWCNT load for **P** materials than for **MB** nanocomposites. Besides, the thermal stability seems to increase with the carbon nanotubes

load for **P** but decrease for the other reported materials. Covalent modifications of the nanofiller show some differences in dispersion and thermal stability dependence to processing conditions as well. Screw speed seems to be the crucial factor influencing the final properties.

4.7. Selection of samples with the best balance of properties

Samples with the best balance of properties after the common extrusion method or the samples expected to show required results after the injection molding step are selected.

The nanocomposites **MB** with the pristine carbon nanotubes are selected in order to perform the investigation on the common industrially accepted method with commercial materials. The study is aimed also towards the influence of carbon nanotube content and processing conditions during the nanocomposite formation on the final properties of injection molded specimen.

Furthermore, **P 5.0 wt. %** is selected in order to investigate direct masterbatch dilution in the injection molding process. It is expected to observe the application of the shear during the dilution of masterbatch in the forming process rather than in extrusion.

5. Modification of conventional melt mixing

Common method of nanocomposites formation by twin screw extrusion gives homogeneous morphologies, described in Chapter 4. Nevertheless, attempts to improve the two-step masterbatch dilution gave the solvent-assisted MWCNT addition method. Feeding the suspension of carbon nanotubes in ethyl alcohol instead of pristine MWCNT was carried out in order to decrease the primary agglomeration coming from the nanofiller production. This method, despite removing the two-step processing limitation, is based on the idea of the primary MWCNT agglomerates breakage before the introduction of carbon nanotubes into the nanocomposite. Formation of the suspension of carbon nanotubes in ethyl alcohol provides relatively good penetration of primary agglomerates by the solvent and the transfer of mixing energy to these agglomerates through the solvent before twin-screw extrusion. The use of solvent is selected in order to provide mild conditions of agglomerates breakage with minimal shortening of carbon nanotubes. Besides, ethyl alcohol is a compromise of low-hazardous solvent with low boiling point, providing relatively stable carbon nanotube suspensions.

5.1. Study of PC/ABS-MWCNT nanocomposites morphology

5.1.1. Influence of nanocomposite processing on the morphology of PC/ABS-MWCNT nanocomposites

Twin-screw extrusion combined with a carbon nanotube-ethyl alcohol suspension feeding gives the reduction of the number of processing steps. At the same time similar level of the nanofiller dispersion is maintained. Furthermore, the control of screw design and shear with the temperature and screw speed occurs,^[58,158-159] making this method similar to the common

masterbatch dilution processing. Specific Mechanical Energy in the process is generally lower for the suspension-based method than for the masterbatch dilution method in the whole range of studied parameters. Explanation of such behavior can be related to the presence of ethyl alcohol in the system, which decreases viscosity of the melt influencing the torque necessary for achieving defined screw speed.

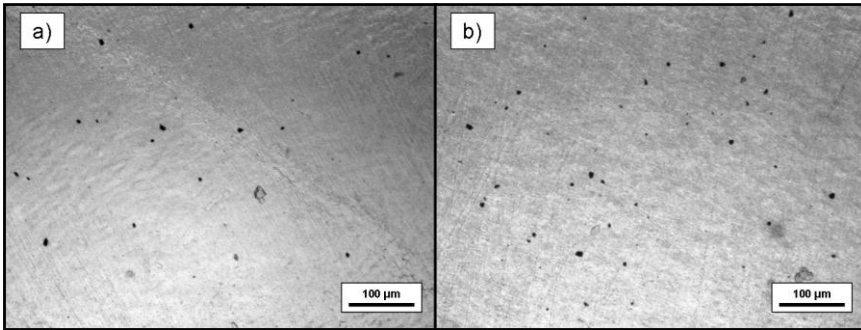


Figure 5.1.1: Light-transmission microscopy image of nanocomposites processed by suspension method (**S**) at 260 °C with 400 rpm: a) 1.0 wt. % MWCNT, b) 3.0 wt. % MWCNT.

A slight decrease of carbon nanotubes dispersion quality is achieved with the advantage of the reduction of one processing step and elimination of the direct nanomaterials handling during the processing. Figure 5.1.1 shows OM images of nanocomposites with various carbon nanotube concentrations formed with suspension method. Similar agglomeration is present in both concentrations: 1.0 wt. % (Figure 5.1.1a) and 3.0 wt. % MWCNT (Figure 5.1.1b). Nevertheless, there is a slight agglomeration increase when MWCNT load increases. This phenomenon is stronger for suspension method, while in the masterbatch dilution, the increase of carbon nanotubes load (within the studied range) is rather insignificant. Perhaps, double processing applied

in the **MB** method is responsible for this effect having higher significance on the material quality than processing with ethyl alcohol.

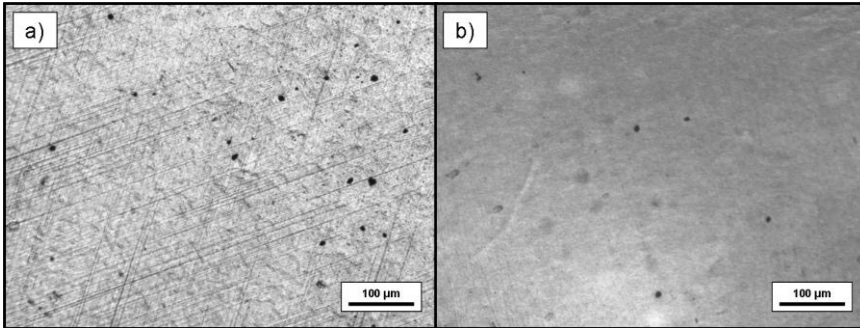


Figure 5.1.2: Light-transmission microscopy image of nanocomposites (2.0 wt. % MWCNT) processed by suspension method (**S**) with 400 rpm: a) 240 °C, b) 260 °C.

Mainly the influence of barrels temperature during the extrusion as a morphology determining parameter was investigated in this study. This is due to the minor influence of screw speed, probably influenced by the presence of ethyl alcohol. Commonly, the processing temperature needs to be selected together with the screw speed (and possibly with the screw design) to give the desired influence on the SME. High temperatures decrease the melt viscosity, so higher shear will be obtained at the same screw speed but at lower temperatures. However, below some defined temperature value, especially at the beginning of the screw, the polymer is not melted completely which can result in incomplete agglomerates penetration by the matrix giving poor morphology of the final material. Light-transmission micrographs of the nanocomposite with 3.0 wt. % MWCNT processed with suspension method at various temperatures in Figure 5.1.2 show the improvement of morphology with the increase of temperature. At 260 °C the agglomerates appear in significantly lower

number and with the narrow size distribution. Such a minor agglomeration behavior in the suspension method even at relatively high MWCNT concentrations allows the investigation of slight changes appearing with the variations of temperature.

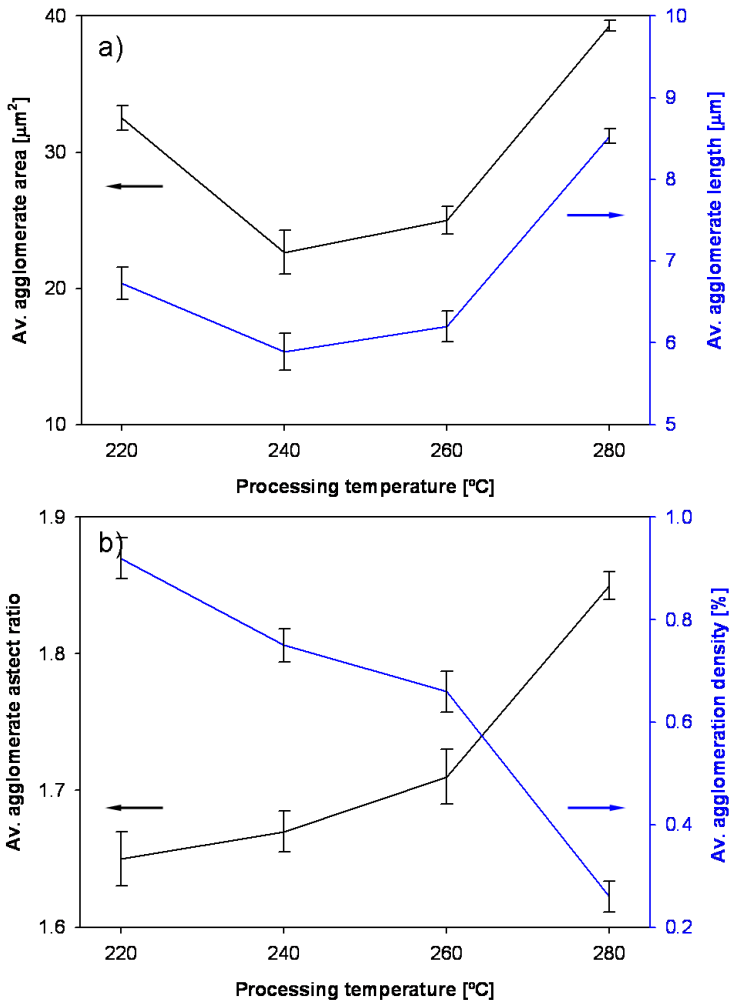


Figure 5.1.3: Agglomerates size distribution in nanocomposite with 1.0 wt. % MWCNT processed by suspension method **S** at 400 rpm.

Observed behavior of the nanocomposite obtained by suspension method varies from the materials processed by powder addition or masterbatch dilution methods (usually the decrease of agglomeration with an increase of melt temperature at the same screw speed). Therefore, more attention needs to be given to the role of ethyl alcohol in the process.

The residual alcohol introduced into the system during the suspension method acts as a plasticizer changing the viscosity of the polymer melt. Nevertheless, the amount of residual solvent is determined by thermogravimetric analyses at the average below 1.0 wt. % of the specimen. This results with significantly lower ability of the system to transfer the energy that helps to break the agglomerates. Nevertheless, penetration of the agglomerates by the used solvent and the polymer melt seems to be improved. This effect is responsible for the observed decrease of the agglomeration at higher processing temperatures: reduced viscosity (related also to the change of the physical state of the solvent) along with the plasticizing effect of the solvent, helps to improve the final morphology of the nanocomposite. However, a slight negative impact on several properties is observed when ethyl alcohol-assisted nanofiller feeding is employed.

Detailed investigation of the agglomeration behavior responding to the changes of processing temperature is shown on the nanocomposite with a lower concentration of carbon nanotubes, 1.0 wt. % MWCNT, but the same behavior exists for the other concentrations of carbon nanotubes. Figure 5.1.3a presents curves of the agglomerate area and the length at the applied barrels temperatures. A strong decrease of agglomerates area and length is observed with the change from 220 °C to 240 °C, while the increase of these parameters is present between 260 °C and 280 °C. This behavior is characteristic for the suspension method and not obvious in powder feeding or masterbatch dilution. The effect can be related to the aforementioned dependence of melt viscosity on barrels temperature. The

optimal conditions regarding melt viscosity at present concentration of ethyl alcohol provide best agglomeration results at moderate barrels temperatures. This behavior was not observed in OM images (Figure 5.1.2). The addition of ethyl alcohol is understood as an aforementioned introduction of a plasticizer to the system, even though it is expected to evaporate during the processing. This effect, along with the decrease of MWCNT agglomeration degree before the feeding, is responsible for the dispersion improvement up to the middle-high temperature. On the other hand, the gradual increase of the agglomerate aspect ratio (Figure 5.1.3b) indicates the change of agglomerate shape with the increase of processing temperature. Lengthening the agglomerates at higher temperatures can be explained with the higher impact of the rotational movement of the screws at these conditions. However, the most significant parameter describing the state of the dispersion, the average agglomeration density presented in Figure 5.1.3b, clearly shows the decrease of the ratio between the global agglomerate area and the total investigated area. In this regard, the increase of barrels temperature during the suspension feeding in nanocomposite formation results with the decrease of agglomeration behavior, even though the relation of the size and shape of individual agglomerates with the temperature is not linear. Concluding, it seems that the best processing conditions for the solvent-assisted nanocomposite processing is moderate barrels temperature. Screw speed is a parameter of a minor importance due to the presence of solvent affecting melt viscosity.

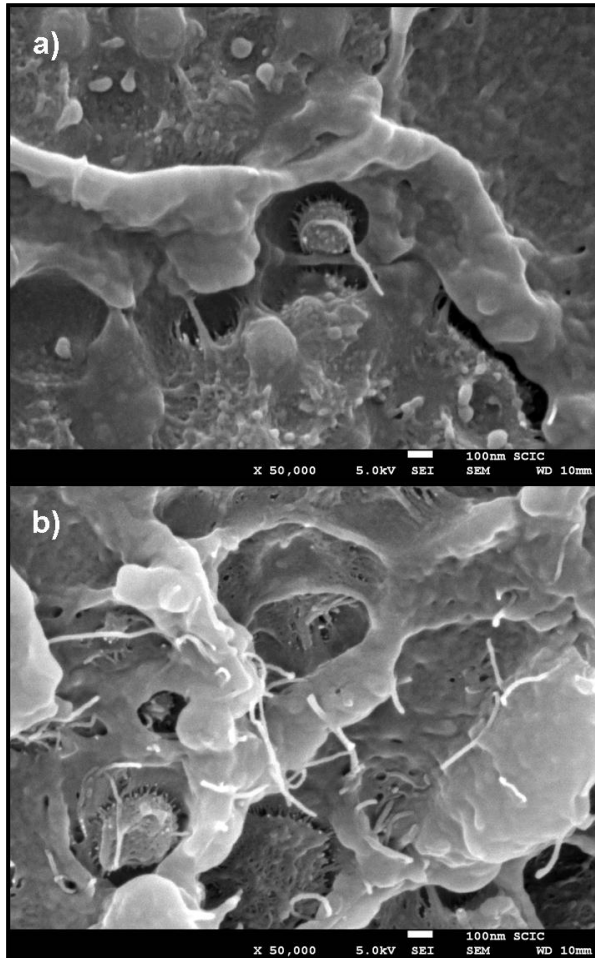


Figure 5.1.4: SEM micrograph of nanocomposite processed by suspension method at 280 °C with 400 rpm: a) 1.0 wt. % MWCNT, b) 2.0 wt. % MWCNT, polycarbonate phase with carbon nanotubes.

Observation of no significant changes of carbon nanotubes location between the main phases of the blend was made on suspension processing method. Polycarbonate is the main phase filled with the nanofiller, similarly to the masterbatch dilution and powder addition methods. Nevertheless, clearly higher presence of the nanofiller in the polybutadiene phase occurs in

solvent-assisted method of nanocomposites production. Figure 5.1.4a shows such an effect of the individual carbon nanotube located in the polybutadiene sphere. Such a coexistence of MWCNT and polybutadiene is observed in high number of micrographs. Therefore, this seems to be the common behavior independent on the processing parameters and understood as the nanofiller-matrix interaction change by the incorporation of solvent. The majority of multi-walled carbon nanotubes are still preferentially located in the polycarbonate as it is shown in Figure 5.1.4b. This is thermodynamically favored and occurs in also in masterbatch dilution and powder addition methods (Figure 4.1.7).^[152,197]

Table 5.1.1: Raman spectroscopy shifts of characteristic MWCNT bands in pristine nanofiller and in nanocomposites processed with solvent-assisted method and masterbatch dilution method.

Material	Band shift [cm^{-1}]	
	D band	G band
MWCNT	1339	1575
S (2.0 wt.%, 400 rpm)	1350	1605
MB (2.0 wt.%, 400 rpm)	1347	1599

Improved morphology in the suspension-based processing was proved also by Raman spectroscopy measurements. The up-shift of D- and G-band of the pristine carbon nanotubes occurs with the improvement of the dispersion quality and the related agglomerate size reduction between the processing methods (Table 5.1.1). The shift recorded for nanocomposite obtained by suspension method with 2.0 wt. % MWCNT processed at 400 rpm shows 1350 cm^{-1} and 1605 cm^{-1} for D- and G-band, respectively. That shows the difference between the pristine nanofiller and the **S** nanocomposite in the range of 2.0 % (while 1.0 % is recorded for **MB** and for **P** materials). Higher

values of D- and G-band shifts for solvent-assisted method than for masterbatch dilution can be interpreted as an increase of the number of individually dispersed carbon nanotubes, not obvious in OM images.

5.1.2. Influence of MWCNT modification on morphology of PC/ABS nanocomposites

Non-covalent modification of multi-walled carbon nanotubes are based on the introduction of the commercial surfactant changing the interactions between the phases of the nanocomposite. Figure 4.1.8 presents the possible interactions between the additive and the nanofiller. The difference with covalent modification (the surface oxidation of MWCNT studied in the Chapter 4) is related to the absence of the chemical bonds and is theoretically maintaining the untouched surface of individual nanotubes. The change of the nanocomposite behavior was observed in nanocomposites with **S-Triton**, due to the physical absorption of surfactant molecules on MWCNT, decreasing the surface tension.^[166] This reduces the agglomeration behavior by modulating the Van der Waals attraction forces between the individual nanotubes. Figure 4.1.8b-d shows the supposed surfactant absorption mechanisms. Examples a) presenting the encapsulation of the individual nanotube and d) with the random adsorption of surfactant molecules are the most probable for the applied MWCNT. Nevertheless, the situation present in Figure 4.1.8d was reported when surfactant is used.^[198]

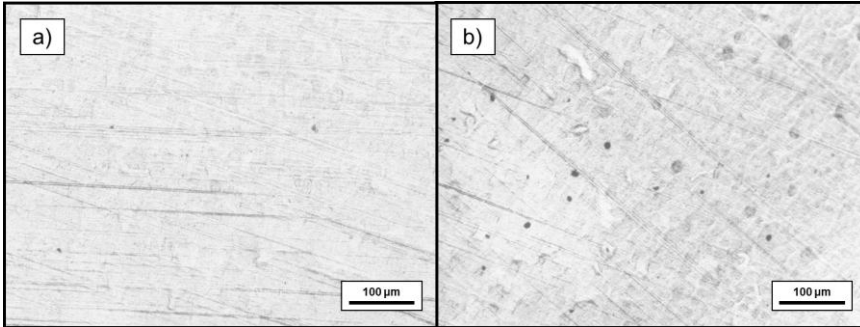


Figure 5.1.5: Light-transmission microscopy image of nanocomposites processed by suspension method with surfactant (**S-Triton**) at 260 °C with 400 rpm: a) 1.0 wt. % MWCNT b) 2.0 wt. % MWCNT.

Non-covalent modification was carried out with the suspension method by the addition of **S-Triton**. The stability of the suspension before feeding seems to be the crucial factor and can be related to the effectiveness of the surfactant. Commonly provided parameter characterizing the surface-active substances is the foam height showing good results for the applied *Triton X-100*. (Table 3.1.3). The stability of the surfactant in this test can be extrapolated to the overall effectiveness of surfactant. Van der Waals forces stabilize the interactions with carbon nanotubes preventing the agglomeration. These observations agree with the OM images present in Figure 5.1.5. The influence of surfactant on the morphology of nanocomposites shows strong decrease of MWCNT agglomeration, this indicates the correlation of the foam height parameter with the morphology of the nanocomposite.

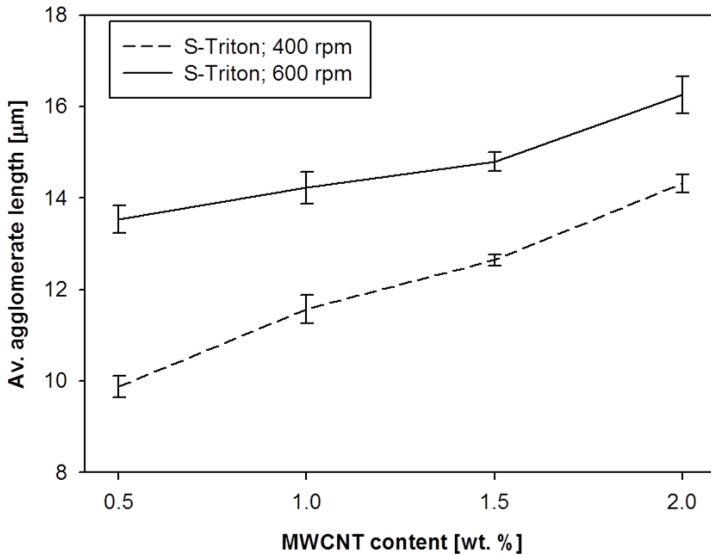


Figure 5.1.6: Dependence of the average agglomerate length on screw speed for **S-Triton** formed at 260°C.

Influence of the nanofiller content for the investigated physical modification of carbon nanotubes shows the increase of the agglomerate length at elevated MWCNT loads (Figure 5.1.6). Nevertheless, such behavior is expected for applied modification. The influence of processing on the effect of surfactant addition was investigated mainly on one processing parameter. The influence of screw speed is studied along the MWCNT loads, revealing the increase of agglomerate length at higher speed (slightly reduced at elevated nanofiller loads). This can be explained by the influence of screw speed on melt viscosity. The general improvement of morphology for **S-Triton** observed in the light-transmission microscopy imaged can be concluded as the decrease of agglomerates number rather than the decrease of their size. Nevertheless, the agglomerates observed after the non-covalent modification of the nanofiller are slightly larger than for the non-modified carbon nanotubes (Figure 5.1.3).

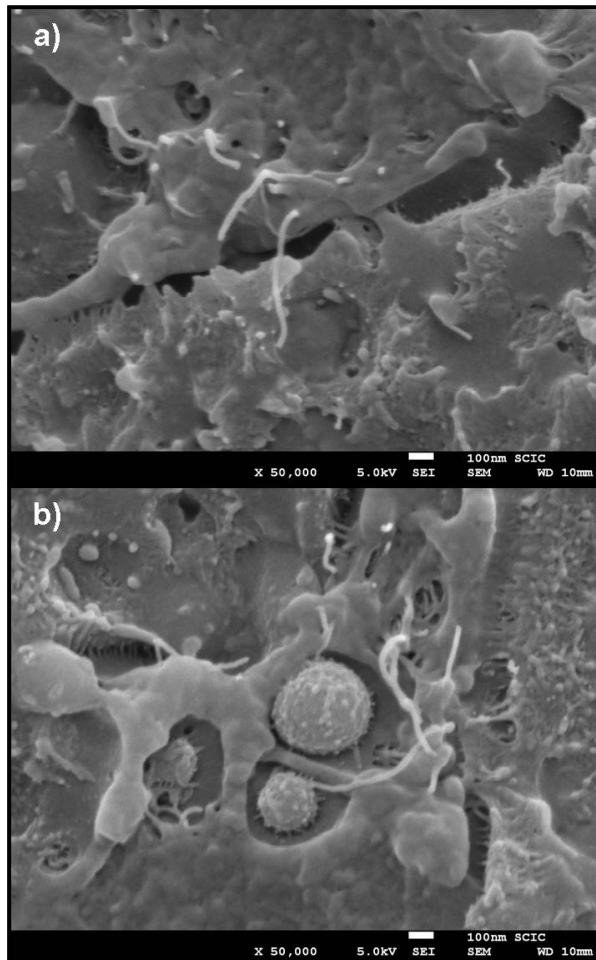


Figure 5.1.7: SEM micrograph of nanocomposite **S-Triton** with 1.0 wt. % MWCNT processed at 260 °C with 400 rpm.

Control of carbon nanotubes localization in the main phases of PC/ABS by the solution processing with surfactant shows the increased MWCNT location in the interfacial region. This is confirmed by SEM and present on the micrographs (Figure 5.1.7a). Carbon nanotubes are located also in polybutadiene phase (Figure 5.1.7b). Nevertheless, the affinity of carbon

nanotubes to PC phase after the non-covalent modification remains almost unchanged. Difference between the effects of surfactant on the nanocomposite is related to the differences in the surface tension and polarity (Table 3.1.3). The difference of surface tensions between the matrix and carbon nanotubes for the nanocomposite with and without surfactant suggests the possible change of MWCNT location after the modification. The following decrease of interfacial tension between ABS-MWCNT is expected for the used surfactant. The individual carbon nanotube wrapped with the surfactant molecules show improved wetting coefficient towards both components of the blend, though. Therefore, no particular change in carbon nanotubes affinity to any component of the blend was further studied.

Observation made in TEM micrographs of the nanocomposites obtained by the suspension method shows the possibility to distinguish PC and ABS (Figure 5.1.8). This is possible even though no staining agent was used. Such behavior is related to the residual MWCNT catalyst in the solutions with ethyl alcohol acting as a contrast agent during compounding. Metal complexes present in the commonly used contrast agents (OsO_4 , RuO_4 , $(\text{NH}_4)_2\text{MoO}_4$, FeCl_3) and in the catalysts usually used for MWCNT formation with CCVD method (TiO_2 , MgO , Ni-Mo, $\text{Fe}^{[199-200]}$) have similar chemical behavior. Moreover, the MWCNT used in this project are an industrial grade-material carrying some amount of catalyst, while the contrast agent is usually used at relatively low concentrations (2 %^[201]).

The change of carbon nanotubes location in the blend after the non-covalent modification is present in Figure 5.1.8b. Carbon nanotubes in Figure 5.1.8a are relatively homogeneously dispersed in the whole polycarbonate component, while in Figure 5.1.8b MWCNT are located mainly in the interface region. It seems that the surfactant changes the interaction MWCNT-polymer rather than MWCNT-MWCNT, as the nanofiller tends to be more bundled in **S-Triton** 1.0 wt. % MWCNT. Nevertheless, there are rather

loose agglomerates of different appearance to these observed after the powder addition or masterbatch dilution processing methods. This is an improvement of the primary agglomerates penetration. The nanofiller is present in a low quantity in ABS and in the interface region, which confirms the change of the affinity only to one phase after the non-covalent modification of the nanofiller. However, the size of bundles below 400 nm confirms better MWCNT dispersion than in the powder method (Table 4.1.2) and in the neat solution feeding (Figure 5.1.3).

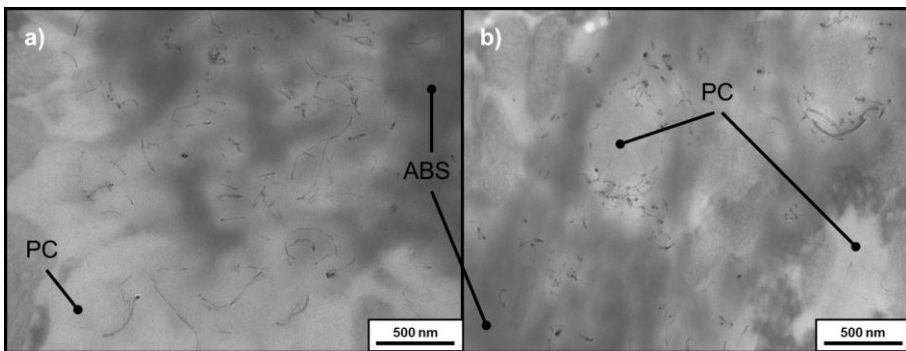


Figure 5.1.8: TEM micrograph of nanocomposites (1.0 wt. % MWCNT) processed at 260 °C with 600 rpm a) **S**, b) **S-Triton**.

5.2. Study of thermal properties of nanocomposites processed by suspension method

5.2.1. Thermal stability of nanocomposites

Suspension feeding providing higher homogeneity than the other researched methods shows analogous thermal degradation behavior to powder feeding of masterbatch dilution method. Figure 5.2.1 show the influence of MWCNT content on the thermal stability of the nanocomposites. Formation of the nanocomposite causes the upshift of the weight derivative for ABS and the opposite action for polycarbonate phase. Such behavior is related to the

uneven division of carbon nanotubes between both phases of the matrix and is independent on nanofiller concentration. Besides, peak intensity varies for ABS phase at different MWCNT loads, which can be understood as the dependence of this phase filling.

The difference between the decomposition temperatures of PC and ABS is observed for materials formed at various processing conditions (Figure 5.2.2). Nevertheless, the decrease of weight derivative maximum (DTG curves) with the formation of the **S** nanocomposite occurs for PC phase and similar increase for ABS phase. Such behavior can be related to the parameter enclosing the degree of matrix degradation during the processing and the final morphology. Furthermore, the aforementioned difference in filling of both phases at various conditions can cause such a behavior.

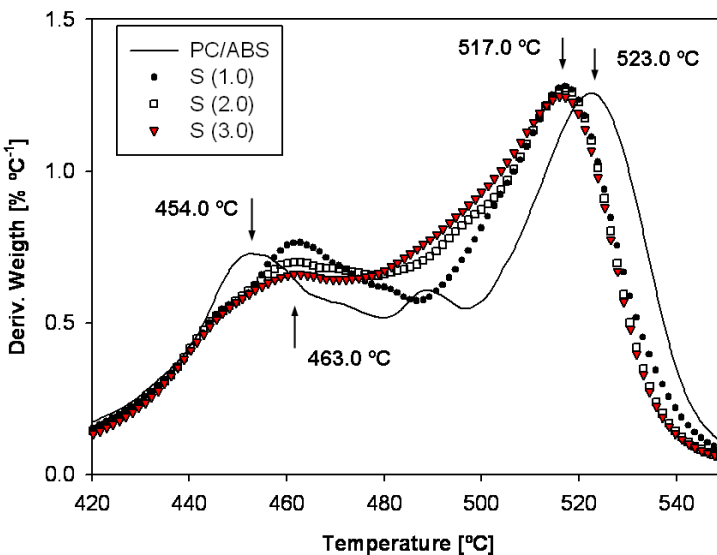


Figure 5.2.1: Weight derivative (DTG curves) for nanocomposites processed at (400 rpm) by suspension method **S**.

Basing on the aforementioned findings, decrease of thermal stability for PC occurs for higher MWCNT content in this phase. Results in Figure 5.2.2 can

be related to the change of MWCNT location to ABS phase with the decreased processing temperature, though. Additionally, the increase of values for ABS present in Figure 5.2.2 agrees with general increase of the thermal stability of this phase at higher MWCNT contents (so also higher MWCNT loads in ABS).

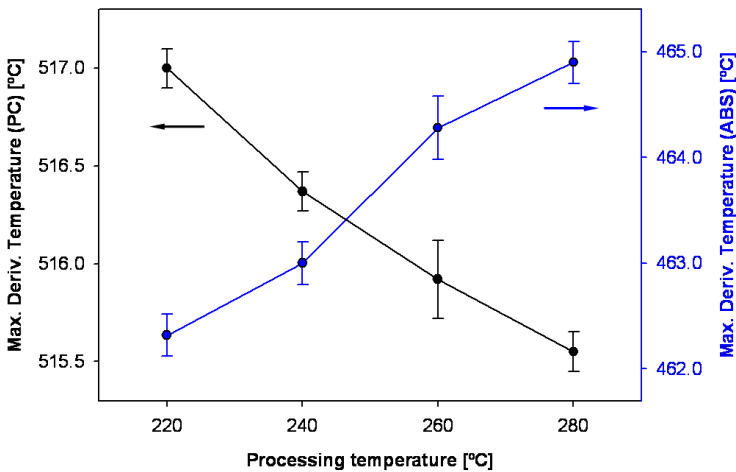


Figure 5.2.2: Dependence of the position of temperature derivative peak maximum on the processing temperature for nanocomposite formed with suspension method with 2.0 wt. % MWCNT .

Interactions between the blend components and the nanofiller are changed when the surfactant is introduced in suspension method. Figure 5.2.3a shows clear decrease of the thermal decomposition temperature for ABS with screw speed increase for surfactant. Nevertheless, the non-covalent modification providing better morphologies results with the increased thermal stability of both blend components. However, the influence of carbon nanotubes load seems to be much stronger in ABS phase than in PC presented in Figure 5.2.3b. The behavior regarding the screw speed differs between the phases and polycarbonate exhibit higher stability at lower shear.

These observations confirm the morphology dependence on the thermal stability. However, non-covalent modification of carbon nanotubes gives different results than the powder addition method (Figure 4.2.2). Increase of the screw speed for nanocomposites processed by powder addition method gives the stability increase in both blend components, while in the presence of ethyl alcohol only polycarbonate shows improved values at higher screw speeds. Besides, this behavior is opposite to the one observed in Figure 5.2.3, which can be related to slight increase of MWCNT in ABS phase at lower screw speeds. These observations confirm that it could be possible to control MWCNT location in blend components with surfactant addition. This could happen by the increase of the MWCNT load at low temperatures and at low screw speed.

Change of the feeding method to the solvent-assisted results with no significant influence on glass transition temperature of PC but the decrease of this value for ABS (Figure 5.2.4). This can be correlated with the decrease of ΔC_p for PC and ABS when the nanofiller load is increased (Figure 5.2.5). Such a behavior differs at various processing temperatures showing the higher dependence of ABS phase on the temperature during the nanocomposite formation. Highest ΔC_p for ABS is observed at 220 °C, while the mid-range barrels temperature gives lower value. This can be related with the quality of nanotube network formed in this phase (or presence of individually dispersed nanofiller) and agrees with the previous findings and the statement regarding MWCNT agglomeration behavior. The dispersion quality affects the mobility of polymer chains. Therefore, the mid-range processing temperatures show the improved morphology in nanocomposites processed by suspension method, which is confirmed by the lower ΔC_p caused by the stronger interactions between polymer chains and nanotube network. The fact of absence of such strong behavior in PC phase can be concluded as an increased feeling of ABS phase in the mid-range processing

temperatures. Moreover, ABS seems to be more sensitive for changes than polycarbonate.

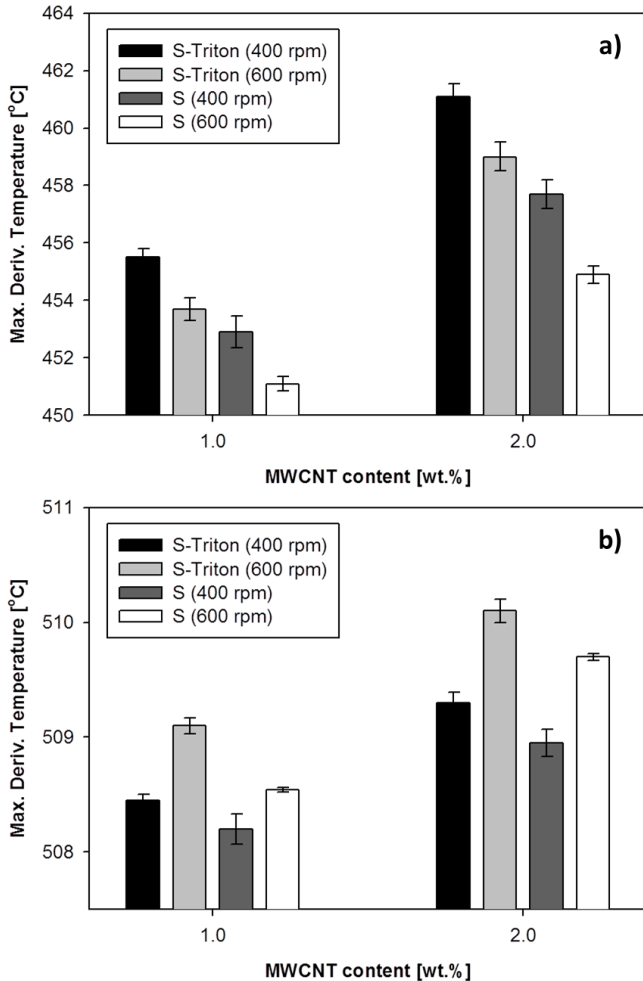


Figure 5.2.3: Temperature derivative peak maximum for nanocomposite **S** and **S-Triton** for blend components: a) ABS, b) PC.

Non-covalent modification of carbon nanotubes present in Table 5.2.1 confirms clearly better morphology of **S-Triton** than for **S** nanocomposites, explained earlier (Figure 5.1.2 and Figure 5.1.5). The former nanocomposite

shows the lower ΔC_p values for ABS component, with no significant change observed when MWCNT load increases. In the same time, the specific heat for PC slightly increases. **S-Triton** (compared to **S**) shows lower ΔC_p for ABS but higher for PC phase, with the additional lower dependence of ABS phase on the screw speed. The surfactant gives higher MWCNT loads in ABS phase, which can be understood from the theory of the decrease of polymer chains mobility (related to the decrease of ΔC_p) for more perfect MWCNT network (or lower carbon nanotubes load). Analysis of the processing parameters dependence on heat capacity does not reveal the significance of screw speed.

Table 5.2.1: Change of heat capacity (ΔC_p) at glass temperature for selected **S-Triton** nanocomposites formed at 260 °C.

Screw speed	MWCNT [wt. %]	ΔC_p [J g ⁻¹ deg ⁻¹]	
		PC	ABS
S-Triton, 400 rpm	1.0	0.148	0.064
	2.0	0.149	0.054
	3.0	0.158	0.052
S-Triton, 600 rpm	1.0	0.153	0.063
	2.0	0.159	0.054
	3.0	0.169	0.051

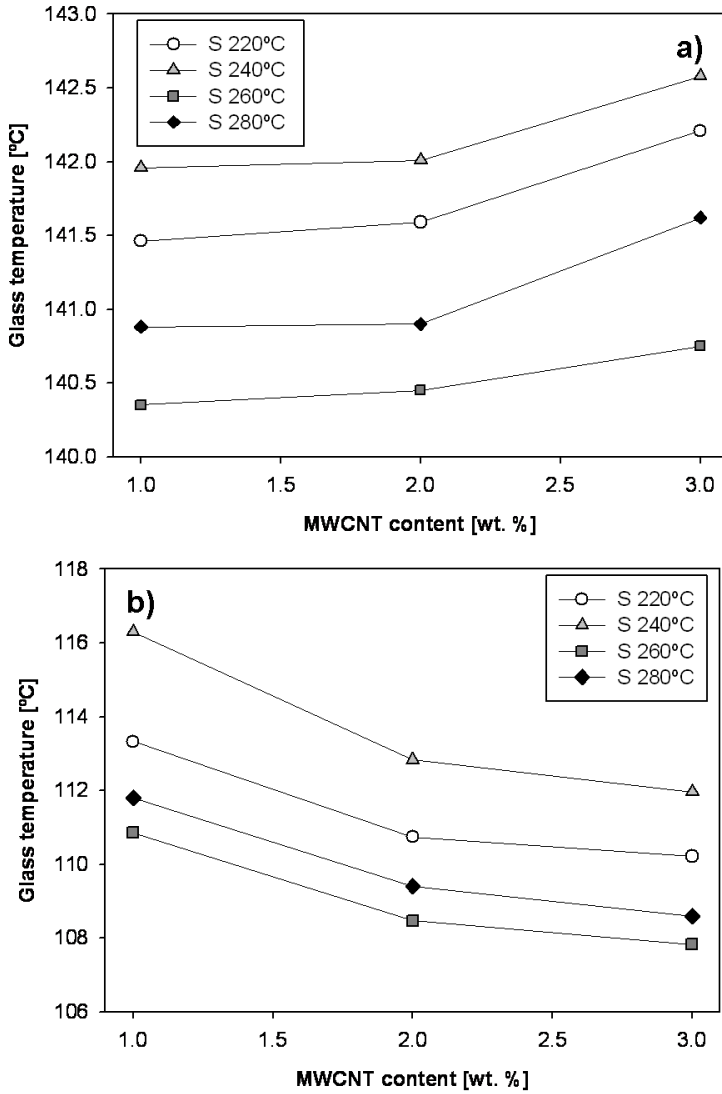


Figure 5.2.4: Glass temperature (T_g) of selected nanocomposites processed by suspension method: a) PC, b) ABS.

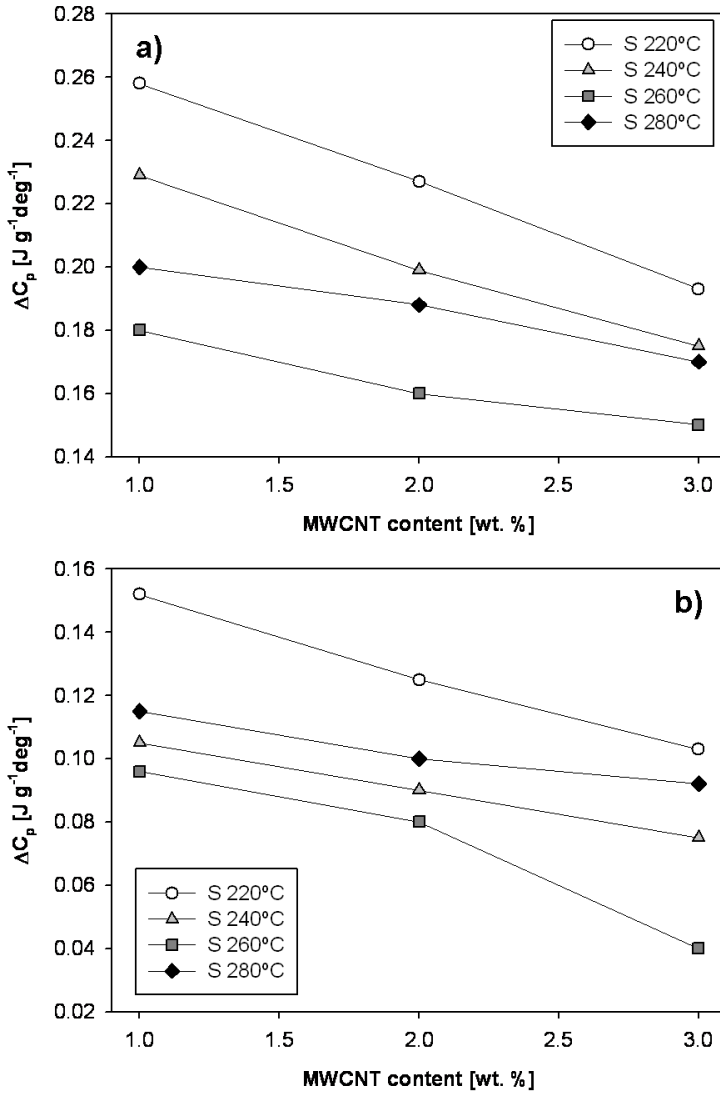


Figure 5.2.5: Change of heat capacity (ΔC_p) at glass temperature for selected nanocomposites processed by suspension method: a) PC, b) ABS.

5.3. Study of mechanical properties in nanocomposites processed by suspension method

Dynamic Mechanical Analyses carried out on nanocomposites processed by suspension method revealed higher influence of the screw speed than the melt temperature. Figure 5.3.1 shows storage modulus curves of the nanocomposite filled with 2.0 wt. % MWCNT processed at various conditions. Material formed at 600 rpm shows clearly higher values before the PC region. The two characteristic points on curves were selected to show the difference. At 120 °C (ABS phase transition zone) the materials show the aforementioned dependence on screw speed, while at 150 °C (PC phase transition zone) such differences do not exist. This is explained as a relatively stronger sensitivity of ABS on processing conditions. Besides, almost no influence of processing temperature was observed.

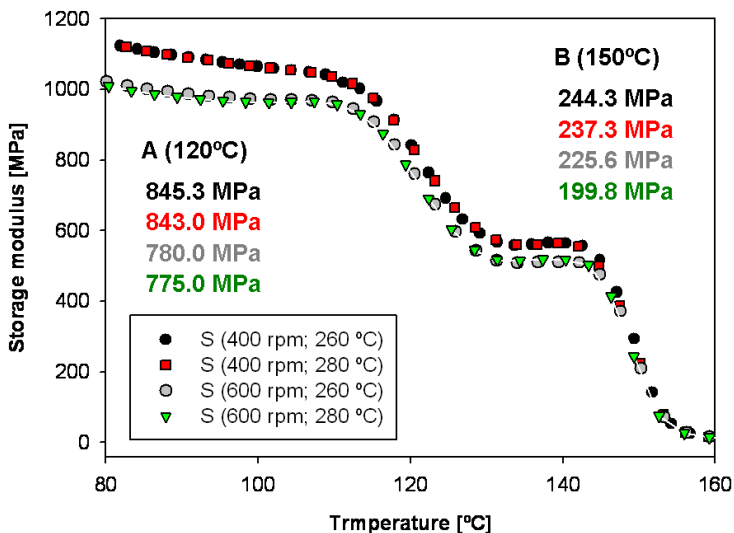


Figure 5.3.1: Storage modulus of nanocomposites with 2.0 wt. % MWCNT formed at various conditions with suspension method; A: Polycarbonate degradation (at 120 °C), B: ABS degradation (at 150 °C).

There, the correlation between the screw speed and the processing temperature has more influence than the selection of the individual parameter.

Non-covalent modification of carbon nanotubes the on mechanical properties shows lower $\tan \delta$ temperature and rather undefined $\tan \delta$ intensity after the introduction of surfactant. Figure 5.3.2 presents these parameters for polycarbonate phase as a dependence on MWCNT load.

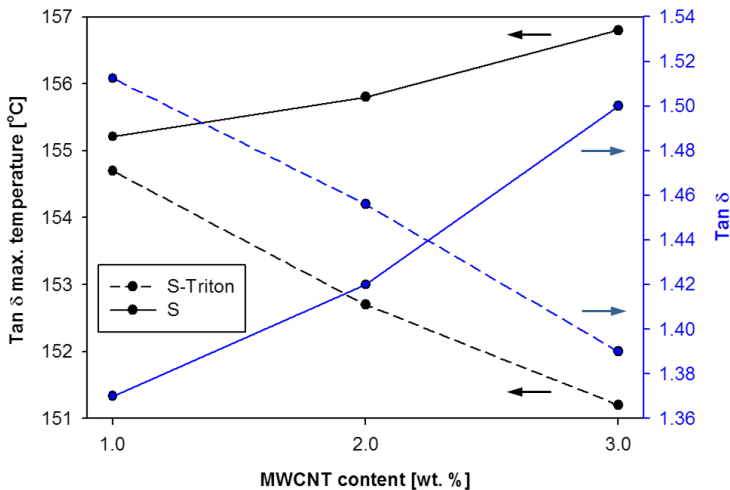


Figure 5.3.2: The dependence of polycarbonate phase $\tan \delta$ peak position on MWCNT load in **S** and **S-Triton** nanocomposites.

For both parameters, the opposite behavior observed for PC before and after addition of surfactant confirmed the change of carbon nanotube-matrix interactions. The upshift of $\tan \delta$ temperature increasing with MWCNT load can be also caused by the presence of ethyl alcohol in the nanocomposite rather than by the surfactant. ABS component changes within a very narrow range between 1.0 wt. % and 3.0 wt. % MWCNT. The change of $\tan \delta$ temperature for ABS ranges between 124.8 °C and 145.2 °C, while the change for $\tan \delta$ intensity between 0.138 °C and 0.139 °C.

Table 5.3.1: Mechanical properties of nanocomposites formed with suspension feeding method at 260 °C and 600 rpm.

Nanocomposite		Mechanical properties		
Method	MWCNT [wt. %]	E ⁽¹⁾ [MPa]	ε-γ ⁽²⁾ [MPa]	ε-b ⁽³⁾ [%]
S	0.0	2164 (±28.6)	50.6 (±2.4)	10.3 (±0.6)
S	1.0	2902 (±14.2)	52.1 (±1.5)	9.1 (±0.5)
S	2.0	2949 (±17.0)	57.7 (±2.3)	8.6 (±0.5)
S-Triton	1.0	2752 (±10.5)	59.9 (±2.1)	6.9 (±0.6)
S-Triton	2.0	2827 (±13.2)	56.7 (±1.5)	6.7 (±0.8)

⁽¹⁾ Young's modulus; ⁽²⁾ Stress at yield point; ⁽³⁾ Elongation at break.

Tensile testing carried out on the representative nanocomposites processed by suspension method (Table 5.3.1) revealed slight decrease of mechanical properties (when compared to powder addition and masterbatch dilution methods), probably due to the presence of trace amounts of ethyl alcohol acting as a plasticizer. Young's modulus increases with the increase of carbon nanotube load for both, suspension feeding method and **S-Triton** nanocomposites. The value of stress at yield point is improved for **S-Triton**. The stress at which nanocomposite begins to deform plastically is generally related to the dispersion quality. The improvement of ε-γ is commonly provided by the decrease of the number of defects in the material (*e.g.* improving the filler dispersion) in order to increase the stress barrier. In case of surfactants, also the interaction between the modified MWCNT and the matrix plays an important role. Additionally, the elongation at break decreases with an addition of surfactant due to the improved morphology. Polymeric chains lose the possibility to move freely in the presence of well-dispersed nanofiller and the breakage of the specimen occurs earlier than for the pristine matrix. Nevertheless, the Young's modulus results are similar

to the values recorded for **P** (Table 4.3.1) while masterbatch dilution gives highest increase of mechanical properties among the investigated materials (Table 4.3.2). The stress at yield point seems to increase more for **S** than for **P** nanocomposites when carbon nanotube content increases. This can be related with stronger agglomeration in the latter nanocomposites at elevated MWCNT loads. Nevertheless, the initial value of the elongation (1.0 wt. % MWCNT) as well as the value at the higher carbon nanotube concentration (2.0 wt. % MWCNT) is 185% and 205% of the ones recorded for **P**. This is a typical behavior for polymers containing plasticizer.

5.4. Comparison of electrical properties of nanocomposites

The introduction of carbon nanotubes into the immiscible polymeric blend significantly improve electrical properties, which was proved in the Chapter 4. Boosted electrical conductivity of the polymers^[152] can be additionally tuned with the additives and the processing parameters. The electrical conductivity graph containing values for PC/ABS-MWCNT nanocomposites processed with **S** and **S-Triton** methods is shown in Figure 5.5.1. Aforementioned **MB** nanocomposite is shown for comparison. Electrical conductivity increases with the increase of MWCNT load for nanocomposites processed by suspension method. The values obtained in this study are similar to the values obtained by the common industrial process of pre-dispersed masterbatch dilution. The percolation threshold is observed at the same carbon nanotubes concentration as in the **MB** nanocomposite. This can be understood as the similar quality of the nanofiller network in both nanocomposites. However, the values of electrical conductivity recorded below the percolation threshold are lower for the suspension method.

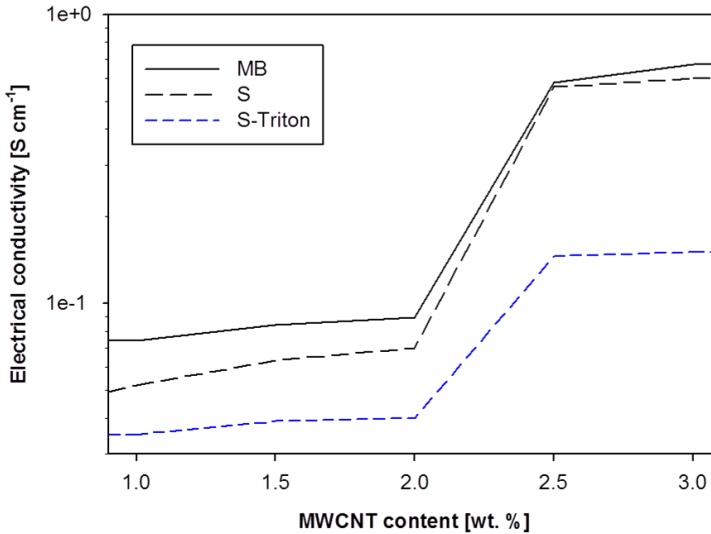


Figure 5.5.1: Volumetric electrical conductivity of selected nanocomposites processed at 400 rpm and 260 °C.

Figure 5.5.2 shows the importance of correct selection and correlation of the screw speed and barrels temperature. The highest values are recorded for the mid-range energy applied to the material during extrusion, which occurs for 400 rpm and 280 °C or 600 rpm and 260 °C. This should be the result of a balance between the nanotubes shortage and the agglomerates breakage. Nevertheless, the selection of high screw speed (responsible for the energy for agglomerates breakage and morphology improvement) and slightly reduced melt temperature seems to be the best option. The behavior of nanocomposites, regarding the effect of melt temperature and screw speed selection on electrical conductivity is similar with the nanocomposites described before.

Besides, the influence of MWCNT modification on the electrical conductivity is shown in Figure 5.5.1. Both nanocomposites with non-covalent modification show the increase of electrical conductivity with the increase of MWCNT concentration. Nevertheless, the surfactant gives lower values after

the percolation threshold than the recorded for **MB** nanocomposite. This can be related to the disturbed contact between the individual carbon nanotubes due to the additive. No change of percolation threshold concentration (with the same electrical conductivity as **MB** before that point) is observed for **S-Triton**. Despite the observed higher degree of nanofiller dispersion (Figure 5.1.5) a clear decrease of electrical conductivity occurs when compared to the non-modified carbon nanotubes-based nanocomposite processed with solvent-assisted method. These differences are also related to the presence of surfactant influencing contact between individual nanotubes. Even though the morphology difference between the two additives favors **S-Triton** to provide more conductive nanocomposites, the neat MWCNT in **S** nanocomposites shows higher values of this parameter.

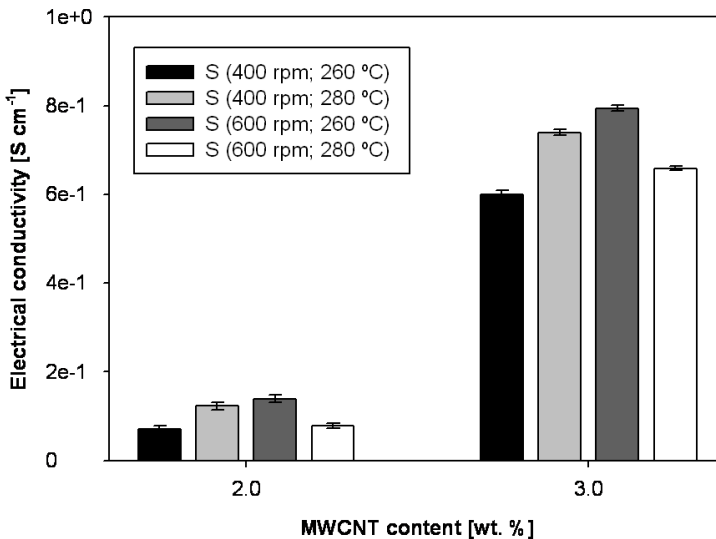


Figure 5.5.2: Comparison of volumetric electrical conductivity of nanocomposites formed with suspension feeding.

5.5. Preliminary conclusions

Preliminary conclusions after the twin screw extrusion with the nanofiller addition in the form of suspension in ethyl alcohol are shown in Table 5.6.1. The performance obtained is studied for various processing parameters and for non-covalent modification of the nanofiller.

The application of MWCNT-suspension feeding results with the behavior similar to dry methods for both types of nanocomposites. Morphology, mechanical- and thermal properties show relatively similar values. However, despite the trends similar to the masterbatch dilution method, there are differences observed between these main types of feeding.

Thermal, electrical and mechanical properties modified with processing parameters need to be compromised in **S** nanocomposites, in order to reach the balance of the final properties. This is similar to the masterbatch dilution method. Melt rheology during the extrusion, understood as a response of material for selected screw speed and processing temperature, is directly related with the electrical conductivity. Moderate values of processing parameters provide better performance of electrical conductivity. Besides, the suspension feeding **S** and the masterbatch dilution **MB** show the potential to form the nanocomposites with an improved morphology. Despite the decreased number of processing steps, the morphology in solvent-assisted method is improved. Nevertheless, similar effect of screw speed is observed for both methods, showing the increase of morphology at elevated values of this parameter. Thermal stability measurements and the study of mechanical properties prove changes of thermodynamically favored location of the nanofiller.

Table 5.6.1: Summary of PC/ABS-MWCNT nanocomposites (formed with solvent-based methods) performance; behavior relates to the increase of parameters defining columns.

Property	MWCNT load	Melt temp.	Screw
<u>Suspension feeding (S) / (S-Triton)</u>			
Dispersion quality	▼ / ▼	▼ / ▼	▲ / ▲
Thermal stability	● / ▼	▼ / ▼	▲ / ▲
Mechanical	▲ / ▲	● / ▲	▼ / ▼
Electrical	▲▲ / ▲▲	▲ ⁽²⁾ / ▲	▲ ⁽²⁾ / ▲

⁽¹⁾ Performance relates mainly to higher values of the parameter; ⁽²⁾ Regarding the results present in Figure 5.5.2; ▲▲/▼▼ – significant increase/decrease of value, ▲/▲ – moderate increase/decrease of value, ● – no significant or not defined change.

6. Injection molding

6.1. Processing conditions

Injection molding of selected nanocomposites was carried out on a BOY Spritzgiessautomaten 12A machine equipped with a CTM-12LH mold temperature control. Characteristics of the injection molding machine are shown in Table 6.1.1. The temperature of nozzle understood as melt temperature was varied between 260°C and 280°C while mold temperature was maintained at 70°C. Injection speed varied between 5 mms⁻¹ and 150 mms⁻¹, dependently on the design of the experiment. The weight of one shot with the sprue and runners was 6.7±0.1 g. Injection pressure, a machine response to the selected parameters, varied in a range 70 to 120±10 bar. Dog-bone and rectangular specimens of geometry present in Table 3.3.1 were prepared and studied. The injection gate in both cases was located on the side of each specimen (Figure 6.1.1) so the melted nanocomposite travelling along the length of the mold cavity.

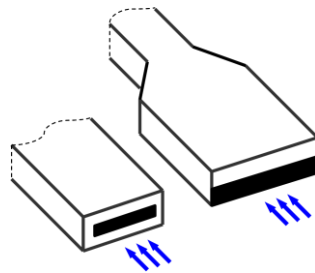


Figure 6.1.1: Injection gate for both injection molded specimens.

Two main feeding methods were applied during this study: common processing (**COM**) of the nanocomposite obtained in extrusion (injection of the **MB** material described in Chapter 3) or pre-dispersed masterbatch dilution carried out directly in injection molding machine (**DD**).

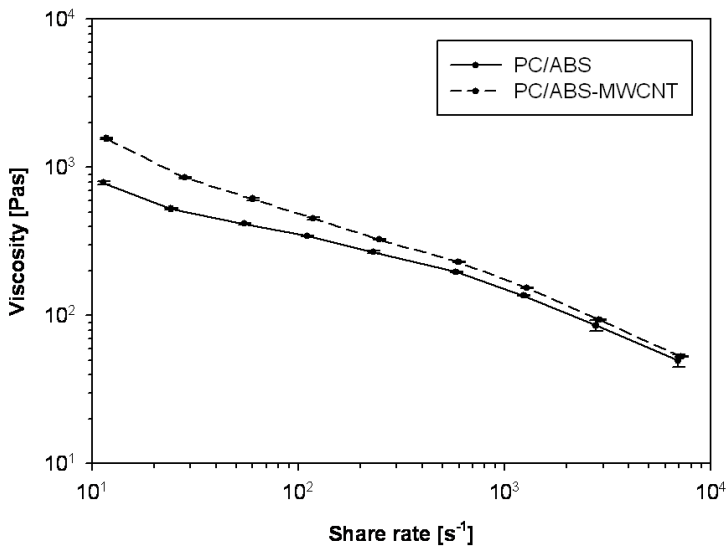


Figure 6.1.2: Results of capillary rheology for PC/ABS and its nanocomposite with 2.0 wt.% MWCNT.

Table 6.1.1: Characteristics of Injection molding machine.

Parameter	Unit	Value
Max. stroke volume (theoretical)	cm ³	20
Max. shot weight ⁽¹⁾	g	19.4
Max. spec. injection pressure	bar	2580
Max. screw stroke	mm	80
Screw torque	Nm	130

⁽¹⁾ Measured in polystyrene

Figure 6.1.2 shows minor differences of viscosity between the neat PC/ABS and PC/ABS-MWCNT with 2.0 wt.% of the nanofiller. This indicates that it is not necessary to change the injection molding parameters between these materials in order to provide similar processing conditions. The

nanocomposite characterized with slightly higher viscosity at lower shear rates gives relatively similar values when the shear increases. Therefore the injection molding conditions in the preliminary stage were studied using pristine PC/ABS. The nanocomposites with various MWCNT concentrations were further processed with no change of injection parameters.

6.1.1. Common injection molding process

Selected nanocomposites, obtained previously using the two-step masterbatch dilution on twin screw extruder, were injection molded with the common method (**COM**) with the processing parameters shown in Table 6.1.2. These processing parameters were selected due to the similarity with the injection molding process applied in industry. Homogeneous material introduced to the hopper does not suffer additional stress. Nevertheless, this method has to be considered as two-step processing: the material formed in the extrusion needs to be diluted to the designed nanofiller concentration and shaped further.

Table 6.1.2: Common injection molding (**COM**) parameters.

MWCNT [wt.%]	Injection speed [mm s ⁻¹]	Melt temp. [°C]
0.5	5; 10; 25; 50; 100; 150	280
1.0	5; 10; 25; 50; 100; 150	280
1.5	5; 10; 25; 50; 100; 150	260, 280
2.0	5; 10; 25; 50; 100; 150	280
3.0	5; 10; 25; 50; 100; 150	280
5.0	5; 10; 25 ⁽¹⁾ ; 50; 75; 100;	280

⁽¹⁾ Additionally injection molded at 260°C, 265°C, 270°C, 275°C.

6.1.2. Masterbatch dilution in injection molding

The pre-dispersed masterbatch with 5.0 wt.% MWCNT load was used in melt compounding to form nanocomposites and was diluted directly in the injection molding process (**DD**). Pellets of the masterbatch together with pellets of pristine matrix were mixed in the hooper and the dilution was carried out in feeding, transition and metering zones of the screw. This experiment, described in Table 6.1.3, resulted in reduction of the processing step affecting the final properties.

Table 6.1.3: Injection molding with reduced number of processing steps (**DD**) parameters.

Final MWCNT concentration	Injection speed	Melt temperature
[wt.%]	[mm s⁻¹]	[°C]
0.5	10; 50; 100	260, 280
1.0	10; 50; 100	260, 280
2.0	10; 50; 100	260, 280
3.0	10; 50; 100	260, 280

6.2. Study of MWCNT dispersion

Injection molding is a commonly used method of plastics processing, and can be applied to MWCNT-based nanocomposites with polymeric matrices. Nevertheless, there are drawbacks due to the size of the filler and interactions with matrix chains in plastics containing MWCNT. The distribution of the nanofiller usually varies in the final part depending on the distance from the injection molding gate and the sample walls.^[202] The latter skin effect can be observed as a gradient of filler load and alignment near the surface of the specimen and arises due to the temperature gradient inside the mold.^[60,97] The skin effect has a comparable impact on the

properties of the material to the position (and shape) of the injection gate. Moreover, the final parameters vary significantly in this common process with the change of the defined control parameter, *e.g.* the injection velocity. This is due to the mutual relation between the set pressures, temperatures, injection velocity and viscoelastic properties of the material. The aforementioned factors influencing MWCNT location in the rectangular specimen are investigated in this work by a number of characterization methods. The material was subtracted from injection molded specimens at various distances from the injection gate (Figure 6.2.1). Various divisions of the rectangular bar were applied dependently on the characterization method used.

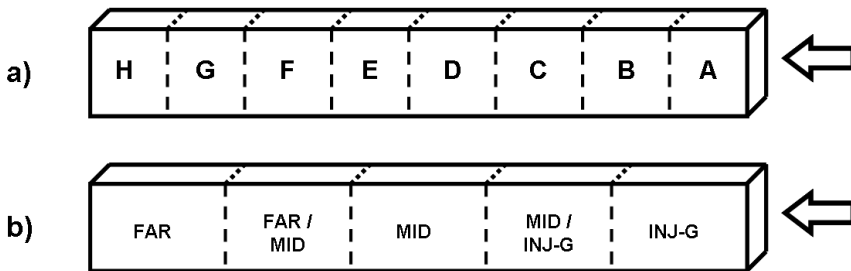


Figure 6.2.1: Schematic zones for sample subtraction from injection molded specimens for different experiments; arrows indicate injection gate; a) sample subtraction for TGA, b) sample subtraction for OM, TEM and Raman spectroscopy.

6.2.2. Morphology of injected samples

Macro-scale optical microscopy reveals the obvious differences in morphology caused by **DD** and **COM** injection molding. Figure 6.2.2, Figure 6.2.3, Figure 6.2.4 and Figure 6.2.5 show OM images from the areas near- and far from the injection gate obtained at low and high injection velocity. For injection molding with the lower number of processing steps (**DD**) (Figure 6.2.2, Figure 6.2.3) the morphology was significantly worse than for

the common injection process (**COM**) where the pre-diluted masterbatch was used. Layered structures appear due to the inefficient mixing provided by the screw, rather transporting characteristics. Insufficient mixing abilities due to the absence of kneading elements impede the efficient blending of the materials with different viscosities. Furthermore, no significant influence of the MWCNT content was observed by any of the characterizing methods.

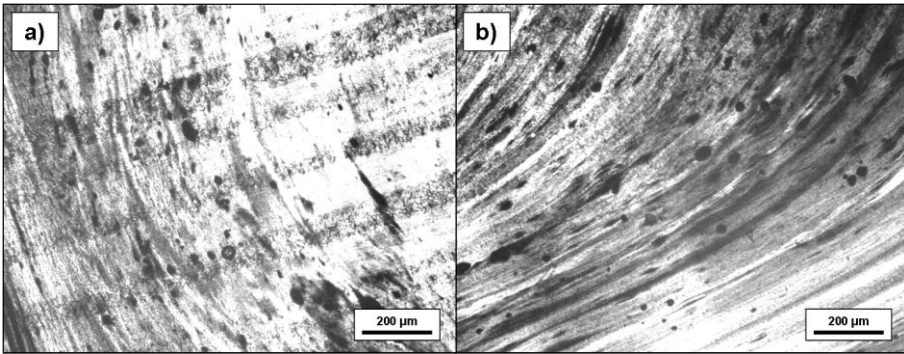


Figure 6.2.2: Nanocomposite with 1.0 wt. % MWCNT injection molded at 280 °C and 10 mms^{-1} with reduced number of processing steps (**DD**): a) near-gate area, b) far-gate area.

Analysis of OM images of the cross-sections of injection molded nanocomposites produced using the commonly applied method provides some understanding of the significance of shear during the processing. The images also indicate the rather poor mixing ability of screw in injection molding machine. The morphology improvement and relative independence on processing parameters was achieved with the addition of one masterbatch dilution step on twin-screw extruder (**COM**). Figure 6.2.4 shows relatively good morphology (compared to Figure 6.2.2 and Figure 6.2.3). Besides, the presence of agglomeration in shaped specimens for all performed experiments proves the difficulty of improving the morphology in injection molding. The morphology quality of nanocomposites is higher

before the injection molding (Figure 4.1.6) than after the processing step (Figure 6.2.6).

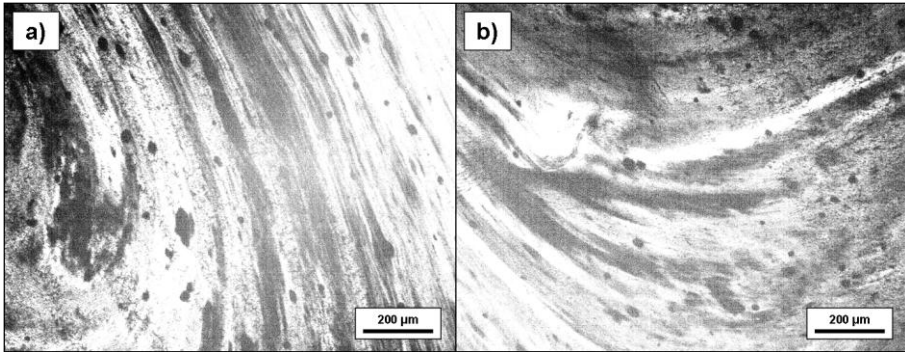


Figure 6.2.3: Nanocomposite with 1.0 wt. % MWCNT injection molded at 280 °C and 100 mms^{-1} with reduced number of processing steps (**DD**): a) near-gate area, b) far-gate area.

The **DD** method shows the unchanged agglomeration behavior at various injection velocities. Figure 6.2.2 representing 10 mms^{-1} and Figure 6.2.3 representing 100 mms^{-1} screw speeds show no clear difference between the agglomeration behavior in the areas near- or far from the injection gate. Nevertheless, the layered structure seems to be reduced to the certain areas at the defined distance from the injection gate when injection speed of 100 mm s^{-1} were used (Figure 6.2.3). That can be understood as the application of moderate shear stress along with the partial relaxation of the melt. Nevertheless, the shear provided is not enough to break the agglomerates. A discontinuous structure is maintained along the length of the specimen injection molded at 10 mms^{-1} (Figure 6.2.2), also due to the insufficient energy applied in the final part of injection cycle.

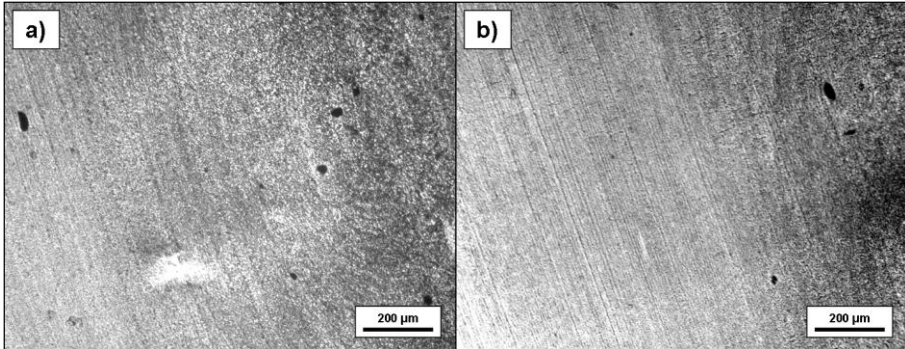


Figure 6.2.4: Nanocomposite with 1.0 wt. % MWCNT injection molded at 280 °C and 10 mm s⁻¹ (**COM**): a) near-gate area, b) far-gate area.

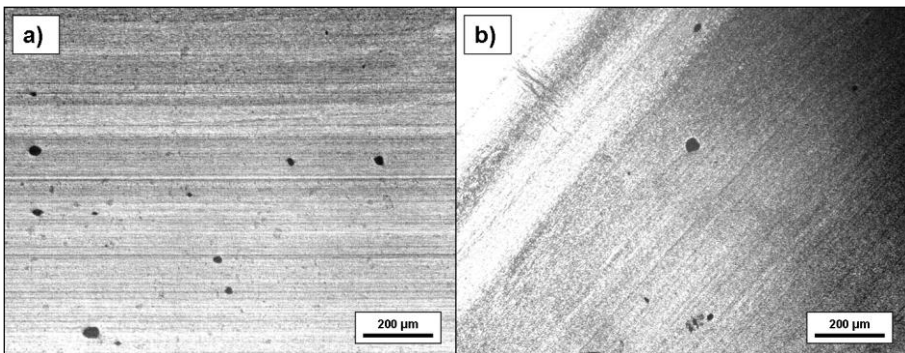


Figure 6.2.5: Nanocomposite with 1.0 wt. % MWCNT injection molded at 280 °C and 100 mm s⁻¹ (**COM**): a) near-gate area, b) far-gate area.

On the contrary, the common injection molding method (**COM**) present in Figure 6.2.4 and Figure 6.2.5 shows morphology with relatively high homogeneity at low and high injection velocities. The agglomeration behavior at both velocities in the **COM** injection molding samples seems to differ more with the distance from the injection gate than in the **DD** method. An increase of agglomeration behavior in samples processed at 100 mms⁻¹ occurs at the area near the injection gate and can be explained as an entanglement of long carbon nanotubes. This causes significant

decrease of the flow ability and the location of such agglomerates in the initial part of the specimen. Figure 6.2.4a and Figure 6.2.5a show areas near the injection gate show more agglomerates (especially in the latter image with the material processed at 100 mms^{-1}). The distance from the gate to the opposite wall of the mold seems to be sufficient enough to provide the shear for agglomerates breakage.

Higher morphology discontinuity in nanocomposites processed with both **COM** and **DD** methods is observed at 100 mms^{-1} (Figure 6.2.3 and Figure 6.2.5). In the latter case, despite the more homogeneous morphology, MWCNT-rich and -deficient layers appear. These regions are of much lower thickness, though. Such effects can be explained by the material-process relationship and appears to be a common problem in injection molding at elevated velocities.

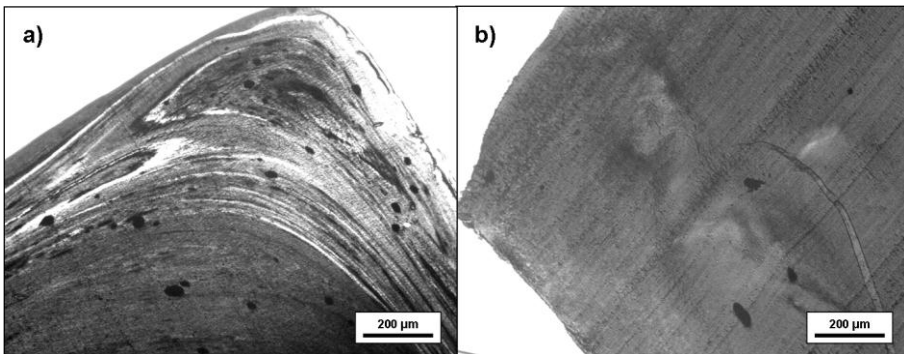


Figure 6.2.6: Edge of the specimen of nanocomposites (1.0 wt. %) injection molded at $280 \text{ }^{\circ}\text{C}$ and 100 mm s^{-1} : a) **DD**, b) **COM**.

Skin effect described in the literature^[60] is clearly present in **DD** materials. Figure 6.2.6a shows much more layered structure near the edge of the sample, amplified in the corner region. Such an effect is commonly related with the temperature difference in the mold causing much faster solidification of the nanocomposite melt which is in contact with the mold.

Figure 6.2.6b representing **COM** method shows no clear skin region. Nevertheless, according to Figure 6.2.7 presenting the principals of this effect and to the research presented below, the difference between the core and the edge of **COM** specimen exists. This observation limits the eventual electrical applications to parts produced by **COM** injection molding due to the greater isolation appearing on the surface of **DD**-injection molded specimens.

Polymer flow in the mold is shown in Figure 6.2.7 including the simplified structure of three sections of the melt: frozen layer, skin- and core polymers. In fact, every new portion of polymer injected into the mold cavity became core polymer while the previous material located in this place is pushed further. This course of injection molding process causes disadvantages in nanocomposites processing. Besides the expected orientation of nanofillers with high aspect ratio (*e.g.* carbon nanotubes), some variety in concentration of MWCNT in various specimen areas occur.

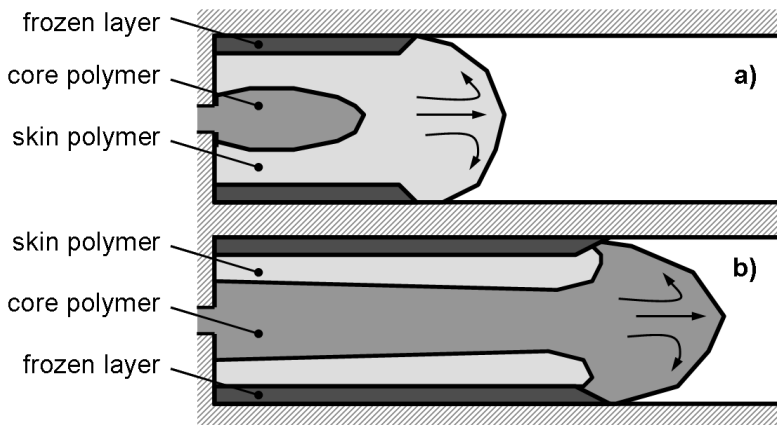


Figure 6.2.7: Fountain flow in the mold cavity: a) initial stage, b) middle/end of injection cycle.

Concluding the above observations, when the materials with reduced number of steps in melt compounding (nanocomposite **P** in Figure 4.1.4) is compared to the analogous material in injection molding (**DD** in Figure 6.2.2), significantly higher agglomeration behavior is observed. These results underline that the crucial step in obtaining final samples is melt compounding. Further processing seems to be used mainly for maintaining the morphology obtained previously. The improvement of the morphology in injection molding seems to be rather difficult to achieve.

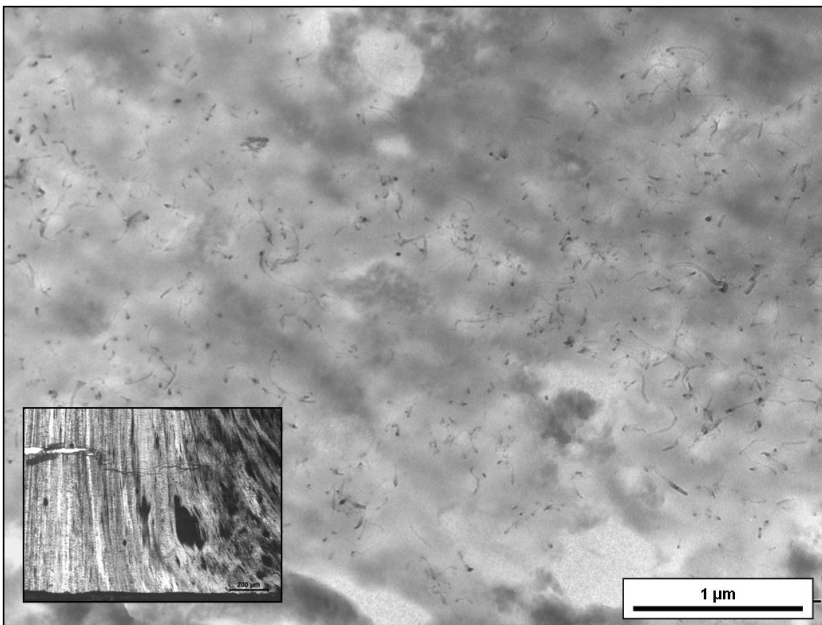


Figure 6.2.8: Nanocomposite with 1.0 wt. % MECNT injection molded at 280 °C and 100 mm s⁻¹ with (**DD**); miniature shows micrograph from OM.

TEM micrographs of nanocomposite with 1.0 wt. % MWCNT injection molded at 100 mms⁻¹ and 50 mm s⁻¹ are present in Figure 6.2.8 and Figure 6.2.9, respectively. Material presented in these micrographs was diluted from 5.0 wt. % MWCNT in injection molding machine (**DD**) so that two

processing steps are present between formation of the nanocomposite and formation of the specimen. Although there is a significant difference in conditions during these two processes, clear changes in the morphology are present in attached OM images rather than in the micrographs. Nevertheless, in both micrographs carbon nanotubes are located in polycarbonate (bright appearance) rather than in ABS (dark areas).

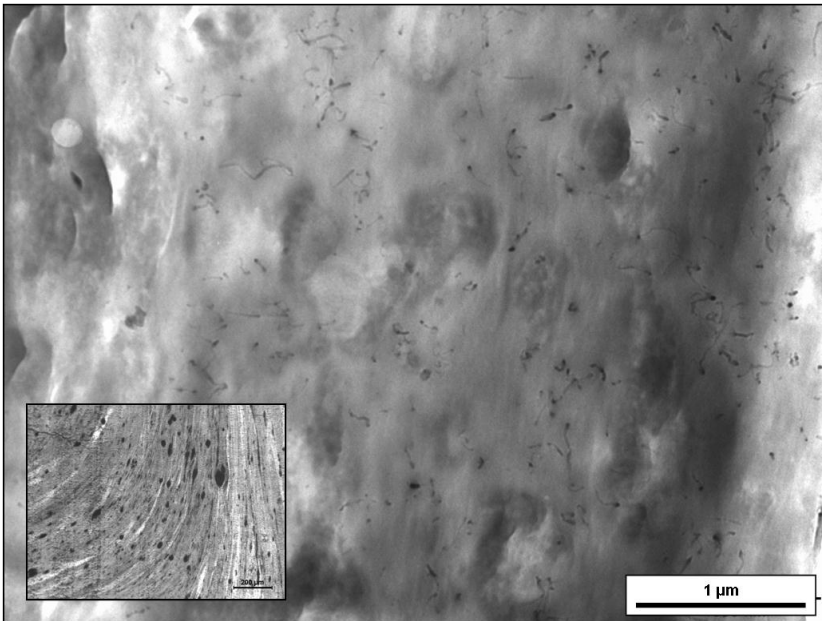


Figure 6.2.9: Nanocomposite with 1.0 wt. % MECNT injection molded at 280 °C and 50 mm s⁻¹ (DD); miniature shows micrograph from OM.

Higher shear applied to the material related with the higher mixing ability of the process is present in the specimen shown in Figure 6.2.8. Nevertheless, according to the observations from Chapter 4, it is difficult to change the location of the nanofiller between the phases of the blend only by shear application. The major part of MWCNT after melt mixing is located in polycarbonate (Figure 4.1.7). However, the specimen processed at 50 mms⁻¹

shows uneven distribution of the well dispersed carbon nanotubes in polycarbonate phase (Figure 6.2.9). The bright area in the micrograph (representing PC) with no nanotubes origin from the pristine matrix used for dilution of the masterbatch. Ineffective mixing results with the MWCNT-rich and -poor regions. Besides, the injection velocity seems to have more obvious influence on the morphology in micro-scale than it is observed in macro-scale. OM images attached to each micrograph show lower degree of agglomeration for material processed at higher injection velocity.

6.2.2. Carbon nanotubes location in the sample

Figure 6.2.10 shows the effect of first injection cycle in 3.0 wt. % MWCNT nanocomposite carried out after the machine was purged with pristine, unfilled PC/ABS. Such a change usually results with residual amount of the latter material in the nozzle. Due to the similarity between these materials such sample can be treated as a polymer flow model. Initial part of the dog-bone specimen near the injection gate is MWCNT-deficient, while the gauge and the region furthest from the injection gate contain more carbon nanotubes. This needs to be understood as a difference of flow behavior of MWCNT-filled and unfilled blend, which is in agreement with further findings. Furthermore, the presence of minor amount of carbon nanotubes in the direct neighborhood of the injection gate is most probably related with the holding pressure. This pressure, applied to compensate the material shrinkage during cooling, is responsible for the injection of residual material into the mold cavity at the final stage of the process. The decrease between the filling and holding pressures caused carbon nanotube concentration differences within the sample, appearing as bright regions. Though the dog-bone and rectangular shapes differ significantly, some assumptions can remain unchanged for both shapes. Besides, every change of the geometry

of the mold results with the change of shear and the formation of flow gradient.

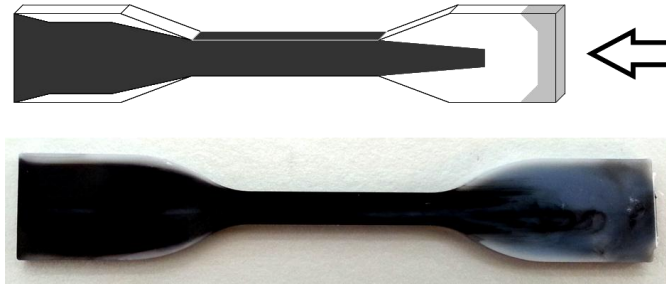


Figure 6.2.10: Demonstration of dog-bone specimen formed by injection molding from PC/ABS-MWCNT with the residual presence of PC/ABS in the nozzle; injection gate is marked with an arrow.

The influence of masterbatch dilution in injection molding on the distribution of multi-walled carbon nanotube-rich regions within the specimen is investigated by Raman spectroscopy. Specimen preparation is cutting of the rectangular injected bar into five sections (Figure 6.2.1b). Laser beam during the experiment was focused on the three areas of the cross-sections present in Figure 6.2.11. However, only two main areas were specified in the results (side and center) due to the high repeatability of the records obtained from side A and side B.

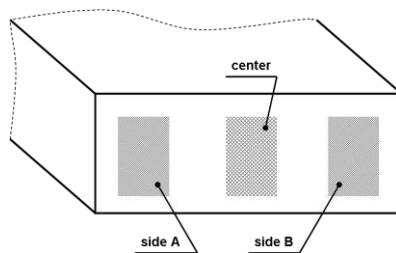


Figure 6.2.11: Raman spectroscopy measurements areas in cross-section of injection molded sample.

Raman spectroscopy results agree with the results obtained by optical- and transmission electron microscopy. D/G intensity ratio was calculated for all the recorded curves following methodology used in Chapter 4. Figure 6.2.12 shows the results of the **DD** injection molding method for nanocomposites with 3.0 wt. % MWCNT. The increase of D/G ratio with the distance from the injection gate, for both zones of the cross-section, is related with the higher MWCNT load (and perhaps with the orientation) in the MID and FAR areas (Figure 6.2.1b). It can be also explained by the disturbed flow of the nanocomposite melt caused by passing the injection gate. This effect is present also at lower carbon nanotubes concentration, shown in Figure 6.2.13, confirming no strong influence of this factor.

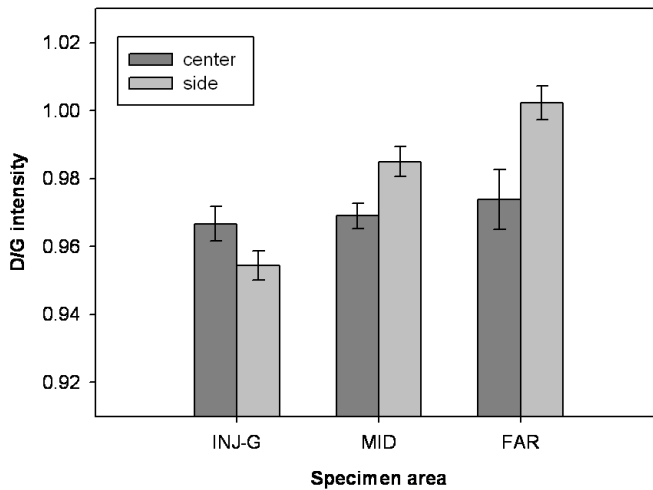


Figure 6.2.12: D/G intensity plotted against the specimen area for nanocomposite with 3.0 wt. % processed by **DD** injection molding at 280 °C and 100 mm s⁻¹.

Comparing this observation with the analogous material obtained by the **COM** injection molding method (Figure 6.2.14) shows similar behavior that is present also at the lower injection velocity (Figure 6.2.15). Therefore, the

obtaining of homogeneous mold filling in case of PC/ABS-MWCNT will be rather difficult, as the tendency to accumulate carbon nanotubes in the far-gate area occurs independently on the processing method, concentration or injection velocity.

Besides, opposite behavior of the core and the side of the specimen for the **DD** method in the areas near- and far from the injection gate are present at both investigated nanofiller concentrations. The middle area of the sample in this method seems to depend on the nanotubes concentration (Figure 6.2.12 and Figure 6.2.13). Following Chapter 4, D/G intensity ratio is understood as an indicator of the quality of MWCNT dispersion and concentration of the nanofiller. This gives the image of nanotubes distribution in the specimen influenced by the total shear applied to the material.

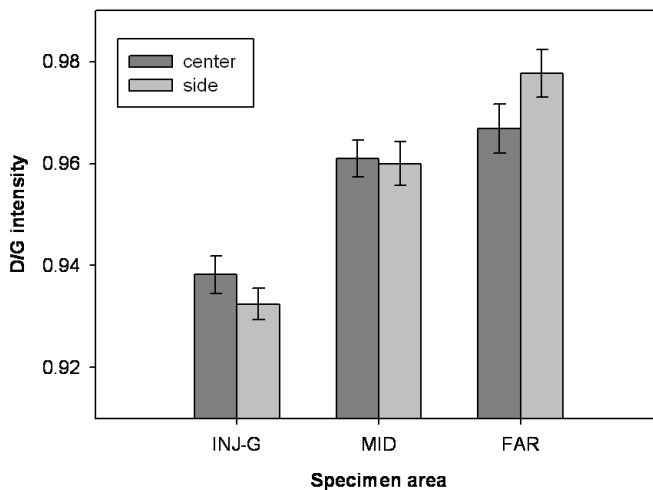


Figure 6.2.13: D/G intensity plotted against the specimen area for nanocomposite with 1.0 wt. % processed by **DD** injection molding at 280 °C and 100 mm s⁻¹.

Discontinuous morphology in the material after the **DD** injection molding results with the lower MWCNT concentration in the core of the cross section (Figure 6.2.2 and Figure 6.2.3). Such variation in the morphology can be

related to the aforementioned fountain flow present in Figure 6.2.7 and the difference in flow-abilities between the matrix and the nanofiller. Melt forehead in the mold cavity is nanofiller-rich due to the higher flow ability of MWCNT than polymeric matrix. This is because the rigid, rod-like shape and not-entangled carbon nanotubes have higher number of freedom degrees. The injection process propels with the skin polymer being pushed aside by the core polymer (Figure 6.2.7). This causes the increase of MWCNT concentration in the side zone of the specimen in the area far from the injection gate.

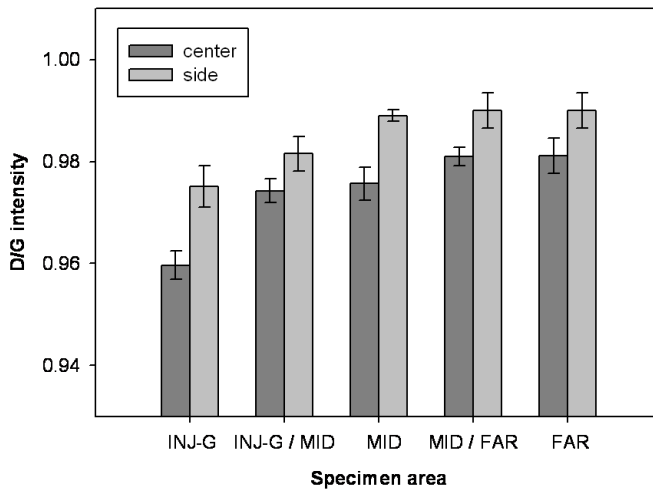


Figure 6.2.14: *D/G intensity plotted against the specimen area for COM injection molding at 280 °C and 100 mm s⁻¹; MWCNT load: 3.0 wt. %.*

However, this behavior in the common injection molding (**COM**) (Figure 6.2.14 and Figure 6.2.15) depends strongly on the injection velocity. These samples show higher precision of results due to the increased number of investigated areas. Significant decrease of injection velocity in the **COM** method gives the opposite behavior of carbon nanotubes in the central part and the side of the cross-section of the specimen. Figure 6.2.15 pictures

clearly higher MWCNT load in the central part along the whole specimen. Perhaps such strong decrease of the injection velocity (compared to Figure 6.2.14) provides change of melt behavior and the decrease of the differences in flow abilities. This causes the opposite behavior of nanotubes-rich and nanotubes-poor part of the blend. Higher D/G ratio in the side area along the whole length of the specimen, for 3.0 wt. % MWCNT sample injection molded at high velocity (Figure 6.2.14) suggests higher amount of carbon nanotubes or/and higher orientation. Besides, the injection molding at 100 mms^{-1} seems to give more homogeneous specimens. The difference of D/G intensity ratio between INJ-G and FAR samples (for both zones of the cross-section) is *c.a.* 0.06 for low- and only 0.02 for high velocity.

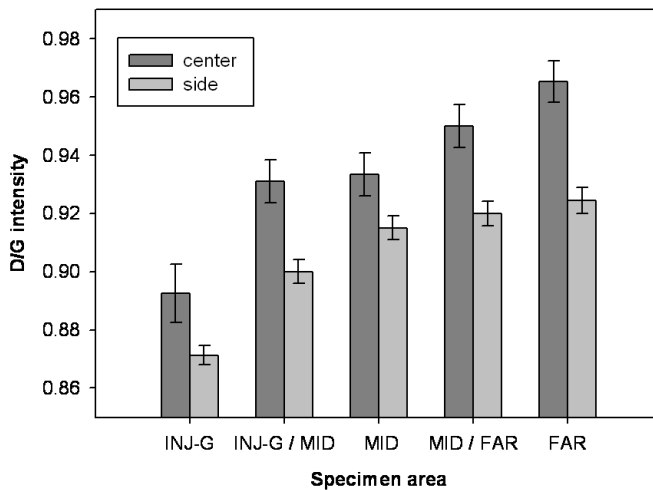


Figure 6.2.15: D/G intensity plotted against the specimen area for **COM** injection molding at $280 \text{ }^\circ\text{C}$ and 10 mm s^{-1} ; MWCNT load: 3.0 wt. %.

However, significantly lower shear at 10 mms^{-1} is homogenizing flow abilities of the nanocomposite phases and does not cause location of MWCNT in the side-area of the cross-section (Figure 6.2.15). The major part of the nanofiller is located rather in the central part of the rectangular bar, what

agrees with Figure 6.2.4. More uniform distribution of carbon nanotubes along the length and the width of the injection molded specimen is perhaps possible at moderate velocities.

Besides, D/G intensity ratio in both types of injection molding methods can include the share of the carbon nanotubes destroyed during the processing. Shortening, the most probable destruction of carbon structures, would cause higher flow ability of the nanotubes with reduced size and related preferential location of this filler in defined areas of the specimen.

Summarizing the location of carbon nanotubes in injection molded samples, common injection molding process **COM** compared with direct masterbatch dilution in injection molding **DD** shows major differences in the initial part of the mold-filling step. This is related to the partial mixing of the matrix and the nanocomposite **DD** causing the difference in flow abilities of phases.

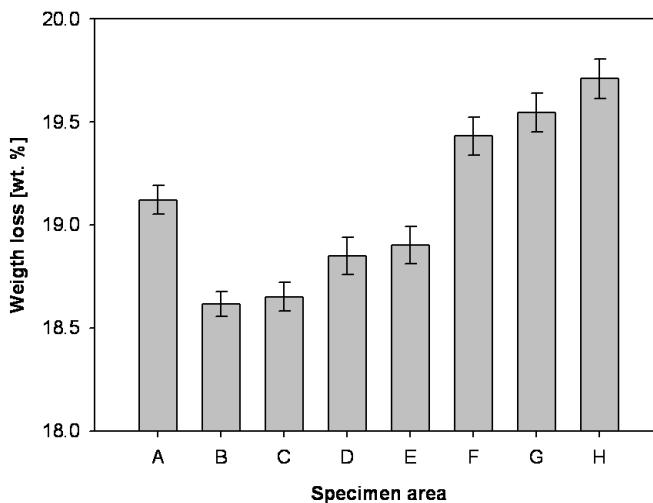


Figure 6.2.16: Weight loss at 600 °C in injection molded (**COM**, 280 °C, 100 mm s^{-1}) nanocomposite with 3.0 wt. % MWCNT.

Besides, the nanofiller location along the injection molded specimen can be determined with TGA. Such experiment was done on the nanocomposite

3.0 wt. % MWCNT processed with the common injection molding method **COM** at high melt temperature and at high injection velocity (Figure 6.2.16). Sample cut into eight parts following the scheme in Figure 6.2.1a was tested on TGA showing various amounts of residual material after the experiment. Even though a part of this residue is related to the aromatic structures form the matrix, these results can be extrapolated to the amount of multi-walled carbon nanotubes in the nanocomposite. MWCNT are located mainly in the area far from the injection gate, what agrees with the above observations. Besides, the amount of inorganic residue in the part A indicating injection gate, is on the level of the central part of the specimen. This can be explained as a shear gradient caused by injection gate or by the holding pressure applied after the mold-filling step. This concentration is the desired nanofiller load undisturbed by the processing parameters. Besides, the nanocomposite melt at high temperatures is known to show different flow ability of the matrix and the nanofiller. Flow abilities of incompatible blend phases unevenly filled should vary as well. Such behavior explains the differences between specimen parts B and H stating clearly higher flow ability for carbon nanotubes. This difference can be possibly minimized with the application of mild injection velocity providing lower shear. Moreover, the behavior present in Figure 6.2.16 agrees with the other results obtained on nanocomposites with lower MWCNT load.

6.2.3. Orientation of carbon nanotubes

Orientation of carbon nanotubes was investigated as a binary parameter (presence or absence of oriented nanotubes) in the nanocomposites with high and low nanofiller load processed with the **COM** method at high injection velocity. Such processing conditions were selected in order to secure higher share of oriented carbon nanotubes. Figure 6.2.17 shows the area from where material for TEM imaging was subtracted.

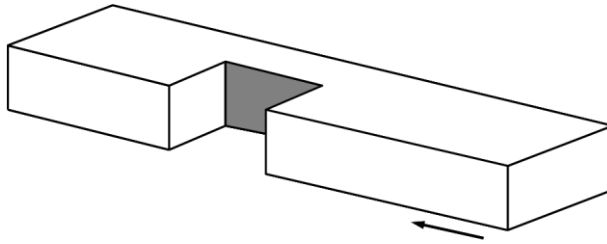


Figure 6.2.17: Scheme of the region observed for oriented nanotubes localization (dark area); arrow shows the direction of nanocomposite flow.

Methodology of this study includes the defined path with the initial part: TEM observation of material from injection molded specimen. Individual carbon nanotubes present in micrographs are defined in optical data analyses program (Figure 6.2.18a) and such network (Figure 6.2.18b) was further investigated. Study of MWCNT alignment is done with the presence of original image in order to provide images with high contrast necessary for precise results.

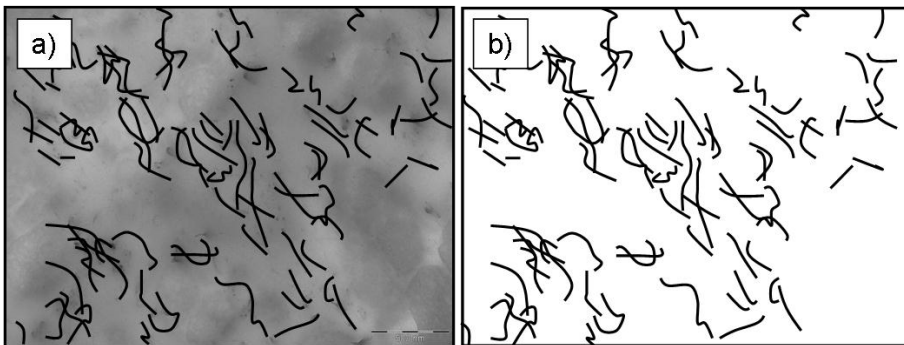


Figure 6.2.18: Methodology of defining individual MWCNT: a) TEM micrograph with marked nanotubes, b) image prepared for analysis by program; sample PC/ABS with 2.0 wt. % of MWCNT injection molded (**COM**) at 100 mm s^{-1} at $280 \text{ }^\circ\text{C}$.

Orientation is investigated as a distribution of angles deviation between the Feret axis of individual carbon nanotubes and the theoretical vector \vec{v} located at 0° to the melt flow. Feret parameter (*e.g.* axis, diameter) is related to the dimension or the other value of the object measured in specified direction. Feret axis was selected for this study due to its specific characteristic. Multi-walled carbon nanotubes in injection molded samples are not straight and application of Feret parameter is crucial for obtaining understandable results. This data was later compared between both materials so that the lower number of individual filler particles occurring for 0.5 wt. % MWCNT was taken into account.

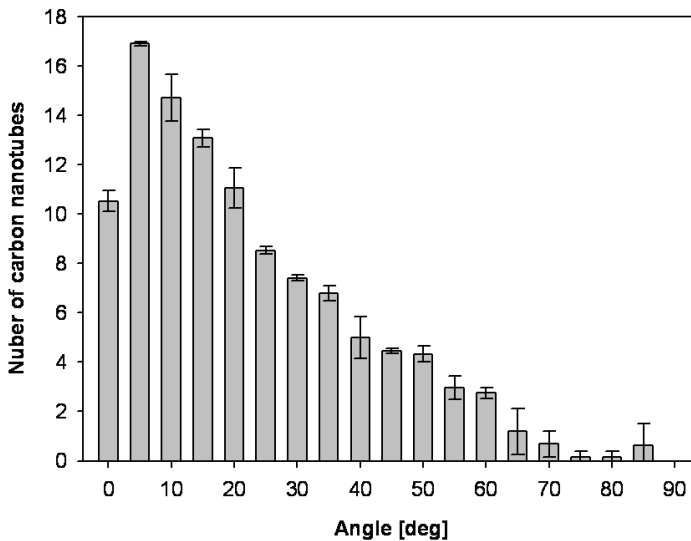


Figure 6.2.19 Distribution of angles of carbon nanotubes appearance representing the orientation of nanofiller; sample PC/ABS with 2.0 wt. % of MWCNT injection molded (COM) at 100 mms^{-1} at 280°C .

Figure 6.2.19 shows the results of nanocomposite with 2.0 wt. % MWCNT while Figure 6.2.20 – with 0.5 wt. % MWCNT. Distribution of deviation angles seems to be very similar at various concentrations of the nanofiller.

Rather minor influence of nanocomposite viscosity on nanotubes orientation within the investigated loads can be concluded. Only *c.a.* 2.5 % of nanotubes in 2.0 wt. % MWCNT are located at an angle above 60° from \vec{v} . This can be understood as no orientation along the melt flow. For the nanocomposite with lower load, this value is slightly higher, *c.a.* 3.8 %. Furthermore, when the highest orientation (below 10°) is considered, also the latter nanocomposite shows higher value: 37.8 % versus 33.1 %. Nevertheless, this difference is clearly decreased confirming the above statement of little influence of the viscosity. Presence of the neighboring nanotubes, which is significantly increased at elevated loads, does not affect significantly the orientation.

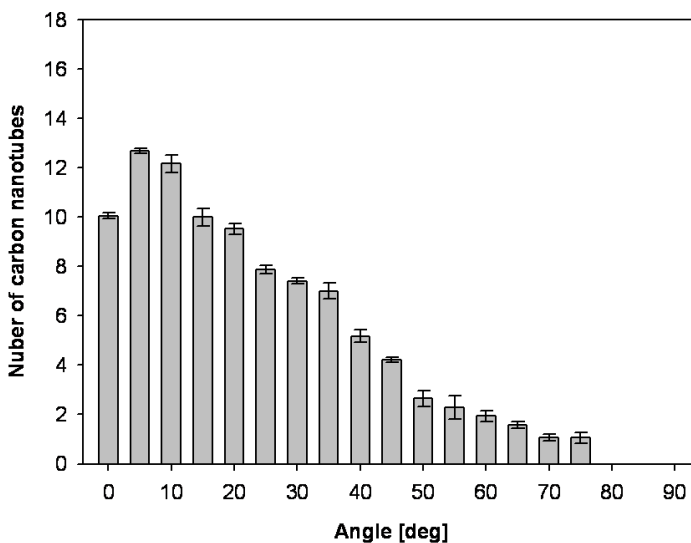


Figure 6.2.20: Distribution of angles of carbon nanotubes appearance representing the orientation of nanofiller; sample PC/ABS with 0.5 wt. % of MWCNT injection molded (**COM**) at 100 mms^{-1} at 280°C .

Lower values of small angles below 5° observed at both investigated loads is most probably related to the methodology. Calculated parameters allow only

relatively well aligned nanotubes to be recorded in this range. This means that the Feret axis should overlap the actual axis of the individual nanotube with high accuracy. Considering relatively high curvature of the nanotubes (Figure 6.2.18b), aforementioned 10° limiting high alignment seems to be a correct value.

Besides, the orientation of carbon nanotubes in different areas of the specimen could be slightly different due to the fountain flow. This phenomenon is not investigated in this part of the work. However, the orientation in the whole specimen should be similar, strongly influenced by the direction of polymer flow. This should not affect further investigated properties.

6.3. Flammability of injection molded nanocomposites

Rather poor flame propagation parameters of polymer materials are commonly improved by the addition of flame retardants. This parameter is crucial for all the applications, *e.g.* in construction or automotive sectors. Increase of ignition temperature or reduction of flame propagation speed is usually achieved. Multi-walled carbon nanotubes are well known non-phosphorous and halogens-free additive decreasing the flammability of the polymeric materials at relatively low concentrations, even though MWCNT are not fire-retardants itself.^[203]

Injection molded samples were compared to the samples obtained in melt compounding and shaped in compression molding. Selected PC/ABS and its nanocomposites processed at the same conditions **COM** shown in Figure 6.3.1 indicates the different behavior towards flame propagation. Flammability of pristine matrix is significantly higher than of nanocomposite, what is unchanged after injection molding. Besides, drips of the burning material are present during testing, which causes shortening of the initial sample (Figure 6.3.1c). The total degradation occurs after relatively short

time (Figure 6.3.1d). After the formation of nanocomposite (2.0 wt. % MWCNT) flammability is clearly decreased with both parameters: burning time and the behavior. Moreover, neither dripping nor shortening of specimen length were observed during burning (Figure 6.3.1b). Nevertheless, total burning of nanocomposite sample occurs with similar flame propagation properties.

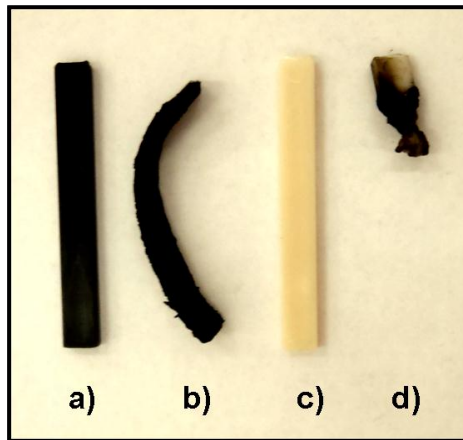


Figure 6.3.1: Various materials injection molded (COM) at 280 °C at 100 mm s^{-1} : a) PC/ABS-MWCNT with 2.0wt. % before and b) after flammability test, c) PC/ABS before and d) after flammability test.

The influence of carbon nanotube content on flammability is shown in Figure 6.3.2. The linear burning rate decreases strongly after the formation of nanocomposite, keeping the same trend with the successive increase of MWCNT concentration. The most probable mechanism regulating flame suppressing in the nanocomposites assumes the flame retardancy depending on the state of MWCNT dispersion. The tight network of well-dispersed carbon nanotubes of possibly high aspect ratios^[204] provides strong barrier resistance to the evolution of volatiles and oxygen ingress to the condensed phase.^[205] This applies to materials processed within one method so that no

significant differences occurs (*e.g.* polymer matrix degradation) influencing the results. Additionally, at the beginning of nanocomposite burning process the protective char is created, providing the heat thermal barrier.^[174] Both effects: homogeneous morphology and graphitization are reported to have the influence on heat release rate for MWCNT-based nanocomposites.^[205-206] Furthermore, self-extinguishing of the specimen was observed after the removal of burner at the higher nanofiller loads. This is related to the increased barrier properties. Such an increase occurs due to the formation of tighter nanofiller network, despite significantly higher agglomeration behavior at elevated MWCNT concentrations.

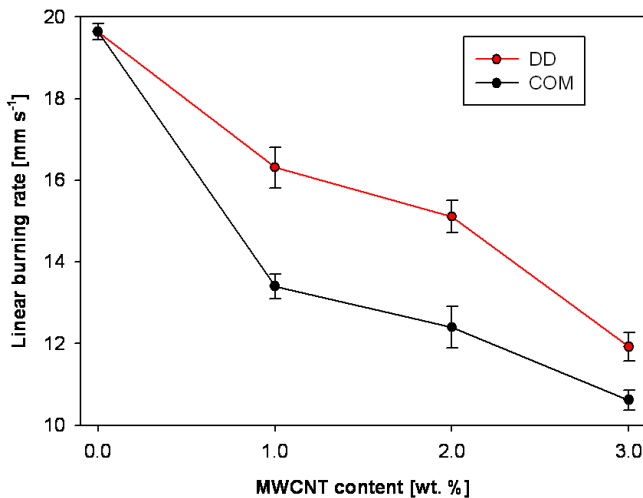


Figure 6.3.2: Linear burning rate for different injection molding (280 °C and 100 mm s⁻¹) methods for nanocomposites.

The linear burning rate as a representative parameter defining flame resistance of polymer-based materials was plotted versus carbon nanotube content for **DD** and **COM** processing in Figure 6.3.2. Injection molding of nanocomposite results with various burning rates dependently on carbon nanotubes load and on morphology (determined by the number of

processing steps). Clear decrease of this parameter is observed, what means that the flame propagation is decreased when more MWCNT is introduced. Besides, **COM** process gives lower than **DD** burning rates along the whole range of carbon nanotubes concentrations. This is related to clearly better morphology of the former material (Figure 6.2.4 and Figure 6.2.5). Better dispersion of carbon nanotubes gives tighter network that improves barrier properties and decreases the emission of gaseous decomposition products.

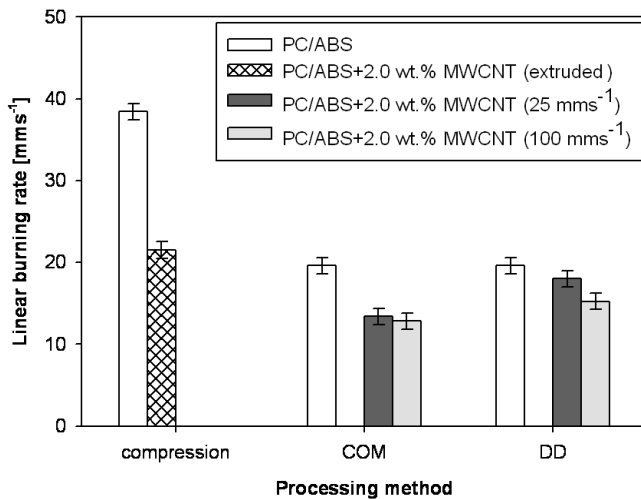


Figure 6.3.3: Linear burning rate for injected (280 °C) and compression molded specimens of nanocomposites with 2.0 wt. % MWCNT and for pristine matrix.

Further investigations on the influence of injection molding parameters and processing method on linear burning rate are shown in Figure 6.3.3. Clear decrease of flammability occurs between compression and injection molding. This effect is present for the pristine matrix and for the nanocomposite, suggesting involvement of polymer chains. Besides, injection velocity increase in both, **DD** and **COM** methods, show the decrease of linear burning rate. Such behavior is related to the above explanation. Tighter packing and orientation of carbon nanotubes and polymer chains in injection

molding is believed to decrease flame propagation. Furthermore, high injection velocity providing higher shear can be related to the decrease of carbon nanotubes agglomeration and an increase of network quality. Regarding the previous preliminary conclusions, the tight network with rather random MWCNT orientation is necessary for good barrier properties improving incombustibility. Nevertheless, higher injection velocity generally providing 1D (MWCNT) or 2D (graphene) nanofiller alignment in the melt flow direction,^[60] show rather minor influence. General conclusion after the comparison of thermal stability of nanocomposites obtained by compounding (Chapter 4) with their flammability shows rather little relation between these properties. Nevertheless, the decrease of flammability seems to occur with the improvement of morphology.

6.4. Mechanical reinforcement in injection molded nanocomposites

Mechanical reinforcement of PC/ABS blend achieved after the incorporation of carbon nanotubes, present in Chapter 4, was studied after the **COM** injection molding method. All recorded data showed clearly the improvement of mechanical properties of PC/ABS with an increase of MWCNT concentration. Figure 6.4.1 shows Young's modulus dependence on the carbon nanotubes concentration at low and high injection velocities. Stabilization of the improvement of mechanical properties present in the form of plateau occurring above 1.0 wt. % MWCNT was explained by the higher nanofiller agglomeration behavior at elevated concentrations. Furthermore, the increase of Young's modulus at elevated injection velocity (and melt temperature) was related to the orientation of carbon nanotubes at these conditions and to the alignment of polymer chains in the direction of the flow. Such an orientation and alignment in the direction of the applied

force during tensile testing provides an anisotropic reinforcement of the material.

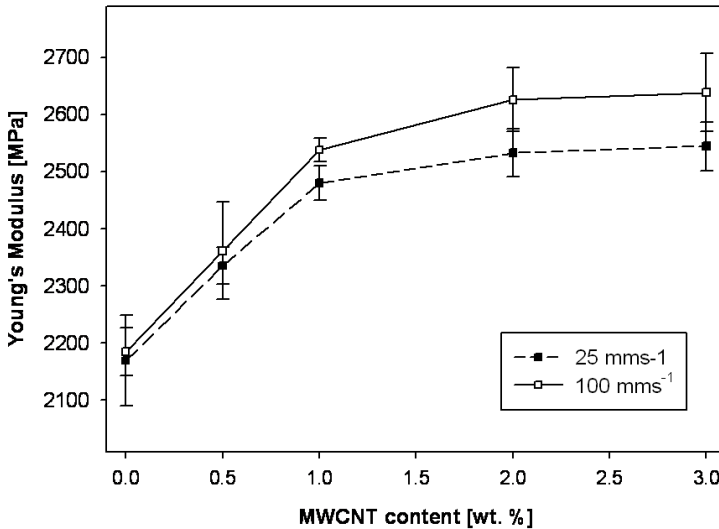


Figure 6.4.1: Young's modulus dependence on injection velocity and MWCNT load in nanocomposites injection molded (COM) at 280 °C.

General increase of the stress at yield point present in Figure 6.4.2 is reported with the increase of carbon nanotubes content and injection speed. The most significant change, not present here, was observed at 270 °C, what can be understood as the higher impact of the processing parameters on material brittleness. Yield stress was constant with the increase of injection velocity at 280 °C. This is due to the higher agglomeration of carbon nanotubes at elevated temperatures. Macro-size agglomerates increase brittleness of the material due to the faster occurrence of the loss of interfacial interactions with matrix. Individual carbon nanotubes creating well-structured network in the material allow higher mobility of polymer chains than agglomerates, which are considered as defects. The general trend showing higher values of yield stress at elevated melt temperatures

and injection velocity is therefore related to the loss of elasticity of the nanocomposite. Plateau for both applied injection velocities occurred above 2.0 wt. % MWCNT marking the influence of increased agglomeration behavior.

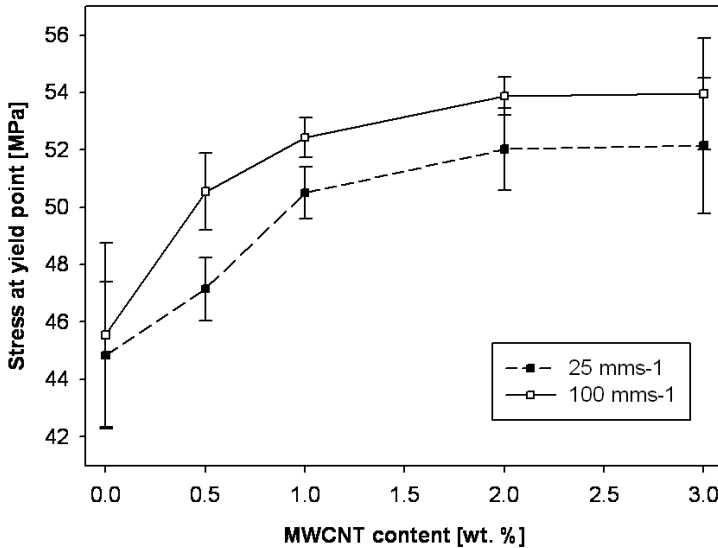


Figure 6.4.2: Yield stress dependence on injection velocity and MWCNT load in nanocomposites injection molded (COM) at 280 °C.

The decrease of elongation at break was observed with an increase of melt temperature and the decrease of injection velocity (Table 6.4.1). Besides, the influence of nanofiller load was typical for MWCNT-filled polymers^[160] and showed the decrease of elongation with an increase of the load. Nevertheless, carbon nanotubes concentration at low loads seems to be of minor significance in PC/ABS-MWCNT when compared to the processing parameters. Reduced elongation at break at elevated injection velocity for the same nanofiller concentration is related to aforementioned orientation of individual nanotubes. Besides, observed ϵ_b decrease between 25 mms⁻¹ and

100 mms^{-1} is followed by the region of relatively higher independence on injection velocity. This is related to the shear change at low values of injection velocity and possibly to the distribution of nanofiller (and agglomerates) in the mold varying at low- and high injection velocities. The former factor seems to be more significant though.

Table 6.4.1: Elongation of nanocomposites injection molded (**COM**) at 280 °C.

MWCNT [wt.%]	Elongation at break	
	25 ⁽¹⁾	100 ⁽¹⁾
0.0	13.06 (± 0.15)	12.44 (± 0.28)
0.5	11.85 (± 0.30)	11.27 (± 0.28)
1.0	11.66 (± 0.12)	11.12 (± 0.11)
2.0	11.53 (± 0.14)	11.07 (± 0.19)
3.0	10.72 (± 0.21)	10.19 (± 0.07)

⁽¹⁾ injection velocity [mms^{-1}]

The effect of particle size was reported and showed the highest importance on elongation at break at rather low filler concentrations (below 15 wt. %).^[207] Expected increase of agglomeration size in PC/ABS-based nanocomposites at elevated temperatures showed such influence on elongation behavior.

Figure 6.4.3 shows the storage modulus at $\tan \delta$ for nanocomposites with higher MWCNT load. Decreased dependence of this parameter on injection velocity above the 50 mms^{-1} forms the plateau for both blend phases. This is related to the elevated values of shear at higher injection velocity. Therefore, no significant increase of storage modulus observed above the 50 mms^{-1} which agrees with the previous findings from tensile testing. Furthermore, the temperature of $\tan \delta$ maximum present in Figure 6.4.4 shows the clear decrease for both blend phases. Appearance of $\tan \delta$

maximum at lower temperatures at elevated injection velocity proves better energy storage by the nanocomposite at these processing conditions.

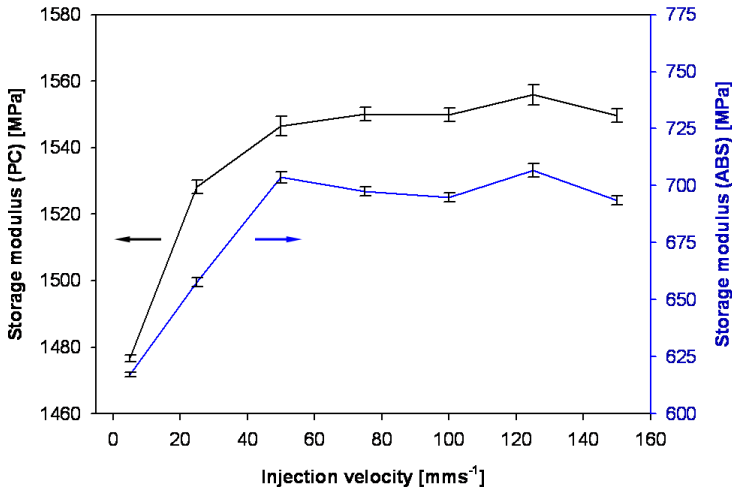


Figure 6.4.3: Storage modulus at $\tan \delta$ maximum for both blend phases versus injection velocity (**COM**, 5.0 wt. %, 280 °C).

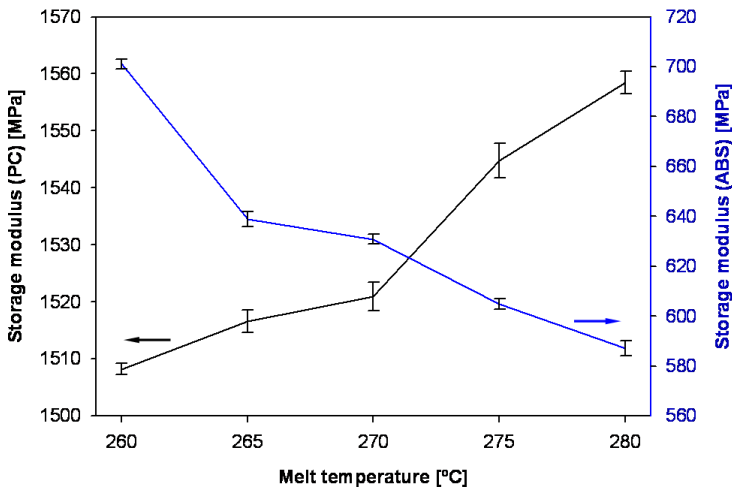


Figure 6.4.4: Storage modulus at $\tan \delta$ maximum for both blend phases versus melt temperature during injection molding (**COM**, 5.0 wt. %, 25 mm s⁻¹).

Such an improvement can be related to higher polymer chains and nanofiller orientation leading to the formation of anisotropic material. Force during DMA test is applied to the specimen in the direction perpendicular to the melt flow, which explains the behavior.

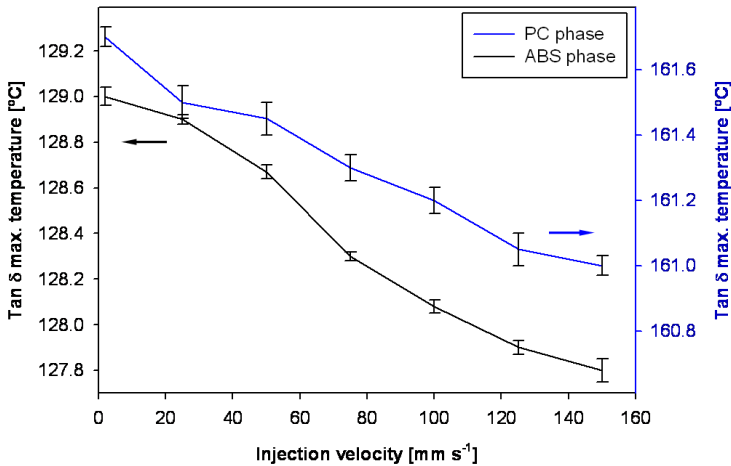


Figure 6.4.5: Temperature at $\tan \delta$ maximum for both blend phases versus injection velocity (COM, 5.0 wt. %, 280 °C).

The influence of the melt temperature during injection molding present in Figure 6.4.5 and Figure 6.4.6 show various behaviors on $\tan \delta$. Storage modulus values at $\tan \delta$ maximum for ABS phase decreases with the temperature, while an increase was observed for polycarbonate in the same conditions. This effect show difference with injection velocity influence on both phases – no plateau was observed within the suggested processing temperatures range. Mechanical properties of PC phase in the injection molded nanocomposites increases at elevated melt temperatures. Nevertheless, that change is only 30 % of the values observed for ABS, decreasing significantly with the increase of the melt temperature during injection molding. Such trend can be understood as carbon nanotubes

location change between the nanocomposite phases with the increase of the melt temperature. It is supposed that MWCNT migrate to polycarbonate due to the higher affinity with this phase, facilitated by the change of melt viscosity.

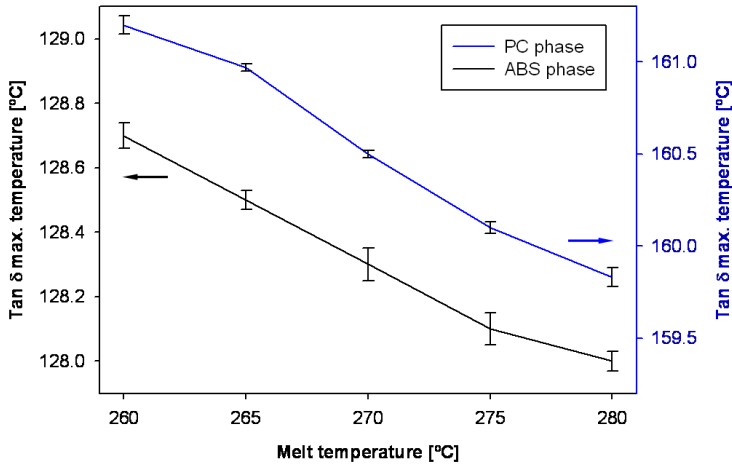


Figure 6.4.6: Temperature at $\tan \delta$ maximum for both blend phases versus melt temperature during injection molding (**COM**, 5.0 wt. %, 25 mm s⁻¹).

Figure 6.4.6 presents temperature of $\tan \delta$ maximum for both blend components for the nanocomposite injection molded at various temperatures. The decrease of this parameter for both phases occurs and the highest values of the processing temperature. Such a slight decrease of the mechanical properties with an increase of melt temperature was probably related to the degradation of polymer chains at elevated temperatures or to the increase of melt viscosity at higher temperatures. This allowed higher MWCNT mobility in the melt and the following agglomeration. Such an effect decreases the amount of nanofiller for the benefit of macro-size particles (agglomerates).

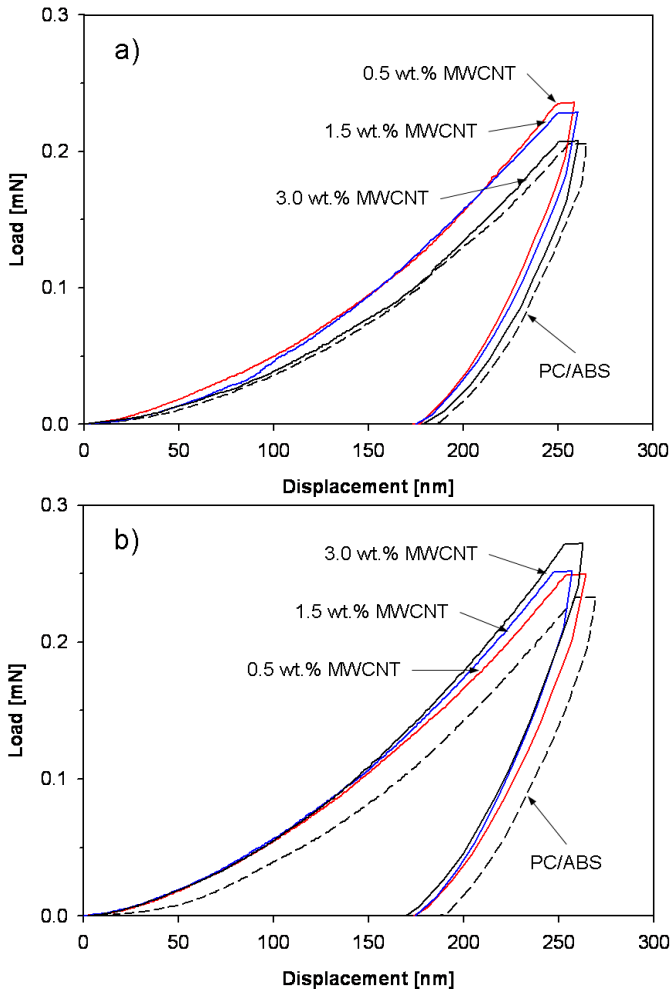


Figure 6.4.7: Nanoindentation results of nanocomposites injection molded (COM) at 280 °C and: a) 25 mms^{-1} , b) 100 mms^{-1} .

Curves recorded at similar conditions for the pristine PC/ABS and for the nanocomposites below 3.0 wt. % MWCNT show lower force values at 25 mms^{-1} (Figure 6.4.7a) than at 100 mms^{-1} (Figure 6.4.7b). Lower force reading can be explained with the increase of material stiffness after the formation of the nanocomposite. This is related with an increase of the elastic modulus and the hardness at higher injection velocity.^[163] Nano-

reinforcement effect causes the down-shift of the load-displacement curves, which was understood as a reduction of the remaining depth with the increase of the nanofiller load. An incorporation of MWCNT into the polymer matrix increases the elastic modulus and hardness of pristine matrix due to the intrinsic strength and high aspect ratio of the individual carbon nanotubes. Hardness has been defined as a resistance of material surface against the deformation caused by a normal force, while the elastic modulus is the ability of material to recover its former shape.^[163] Therefore, it is expected that at elevated MWCNT concentration the interaction of the indenter with nanotubes increases. Consequently, the elastic modulus and the hardness should show higher values with an increase of MWCNT content. Resistance of the material against the deformation caused by the normal load was improved and higher elastic recovery was observed.

After the introduction of 3.0 wt. % MWCNT, Young's modulus (Figure 6.4.8) increased 36 % at 25 mms⁻¹ and 14 % at 100 mms⁻¹. Hardness (Table 6.4.2) increased 46 % at 25 mms⁻¹ and 21 % for 100 mms⁻¹. Such behavior was reported earlier for other polymers.^[163,208] An increase of hardness (Table 6.4.2) indicates higher resistance of the material against the deformation caused by a normal load. Similarly, an increase in the yield stress was observed in macroscopic tests and therefore a good correlation with tensile test results can be reported. However, a decrease in nanoindentation properties was observed for 3.0 wt. % MWCNT at 25 mms⁻¹. This may be caused by the non-homogeneous distribution of the agglomerates (e.g. wide distribution of agglomerates size). Moreover, this value is similar to the pristine PC/ABS, which confirms moderate loads required for an effective reinforcement at the reduced injection velocities. Higher nanoindentation properties were observed for elevated injection velocities on the Young's modulus (Figure 6.4.8) and the hardness (Table 6.4.2). The improvement of both parameters with an increase of MWCNT content was observed and a plateau is present above 0.5 wt. %. Samples injection molded at 100 mms⁻¹ show slightly lower Young's modulus and hardness than PC/ABS

samples after the Ar ion beam irradiation (3.4 GPa and 0.2 GPa, respectively).^[162]

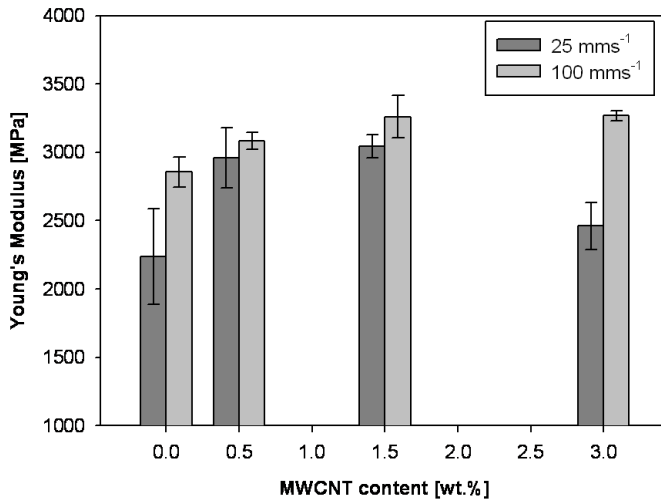


Figure 6.4.8: Young's modulus dependence on injection velocity and MWCNT load in nanocomposites injection molded (COM) at 280 °C; results based on nanoindentation.

Mechanical properties measured by tensile test showed the same tendency as the values from nanoindentation. The continuous increase in Young's modulus and stress at yield point with carbon nanotubes increase occurred. Young's modulus and stress at yield point are also higher at elevated injection velocity, probably due to the higher carbon nanotubes orientation. Nevertheless, the elastic modulus determined by nanoindentation is higher than the macroscopic one. This reveals more remarkable nanofiller influence in nanoscale, taking into account the local character of the measurements. In addition, macroscopic mechanical test (tensile test) is less sensitive to carbon nanotubes distribution than the nanoindentation measurements. However, the values of Young's modulus and hardness at 25 mms⁻¹ for 3.0 wt. % MWCNT are similar to the values of pristine PC/ABS as

a consequence of non-homogeneous dispersion. There is no evidence of this effect in macroscopic response.

Table 6.4.2: Hardness and plasticity based on nanoindentation results on injection molded (COM) nanocomposites.

MWCNT [wt. %]	Hardness [MPa]		Plasticity index	
	25 ⁽¹⁾	100 ⁽¹⁾	25 ⁽¹⁾	100 ⁽¹⁾
0.0	132 (±31)	197 (±27)	0.70 (±0.04)	0.64 (±0.03)
0.5	186 (±30)	215 (±9)	0.65 (±0.04)	0.61 (±0.03)
1.5	190 (±17)	207 (±10)	0.64 (±0.03)	0.62 (±0.02)
3.0	142 (±23)	231 (±4)	0.67 (±0.03)	0.63 (±0.02)

⁽¹⁾ injection velocity [mms^{-1}]

Plasticity index present in Table 6.4.2 decreases with an increase of MWCNT content below 3.0 wt. % MWCNT, indicating the improvement in elastic recovery of nanocomposites after removing the external load. Similar behavior was reported for epoxy-based vinyl-ester polymer matrix with graphene nanoplatelets.^[163] An exceptional increase of plasticity index for 3.0 wt. % MWCNT at 25 mms^{-1} was observed. This is due to the agglomeration of the carbon nanotubes at elevated loads^[170,208] caused by the low injection velocity. On the other hand, the reduction of the plasticity index at 100 mms^{-1} (stating improved plastic recovery) was obtained at low nanofiller loads with a plateau above 0.5 wt. %.

6.5. Electrical properties of injection molded nanocomposites

Two methods of electrical properties determination of PC/ABS-MWCNT nanocomposites (Figure 3.4.12) related to surface- and volumetric electrical conductivity are applied to investigate the performance achieved after injection molding. Figure 6.5.1 illustrates the electrical conductivity

dependence on the MWCNT content and on the injection velocity for PC/ABS-MWCNT nanocomposites processed at 280 °C. The conductivity increases with the nanofiller content. Electrical conductivity remains within one order of magnitude between the extreme values of each material (*e.g.* 4.8 E-3 Scm^{-1} for 3.0 wt. % and 1.2 E-3 Scm^{-1} for 1.5 wt. %) with higher values appearing at low injection velocities. This can be explained by the theory of carbon nanotubes location in the core of the specimen^[209] confirmed by Figure 6.2.10 and Figure 6.2.13 and based on the direct influence of shear gradient for various injection velocities.

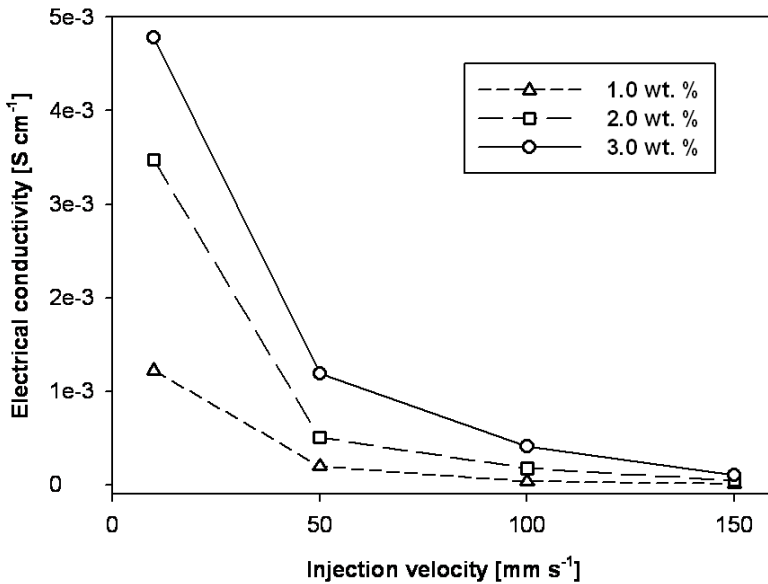


Figure 6.5.1: Electrical conductivity of nanocomposite injection molded at 280 °C.

Figure 6.5.2 shows the relation between surface and volumetric conductivity of samples obtained with the direct masterbatch dilution in injection molding machine. Electrical conductivities are similar at low injection velocity, which proves the similar morphologies in sample skin and core. From 60 mm s⁻¹ onwards both conductivities are constant: 0.1 Scm^{-1} and 1.1 Scm^{-1} for

surface and volumetric conductivity, respectively. The core of the specimen is MWCNT-rich at higher injection velocities and the nanofiller is oriented in the direction of the flow. This causes the increase of volume electrical conductivity giving also more differences between volume and surface conductivities. However, this phenomenon seems to have no strong relation with agglomeration. At higher injection velocities the surface conductivity is measured in low MWCNT concentration skin region, so the lower values are observed.

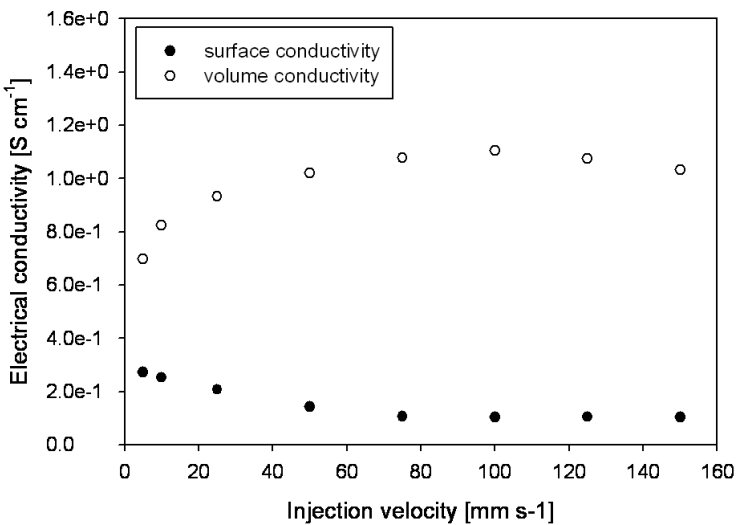


Figure 6.5.2: Electrical conductivity of nanocomposite with 5.0 wt. % MWCNT injection molded (**COM**) at 280 °C.

The sensitivity of the surface conductivity to the skin layer at low injection velocity was already presented by Villmow *et al.*^[60] Figure 6.5.3 shows the analogous studies of both electrical conductivities dependence on the melt temperature during processing. Volumetric and surface conductivity show the opposite behavior, with the closest values between 270 °C and 275 °C which seem to be the best temperature for obtaining homogeneous samples.

However, the differences are significantly lower than the in the previous study, indicating higher influence on injection velocity on electrical conductivity.

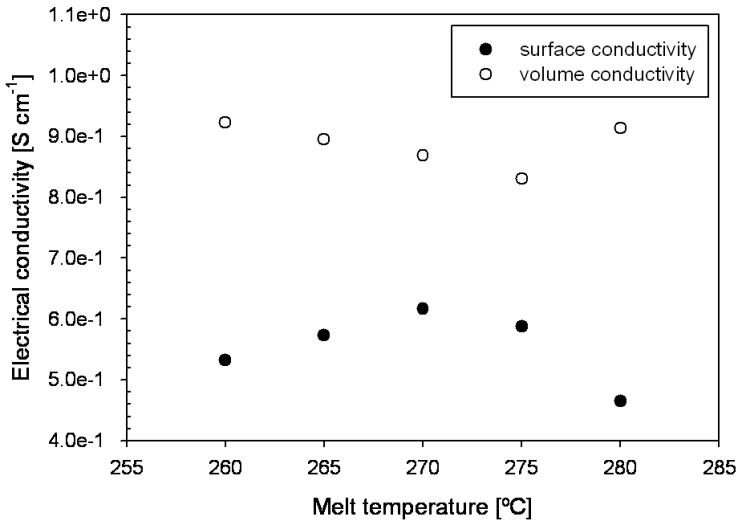


Figure 6.5.3: Electrical conductivity of nanocomposite with 5.0 wt. % MWCNT injection molded (**COM**) at 25 mm s^{-1} .

Direct masterbatch dilution **DD** in injection molding results with different electrical properties behavior of the nanocomposite with respect to the injection velocity. Such differences between **DD** and **COM** methods are present at low- (Figure 6.5.4) and high (Figure 6.5.6) MWCNT loads. Intensive change of the electrical conductivity at low injection velocities was already observed with the opposite trend (Figure 6.5.1). Reversed behavior of the material in **DD** and **COM** processing is based on the different nature of both methods. The former one includes mixing of masterbatch and pristine matrix in injection molding, which is hampered due to the viscosity difference and transporting (not mixing) character of the screw. Therefore, the higher injection speed providing higher shear results with higher

homogeneity of the material and the following formation of co-continuous nanocomposite. The **COM** injection molding on the contrary shows slight decrease of morphology (or maintaining the dispersion state achieved in melt-mixing) rather than the effective breakage of agglomerates.

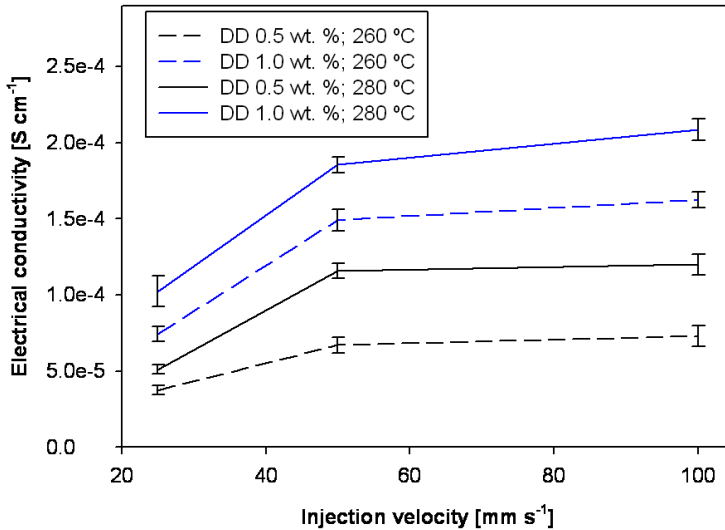


Figure 6.5.4: Electrical conductivity of nanocomposites (lower MWCNT loads) diluted in injection molding with **DD** method.

Furthermore, in both cases melt temperature during injection molding shows influence on the electrical conductivity. Elevated values of the temperature provide higher conductivity and this effect is more obvious for nanocomposites with low carbon nanotube loads (Figure 6.5.4). This is most probably due to the viscosity difference between the masterbatch and the pristine matrix. At elevated temperatures both melts have the decreased viscosity, which facilitates mixing and carbon nanotubes migration between the nanofiller-rich and -poor phases.

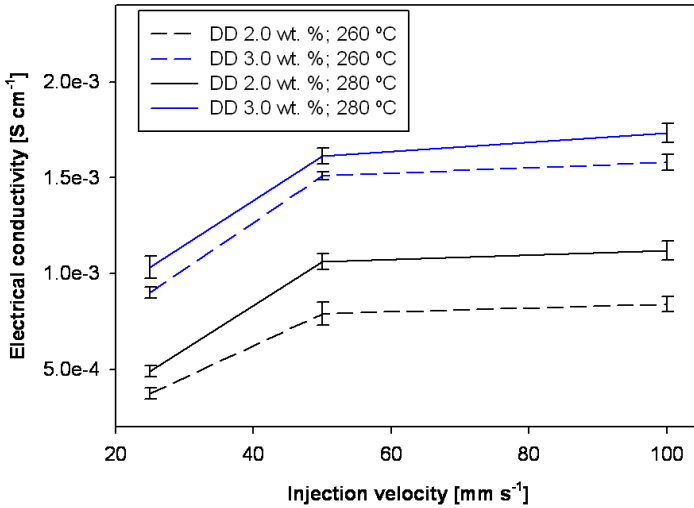


Figure 6.5.5: Electrical conductivity of nanocomposites (higher MWCNT loads) diluted in injection molding with **DD** method.

6.5.1. Recovery of conductive network

The recovery of electrical conductivity was investigated after various material processing routes (Figure 6.5.6). The experiment reported in Table 6.5.1 consists of three groups of PC/ABS-MWCNT nanocomposites. Materials were principally processed by injection molding and compression molding. This was followed by grinding the specimens and compression molding such obtained materials. Raw material for the first processing step (first compression or injection molding: Figure 6.5.6a or Figure 6.5.6b, respectively) was produced with masterbatch dilution in extruder (samples **COM** from Table 6.5.1) or in injection molding machine (samples **DD**). Significant differences between electrical conductivity of two different processing paths of one material are showed in Table 6.5.1. Compression molded nanocomposite with 3.0 wt. % MWCNT shows electrical conductivity over two orders of magnitude higher than the same nanocomposites after

injection molding. Nanocomposite diluted in injection molding shows lower electrical conductivities than the previous method for both velocities.

Table 6.5.1: Electrical conductivity after various processing paths done on injected (280 °C) nanocomposites; values are in $S\text{cm}^{-1}$.

Proc. ⁽¹⁾	Inj. veloc. ⁽²⁾	COM ⁽³⁾		DD ⁽⁴⁾	
		1.5 wt.%	3.0 wt.%	1.5 wt.%	3.0
C 01	(a) -	1.62E-01	2.38E-01	-	-
C 02	(c) -	3.18E-01	1.76E-01	-	-
I 01	(b) 10	-	8.29E-03	3.52E-04	6.94E-03
	(b) 100	-	3.81E-03	1.97E-04	2.76E-03
C 01	(d) 10	-	3.73E-01	5.44E-02	1.98E-01
	(d) 100	-	3.21E-01	5.97E-02	2.47E-01

⁽¹⁾ Processing: C-compression molding, I- injection molding; ⁽²⁾ Injection velocity [mms^{-1}]; ⁽³⁾ Two processing steps before 1st processing; ⁽⁴⁾ one processing step before 1st processing

Grinding the samples after the first processing and the following compression molding of that material shows the expected results of leveled electrical conductivities in the final specimens. Both, masterbatch dilution in extrusion and in injection molding, show significant differences of conductivity between the first and the second processing. An increase of two orders of magnitude for previously injected samples was observed. Moreover, after the re-compression, electrical conductivity becomes constant between both processing velocities and both methods. The final values are similar within one nanofiller concentration, which can be explained as the relaxation of carbon nanotube network. These results show that non-homogeneously distributed nanofiller leaves the possibility of electrical conductivity recovery

after the formation of the final part. Similar effects are reported in the literature for the increase of electrical conductivity of nanocomposite melt^[95] or the change of electrical properties after the specimen annealing.^[210] In both examples the changes are related to the viscoelastic relaxation of the polymer matrix allowing the reorientation of loosely-packed agglomerates and not entangled carbon nanotubes. This explanation applies also to the presented observations.

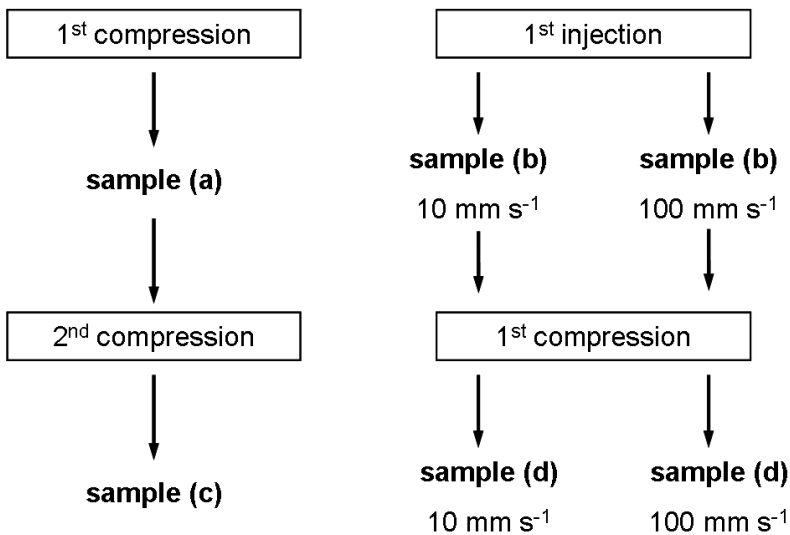


Figure 6.5.6: Scheme of nanocomposite re-processing paths for conductive network recovery presented in Table 6.5.1.

Results present in Table 6.5.2 are the confirmation of the above findings. Besides the higher electrical conductivity observed at elevated injection velocity, all values of electrical conductivity recorded after DMA are higher than before this experiment. This is related to the recovery (or formation) of carbon nanotube network after temperature- and stress treatment. Vibration at frequency 1 Hz along with the temperature slightly above PC glass transition temperature provides good conditions for nanofiller movement.

Chains relaxation allows higher number of MWCNT freedom degrees what results with significant nanotube-nanotube contact improvement and the following increase of the electrical conductivity.

Table 6.5.2: Electrical conductivity change after DMA test on injected (280 °C) nanocomposites (**MB**); values are in Scm^{-1} .

MWCNT [wt. %]	Before DMA		After DMA	
	25⁽¹⁾ mms⁻¹	100⁽¹⁾ mms⁻¹	25⁽¹⁾ mms⁻¹	100⁽¹⁾ mms⁻¹
0.5	5.11 E-05	1.07 E-04	2.81 E-04	4.00 E-04
1.0	8.25 E-05	2.08 E-04	4.43 E-04	5.03 E-04
2.0	1.45 E-04	2.73 E-04	5.56 E-04	6.46 E-04

⁽¹⁾ Injection velocity

6.6. Preliminary conclusions

Preliminary conclusions on injection molding of PC/ABS-MWCNT are present in Table 6.6.1. Two independent variations of processing were studied along with the influence of the most important processing parameters.

Application of the method basing on direct dilution of masterbatch in injection molding machine does not bring improvement in the morphology, compared to the common injection molding. Besides variations in MWCNT dispersion quality, the location of nanofiller is different in these methods. Orientation of carbon nanotubes along the melt flow in the common method is relatively high. Increased flammability of injection molded specimen, compared to compression molded nanocomposites, along with the improvement of mechanical properties is related to tighter packing of polymer chains and nanofiller. Nanoindentation test shows the influence of nano-scale filler on micro- and macro-scale mechanical properties. Electrical

conductivity, slightly decreased after injection molding, show higher values when the samples are re-processed and the nanotubes network is rearranged. This gives the possibility of carbon nanotube-filled nanocomposites application also after recycling.

Table 6.6.1: Summary of the performance of injection molded PC/ABS-MWCNT nanocomposites; behavior relates to the increase of parameters defined in columns.

Property	MWCNT load	Injection gate distance	Injection velocity	Melt temperature
<u>Common processing (COM)</u>				
Morphology	▼	▲	●	NA
Thermal stability	▲	NA	NA	NA
Flammability	▼	NA	▼	NA
Mechanical	▲	NA	▲	▼
Electrical	▲	NA	▲	NA
<u>Direct dilution processing (DD)</u>				
Morphology	▼▼	▲	●	NA
Thermal stability	▲	NA	NA	NA
Flammability	▼	NA	▼	NA
Mechanical	▲	NA	NA	▲
Electrical	▲	NA	▼▼	NA

▲/▼ – significant increase/decrease of value, ▲/▲ – moderate increase/decrease of value, ● – no significant or not defined change.

7. Modelling of injection molded nanocomposites

Computational simulation of polymer processing supports the understanding of material behavior and enables a complete study of manufacturing processes of short fiber-reinforced polymers. Injection molding, in its complexity, requires the support of mathematical methods for full understanding, especially for nanocomposites processing. Microfiller orientation in the specimen obtained by injection molding differs dependently on the distance from the mold wall and from the injection gate. Variations of shear and melt-mold temperature exchange coefficients influence the orientation of one-dimensional filler, which can be described by mathematical model with relatively good accuracy. Nevertheless, the accuracy of such model is questioned when the nano-scale filler is used for calculations. Different interactions between the matrix and the nanofiller causing difference in flow behavior require modification of the previous mathematical model.

In this chapter, the orientation of carbon nanotubes is investigated in injection molded specimens. Influence of the orientation on the position from injection gate is studied. Besides, the resulting output from the calculations is compared with the experimental data in order to estimate the data fitting.

7.1. Methodology and basic assumptions

7.1.1. A short description of numerical models

Fokker-Planck mathematical model, known as Kolmogorov equation,^[211] is a widely accepted method to solve stochastic differential equations, *e.g.* for engineering solutions). The general concept of Brownian particle in a fluid (*e.g.* describing a hypothetical system with a certain number of freedom

degrees) described by this model has an advantage of the limited parameters use.^[212] Equation 7.2 shows Fokker-Planck model for $n(t,x)$:

$$(7.1) \quad \begin{aligned} \frac{\partial n(t,x)}{\partial t} = & -\frac{d}{dx} [n(t,x)a(x)] + \frac{d^2}{dx^2} [n(t,x)\mathfrak{S}(x)] = \\ & -a(x)\frac{\partial n(t,x)}{\partial x} - a'(x)n(t,x) + \frac{\partial^2 n(t,x)}{\partial x^2} \mathfrak{S}(x) + \\ & 2\frac{\partial n(t,x)}{\partial x} \mathfrak{S}'(x) + \mathfrak{S}''(x)n(t,x) \end{aligned}$$

The necessity of extended calculations disables the application of other than Tucker-Folgar models (*e.g.* Fokker-Planck) to solve large scale industrial problems. Therefore, the Tucker-Folgar method (Equation 7.2) simplifies the calculation process by using fiber orientation tensors defined as moments of the distribution function.^[213] The fiber orientation tensor (α_{ij}) defining the orientation on 3D meshes depends on the vortical tensor (describing local rotary motions of polymer melt) ($\frac{1}{2}\omega_{ij}$) and the deformation rate tensor ($\frac{1}{2}\gamma_{ij}$). The C_i coefficient defines fiber-fiber interactions and is determined basing on the experimental data.

$$(7.2) \quad \begin{aligned} \frac{D\alpha_{ij}}{D_t} = & -\frac{1}{2}(\omega_{ik}\alpha_{kj} - \alpha_{ik}\omega_{kj}) \\ & + \frac{1}{2}\lambda(\dot{\gamma}_{ik}\alpha_{kj} + \alpha_{ik}\dot{\gamma}_{kj} - 2\alpha_{ijkl}\dot{\gamma}_{kl}) \\ & + 2C_i\dot{\gamma}(\delta_{ij} - 3\alpha_{ij}) \end{aligned}$$

The major challenge in applying the Tucker-Folgar model into PC/ABS-MWCNT nanocomposite study is related with the usual use of this method to solve macro-scale problems. Commonly simulated carbon or glass

short-fiber reinforcement does not show such strong fiber-fiber interactions as seen for nano-scale fillers, such as carbon nanotubes.^[145] In this case the C_f coefficient needs to be correctly selected in order to simulate expected conditions.

Finite elements method, a mathematical method having wider application than aforementioned models, can be applied to calculate orientation tensors of one-dimensional fillers in polymer matrix, too. It is a common method used for calculation of numerical approximations to the unknown analytical solution.^[214-215] After cutting the specimen volume into smaller elements and interconnecting them at nodes, the set of basic functions defining the process are calculated. Such a simplification forms a convenient, universal approach. Nevertheless, disadvantages of formation of a closed solution (disabling study of once-defined system at various conditions) and easiness of mistakes need to be taken into account.

Computational simulation of multi-walled carbon nanotubes behavior in PC/ABS immiscible blend during injection molding process was carried out with the use of various types of software. Moldex 3D-Fiber (CoreTech System Co., Ltd.) software simulates the 3-D orientation of carbon nanotubes in the process of mold filling during injection molding. The anisotropy of the nanocomposite, responsible for the physical properties of the final part were predicted with the support of OpenFOAM (OpenCFD Ltd. at ESI Group) software defining the laws of fluid flow.

7.1.2. Assumptions used for the calculation

Data-feed for the computational simulation contains study of the nanocomposite viscosity present in Figure 6.2.1 along with the carbon nanotubes and matrix characteristics present in Chapter 3. The injection molding conditions simulated in this calculation were similar to the conditions applied for the experimental tests. The nanocomposite injected

into the mold cavity at $280\text{ }^{\circ}\text{C}$ at 100 mms^{-1} was described in Table 3.3.1. The carbon nanotube content in nanocomposite was simulated at 2.0 wt. %. This concentration was a compromise between expected high freedom of individual carbon nanotubes and relatively high nanofiller load.

Simulations were carried out for 13 sets of (X, Y) coordinates selected along the specimen length, shown in Figure 7.1.1. Section N=13 represents the area near the injection gate while N=1 is the area at opposite end of the mold cavity. These sets of coordinates are evenly spaced along the y axis being the direction of the melt flow marked in Cartesian coordinate system in Figure 7.1.1. Calculations are performed for the central area of the mold cavity, marked as a gray area. Each of these coordinates has the tensors of 15-30 nodes spread throughout the specimen height, designated as the z axis in Figure 7.1.1.

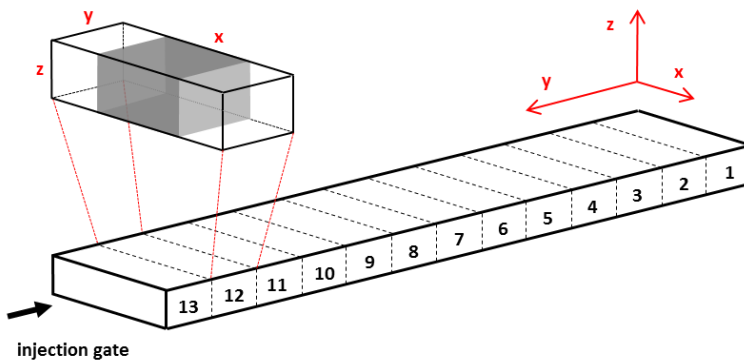


Figure 7.1.1: Schematic explanation of theoretical sample division in computational modeling process with the definition of axes; gray area shows the investigated area.

The resulting data is shown as a set of 13 graphs of the tensors at each (X, Y) coordinate. Each graph contains the distribution of the nanofiller share that is parallel to the defined axis of the Cartesian coordinate system (x, y or z in Figure 7.1.1). The change is plotted along the height of the specimen

(x in Figure 7.1.1). Besides, a graph that shows the standard deviation for each tensor along the length of the specimen is shown to highlight the change in standard deviation in this direction.

7.2. Calculation results

Differences in orientation of carbon nanotubes in various parts of the final injection molded specimen can be observed in Figure 7.2.1. Orientation is strictly related to the melt flow in the mold cavity.

Graphs of all three tensors for selected coordinates $N=1, 4, 7, 10$ and 13 show that the stabilization of the flow provides the constant orientation of MWCNT along the specimen height before the segment 10.

That makes *c.a.* 23 % of the specimen length after the injection gate. Above that distance, the fountain flow of injected melt can be assumed to provide a homogeneous morphology with oriented nanofiller. Besides, all the reported graphs show a significantly higher percentage of carbon nanotubes oriented along the y axis (length of the specimen), which is an expected result. Tensor x , showing the orientation of carbon nanotubes along the width of the specimen, is on the level of *c.a.* 20 % for all the examples shown in Figure 7.2.1, except the injection gate region. This effect is caused by the fountain flow. Furthermore, the disturbances present for all the coordinates in the *c.a.* 0.0-0.5 mm and 1.5-2.0 mm are caused by material behavior near the skin region.

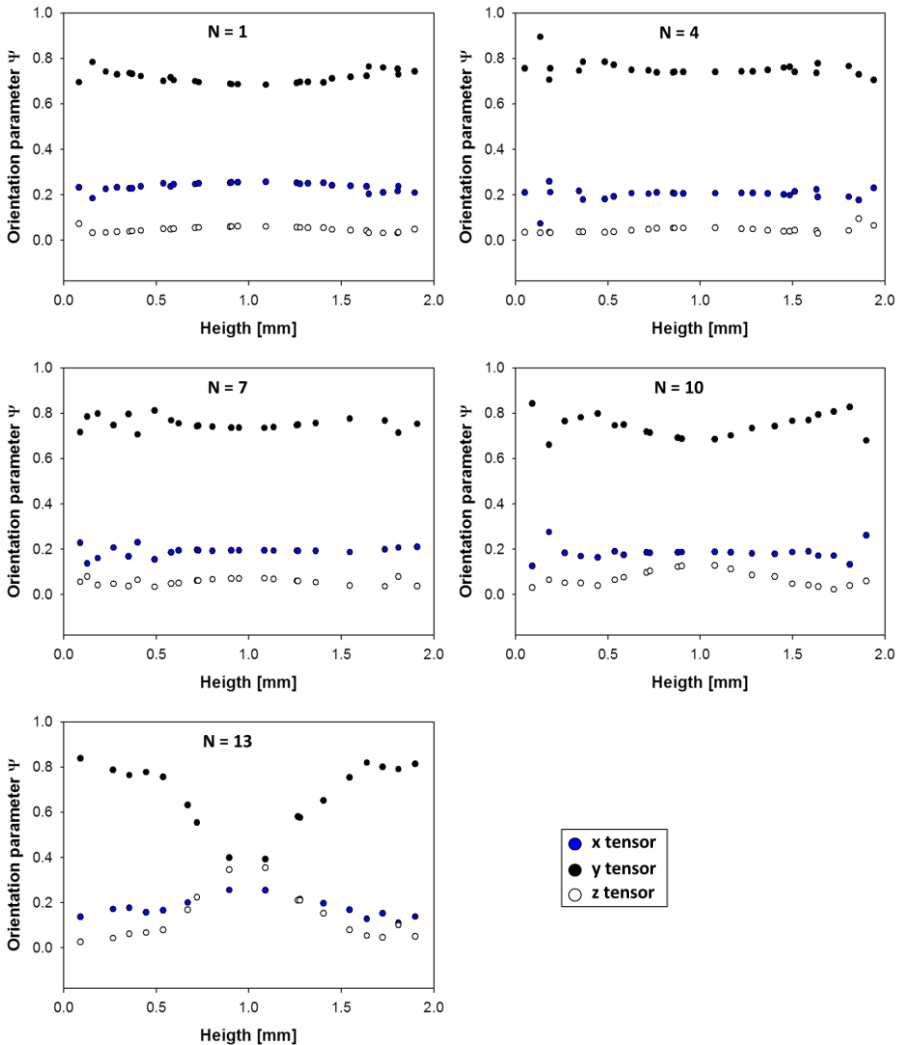


Figure 7.2.1: Graphs showing x , y and z tensors at selected coordinates.

Considering the graph of material at coordinate $N=13$ in Figure 7.2.1 in more detail, it can be observed that the homogenization of MWCNT orientation tensors occurs along all the axes of the Cartesian coordinate system. The injection gate region (also for $N=12$ or 11 , not shown here) is characterized by non-laminar and rather turbulent flow causing little or no

alignment of nanotubes. This is shown as low values of the orientation parameter ψ for x , y and z , ranging between 20 and 40 %. Nevertheless, the skin region (at specimen height below 0.5mm and above 1.5mm) of coordinate $N=13$ shows material behavior similar to other parts of the specimen. This suggests that the effect of poor MWCNT orientation in the core region at injection gate is related to the application of holding pressure. The residual nanocomposite melt injected into the mold cavity at the end of the cycle is isotropic and no conditions to change this state occur. Therefore the considered area should be also isotropic. Besides, this study shows change of nanotubes orientation in injection gate area from tensor y towards z , not along the expected x axis.

Individual study on each tensor along the mold cavity length give similar results at those at the far-gate region, but different nanofiller orientation behavior near the gate area. Figure 7.2.2 shows the x tensor at the beginning ($N=13$ to $N=10$) and at the end ($N=3$) of the specimen. The constant orientation of carbon nanotubes of *c.a.* 21 % is independent on the specimen height. Further interpretation of this graph shows a clear decrease of the percentage of nanotubes oriented along the mold width with shortening the distance from injection gate. Moreover, the distribution of MWCNT orientation along the x axis (explained in Figure 7.1.1) show the aforementioned effect of holding pressure.

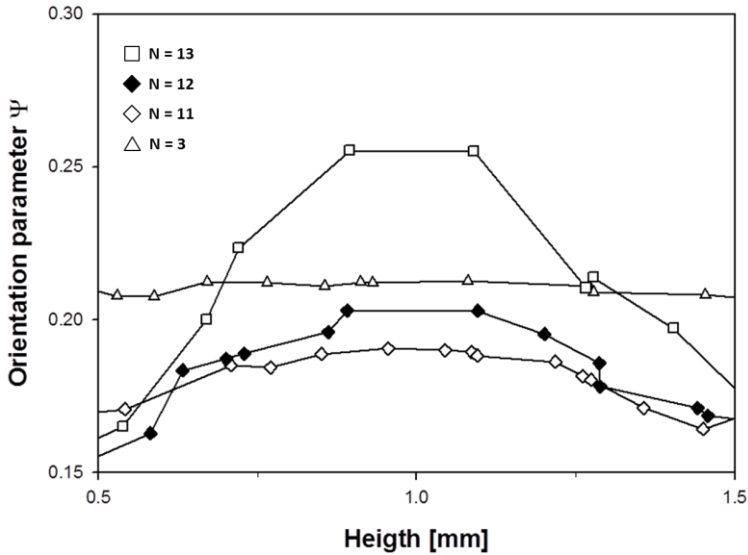


Figure 7.2.2: Curves of x tensor versus specimen height.

Figure 7.2.3 shows a detailed insight into the evolution of the y tensor along the injected specimen length. Coordinates $N=1$ (not shown here for clarity) to $N=7$ show no significant change with shortening the distance to injection gate and a value of orientation parameter is c.a. 75 %. This can be understood as the situation where the majority of carbon nanotubes are oriented along the specimen length. A significant change in orientation parameter with an increasing pith between the coordinates starts from $N=9$, so near the 30 % of the specimen length counting from injection gate. Unlike in the evolution of tensor x , here the decrease of MWCNT orientation occurs in the specimen core region. The constant value of orientation parameter in the skin region suggests the occurrence of a frozen nanocomposite layer in the initial phase of the cycle independent of the specimen area (coordinates). Besides, the drop of orientation to 40 % shows the significance of holding pressure and the fountain flow.

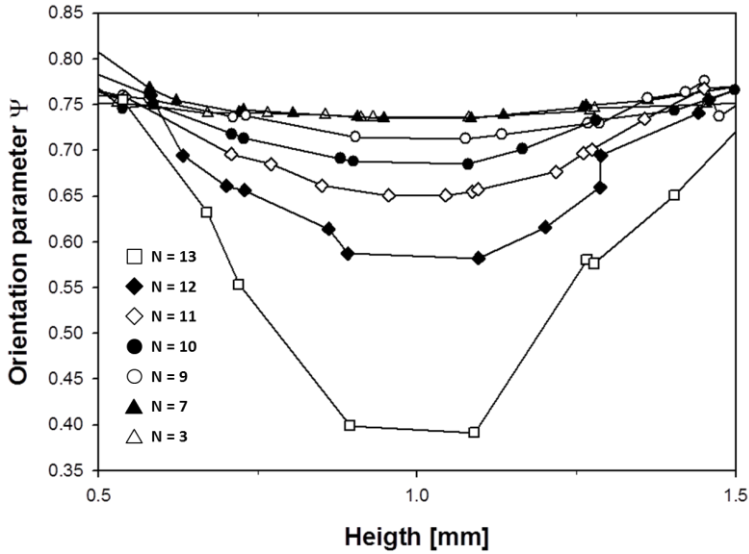


Figure 7.2.3: Curves of γ tensor versus specimen height.

The opposite trend in the evolution of nanofiller orientation is observed with shortening the distance to injection gate (Figure 7.2.4). Orientation along the z tensor increases near the injection gate, causing a large share of the total nanofiller load to be present at the very beginning of the specimen (N-12, 13). Before that, the gradual increase of orientation along the thickness, the least expected, is on the level 5-15 %. The negligible share of this tensor can be explained if the front of the nanocomposite melt advances mainly across and along the sample, due to the dimensions of the mold (width: 2 mm, thickness: 10 mm). Therefore, such an increase of MWCNT orientation along the z axis in the core region compared to the initial value at N=3 only confirms the formation of aforementioned isotropic state near the injection gate.

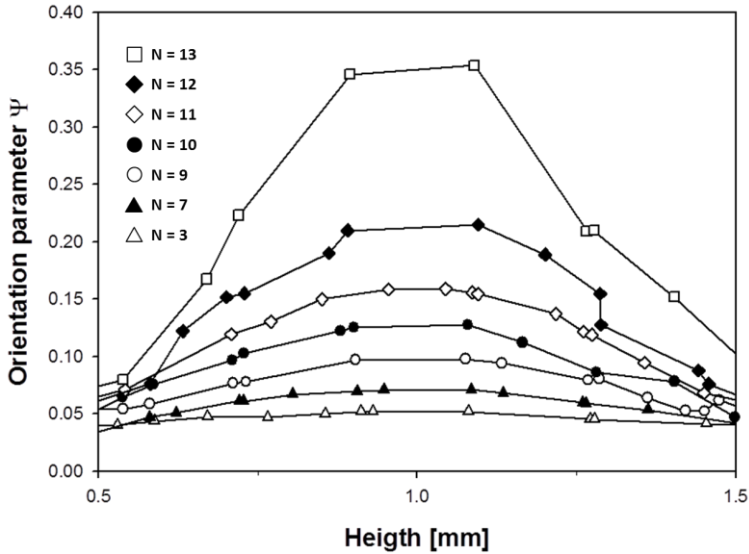


Figure 7.2.4: Curves of z tensor versus specimen height.

Nevertheless, standard deviation plotted versus specimen length individually for each tensor in Figure 7.2.5 shows rather poor accuracy in the initial part of the specimen ($N=13$ to $N=8$). The accuracy of the z tensor shows trend similar to the other curves. However, the values near $N=13$ are unexpectedly high, especially concerning the low values of the orientation parameter. This can be explained by the highly unpredictable isotropic character of the specimen in the injection gate area. Furthermore, a significant increase of standard deviation value occurs at $N=3$ for x and y tensors representing the main direction of the fountain flow. Such an effect is most probably related to the disturbances of the end of mold cavity. The advancing melt suddenly stops causing changes in morphology.

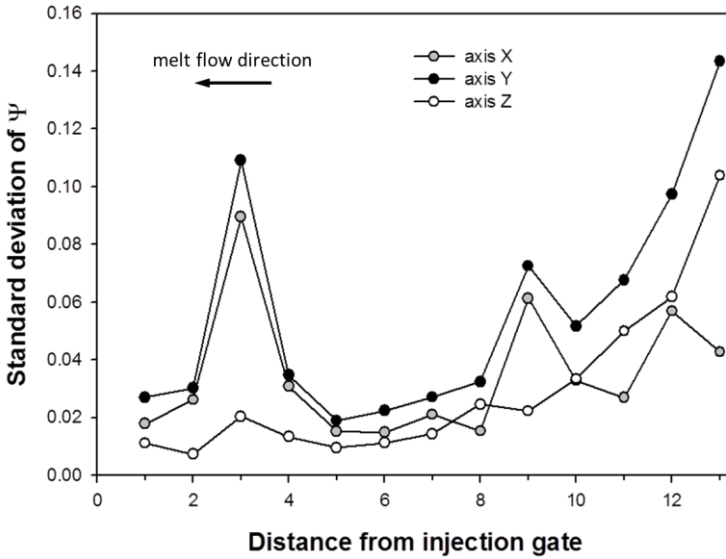


Figure 7.2.5: Standard deviation for each tensor along the specimen length.

7.2.1. Comparison between theoretical and experimental data

Comparison between the aforementioned results of computational modeling of MWCNT orientation in injection molded specimen and the experimental data present in Chapter 6 were carried out. Both methods used for the determination of carbon nanotube orientation differ significantly, which makes a full comparison difficult. Nevertheless, tensors x and y of coordinates N=3 to N=7 at the half-height (*c.a.* 1.0 mm) can be used for experimental and theoretical data fitting, due to relatively high similarity with the area of sample subtraction for experimental tests.

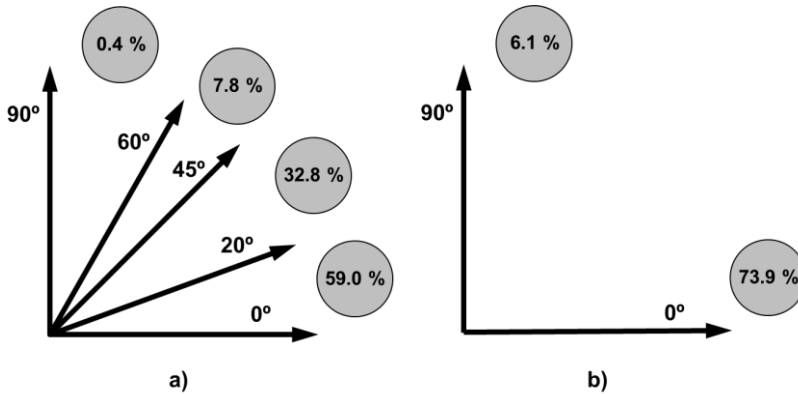


Figure 7.3.1: Percentage of carbon nanotubes fitting the area defined by vectors a) experimental values, b) calculated values.

Figure 7.3.1a shows the result of the study of Feret's axes (described in Chapter 6), used as a definition of individual carbon nanotubes in experimental tests. Only 0.4 % of the total MWCNT quantity is parallel (or is within 30°) to z axis, defined in Figure 7.1.1. This is clearly a lower value than the calculated 6.1 % (Figure 7.3.1b). Besides, carbon nanotubes defined with tensor y create a lower share in experimental method (59.0 %) than calculated (73.9 %). The experimental result (8.2 %) gets closer to the mathematical model for z tensor, when the considered area is 0° to 45° and 45° to 90°. Nevertheless, the difference between both methods can be related to various factors and the precision of determining individual carbon nanotubes orientation by experimental methods may be insufficient. This arises from nanotube curvature and application of the Feret parameter. On the other hand, the Tucker-Folgar method still requires improvement in order to provide correct simulation for nanocomposites.

7.3. Preliminary conclusion

Similarity of the nanocomposite morphology described by the applied mathematical model and studied on specimens after injection molding

suggest that an agreement between the Tucker-Folgar method and experimental data exists. Both investigation methods show change of carbon nanotube orientation along the specimen length towards the direction perpendicular to melt flow with the decrease of distance from injection gate. This effect must have negative influence on properties such as electrical conductivity. Furthermore, the skin region observed earlier is well defined in the applied mathematical model. The expectations of relative similarity of MWCNT orientation along the whole specimen length should be changed after introduction of the presented model. It is clear that the injection gate influencing the melt flow.

8. Conclusions and future research

8.1. Conclusions

The effect of processing conditions and nanofiller feeding method during the twin-screw extrusion was investigated in the initial part of this study. The results from various analytical techniques used to fully characterize the nanocomposite and determine its behavior gave the overview of properties improvement.

- Study of morphology revealed the influence of processing parameters on the MWCNT dispersion in nanocomposites. The nanofiller dispersion quality decreased with the nanofiller load showing relation with the specific mechanical energy. Besides, no significant change of the location of majority of carbon nanotubes in the polycarbonate phase was observed in any of the applied nanofiller feeding method. However, masterbatch dilution showed the importance of two processing cycles in the nanocomposite formation step.
- Thermal properties showed dependence with the dispersion of MWCNT in the polymer matrix. The change of the heat capacity at the glass transition temperatures indicated the increase of carbon nanotube content in the ABS phase at elevated loads.
- Mechanical percolation was significantly lower than electrical percolation, indicating difficulties in the formation of conductive path. An improvement of mechanical properties with an increase of the MWCNT load was correlated with the theoretical values from the modified Halpin-Tsai method.
- Electrical conductivity improvement with MWCNT load increase was observed to be dependent on the processing conditions.

- Use of surface-modified carbon nanotubes in masterbatch dilution method show little impact on the influence of the processing parameters. Electrical percolation in the nanocomposites with MWCNT-COOH was lower than for pristine MWCNT. However, the destruction of charge paths by the surface oxidation caused significant decrease of electrical conductivity.
- Modification of nanofiller feeding method with the introduction of carbon nanotubes suspension in ethyl alcohol allowed reduction of the number of processing cycles with maintaining similar material properties.
- Introduction of non-covalent modification of the nanofiller gave an improvement in the final morphology. Electrical conductivity dependence on processing parameters was studied. Besides, no significant change of studied properties comparing to the suspension feeding method with the pristine nanofiller was observed.

Selected nanocomposites from twin-screw extrusion were injection molded in order to investigate the influence of processing parameters during the common industrially-accepted material shaping process.

- Application of the method basing on the direct dilution of masterbatch in injection molding machine brought no improvement in the morphology, compared to the common injection molding. The common injection molding gave strong nanofiller agglomeration in the final material.
- Orientation of carbon nanotubes along the melt flow in the common method is relatively high, which is confirmed further with the mathematical calculations. Relatively good agreement between the Tucker-Folgar method and the experimental data was observed, showing the change of carbon nanotube orientation behavior with the decrease of the distance from injection gate.

- Decreased flammability of injection molded specimen, compared to compression molded nanocomposites, along with the improvement of mechanical properties is related to tighter packing of polymer chains and carbon nanotubes. Nanoindentation test showed the influence of nano-scale filler on micro- and macro-scale mechanical properties.
- Electrical conductivity of the final material changed between high- or low shear applied during processing. The highest volumetric electrical conductivity appears at low shear. The differences between surface and volumetric conductivities revealed higher homogeneity of the specimens at low shear rate, implemented by low injection velocities and moderate melt temperatures.
- The re-creation of carbon nanotube network and the recovery of electrical conductivity in re-processed PC/ABS-MWCNT nanocomposites subjected previously to various processing paths was observed.

8.2. Suggestions for future research

Immiscible blend-based nanocomposites investigated within this thesis can be used in a wide range of industrial applications due to the combined properties of polymeric blend and carbon-based nanofiller. Thus, this technology can be further explored towards various directions.

- Nanocomposite formation should be further studied, focusing on the additives improving more homogeneous distribution of the nanofiller in the phases of an immiscible blend. Achievement of this goal is difficult when only feeding method or processing parameters are changed.
- Multi-phase blends with semi-crystalline character (*e.g.* PA6/PP) filled with multi-walled carbon nanotubes should be studied with the analogous approach. The influence of the nanofiller on crystallinity should have interesting effect on mechanical properties of these nanocomposites.

- The study of co-filled nanocomposites recently attracts attention. Macro-nano filler systems represented by glass fibers-carbon nanotubes should be in the area of particular interest. Such combination of the fillers would allow significant increase of mechanical properties provided by the macro filler and an increase of electrical properties due to the incorporation of carbon nanotubes.
- Injection molding of multi-phase polymeric systems filled with carbon nanotubes should be investigated in order to achieve optimal conditions for homogeneous nanofiller distribution. Complex specimen shapes should be introduced to such study in order to provide more complete data.
- Computational modeling of the location and orientation of carbon nanotubes in injection molded specimens should be expanded on the influence of processing parameters and correlated with the results of Raman spectroscopy.

LITERATURE

- [1] A. Gödel, P. Pötschke, Carbon nanotubes in multiphase polymer blends; In Polymer-Carbon Nanotube Composites: Synthesis, Properties and Applications; Editors: T. McNally, P. Pötschke; ISBN 1-84569-761-8; Woodhead Publishing, **2011**, Chapter 19.
- [2] J.L. Carvile, H.T. Luu, L.S. Bassett, D.A. Driscoll, C. Yuan, Y.G. Chang, X.Y. Ye, A.M. Calafat, K.B. Michels, Polycarbonate Bottle Use and Urinary Bisphenol A Concentrations; *Environ. Health. Perspect.*, **2009**, 117, 1368-1372.
- [3] *www.matweb.com*, visited: 13/12/2013.
- [4] S. Balakrishnan, N.R. Neelakantan, D. Nabi Saheb, J.P. Jog, Rheological and morphological behaviour of blends of polycarbonate with unmodified and maleic anhydride grafted ABS; *Polymer*, **1998**, 39, 5765-5771.
- [5] Y. Sun, Z.-X. Guo, J. Yu, Effect of ABS Rubber Content on the Localization of MWCNTs in PC/ABS Blends and Electrical Resistivity of the Composites; *Macromol. Mater. Eng.*, **2010**, 295, 263-268.
- [6] Z. Spitalsky, D. Tasis, K. Papagelis, C. Galiotis, Carbon nanotube-polymer composites: Chemistry, processing, mechanical and electrical properties; *Prog. Polym. Sci.*, **2010**, 35, 357-401.
- [7] K. Prashantha, J. Soulestin, M.F. Lacrampe, P. Krawczak, G. Dupin, M. Claes, A. Tewari, Electrical and dielectric properties of multi-walled carbon nanotube filled polypropylene nanocomposites; *Polym. Polym. Compos.*, **2010**, 18, 489-494.
- [8] S. Bose, A.R. Bhattacharyya, A.R. Kulkarni, P. Pötschke, Electrical, rheological and morphological studies in co-continuous blends of polyamide 6 and acrylonitrile-butadiene-styrene with multiwall carbon nanotubes prepared by melt blending; *Comp. Sci. Tech.*, **2009**, 69, 365-372.
- [9] B. Marinho, M. Ghislandi, E. Tkalya, C.E. Koning, G. de With, Electrical conductivity of compacts of graphene, multi-wall carbon nanotubes, carbon black, and graphite powder, *Powder Technol.*, 221, **2012**, 351-358.

- [10] A.-C. Dupuis, The catalyst in the CCVD of carbon nanotubes – a review; *Prog. Mater. Sci.*, **2005**, 50, 929-961.
- [11] C.N.R. Rao, FRS, A. Govindaraj, Nanotubes and Nanowires, ISBN 18-4973-058; RSC Publishing, **2005**.
- [12] T. Guo, P. Nikolaev, A. Thess, D.T. Colbert, R.E. Smalley, Catalytic growth of single-walled nanotubes by laser vaporization; *Chem. Phys. Lett.*, **1995**, 243, 49-54.
- [13] K. Hata, D.N. Futaba, K. Mizuno, T. Namai, M. Yumura, S. Iijima, Water-Assisted Highly Efficient Synthesis of Impurity-Free Single-Walled Carbon Nanotubes; *Science*, **2004**, 306, 1362-1364.
- [14] Y.C. Choi, Y.M. Shin, Y.H. Lee, B.S. Lee, G.-S. Park, W.B. Choi, N.S. Lee, M.K. Jong, Controlling the diameter, growth rate, and density of vertically aligned carbon nanotubes synthesized by microwave plasma-enhanced chemical vapor deposition; *Appl. Phys. Lett.*, **2000**, 76, 2367-2369.
- [15] F.R. Garcia-Garcia, M. Perez-Cabero, D.M. Newskaia, I. Rodriguez-Ramos, A. Guerrero-Ruiz, Improving the synthesis of high purity carbon nanotubes in a catalytic fluidized bed reactor and their comparative test for hydrogen adsorption capacity; *Catal. Today*, **2008**, 133-135, 815-821.
- [16] N. Popovska, K. Danova, I. Jipa, U. Zenneck, Catalytic growth of carbon nanotubes on zeolite supported iron, ruthenium and iron/ruthenium nanoparticles by chemical vapor deposition in a fluidized bed reactor; *Powder Technol.*, **2011**, 207, 17-25.
- [17] <http://www.ifw-dresden.de>, visited: 13/12/2013.
- [18] Y. Murakami, Y. Miyauchi, S. Chiashi, S. Maruyama, Generation of Single-Walled Carbon Nanotubes from Alcohol and Generation Mechanism by Molecular Dynamics Simulations; *Chem. Phys. Lett.*, **2003**, 374, 53-58.
- [19] D.E. Resasco, W.E. Alvarez, F. Pompeo, L. Balzano, J.E. Herrera, B. Kitiyanan, A. Borgna, A scalable process for production of single-walled carbon nanotubes (SWCNT's) by catalytic disproportionation of CO on a solid catalyst; *J. Nanoparticle Res.*, **2002**, 4, 131-136.

- [20] R.T.K. Baker, P.S. Harris, J. Henderson, R.B. Thomas, Formation of Carbonaceous deposits from the reaction of methane over nickel; *Carbon*, **1975**, 13, 17-22.
- [21] A. Oberlin, M. Villey, A. Combaz, Pyrolysis mechanism as studied by electron microscopy, DTA, IR and ESR; *Carbon*, **1978**, 16, 73-74.
- [22] A. Star, Y. Lu, K. Bradley, G. Gruner, Nanotube Optoelectronic Memory Devices; *Nano Lett.*, **2004**, 9, 1587-1591.
- [23] M. Endo, K. Takeuchi, S. Igarashi, K. Kobori, M. Shiraishi, H.W. Kroto, The production and structure of pyrolytic carbon nanotubes (PCNTs); *J. Phys. Chem. Solids*, **1993**, 54, 1841-1848.
- [24] S.R.C. Vivekchand, A. Govindaraj, Md. Motin Seikh, C.N.R. Rao, New Method of Purification of Carbon Nanotubes Based on Hydrogen Treatment; *J. Phys. Chem. B*, **2004**, 108, 6935-6937.
- [25] A.U. Yalovenko, AFM investigation of carbon nanotubes (www.ntmtd.com, visited: 15/12/2013).
- [26] K. Tanaka, T. Yamabe, K. Fukui, The Science and Technology of Carbon Nanotubes; ISBN 0-08-042696-4; Elsevier, **1999**.
- [27] Q. Wang, Effective in-plane stiffness and bending rigidity of armchair and zigzag carbon nanotubes, *Int. J. Solids Struct.*, **2004**, 41, 5451-5461.
- [28] B. Scheibe, M.H. Rummeli, E. Borowiak-Palen, R.J. Kalenczuk, Separation of surfactant functionalized single-walled carbon nanotubes via free solution electrophoresis method; *Cent. Eur. J. Phys.*, **2011**, 9, 325-329.
- [29] L.M. Sheng, L. Shi, K. Am, L.M. Yu, Y. Ando, X.L. Zhao, Effective and efficient purification of single-wall carbon nanotubes based on hydrogen treatment; *Chem. Phys. Lett.*, **2011**, 502, 101-106.
- [30] www.helixmaterial.com, visited: 13/12/2013.
- [31] A. Krishnan, E. Dujardin, T.W. Ebbesen, P.N. Yianilos, M.M.J. Treacy, Young's modulus of single-walled nanotubes; *Phys. Rev. B*, **1998**, 58, 14013-14019.
- [32] N. Yao, V. Lordi, Young's modulus of single-walled nanotubes; *J. Appl. Phys.*, **1998**, 84, 1939-1943.
- [33] www.nanocyl.com, visited: 13/12/2013.

- [34] R. Khare, S. Bose, Carbon nanotube based composites – a review; *J. Min. Mater Charact. Eng.*, **2005**, 4, 31-46.
- [35] R. Haggemueller, H.H. Gommans, A.G. Rizler, J.E. Fisher, K.I. Winey, Aligned single-wall carbon nanotubes in composites by processing method; *Chem. Phys. Lett.*, **2000**, 330, 219-225.
- [36] G. Sui, S. Jana, W.H. Zhong, M.A. Fuqua, C.A. Ulven, Dielectric properties and conductivity of carbon nanotube/semi-crystalline polymer composites; *Acta Mater.*, **2008**, 56, 2381-2393.
- [37] M.A. Coler, F.R. Barnet, A. Lightbody, H.A. Perry, Conductive Plastic Materials; *Proc. Inst. Radio Eng.*, **1950**, 38, 117.
- [38] Y.-C. Zhang, D. Zheng, H. Pang, J.-H. Tang, Z.-M. Li, The effect of molecular chain polarity on electric field-induced aligned conductive carbon nanotube network formation in polymer melt; *Comp. Sci. Tech.*, **2012**, 72, 1875-1881.
- [39] K. Prashantha, J. Soulestin, M.F. Lacrampe, P. Krawczyk, G. Dupin, M. Claes, Masterbatch-based multi-walled carbon nanotube filled polypropylene nanocomposites: Assessment of rheological and mechanical properties; *Comp. Sci. Tech.*, **2009**, 69, 1756-1763.
- [40] J.H. Jou, C.P. Wang, M.H. Wu, H.W. Lin, H.C. Pan, B.H. Liu, High-efficiency flexible white organic light-emitting diodes; *J. Mater. Chem.*, **2010**, 20, 6626-6629.
- [41] M. Monthieux, V.L. Kuznetsov, Who should be given the credit for the discovery of carbon nanotubes?; *Carbon*, **2006**, 44, 1621-1623.
- [42] J.-M. Thomassin, I. Huynen, R. Jerome, C. Detrembleur, Functionalized polypropylenes as efficient dispersing agents for carbon nanotubes in a polypropylene matrix; application to electromagnetic interference (EMI) absorber materials; *Polymer*, **2010**, 51, 115-121.
- [43] H. Cabeci, R. Guzman de Villoria, A.J. Hart, B.L. Wardle, Multifunctional properties of high volume fraction aligned carbon nanotube polymer composites with controlled morphology; *Comp. Sci. Tech.*, **2009**, 69, 2649-2656.

- [44] J. Sandler, M.S.P. Shaffer, T. Prasse, W. Bauhofer, K. Schulte, A.H. Windle, Development of a dispersion process for carbon nanotubes in an epoxy matrix and the resulting electrical properties; *Polymer*, **1999**, 40, 5967-5971.
- [45] J.K.W. Sandler, J.E. Kirk, I.A. Kinloch, M.S.P. Shaffer, A.H. Windle, Ultra-low percolation threshold in carbon-nanotube-epoxy composites; *Polymer*, **2003**, 44, 5893-5899.
- [46] X. Gong, J. Liu, S. Baskaran, R.D. Voise, J.S. Young, Surfactant-Assisted Processing of Carbon Nanotube/Polymer Composites; *Chem. Mater.*, **2000**, 12, 1049-1052.
- [47] S. Cui, R. Canet, A. Derre, M. Couzi, P. Delhaes, Characterization of multiwall carbon nanotubes and influence of surfactant in the nanocomposite processing; *Carbon*, **2003**, 41, 797-809.
- [48] I.N. Mazov, I.A. Ilinykh, V.L. Kuznetsov, A.A. Stepashkin, K.S. Ergin, D.S. Muratov, V.V. Tcherdyntsev, D.V. Kuznetsov, J.P. Issi, Thermal conductivity of polypropylene-based composites with multiwall carbon nanotubes with different diameter and morphology, *J. Alloys Compd.*, **2014**, 15, S440-S442.
- [49] L.-H. Du, J. Bai, H.-M. Cheng, The present status and key problems of carbon nanotube based polymer composites; *Polym. Lett.*, **2007**, 1, 253-273.
- [50] S.H. Lee, J.H. Kim, S.H. Choi, S.Y. Kim, K.W. Kim, J.R. Youn, Effects of filler geometry on internal structure and physical properties of polycarbonate composites prepared with various carbon fillers; *Polym. Int.*, **2009**, 58, 354-361.
- [51] G. Broza, M. Kwiatkowska, Z. Roslaniec, K. Schulte, Processing and assessment of poly(butylene terephthalate) nanocomposites reinforced with oxidized single wall carbon nanotubes; *Polymer*, **2005**, 46, 5860-5867.
- [52] D.H. Park, K.H. Yoon, Y.-B. Park, Y.S. Lee, Y.J. Lee, S.W. Kim, Electrical resistivity of polycarbonate/multiwalled carbon nanotube composites under varying injection molding conditions; *J. Appl. Polym. Sci.*, **2009**, 113, 450-455.

- [53] S. Pegel, P. Potschke, T. Villmow, D. Stoyan, G. Heinrich, Spatial statistics of carbon nanotube polymer composites; *Polymer*, **2009**, 50, 2123-2132.
- [54] M. Morcom, K. Atkinson, G.P. Simon, The effect of carbon nanotube properties on the degree of dispersion and reinforcement of high density polyethylene; *Polymer*, **2010**, 51, 3540-3550.
- [55] L. Yang, F. Liu, H. Xia, X. Qian, K. Shen, J. Zhang, Improving the electrical conductivity of a carbon nanotube/polypropylene composite by vibration during injection-moulding; *Carbon*, **2011**, 49, 3274-3283.
- [56] P. Pötschke, S.M. Dudkin, I. Alig, Dielectric spectroscopic on melt processed polycarbonate – multiwalled carbon nanotube composites; *Polymer*, **2003**, 44, 5023-5030.
- [57] P. Pötschke, M. Abdel-Goad, I. Alig, S. Dudkin, D. Lellinger, Rheological and dielectrical characterization of melt mixed polycarbonate-multiwalled carbon nanotube composites; *Polymer* **2004**, 45, 8863-8870.
- [58] T. Villmow, B. Kretschmar, P. Pötschke, Influence of screw configuration, resistance time, and specific mechanical energy in twin-screw extrusion of polycaprolactone/multi-walled carbon nanotube composites; *Comp. Sci. Tech.* **2010**, 70, 2045-2055.
- [59] S. Pegel, P. Pötschke, G. Petzold, I. Alig, S.M. Dudkin, D. Lellinger, Dispersion, agglomeration, and network formation of multiwalled carbon nanotubes in polycarbonate melts; *Polymer*, **2008**, 49, 974-984.
- [60] T. Villmow, S. Pegel, P. Pötschke, U. Wagenknecht, Influence of injection molding parameters on the electrical resistivity of polycarbonate filled with multi-walled carbon nanotubes; *Compos. Sci. Technol.*, **2008**, 68, 777-789.
- [61] H.M. Duong, N. Tamamoto, K. Bui, D.V. Papavassiliou, S. Maruyama, B.L. Wardle, Morphology Effects on Nonisotropic Thermal Conduction of Aligned Single-Walled and Multi-Walled Carbon Nanotubes in Polymer Nanocomposites; *J. Phys. Chem. C*, **2010**, 114, 8851-8860.
- [62] S. Sathyanarayana, G. Olowojoba, P. Weiss, B. Calgar, B. Pataki, I. Mikonsaari, C. Hübner, F. Hening, Compounding of MWCNTs with PS in a Twin-Screw Extruder with Varying Process Parameters: Morphology,

- Interfacial Behavior, Thermal Stability, Rheology, and Volume Resistivity; *Macrom. Mater. Eng.*, **2013**, 298, 89-105.
- [63] C. McClory, P. Potschke, T. McNally, Influence of Screw Speed on Electrical and Rheological Percolation of Melt-Mixed High-Impact Polystyrene/MWCNT Nanocomposites; *Macromol. Mater. Eng.*, **2011**, 296, 59-69.
- [64] J. Sandler, G. Broza, M. Nolte, K. Schulte, Y.-M. Laam, M.S.P. Shaffer, Crystallization of carbon nanotube and nanofiber polypropylene composites; *J. Macromol. Sci. B*, **2003**, 42, 479-488.
- [65] H. Zhang, Z. Zhang, Impact behavior of polypropylene filled with multi-walled carbon nanotubes; *Eur. Pol. Sci.*, **2007**, 43, 3197-3270.
- [66] D.-H. Xu, Z.-G. Wang, J.F. Douglas, Influence of Carbon Nanotube Aspect Ratio on Normal Stress Differences in Isotactic Polypropylene Nanocomposite Melts, *Macromolecules*, **2008**, 41, 815-825.
- [67] S. P. Bao, S.C. Tjong, Mechanical behavior of polypropylene/carbon nanotube nanocomposites: The effect of loading rate and temperature; *Mater. Sci. Eng. A*, **2008**, 485, 508-516.
- [68] K. Kalaitzidou, H. Fukushima, P. Askeland, L.T. Drzal, The Nucleating Effect of Exfoliated Graphite Nanoplatelets on the Crystallization of Polypropylene Nanocomposites; *J. Mater. Sci.*, **2008**, 43, 2895-2907.
- [69] I. Alig, D. Lellinger, S.M. Dudkin, P. Pötschke, Conductivity spectroscopy on melt processed polypropylene-multiwalled carbon nanotube composites: Recovery after shear and crystallization; *Polymer*, **2007**, 48, 1020-1029.
- [70] J.A. King, B.A. Johnson, M.D. Via, C.J. Ciarkowski, Electrical conductivity of carbon-filled polypropylene-based resins; *J. Appl. Polym. Sci.*, **2009**, 112, 425-433.
- [71] F. Thiebaud, J.C. Gelin, Characterization of rheological behaviors of polypropylene/carbon nanotubes composites and modeling their flow in a twin-screw mixer; *Compos. Sci. Technol.*, **2010**, 70, 647-656.
- [72] J.-W. Lee, J.-C. Lee, J. Pandey, S.-H. Ahn, Y.J. Kang, Mechanical Properties and Sound Insulation Effect of ABS/Carbon-black Composites; *J. Compos. Mater.*, **2010**, 44, 1701-1716.

- [73] D. Mari, R. Schaller, Mechanical spectroscopy in carbon nanotube reinforced ABS; *Mater. Sci. Eng. A*, **2009**, 521-522, 255-258.
- [74] R. Balart, J. Lopez, D. Garcia, M. Dolores Salvador, Recycling of ABS and PC from electrical and electronic waste. Effect of miscibility and previous degradation on final performance of industrial blends; *Eur. Polym. J.*, **2005**, 41, 2150-2160.
- [75] O. Meincke, D. Kaempfer, H. Weickmann, C. Friedrich, M. Vathauer, H. Warth, Mechanical properties and electrical conductivity of carbon-nanotube filled polyamide-6 and its blends with acrylonitrile/butadiene/styrene; *Polymer*, **2004**, 45, 739-748.
- [76] Z. Shen, S. Bateman, D.Y. Wu, P. McMahon, M. Dell'Olio J. Gotama, The effects of carbon nanotubes on mechanical and thermal properties of woven glass fibre reinforced polyamide-6 nanocomposites; *Comp. Sci. Tech.*, **2009**, 69, 239-244.
- [77] E. Logakis, C. Pandis, V. Peoglos, P. Pissis, J. Pionteck, P. Pötschke, M. Micusik, M. Omastova, Electrical/dielectric properties and conduction mechanism in melt processed polyamide/multi-walled carbon nanotubes composites; *Polymer*, **2009**, 50, 5103-5111.
- [78] P. Ding, S. Su, S. Tang, Y. Liu, L. Shi, Highly thermal conductive composites with polyamide-6 covalently-grafted graphene by an in situ polymerization and thermal reduction process, *Carbon*, **2014**, 66, 576-584.
- [79] H. Meng, G.X. Sui, G.Y. Xie, R. Yang, Friction and wear behavior of carbon nanotubes reinforced polyamide 6 composites under dry sliding and water lubricated condition; *Comp. Sci. Tech.*, **2009**, 69, 606-611.
- [80] B. Krause, P. Pötschke, L. Haussler, Influence of small scale melt mixing conditions on electrical resistivity on carbon nanotube-polyamide composites; *Comp. Sci. Tech.*, **2009**, 69, 1505-1515.
- [81] I.Y. Pang, T. Liu, W.D. Zhang, H. Schonherr, G.J. Vancso, Rubber network in elastomer nanocomposites; *Eur. Polym. J.*, **2007**, 43, 4136-4150.
- [82] P.V. Codgire, A.R. Bhattacharyya, S. Bose, N. Gupta, A.R. Kulkarni, A. Misra, Control of multiwall carbon nanotubes dispersion in polyamide 6 matrix: An

- assessment through electrical conductivity; *Chem. Phys. Lett.*, **2006**, 432, 480-485.
- [83] P. Pötschke, T.D. Fornes, D.R. Paul, Rheological behavior of multiwalled carbon nanotube/polycarbonate composites; *Polymer*, **2002**, 43, 3247-3255.
- [84] J.A. King, M.D. Via, J.A. Caspary, M.M. Jubinski, I. Miskioglu, O.P. Millisand G.R. Bogucki, Electrical and thermal conductivity and tensile and flexural properties of carbon nanotube/polycarbonate resins; *J. Appl. Polym. Sci.*, **2010**, 118, 2512-2520.
- [85] C. Liu, J. Zhang, J. He, G. Hu, Gelation in carbon nanotube/polymer composites; *Polymer*, **2003**, 44, 7529-7532.
- [86] W. Ding, A. Eitan, F.T. Fisher, X. Chen, D.A. Dikin, R. Andrews, L.C. Brinson, L.S. Schandler, R.S. Ruoff, Direct Observation of Polymer Sheathing in Carbon Nanotube-Polycarbonate Composites; *Nano Lett.*, **2003**, 3, 1593-1597.
- [87] M. Fernandez, M. Landa, M.E. Munoz, A. Santamaria, Thermal and Viscoelastic Features of New Nanocomposites Based on a Hot-Melt Adhesive Polyurethane and Multi-Walled Carbon Nanotubes, *Macromol. Mater. Eng.*, **2010**, 295, 1031-1041.
- [88] R. Zhang, A. Dowden, H. Deng, M. Baxendale, T. Peijs, Conductive network formation in the melt of carbon nanotube/thermoplastic polyurethane composite; *Compos. Sci. Technol.*, **2009**, 69, 1499-1504.
- [89] S.A. Abdullah, A. Iqbal, L. Frommann, Melt mixing of carbon fibers and carbon nanotubes incorporated polyurethanes; *J. Appl. Polym. Sci.*, **2008**, 110, 196-202.
- [90] <http://www.diytrade.com>, visited: 13/12/2013.
- [91] K. Kohlgrüber, Co-Rotating Twin-Screw Extruders: Fundamentals, Technology, and Applications; ISBN 1-569-904-227; Hanser Publishers, **2008**.
- [92] G. Miquelard-Garnier, A. Guinault, D. Fromonteil, S. Delalande, C. Sollogoub, Dispersion of carbon nanotubes in polypropylene via multilayer coextrusion: Influence on the mechanical properties; *Polymer*, **2013**, 54, 4290-4297.

- [93] G. Menges, W. Michaeli, P. Mohren, How to Make Injection Molds; ISBN 9-781-569902-820; Hanser Publishers, **1993**.
- [94] P. Pötschke, B. Krause, B. Buschhorn, S. Köpke, M. Müller, T. Villmow, K. Schulte, Improvement of carbon nanotube dispersion in thermoplastic composites using a three roll mill at elevated temperatures, *Comp. Sci. Tech.*, **2013**, 74, 78-84.
- [95] I. Alig, D. Lellinger, E. Engel, T. Skipa, P. Pötschke, Destruction and formation of a conductive carbon nanotube network in polymer melts: In-line experiments; *Polymer*, **2008**, 49, 1902-1909.
- [96] B. Krause, T. Villmow, R. Boldt, M. Mende, G. Petzold, P. Pötschke, Influence of dry grinding in a ball mill on the length of multiwalled carbon nanotubes and their dispersion and percolation behavior in melt polycarbonate composites; *Comp. Sci. Tech.*, **2011**, 71, 1145-1153.
- [97] J. Tiusanen, D. Vlasveld, J. Vuorinen, Review on the effects of injection moulding parameters on the electrical resistivity of carbon nanotube filled polymer parts, *Comp. Sci. Tech.*, **2012**, 72, 1741-1752.
- [98] H.P. Thielges, Fiber damage during injection molding of reinforced plastics (Unpublished doctoral dissertation), RWTH Aachen University, **1992**.
- [99] R. Bailey, H. Kraft, A Study of Fibre Attrition in the Processing of Long Fibre Reinforcement Thermoplastics; *Intern. Polym. Proc.*, **1987**, 2, 94-101.
- [100] T.A. Osswald, L.-S. Turng, P.J. Gramann, Injection Molding Handbook; ISBN 156-9904-200; Hanser Publishers, **2002**.
- [101] S.-N. Li, B. Li, Z.-M. Li, Q. Fu, K.-Z. Shen, Morphological manipulation of carbon nanotube/polycarbonate/polyethylene composites by dynamic injection packing molding; *Polymer*, **2006**, 47, 4497-4500.
- [102] P. Pötschke, A. R. Bhattacharyya, A. Janke, Morphology and electrical resistivity of melt mixed blends of polyethylene and carbon nanotube filled polycarbonate; *Polymer*, **2003**, 44, 8061-8069.
- [103] S. Richter, M. Saphiannikova, D. Jehnichen, M. Bierdel, G. Heinrich, Experimental and theoretical studies of agglomeration effects in multi-walled carbon nanotube-polycarbonate melts; *Polym. Lett.*, **2009**, 3, 753-768.

- [104] D. Lellinger, D. Xu, A. Ohneiser, T. Skipa, I. Alig, Influence of the injection moulding conditions on the in-line measured electrical conductivity of polymer-carbon nanotube composites; *Phys. Sta. Sol. (B)*, **2008**, 245, 2268-2271.
- [105] S.-Y. Fu, B. Lauke, R.K.Y. Li, Y.-W. Mai, Effects of PA6,6/PP ratio on the mechanical properties of short glass fiber reinforced and rubber-toughened polyamide 6,6/polypropylene blends; *Comp. B*, **2006**, 37, 182-190.
- [106] J.N. Coleman, U. Khan, W.J. Blau, Y.K. Gunko, Small but strong: a review of the mechanical properties of carbon nanotube-polymer composites; *Carbon*, **2006**, 44, 1624-1652.
- [107] X.L. Xie, Y.W. Mai, X.P. Zhou, Dispersion and alignment of carbon nanotubes in polymer matrix: A review; *Mater. Sci. Eng. R*, **2005**, 49, 89-112.
- [108] G.R. Kasaliwal, S. Pegel, A. Goldel, P. Potschke, G. Heinrich, Analysis of agglomerate dispersion mechanisms of multiwalled carbon nanotubes during melt mixing in polycarbonate; *Polymer*, **2010**, 51, 2708-2720.
- [109] J.-H. Shi, B.X. Yang, S.H. Goh, Covalent functionalization of multiwalled carbon nanotubes with poly(styrene-co-acrylonitrile) by reactive blending; *Eur. Pol. Sci.*, **2009**, 45, 1002-1008.
- [110] C. Penu, G. H. Hu, C. Fonteix, P. Marchal, L. Choplin, Effects of carbon nanotubes and their state of dispersion on the anionic polymerization of ϵ -caprolactam; *Polym. Eng. Sci.*, **2010**, 50, 2287-2297.
- [111] D. Prifits, G. Sakellariou, J.W. Mays, N. Hadjichristidis, Novel diblock copolymer-grafted multiwalled carbon nanotubes via a combination of living and controlled/living surface polymerizations; *J. Polym. Sci. A*, **2010**, 48, 1104-1112.
- [112] J.L. Chen, K.H. Hsieh, Polyacrylamide grafted on multi-walled carbon nanotubes for open-tubular capillary electrochromatography: comparison with silica hydride and polyacrylate phase matrices; *Electrophoresis*, **2010**, 31, 3937-3948.

- [113] Y. S. Li, C.H. Xu, Y.M. Xu, Covalent Attachment of Organic Groups onto Single-walled Carbon Nanotubes via Copper (I)-promoted Radical Addition; *Chem. Lett.*, **2010**, 39, 1000-1002.
- [114] S.Y. Li, H. Chen, D.M. Cui, J.Z. Li, Z.J. Zhang, Y.H. Wang, T. Tang, Structure and properties of multi-walled carbon nanotubes/polyethylene nanocomposites synthesized by in situ polymerization with supported Cp_2ZrCl_2 catalyst; *Polym. Compos.*, **2010**, 31, 507-515.
- [115] A. Ravasio, L. Boggioni, I. Tritto, C. D'Arrigo, A. Perico, J. Hitzbleck, J. Okuda, A non-PFT (polymerization filling technique) approach to poly(ethylene-*co*-norborane)/MWNTs nanocomposites by *in situ* copolymerization with scandium half-sandwich catalyst; *J. Polym. Sci. A*, **2009**, 47, 5709-5719.
- [116] G.-P. Wu, Y.-Y. Wang, D.-H. Lee, C.-X. Lu, W.-Z. Shen, X.-T. Li, Z.-H. Feng, Direct electrochemical attachment of carbon nanotubes to carbon fiber surfaces; *Carbon*, **2011**, 49, 2152-2155.
- [117] S.H. Qin, D.Q. Qin, W.T. Ford, J.E. Herrera, D.E. Resasco, Grafting of poly(4-vinylpyridine) to single-walled carbon nanotubes an assembly of multilayers films; *Macromolecules*, **2004**, 37, 9963-9967.
- [118] H. Kong, C. Gao, D. Y. Yan, Constructing amphiphilic brushes on the convex surfaces of multi-walled carbon nanotubes by *in situ* atom transfer radical polymerization; *J. Mater. Chem.*, **2004**, 14, 1401-1405.
- [119] C. Boyer, M.H. Stenzel, T.P. Davis, Building nanostructures using RAFT polymerization; *J. Polym. Sci. A*, **2011**, 49, 551-595.
- [120] T.H. Hu, H.L. Xie, L. Chen, G.Q. Zhong, H.L. Zhang, Preparation and orientation behavior of multi-walled carbon nanotubes grafted with a side-chain azobenzene liquid crystalline polymer; *Polym. Int.*, **2011**, 60, 93-101.
- [121] H.Y. Tang, D.H. Zhang, Poly(γ -benzyl-L-glutamate)-functionalized single-walled carbon nanotubes from surface-initiated ring-opening polymerizations of *N*-carboxylanhydride; *J. Polym. Sci. A*, **2010**, 48, 2340-2350.
- [122] L.A. Zeng, H.B. Wang, G.X. Fu, J.W. Jiang, X.F. Zhang, A new approach for synthesis of the comb-shaped poly (ϵ -caprolactone) brushes on the surface

- of nano-hydroxyapatite by combination of ATRP and ROP; *J. Colloid Interface Sci.*, **2010**, 352, 36-42.
- [123] K.A. Wepasnick, B.A. Smith, K.E. Schrote, H.K. Wilson, S.R. Diegelmann, D.H. Fairbrother, Surface and structural characterization of multi-walled carbon nanotubes following different oxidative treatments; *Carbon*, **2011**, 49, 24-36.
- [124] P.-C. Ma, N.A. Siddiqui, G. Marom, J.-K. Kim, Dispersion and functionalization of carbon nanotubes for polymer-based nanocomposites: A review; *Comp. A*, **2010**, 41, 1345-1367.
- [125] M. Ganss, B.K. Satapathy, M. Thunga, R. Weidish, P. Pötschke, D. Jehnichen, Structural interpretations of deformation and fracture behavior of polypropylene/multi-walled carbon nanotube composites; *Acta Mater.*, **2008**, 56, 2247-2261.
- [126] J. Sandler, M.S.P. Shaffer, A.H. Windle, M.P. Halsall, M.A. Montes-Moran, C.A. Cooper, R.J. Young, Variations in the Raman peak shift as a function of hydrostatic pressure for various carbon nanostructures: A simple geometric effect; *Phys. Rev. B*, **2003**, 67, 354171-354178.
- [127] J. Sandler, A.H. Windle, P. Werner, V. Altstadt, M.V. Es, M.S.P. Shaffer, Carbon-nanofibre-reinforced poly(ether ether ketone) fibres; *J. Mater. Sci.*, **2003**, 38, 2135-2141.
- [128] V. Skakalova, U. Dettlaff-Weglikowska, S. Roth, Electrical and mechanical properties of nanocomposites of single wall carbon nanotubes with PMMA; *Synth. Met.*, **2005**, 152, 349-352.
- [129] W. Bauhofer, J.Z. Kovacs, A review and analysis of electrical percolation in carbon nanotube polymer composites; *Compos. Sci. Tech.*, **2009**, 69, 1486-1498.
- [130] S. Kumar, B. Li, S. Caceres, R.G. Maguire, W.-H. Zhong, Dramatic property enhancement in polyetherimide using low-cost commercially functionalized multi-walled carbon nanotubes via a facile solution processing method; *Nanotech.*, 2009, 20, 465708.

- [131] L. Liu, K.C. Etika, K.-S. Liao, L.A. Hess, D.E. Bergbreiter, J.C. Grunlan, Comparison of covalently and noncovalently functionalized carbon nanotubes in epoxy; *Macromol. Rapid Commun.*, **2009**, 30, 627-632.
- [132] D.R. Paul, R.M. Robeson, Polymer nanotechnology: Nanocomposites; *Polymer*, **2008**, 49, 3187-3204.
- [133] E.J. Siochi, D.C. Working, C. Park, P.T. Lillehei, J.H. Rouse, C.C. Topping, A.R. Bhattacharyya, S. Kumar, Melt processing of SWCNT-polyimide nanocomposite fibers; *Compos. B*, **2004**, 35, 439-446.
- [134] <http://www.tda.com>, visited: 13/12/2013.
- [135] B. Li, Y.-C. Zhang, Z.-M. Li, S.-N. Li, X.-N. Zhang, Easy Fabrication and Resistivity-Temperature Behavior of an Anisotropically Conductive Carbon Nanotube-Polymer Composite; *J. Phys. Chem. B*, **2010**, 114, 689-696.
- [136] M.R.S. Castro, N. Al-Dahoudi, P.W. Oliveira, H.K. Schmidt, Multi-walled carbon nanotube-based transparent conductive layers deposited on polycarbonate substrate; *J. Nanopart. Res.*, **2009**, 11, 801-806.
- [137] A. Chandra, A.J. Kramschuster, X. Hu, S. Turng, Effect on injection molding parameter on the electrical conductivity of polycarbonate/carbon nanotube nanocomposites; *Proc. Annual Technical conference of the Society of Plastics Engineers*, **2007**, 3, 2184-2188.
- [138] J.A. Elliott, J.K.W. Sandler, A.H. Windle, R.J. Young, M.S.P. Shaffer, Collapse of single-wall carbon nanotubes is diameter dependent; *Phys. Rev. Lett.*, **2004**, 92, 95501.
- [139] J.C. Halpin, J.L. Kardos, Halpin-Tsai Equations: A review; *Pol. Eng. Sci.*, **1976**, 16, 344-352.
- [140] I.V. Singh, M. Tanaka, M. Endo, Effect of interface on the thermal conductivity of carbon nanotube composites; *Int. J. Therm. Sci.*, **2007**, 46, 842-847.
- [141] F.P. Folgar, C.L. Tucker, Orientation behavior of fibers in concentrated suspensions; *J. Reinf. Plast. Comp.*, **1984**, 3, 98-119.
- [142] J.H. Phelps, A.I. Abd El-Rahman, V. Kunc, C.L. Tucker III, A model for fiber length attrition in injection-molded long-fiber composites; *Composites Part A*, **2013**, 51, 11-21.

- [143] C.L. Tucker, S.G. Advani, Processing of shorter systems; In Flow and Rheology in Polymer Composites Manufacturing; Editor: S.G. Advani; Amsterdam: Elsevier, **1994**, Chapter 6.
- [144] G.B. Jeffery, The motion of ellipsoidal particles immersed in a viscous fluid; *Proc. Roy. Soc. A*, **1922**, 102, 161-179.
- [145] A. Londono, Mechanistic models for fiber flow (Unpublished doctoral dissertation), University of Wisconsin-Madison, **2009**.
- [146] J.H. Phelps, C.L. Tucker, An anisotropic rotary diffusion model for fiber orientation in short- and long-fiber thermoplastics; *J. Non-Newtonian Fluid Mech.*, **2009**, 156, 165-176.
- [147] S. Yamamoto, T. Matsuoka, A method for dynamic simulation of rigid and flexible fibers in a flow field; *J. Chem. Phys.*, **1993**, 98, 664-650.
- [148] S. Yamamoto, T. Matsuoka, Viscosity of dilute suspensions of rodlike particles: A numerical simulation method; *J. Chem. Phys.*, **1994**, 100, 3317-3324.
- [149] S. Yamamoto, T. Matsuoka, Dynamic simulation of fiber suspensions in shear flow; *J. Chem. Phys.*, **1995**, 102, 2254-2260.
- [150] Z.M. Ariff, A.A. Bakar, M.N.Z. Arif, Process Parameters Dependence of Acrylonitrile-Butadiene-Styrene (ABS) flow Patterns Inside a Capillary Rheometer; *National Symposium on Polymeric Materials*, **2002**, 203-212.
- [151] S. Sathyanarayana, M. Wegrzyn, G. Olowojoba, A. Benedito, E. Gimenez, C. Hübner, F. Henning, Multiwalled carbon nanotube incorporated into a miscible blend of poly(phenylenether) polystyrene – Processing and characterization; *Polym. Lett.*, **2013**, 7, 621-635.
- [152] Z.Y. Xiong, L. Wang, Y. Sun, Z.X. Guo, J. Yu, Migration of MWCNTs ducting melt preparation of PC/ABS/MWCNT conductive composites via PC/MWCNT masterbatch approach; *Polymer*, **2013**, 54, 447-455.
- [153] M.R. Nobile, Rheology of polymer-carbon nanotube composites melts; In Polymer-Carbon Nanotube Composites: Synthesis, Properties and Applications; Editors: T. McNally, P. Pötschke; ISBN 1-84569-761-8; Woodhead Publishing, **2011**, Chapter 15.

- [154] S.F. Ahmed, J.W. Ji, M.W. Moon, Y.J. Jang, B.H. Park, S.H. Lee, K.R. Lee, The Morphology and Mechanical Properties of Polycarbonate/Acrylonitrile Butadiene Styrene Modified by Ar Ion Beam Radiation; *Plasma Process. Polym.*, **2009**, 6, 860-865.
- [155] S. Nuriel, L. Liu, A.H. Barber, H.D. Wagner, Direct Measurement of Carbon Nanotubes Surface Tension; *Chem. Phys. Lett.*, **2005**, 404, 263-265.
- [156] A.H. Barber, S.R. Cohen, H.D. Wagner, Static and Dynamic Wetting Measurements of Single Carbon Nanotubes; *Phys. Rev. Lett.*, **2004**, 92, 186103.
- [157] M. Sumita, K. Sakata, S. Asai, K. Miyasaka, H. Nakagawa, Dispersion of Fillers and the Electrical Conductivity of Polymer Blends Filled with Carbon Black; *Polym. Bull.*, **1991**, 25, 265-271.
- [158] T. Villmow, P. Pötschke, S. Pegel, L. Häussler, B. Kretzschmar, Influence of twin-screw extrusion conditions on the dispersion of multi-walled carbon nanotubes in a poly(lactic acid) matrix; *Polymer*, 49, **2008**, 3500-3509.
- [159] T. Domenech, E. Peuvrel-Disdier, B. Vergnes, The importance of specific mechanical energy during twin screw extrusion of organoclay based polypropylene nanocomposites, *Comp. Sci. Tech.*, **2013**, 75, 7-14.
- [160] T. McNally, P. Pötschke, P. Halley, M. Murphy, D. Martin, S.E.J. Bell, G.P. Brennan, D. Bein, P. Lemonie, J.P. Quinn, Polyethylene multiwall carbon nanotube composites; *Polymer*, **2005**, 46, 8222-8232.
- [161] L. Deng, S.J. Eichhorn, C.C. Kao, R. J. Young, The effective Young's modulus of carbon nanotubes in composites; *ACS Appl. Mater. Interfaces*, **2011**, 3, 433-440.
- [162] C.A. Cooper, R.J. Young, M. Halsall, Investigation into the deformation of carbon nanotubes and their composites through the use of Raman spectroscopy; *Composites A*, **2001**, 32, 401-411.
- [163] X. Yan, T. Itoh, Y. Kitahama, T. Suzuki, H. Sato, T. Miyake, Y. Ozaki, A Raman Spectroscopy Study on Single-Wall Carbon Nanotube/Polystyrene Nanocomposites: Mechanical Compression Transferred from the Polymer to Single Wall Carbon Nanotubes; *J. Phys. Chem. C*, **2012**, 116, 17897-17903.

- [164] H.K.F. Cheng, T. Basu, N.G. Sahoo, L. Li, S.H. Chan, Current Advances in the Carbon Nanotube/Thermoplastic Main-Chain Liquid Crystalline Polymer Nanocomposites and Their Blends; *Polymers*, **2012**, 4, 889-912.
- [165] N. Lebovka, T. Dadakova, L. Lysetskiy, O. Melezhyk, G. Puchkovska, T. Gavrilko, J. Baran, M. Drozd, Phase transitions, intermolecular interactions and electrical conductivity behavior in carbon multiwalled nanotubes/nematic liquid crystal composites; *J. Mol. Struct.*, **2008**, 887, 135-143.
- [166] X. Wang, S. Chen, Graphene-Based Nanocomposites; In Physics and Applications of Graphene – Experiments, Editor: S. Mikhailov; ISBN 978-953-307-217-3; InTech, **2011**, Chapter 8.
- [167] W.-J. Chou, C.-C. Wang, C.-Y. Chen, Characteristics of polyimide-based nanocomposites containing plasma-modified multi-walled carbon nanotubes; *Comp. Sci. Tech.*, **2008**, 68, 2208-2213.
- [168] K. Czanikova, N. Torras, J. Esteve, I. Krupa, P. Kasak, E. Pavlova, D. Racko, I. Chodak, M. Omastova, Nanocomposite photoactuators based on ethylene vinyl acetate copolymer filled with carbon nanotubes; *Sensor. Actuat. B-Chem.*, **2013**, 701-710.
- [169] H.-C. Kuan, C.-C.M. Ma, W.-P. Chang, S.-M. Yuen, H.-H. Wu, T.-M. Lee, Synthesis, thermal, mechanical and rheological properties of multiwall carbon nanotube/waterborne polyurethane nanocomposite; *Comp. Sci. Tech.*, **2005**, 65, 1703-1710.
- [170] S.P. Su, Y.H. Xu, C.A. Wilkie, Thermal degradation of polymer-carbon nanotube composites; In Polymer-Carbon Nanotube Composites: Synthesis, Properties and Applications; Editors: T. McNally, P. Pötschke; ISBN 1-84569-761-8; Woodhead Publishing, **2011**, Chapter 16
- [171] I. Groves, T. Lever, N. Hawkins, Thermal Analysis Application Brief. Differentiation Between Grades of ABS by Hi-Res TGA, TA-127.
- [172] Enhanced Separation of Components in ABS Polymer: Using AutoStepwise TGA; *Perkin Elmer Application Note*, **2010**.

- [173] M. Suzuki, C.A. Wilkie, The thermal degradation of acrylonitrile-butadiene-styrene terpolymer as studied by TGA/FTIR; *Polym. Degrad. Stab.*, **1995**, 47, 217-221.
- [174] L.F. Tong, H.Y. Ma, Z.P. Fang, Thermal decomposition and flammability of acrylonitrile-butadiene-styrene/multi-walled carbon nanotubes composites; *Chin. J. Polym. Sci.*, **2008**, 26, 331-339.
- [175] J.E. Robertson, Thermal Degradation Studies of Polycarbonate (Unpublished doctoral dissertation), Virginia Polytechnic Institute and state University, **2001**.
- [176] G. Gedler, M. Antunes, V. Realinho, J.I. Velasco, Thermal stability of polycarbonate-graphene nanocomposite foams; *Polym. Degrad. Stab.*, **2012**, 97, 1297-1304.
- [177] L. Lee, Mechanisms of thermal degradation of phenolic condensation polymers. I. Studies on the thermal stability of polycarbonate; *J. Polym. Sci. A*, **1964**, 2, 2859-2873.
- [178] A. Davis, J.H. Golden, Quantitative analysis of bisphenol A by direct gas chromatography; *J. Gas. Chrom. A*, **1967**, 26, 254-255.
- [179] A. Davis, J.H. Golden, Thermal degradation of polycarbonate; *J. Chem. Soc. B*, **1968**, 45-47.
- [180] A. Davis, J.H. Golden, Stability of Polycarbonate; *J. Macromol. Sci. Rev. Macromol. Chem. Phys.*, **1969**, 3, 49-68.
- [181] R. Zhong, Y. Hu, N. Liu, S. Wang, G. Liao, Evaluation of the thermal degradation of PC/ABS/montmorillonite nanocomposites; *Polym. Adv. Technol.*, **2005**, 16, 725-731.
- [182] S. Wang, Y. Hu, L. Song, Z. Wang, Z. Chen, W. Fan, Preparation and thermal properties of ABS/montmorillonite nanocomposite; *Polym. Degrad. Stab.*, **2002**, 77, 423-426.
- [183] S. Wang, Y. Hu, L. Song, J. Liu, Z. Chen, W. Fan, Synthesis and characterization of polycarbonate/ABS/montmorillonite nanocomposites; *Polym. Degrad. Stab.*, **2003**, 80, 157-161.

- [184] R. Zhong, Y. Hu, S. Wang, L. Song, Thermogravimetric evaluation of PC/ABS/montmorillonite nanocomposite; *Polym. Degrad. Stab.*, **2004**, 83, 423-428.
- [185] Z. Li, S.J. Wilkins, K.S. Moon, C.P. Wong, Carbon Nanotubes/Polymer Nanocomposites: Improved or Reduced Thermal Stabilities; *Mater. Sci. Forum*, **2012**, 722, 77-86.
- [186] R. Arasteh, M. Omid, A.H.A. Rousta, H. Kazerooni, A Study on Effect of Waviness of Mechanical Properties of Multi-Walled Carbon Nanotube/Epoxy Composites Using Halpin-Tsai Theory; *J. Macromol. Sci. B*, **2011**, 50, 2464-2480.
- [187] V.K. Srivastava, S. Singh, A Micro-Mechanical Model of Elastic Modulus of Multi-Walled Carbon Nanotube/Epoxy Resin Composites; *Int. J. Comp. Mater.*, **2012**, 2, 1-6.
- [188] Z. Jiang, P. Hornsby, R. McCool, A. Murphy, Mechanical and Thermal Properties of Polyphenylene Sulfide/Multiwalled Carbon Nanotube Composites; *J. Appl. Polym. Sci.*, **2012**, 123, 2676-2683.
- [189] K. McReeedy, H. Keskkula, Application of thermogravimetric analysis to the thermal decomposition of polybutadiene; *J. Appl. Polym. Sci.*, **2003**, 22, 999-1005.
- [190] W.P. Cox, E.H. Merz, Correlation of dynamic and steady flow viscosities; *J. Polym. Sci. A*, **1958**, 28, 619-622.
- [191] T.S.R Al-Hadithi, H.A. Barnes, K.Walters, The relationship between the linear (oscillatory) and nonlinear (steady-state) flow properties of a series of polymer and colloidal systems; *Colloid Polym. Sci.*, **1992**, 270, 40-46.
- [192] K.Q. Xiao, L.C. Zhang, I. Zarudi, Mechanical and rheological properties of carbon nanotube-reinforced polyethylene composites; *Com. Sci. Technol.*, **2007**, 67, 177-182.
- [193] J. Chen, Y.Y. Shi, J.H. Yang, N. Zhang, T. Huang, C. Chen, Y. Wang, Z.W. Zhou, A simple strategy to achieve very low percolation threshold via the selective distribution of carbon nanotubes at the interface of polymer blends; *J. Mater. Chem.*, **2012**, 22, 22398-223404.

- [194] M. Sumita, K. Sakata, Y. Hayakawa, S. Asai, K. Miyasaka, M. Tanemura, Double percolation effect on the electrical conductivity of conductive particles filled polymer blends; *Colloid. Pol. Sci.*, **1992**, 270, 134-139.
- [195] P. Pötschke, A.R. Bhattacharyya, A. Janke, Carbon nanotube-filled polycarbonate composites produced by melt mixing and their use in blends with polyethylene; *Carbon*, **2004**, 42, 965-969.
- [196] R. Ibara-Gomez, A. Marquez, L.F. Ramos-de Valle, O.S. Rodriguez Fernandez, Influence of the blend viscosity and interface energies on the preferential location of CB and conductivity of BR/EPDM blends; *Rubber Chem. Rechnol.*, **2003**, 76, 969-978.
- [197] M. Gultner, A. Goldel, P. Pötschke, Tuning the localization of functionalized MWCNTs in SAN/PC blends by a reactive component; *Comp. Sci. Tech.*, **2011**, 72, 41-48.
- [198] N.G. Sahoo, S. Rana, J.W. Cho, L. Li, S.H. Chan, Polymer nanocomposites based on functionalized carbon nanotubes; *Prog. Polym. Sci.*, **2010**, 35, 837-867.
- [198] M. Kumar, Carbon Nanotube Synthesis and Growth Mechanism; In Carbon Nanotubes – Synthesis, Characterization, Applications; Editor: S. Yellampalli; ISBN 978-953-307-497-9; InTech, **2012**, Chapter 8.
- [200] Y. Wang, Z. Luo, B. Li, P.S. Ho, Z. Yao, L. Shi, E.N. Bryan, R.N. Nemanich, Comparison study of catalyst nanoparticle formation and carbon nanotube growth: Support effect; *J. Appl. Phys.*, **2007**, 101, 124310-124318
- [201] S. Angermüller, H. D. Fahimi, Imidazole-buffered osmium tetroxide: an excellent stain for visualization of lipids in transmission electron microscopy; *Histochem. J.*, **1982**, 14, 823-835.
- [202] B. Kiss-Pataki, J. Tiusanen, G. Dobrik, Z. Vertesy, Z.E. Horvath, Visualization of the conductive paths in injection moulded MWCNT/polycarbonate nanocomposites by conductive AFM; *Comp. Sci. Tech.*, **2014**, 90, 102-109.
- [203] K. Grzybowski, Potential Application of Carbon Nanotubes (CNT) as a flame retardant additive – technical and market analysis, *Frost & Sullivan Market Insight*, **2009**.

- [204] B.H. Cipriano, T. Kashiwagi, S.R. Raghavan, Y. Yang, E.A. Grulke, K Yamamoto, J.R. Shields, J.F. Douglas, Effects of aspect ratio of MWCNT on the flammability properties of polymer nanocomposites; *Polymer*, **2007**, 48, 6086-6096.
- [205] F. Gao, G. Beyer, Q. Yuan, A mechanistic study of fire retardancy of carbon nanotube/ethylene vinyl acetate copolymers and their clay composites; *Polym. Degrad. Stab.*, **2005**, 89, 599-564.
- [206] T. Kashiwagi, F.M. Du, J.F. Douglas, R. Harris, J.R. Shields, Nanoparticle networks reduce the flammability of nanocomposites; *Nature Mater.*, **2005**, 4, 928-933.
- [207] H. Raghu, S. Bose, P.A. Mahanwar, Effect of Particle Size of Filler on Coloration and Properties of High Density Polyethylene; *J. Min. Mater. Charact. Eng.*, **2006**, 5, 87-100.
- [208] B. Schartel, U. Braun, U. Knoll, M. Bartholmai, H. Goering, D. Neubert, P. Pötschke, Mechanical, thermal, and fibre behavior of bisphenol a polycarbonate/multiwall carbon nanotube nanocomposite; *Polym. Eng. Sci.*, **2008**, 48, 149-158.
- [209] C.Y. Lew, C. Dewaghe, M. Claes, Surface treatment of carbon nanotubes via plasma technology; In *Polymer-Carbon Nanotube Composites: Synthesis, Properties and Applications*; Editors: T. McNally, P. Pötschke; ISBN 1-84569-761-8; Woodhead Publishing, **2011**, Chapter 2.
- [210] B.H. Cipriano, A.K. Kota, A.L. Gershon, C.J. Laskowski, T. Kashiwagi, H.A. Bruck, S.R. Raghavan, Conductivity Enhancement of Carbon Nanotube and Nanofiber-based Polymer Nanocomposites by Melt Annealing; *Polymer*, **2008**, 49, 4846-4851.
- [211] A. Kolmogoroff, Über die analytischen Methoden in der Wahrscheinlichkeitsrechnung, *Math. Ann.*, **1931**, 104, 415-458.
- [212] J.L. Garcia-Palacios, Introduction to the Theory of Stochastic Processes and Brownian Motion Problems, Lecture notes, University of Zaragoza, **2004**.
- [213] J. Linn, The Folger-Tucker Model as a Differential Algebraic System for Fiber Orientation Calculation; *Berichte des Fraunhofer ITWM*, 75, **2005**.

- [214] R. Johansson, D. Konijnendijk, Injection Molding Simulation – A Finite Element Approach to Analyse the Thermodynamics in an IM Tool (Unpublished master dissertation), Lund University, **2007**.
- [215] E. Süli, Lecture Notes on Finite Element Methods for Partial Differential Equations, University of Oxford, **2012**.

